Structural Characterization of Bacterial Antimicrobial Peptides

by

Christopher Thomas Lohans

A thesis submitted in partial fulfillment of the requirements for the degree of

Doctor of Philosophy

Department of Chemistry
University of Alberta

© Christopher Thomas Lohans, 2014

Abstract

Paenibacillus polymyxa NRRL B-30509, *Paenibacillus terrae* NRRL B-30644 and *P. polymyxa* NRRL B-30507 were found to produce several bacteriocins and non-ribosomal peptides. All three strains produce tridecaptins, non-ribosomal lipopeptides antimicrobially active against food pathogen *Campylobacter jejuni*. Two of these strains also produce polymyxins, lipopeptides also active against Gram-negative bacteria. Highly cyclized lantibiotics paenicidins A and B were isolated from *P. polymyxa* NRRL B-30509 and *P. terrae* NRRL B-30644, respectively. The lanthionine (Lan) and methyllanthionine (MeLan) post-translational modifications of paenicidin A were characterized by a novel partial desulfurization strategy, revealing the connectivity of three interlocking thioether-containing rings. Biosynthetic gene clusters responsible for the production of the tridecaptins and paenicidins were identified in the genome sequences of these strains.

Carnobacterium maltaromaticum C2 produces carnolysin, a novel two-component lantibiotic with homology to enterococcal cytolysin. The post-translational modifications of carnolysins A1′ and A2′ were characterized with NMR spectroscopy and tandem mass spectrometry, revealing the Lan and MeLan bridging patterns. Like cytolysin, carnolysin contains unusual LL-Lan and LL-MeLan stereoisomers in the corresponding positions. However, carnolysin also contains D-alanine and D-aminobutyrate residues not found in cytolysin. The carnolysin biosynthetic gene cluster was identified in the genome of *C. maltaromaticum* C2. Heterologous expression of carnolysin in *Escherichia coli* was achieved by expressing the carnolysin precursor peptides with lantibiotic synthetase CrnM and reductase CrnJ. Antimicrobially active

products were obtained by proteolytically removing the N-terminal leader sequences of the carnolysins isolated from *C. maltaromaticum* C2. These digested peptides were active against an array of Gram-positive indicator organisms, while not demonstrating the hemolytic activity associated with cytolysin at the levels tested.

Enterocin 7A and 7B are leaderless bacteriocins produced by *Enterococcus faecalis* 710C. The impact of solvent on the secondary structure of enterocin 7A was examined by circular dichroism spectroscopy, revealing a high degree of α-helicity in fully aqueous conditions. The solution structure of enterocin 7A was solved based on NMR spectroscopic data, demonstrating that this peptide consists primarily of three amphiphilic α-helices burying a hydrophobic core. The structures of enterocins 7A and 7B resembled a region of the circular bacteriocin carnocyclin A, potentially having implications regarding the mode of action of these leaderless bacteriocins.

The cysteines involved in the N-terminal disulfide bridge of class IIa bacteriocin leucocin A were replaced with leucine residues to probe the impact of this substitution on structure. While this mutant peptide retained antimicrobial activity, consistent with similar leucocin A mutants. The solution structure of (C9L,C14L)-leucocin A in aqueous trifluoroethanol was studied by NMR spectroscopy. Instead of the N-terminal three-strand β-sheet found in wild-type leucocin A, the N-terminus of the mutant structure is α-helical. However, this may not represent the active conformation of this peptide, and the structure of the N-terminus may be influenced by the choice of solvent.

Preface

Parts of Chapter 2 of this thesis have been published as Lohans et al. *J. Am. Chem. Soc.* **2012,** *134,* 19540-19543 and Lohans et al. *ChemBioChem* **2014,** *15,* 243-249. I was responsible for isolating the peptides, characterizing them using mass spectrometry and NMR spectroscopy, and determining their spectra of activity. I also isolated and sequenced the genomes of the producer strains and performed bioinformatic analyses. The other authors synthesized chemical standards and peptides, chemically modified the peptides obtained, assisted with the interpretation of mass spectral data, and assisted with gene cluster sequencing. For these two manuscripts, I performed approximately 70 % of the work, and wrote the majority of both manuscripts.

Chapter 3 has been published as Tulini et al. *Int. J. Food Microbiol.* **2014,** *173,* 81-88 and Lohans et al. *J. Am. Chem. Soc.* **2014,** *136,* 13150-13153. I was responsible for isolating the peptides and characterized them using mass spectrometry and NMR spectroscopy. I identified the gene clusters responsible for their production, and did the cloning experiments for the heterologous expression in *E. coli*. I also expressed the enzymatic biosynthetic machinery and showed its activity *in vitro*. Finally, I performed the antimicrobial testing for some of these peptides. The other authors performed preliminary peptide isolation experiments and mass spectral characterization, tested the antimicrobial spectrum of some of these peptides, and assisted with the cloning experiments. For the first manuscript, I performed approximately 50 % of the work, while for the second, I performed approximately 90 % of the work. I assisted with the writing of the first manuscript, while I wrote the majority of the second manuscript.

Chapter 4 has been published as Lohans et al. *Biochemistry* **2013,** *52,* 3987-3994. I isolated enterocin 7A, performed the circular dichroism experiments and acquired NMR spectroscopic data. I interpreted the NMR data and performed the structure calculation experiments for this peptide, in addition to performing antimicrobial testing. The other authors assisted with acquisition of NMR spectroscopic data, structurally analyzed a separate peptide, and performed isothermal calorimetry experiments. I performed approximately 55 % of the work on this project, and wrote the majority of the manuscript.

Chapter 5 has been published as Sit et al. *ChemBioChem* **2012,** *13,* 35-38. I performed the cloning experiments to express a single peptide mutant in *E. coli*. I isolated the peptide, cleaved it, and obtained NMR spectroscopic data. I analyzed these data to assign chemical shifts and performed all of the structure calculations for this mutant. The other authors performed similar experiments with other peptide mutants to determine their structures. I performed approximately 40 % of the work in this manuscript, and assisted with its writing.

Acknowledgements

First and foremost, I would like to thank Prof. John Vederas for providing me the opportunity to do my doctoral studies in his lab. His enthusiasm and passion for research and science in general is nearly unmatched, and he has passed on this interest to me. I thank him for offering support and suggestions whenever asked, while also allowing and encouraging me to develop independence and confidence in research. I do not think that there could have been a better environment for my graduate studies, and for that I am grateful.

Working in the Vederas lab, I have had the opportunity to work with a fantastic group of people who have made the lab a great environment in which to spend these years. I am grateful to Dr. Marco van Belkum, Dr. Brandon Findlay, Shaun McKinnie, Stephen Cochrane and Kaitlyn Towle for their assistance in the preparation of this thesis. I am thankful to all Vederas group members who have taken time to teach me all of the skills necessary to reach this point. Although I have profited from the experiences and advice of all Vederas group members, I would in particular like to thank Marco, Dr. Leah Martin-Visscher and Dr. Clarissa Sit. Thank you to the visiting and undergraduate students with whom I have had the opportunity to work and collaborate: Maude Giroud, Fabricio Tulini, Sara Arbulu, Manon Bels and Jessica Li.

I am especially grateful to the fantastic non-academic staff in the Department of Chemistry. In particular, I would like to thank Mark Miskolzie and Dr. Ryan McKay of the NMR facility, Jing Zheng, Dr. Randy Whittal and Bela Reiz of the MS facility, and Wayne Moffat of the Analytical Instrumentation laboratory for their tireless help with all questions and research problems, often acting beyond the expectations of their post.

Thanks to the Natural Sciences and Engineering Research Council and the University of Alberta for scholarships allowing me to focus on my studies in the lab.

Thanks to Che for going through this process with me, for understanding the stresses and demands inherent in graduate studies, and for always being supportive and encouraging. I would also like to thank my parents for providing me with the opportunity to pursue a university education, for encouraging me to pursue whatever I desired, and for instilling in me a deep appreciation for learning and education.

Table of Contents

List of Tables

List of Figures

List of Abbreviations

A	adenylation
a.a.	amino acids
ABC	ATP-binding cassette
Abu	2-aminobutyrate
AEBSF	4-(2-aminoethyl)benzenesulfonyl fluoride
Amp	ampicillin
APBS	adaptive Poisson-Boltzmann solver
APT	all-purpose Tween
ATCC	American type culture collection
ATP	adenosine triphosphate
AviCys	aminovinylcysteine
AviMeCys	aminovinylmethylcysteine
BLAST	basic local alignment search tool
bp	base pairs
C	condensation
^{13}C-HSQC	^{13}carbon-heteronuclear single quantum coherence
CAA	casamino acids
CbnB2	carnobacteriocin B2
CbnBM1	carnobacteriocin BM1
CbnX	carnobacteriocin X
CD	circular dichroism
CoA	coenzyme A

COSY	correlation spectroscopy
CrnA1	carnolysin A1
CrnA2	carnolysin A2
CylL$_L$	cytolysin L_L
CylL$_S$	cytolysin L_S
CYANA	combined assignment and dynamics algorithm for NMR applications
Dab	2,4-diaminobutyrate
Dha	dehydroalanine
Dhb	dehydrobutyrine
DMF	dimethylformamide
DNA	deoxyribonucleic acid
dNTP	deoxynucleotide triphosphate
DPC	dodecylphosphocholine
DSS	2,2-dimethyl-2-silapentane-5-sulfonic acid
DTT	dithiothreitol
E	epimerase
EDTA	ethylenediaminetetraacetic acid
EI-MS	electron ionization-mass spectrometry
ESI	electrospray ionization
ESI-qTOF MS	electrospray ionization-quadrupole time of flight mass spectrometry
FADH	flavin adenine dinucleotide

FDA	U.S. Food and Drug Agency
FTICR	Fourier-transform ion cyclotron resonance
GC	gas chromatography
GC-MS	gas chromatography-mass spectrometry
GRAS	generally recognized as safe
HATU	2-(1H-7-azabenzotriazol-1-yl)-1,1,3,3-tetramethyluronium hexafluorophosphate
HCCA	α-cyano-4-hydroxycinnamic acid
HPLC	high-performance liquid chromatography
HR-ESI MS	high-resolution electrospray ionization mass spectrometry
IM	inner membrane
IPTG	isopropyl β-D-1-thiogalactopyranoside
Kan	kanamycin
Kyn	kynurenine
LAB	lactic acid bacteria
Lan	lanthionine
LB broth	Luria-Bertani broth
LC	liquid chromatography
LC-MS/MS	liquid chromatography-tandem mass spectrometry
LeuA	leucocin A
LPS	lipopolysaccharide
MALDI-TOF MS	matrix-assisted laser desorption ionization-time of flight mass spectrometry

MALDI-TOF/TOF MS	matrix-assisted laser desorption ionization-time of flight time of flight mass spectrometry
MBP	maltose binding protein
MeLan	methyllanthionine
mGlu	3-methylglutamic acid
MHB	Mueller-Hinton broth
MIC	minimum inhibitory concentration
MPT	mannose phosphotransferase
MRSA	methicillin-resistant *Staphylococcus aureus*
MS	mass spectrometry
MS/MS	tandem mass spectrometry
MW	molecular weight
^{15}N-HSQC	^{15}nitrogen-heteronuclear single quantum coherence
NADPH	nicotinamide adenine dinucleotide phosphate
NANUC	National High Field Nuclear Magnetic Resonance Centre
Ni-NTA	nickel-nitrilotriacetic acid
NMR	nuclear magnetic resonance
NOE	nuclear Overhauser effect
NOESY	nuclear Overhauser effect spectroscopy
NRPS	non-ribosomal peptide synthetase
NRRL	Northern Regional Research Laboratory
OD_{600}	optical density at 600 nm
OM	outer membrane

ORF	open reading frame
PCR	polymerase chain reaction
PPi	inorganic pyrophosphate
PTM	post-translational modification
RMSD	root-mean-square deviation
ROESY	rotating frame nuclear Overhauser effect spectroscopy
rRNA	ribosomal ribonucleic acid
SAM	S-adenosylmethionine
SDS-PAGE	sodium dodecyl sulfate-polyacrylamide gel electrophoresis
SIM	single ion monitoring
SP Sepharose	sulfopropyl Sepharose
SPE	solid-phase extraction
SRCAM	State Research Center for Applied Microbiology
T	thiolation
TAE	Tris-acetate-EDTA
TALOS	torsion angle likelihood obtained from shift and sequence similarity
TBE	Tris-borate-EDTA
TCEP	tris(2-carboxyethyl)phosphine
TE	thioesterase
TE	Tris-EDTA
TFA	trifluoroacetic acid
TFE	trifluoroethanol

TOCSY	total correlation spectroscopy
USDA	United States Department of Agriculture
UV	ultraviolet

Chapter 1

Antimicrobial peptides produced by bacteria

1.1. Introduction

Bacterial secondary metabolites represent a source of highly diverse natural products with a wide variety of functions. Many of these metabolites have received a great deal of interest due to their antimicrobial properties and potential therapeutic applications (Figure 1.1). Furthermore, a substantial portion of the currently used commercial pharmaceuticals are either natural products or derivatives thereof.[1] However, the development of bacterial resistance is a critical issue decreasing the utility of many medically important antibiotics. Therefore, it is essential to search for new antimicrobial agents, ensuring that suitable therapeutics are available for the treatment of bacterial infections. While antimicrobial peptides produced by bacteria have not nearly been considered to the same extent as typical small molecule antibiotics, there is a growing body of research exploring their suitability for numerous potential applications.[2]

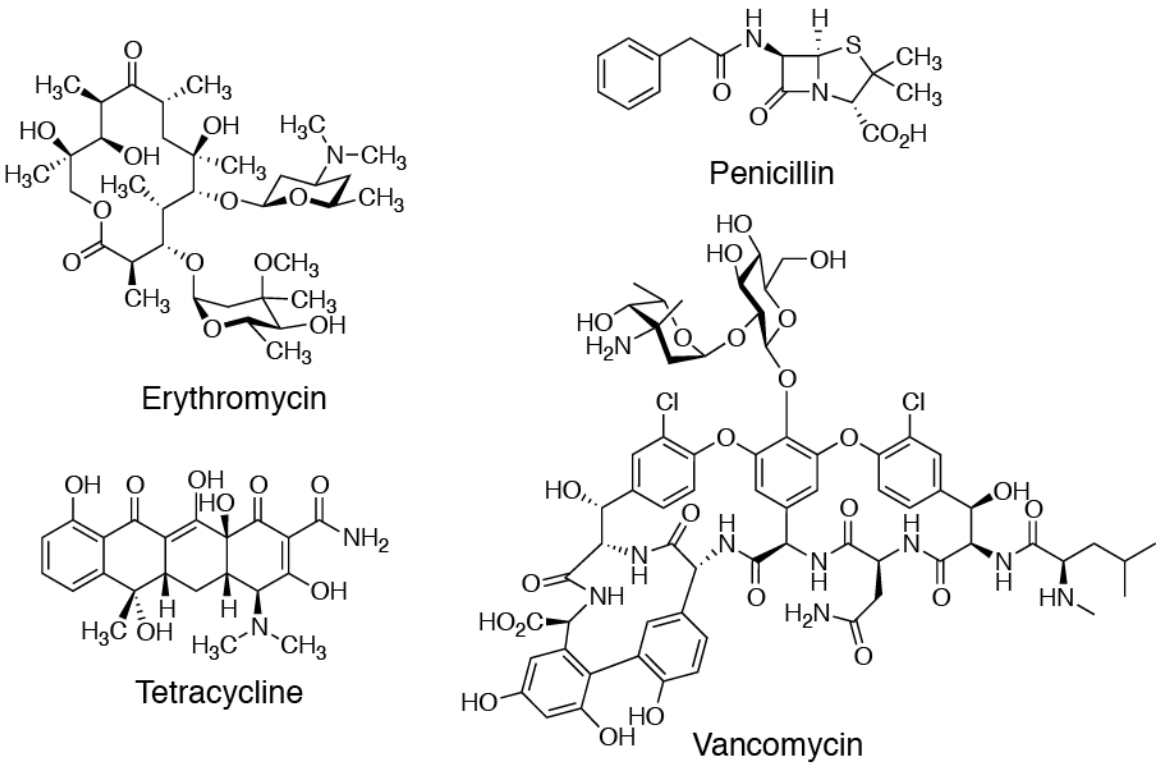

Figure 1.1. Structures of selected antibiotics produced by bacteria.

The majority of bacteria produce ribosomally synthesized antimicrobial peptides, referred to as bacteriocins.[3] These bacteriocins offer their producer strains a selective advantage over similar strains in their ecological niches. Bacteriocins produced by Gram-positive bacteria have been given particular attention due to their potential applications for the preservation of food and their efficacy against Gram-positive pathogenic bacteria.[4] Nisin, produced by strains of the lactic acid bacterium *Lactococcus lactis*, is one of the best studied bacteriocins and is used as a food preservative in many countries.[3] Due to the development of bacterial resistance to conventional antibiotics, bacteriocins have been receiving a greater degree of attention for their potential therapeutic use.[2,5] Despite the long history of the availability of nisin for application in foods, only low levels of resistance have developed.[3]

Gram-positive bacteriocins show great diversity with regards to their structures and post-translational modifications. Several different classification schemes for bacteriocins have been proposed on the basis of these properties.[3] Generally, these schemes consist of at least three classes. Class I bacteriocins, more commonly referred to as lantibiotics, are characterized by the presence of the thioether-containing amino acids lanthionine (Lan) and methyllanthionine (MeLan). The class II bacteriocins do not contain Lan or MeLan, and are smaller than 10 kDa. Class II is further organized into several subclasses according to structure and biosynthesis, such as the class IIa (or pediocin-type) bacteriocins. Finally, the class III bacteriocins (also referred to as bacteriolysins) are large heat-labile proteins.

While the production of bacteriocins is widespread amongst bacteria, non-ribosomal peptide synthetase (NRPS)-derived natural products are less ubiquitous. However, *Streptomyces* spp. and *Bacillus* spp. biosynthesize a diverse array of non-ribosomal peptides. In addition to notable glycopeptide antibiotics such as vancomycin and teicoplanin, NRPSs produce a wide variety of antimicrobial lipopeptides. Daptomycin, a cyclic lipopeptide produced by strains of *Streptomyces roseosporus*, was approved for use in adults by the FDA in 2003 and is often used as a treatment for skin and soft tissue infections.[6] Polymyxin, a cyclic lipopeptide isolated from strains of *Paenibacillus polymyxa*, is used for the topical treatment of certain skin infections.[7]

Although bacterial metabolites have proven valuable with numerous therapeutic applications, there are also disadvantages and drawbacks associated with many of them. The primary concern is the development of bacterial resistance, which has undermined the usefulness of many important antibiotics such as vancomycin and tetracycline.

Additionally, issues of toxicity restrict the usefulness of many antibacterial agents. For example, polymyxins display nephrotoxic activity that precludes many potential applications.[7] Chemical stability represents another issue of concern: nisin has been found to degrade at physiological pH, limiting its potential utility in therapeutic roles. For these reasons, it is paramount to continue the search for new antibiotic candidates. The reservoir of natural products produced by bacteria has yielded many important drugs and lead compounds. However, this reservoir has not been fully explored nor has the potential of numerous partially characterized isolates been realized.

1.2. Lantibiotics

1.2.1. Introduction

As mentioned above, the lantibiotics are a group of highly post-translationally modified bacteriocins typified by the presence of lanthionine (Lan) and methyllanthionine (MeLan) residues. The term 'lanthipeptide' has also been used to refer to this group, to encompass similar peptides that are not antimicrobial.[8] Much of the interest regarding the lantibiotics relates to their potent antimicrobial activity against important Gram-positive pathogens, including *Staphylococcus*, *Clostridium* and *Enterococcus* spp.[8,9] As indicated above, the lantibiotic nisin has been used for food preservation for several decades.[10] Actagardine derivative NVB302 has completed phase I clinical trials for the treatment of *Clostridium difficile* infections, while lacticin 3147 shows promise for treating systemic *Staphylococcus aureus* infections.[11,12]

The post-translational modifications found in lantibiotics are primarily centered around serine, threonine and cysteine residues (Figure 1.2). Enzymatic dehydration of serine or threonine yields dehydroalanine (Dha) and dehydrobutyrine (Dhb), respectively.

Some of these Dha and Dhb residues are not further modified, and occur in the mature lantibiotic. The enzyme-catalyzed conjugate addition of a cysteine thiol onto the β-position of Dha or Dhb forms the thioether bridge of Lan or MeLan, respectively. These Lan and MeLan residues serve to conformationally constrain the peptide structure, and may also impart resistance to proteases. The DL-Lan and DL-MeLan stereoisomers have almost exclusively been found in lantibiotics, although the LL-stereoisomers have been recently discovered in enterococcal cytolysin and haloduracin.[13]

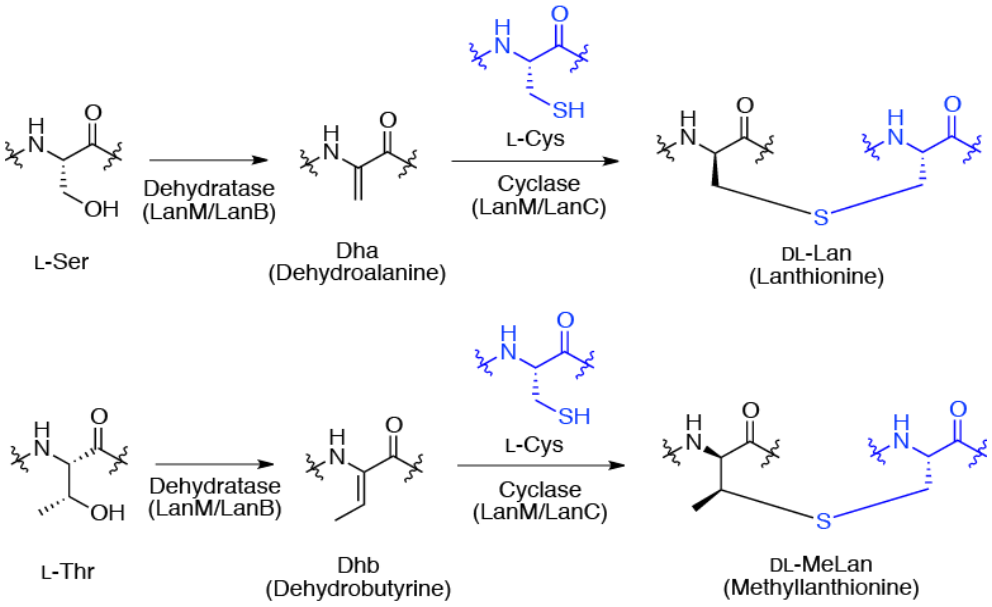

Figure 1.2. Biosynthesis of dehydroalanine, dehydrobutyrine, lanthionine and methyllanthionine residues in lantibiotics.

Lantibiotics demonstrate a wide variety of Lan and MeLan ring topologies. Additionally, numerous post-translational modifications beyond Dha/Dhb and Lan/MeLan are found. However, there are structural motifs conserved between certain groups of lantibiotics, essential for their particular modes of action. Nisin has five Lan and MeLan rings, two of which are interlocking (Figure 1.3). The A and B rings of nisin,

similar to those found in many other lantibiotics, are involved in binding to peptidoglycan precursor lipid II.[14] Lactocin S is largely linear, containing only two Lan residues near the C-terminus (Figure 1.3). This lantibiotic also possesses other post-translational modifications, namely three D-alanine residues and an N-terminal 2-oxopropyl group.[15] Several two-component lantibiotics have been discovered that require the presence of both components for potent antimicrobial activity. Haloduracin is one such two-component lantibiotic, produced by *Bacillus halodurans*.[16] Haloduracin α is a globular lantibiotic with an unusual disulfide bridge and three Lan and MeLan bridges, while haloduracin β is somewhat more linear in structure (Figure 1.3).

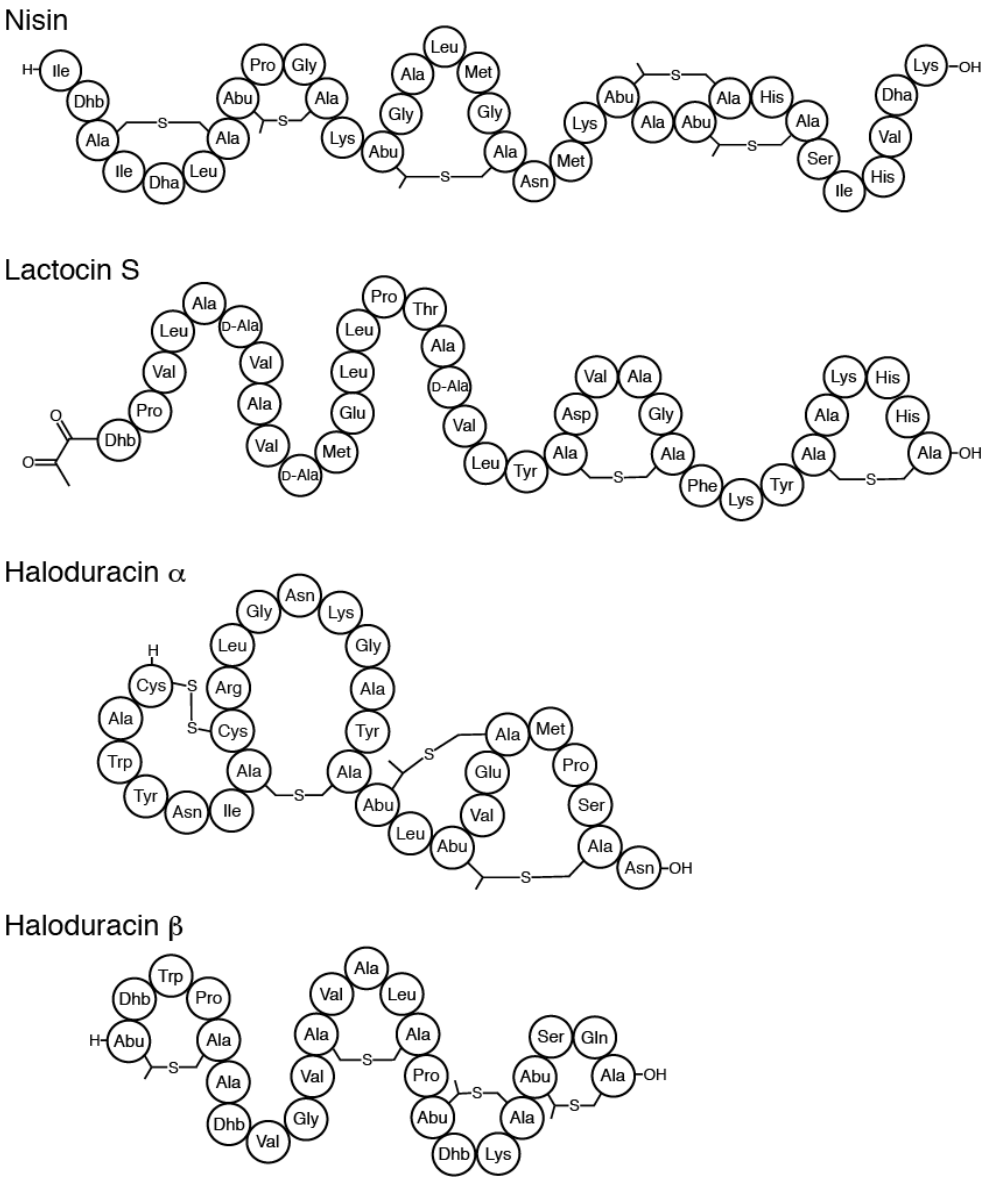

Figure 1.3. Bead structures of representative lantibiotics.

1.2.2. Biosynthesis

Like most other classes of bacteriocins, lantibiotics are biosynthesized with an N-terminal leader sequence. The leader peptide is typically recognized by biosynthetic enzymes, including those involved in the formation of Lan and MeLan residues.[17] This leader sequence then may direct the modified precursor peptide to a transporter protein,

essentially trafficking it for export. During or following export, the leader peptide is proteolytically removed yielding the mature peptide.

Different types of biosynthetic machinery are used for the formation of Lan and MeLan residues. Lantibiotics are often classified based on the characteristics of these biosynthetic enzymes.[8] Class I lantibiotics, such as nisin, rely on two separate enzymes to catalyze the dehydration and cyclization required for Lan/MeLan formation. A dehydratase enzyme, generically called LanB, is responsible for the dehydration of Ser and Thr to Dha and Dhb. Then, the cyclase enzyme, generically called LanC, catalyzes thioether bridge formation between Dha/Dhb and Cys. Insight into the mechanism of Dha and Dhb formation was obtained during the study of the role of LanB-type dehydratase NisB in the biosynthesis of nisin. Mutational analysis of NisB yielded mutant enzymes which modified the nisin precursor peptide NisA by glutamylating select serine and threonine residues.[18] In wild-type NisB, the activated hydroxyl groups would then undergo an elimination reaction yielding Dha and Dhb.

The class II lantibiotics require only a single enzyme to catalyze the formation of Lan and MeLan residues. This type of lantibiotic synthetase, generically referred to as LanM, consists of two domains: an N-terminal dehydratase domain and a C-terminal cyclase domain. LctM, the lantibiotic synthetase involved in the biosynthesis of lacticin 481, was successfully reconstituted *in vitro*.[19] LctM first phosphorylates serine and threonine residues using ATP and Mg^{2+}, and then eliminates the phosphate ester to yield Dha and Dhb.[20] All two-component lantibiotics described to date, such as haloduracin and lichenicidin, belong to class II. Some of these two-component lantibiotics require a separate lantibiotic synthetase for each component (e.g., lacticin 3147), while others

require only a single synthetase to modify both components (e.g., enterococcal cytolysin).[21] Class III and IV lantibiotics have been grouped on the basis of their biosynthetic machinery, but will not be further considered here.[8]

The leader sequences of the modified lantibiotic precursor peptides may be removed in several different ways. Following the installation of Lan and MeLan residues, the modified lantibiotic precursor peptides are exported by an ATP-binding cassette (ABC) transporter. Some lantibiotic transporters, such as that involved in lacticin 481 biosynthesis,[22] have a fused protease domain allowing for the concomitant removal of the leader sequence and export. Other lantibiotics are proteolytically processed through the action of an extracellular protease. NisP, the protease involved in nisin biosynthesis, is anchored to the external surface of the producer membrane via a C-terminal hydrophobic region.[23] Yet other lantibiotics (e.g., subtilin) are not expressed in conjunction with a protease, instead relying on a protease expressed as part of a different pathway.[24]

As protection against the antimicrobial properties of lantibiotics, producer bacteria use immunity proteins.[25] Two general approaches have been found, involving the use of a LanI-type immunity protein or a specialized ABC transporter system.[25] While the different LanI immunity proteins display very little sequence homology to each other, they tend to operate by a similar mechanism. The LanI-type immunity protein associated with nisin, NisI, is either processed into a lipoprotein situated on the extracellular surface or excreted intact. Once extracellularly situated, NisI binds to nisin and prevents pore formation in the membrane.[26] Immunity to nisin is also mediated by the ABC transporter system NisFEG.[25] These LanFEG-type transporters likely expel membrane-associated lantibiotics, thereby preventing the formation of membrane pores.

1.2.2.1. Other post-translational modifications

In addition to Dha, Dhb, Lan and MeLan residues, many lantibiotics display various other post-translational modifications. While many of these modifications are based on enzymatic manipulations of Dha/Dhb and Lan/MeLan residues, others are thought to occur spontaneously. Several lantibiotics possess an N-terminal α-ketoamide; for example, lacticin 3147 A2 bears a 2-oxobutyryl group on Dhb-1 (Figure 1.4A).[27] These α-ketoamides are derived from proteolytic cleavage immediately N-terminal to a Dha or Dhb residue. The Dha/Dhb residue may then tautomerize and react with water to form the corresponding ketone. Some lantibiotics feature further modification of these α-ketoamide groups: epilancin 15X bears a lactyl group on the N-terminus resulting from enzymatic reduction of the N-terminal pyruvoyl group derived from Dha (Figure 1.4B).[28]

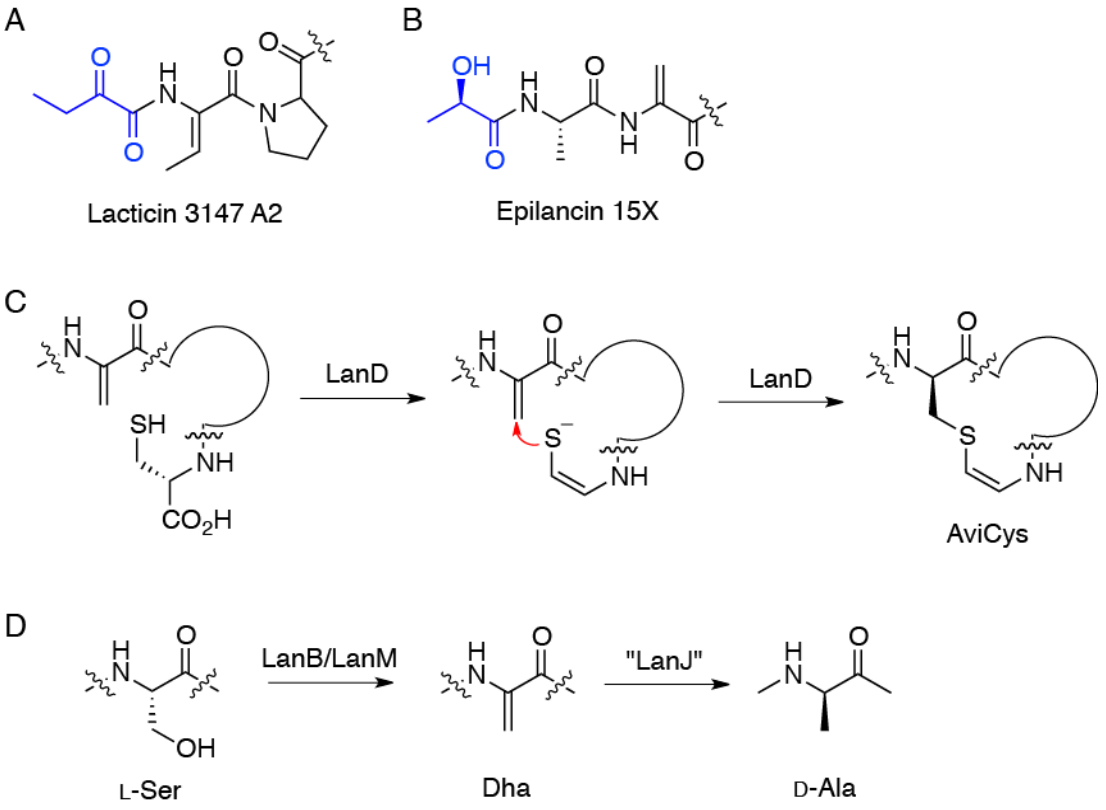

Figure 1.4. Representative post-translational modifications of lantibiotics. Structures of (A) 2-oxobutyryl group of lacticin 3147 A2 and (B) pyruvoyl group of epilancin 15X. (C) Formation of aminovinylcysteine (AviCys). (D) Installation of D-Ala via dehydration and reduction.

Several lantibiotics such as mersacidin and gallidermin have an unusual aminovinylcysteine (AviCys) residue at the C-terminus.[29] AviCys formation is catalyzed by a LanD-type enzyme, which decarboxylates a terminal cysteine residue through a flavin-dependent mechanism and generates a reactive enethiolate species (Figure 1.4C).[30] The sulfur of the enethiolate may then nucleophilically attack the β-carbon of Dha or Dhb, thereby forming AviCys or AviMeCys respectively.

Three lantibiotics have been found to contain D-Ala residues: lactocin S and the two A1 and A2 subunits of lacticin 3147.[15,31] Apart from the carnolysins (described in Chapter 3) and polytheonamides, these bacteriocins are the only prokaryotic ribosomally synthesized peptides known to contain D-amino acids.[32] The D-Ala residues are derived

from the stereoselective reduction of Dha, which ultimately inverts the stereocenter from L-Ser to D-Ala (Figure 1.4D). Mutation of these L-serine residues to L-alanine resulted in peptides with greatly decreased levels of activity.[33] In the biosynthesis of lacticin 3147, this transformation is catalyzed by the reductase LtnJ.[33] Several LtnJ homologs from other bacterial species are capable of reducing Dha residues found in the lacticin 3147 precursor peptides.[34]

There are a wide variety of post-translational modifications found in lantibiotics not based on modifications of Dha and Dhb. Contrasting the N-terminal α-ketoamides found in several lantibiotics, paenibacillin features an acetyl group on the N-terminal residue.[35] Microbisporicin, isolated from the actinomycete *Microbispora corallina*, features a chlorinated tryptophan residue and a dihydroxylated proline residue.[36] While originally considered rare, a growing number of lantibiotics such as bovicin HJ50[37] and the haloduracin α subunit[16] contain disulfide bridges.

1.2.3. Mode of action

The antimicrobial mode of action of several lantibiotics has been investigated, revealing commonality among structurally diverse peptides. Several different lantibiotic structural motifs have been found to interact with lipid II, a precursor in the biosynthesis of peptidoglycan. The globular lantibiotic mersacidin exerts its antimicrobial effects by binding to lipid II, physically sequestering it from the enzymes involved in peptidoglycan biosynthesis and inhibiting cell wall synthesis.[38,39] The solution structure of nisin bound to lipid II was characterized using NMR spectroscopy,[14] revealing a so-called "pyrophosphate cage" binding motif wherein the A and B rings of nisin surround the pyrophosphate group of lipid II. In addition to inhibiting peptidoglycan biosynthesis,

binding of nisin to lipid II leads to pore formation.[40] Fluorescence and circular dichroism experiments were used to probe the stoichiometry of these complexes, suggesting that the pores consist of eight molecules of nisin and four molecules of lipid II.[41]

The mode of action of the two-component lantibiotics has also been the subject of study. Characterization of lacticin 3147 suggested that the two peptides together exert a similar mode of action to nisin.[42] First, the A1 peptide may bind to lipid II, potentially through a similar binding mode as mersacidin. Then, the A2 peptide may bind to the LtnA1 lipid II complex, resulting in inhibition of cell wall biosynthesis and pore formation. Studies of haloduracin suggested a similar overall mode of action to lacticin 3147, despite great differences in the N-termini of these peptides.[43]

1.3. Leaderless bacteriocins

1.3.1. Introduction

The majority of bacteriocins are biosynthesized with N-terminal leader peptides.[17] These leader sequences are often essential for the installation of proper post-translational modifications, and are recognized by biosynthetic enzymes. These sequences are also recognized by transporter proteins facilitating the export of bacteriocins, along with concomitant proteolytic removal of this N-terminal extension. Additionally, leader sequences have been suggested to protect the producing organism from the antimicrobial effects exerted by the bacteriocin. However, the leaderless bacteriocins represent a growing group of cationic peptides that are classified on the basis of their biosynthesis without a leader sequence.

The first peptides of this class to be described were enterocins L50A and L50B, two similar bacteriocins produced by *Enterococcus faecium* L50.[44] Identification of the

structural genes encoding these peptides led to the realization that no N-terminal leader sequence or signal peptide was encoded. Studies revealed that expression of only the structural gene was required to obtain antimicrobial activity, suggesting that no post-translational modifications were required for the maturation of enterocin L50A and L50B. While antimicrobial testing revealed significant synergistic activity between enterocin L50A and L50B, both peptides demonstrated substantial antimicrobial activity individually as well. Sequence analysis of these peptides revealed no major similarities to other bacteriocins, instead suggesting homology to a group of cytolytic peptides produced by staphylococci.[44]

Since that initial report, numerous diverse peptides have been classified as leaderless bacteriocins (Figure 1.5). Several of these peptides, such as enterocin MR10A and MR10B, resemble enterocin L50A and L50B.[45] Longer leaderless bacteriocins have also been described, such as aureocin A53 from *Staphylococcus aureus* A53 and lacticin Q from *Lactococcus lactis* QU 5.[46,47] *L. lactis* BGMN1-5 produces LsbB, a 30 residue leaderless bacteriocin with little homology to these other peptides.[48] *S. aureus* A70 produces four similar peptides of 30-31 amino acids, named aureocin A70.[49]

```
Enterocin L50A      MGAIAKLVAKFGWPIVKKYYKQIMQFIGEGWAINKIIEWIKKHI 44
Enterocin L50B      MGAIAKLVTKFGWPLIKKFYKQIMQFIGQGWTIDQIEKWLKRH  43
                    ********:*****::**:*********:**:*::* :*:*:*

Lacticin Q          MAGFLKVVQLLAKYGSKAVQWAWANKGKILDWLNAGQAIDWVVSKIKQILGIK 53
Aureocin A53        MS-WLNFLKYIAKYGKKAVSAAWKYKGKVLEWLNVGPTLEWVWQKLKKIAGL- 51
                    *: :*:.:: :****.***. **  ***:*:***.* :::** .*:*:* *:

LsbB                MKTILRFVAGYDIASHKKKTGGYPWERGKA 30

Aureocin A70
AurA                MGKLAIKAGKIIGGGIASALGWAAGEKAVGK 31
AurB                MGAVAKFLGKAALGGAAGGATYAGLKKIFG- 30
AurC                MGALIKTGAKIIGSGAAGGLGTYIGHKILGK 31
AurD                MGAVIKVGAKVIGWGAASGAGLYGLEKILKK 31
                    ** :    .*    * *..      .* .
```

Figure 1.5. Amino acid sequences of representative leaderless bacteriocins. Conserved residues are indicated with an asterisk, conservative substitutions with a colon, and residues with weakly similar properties with a period.

1.3.2. Biosynthesis

Relative to the other classes of bacteriocins, the biosynthetic and immunity proteins involved in the production of leaderless bacteriocins are not well understood. Several gene clusters associated with leaderless bacteriocins have been described, including enterocin L50,[44] aureocin A53,[46] epidermicin NI01[50] and BHT-B.[51] Comparison of the gene clusters for aureocin A53 and epidermicin NI01, which showed similar organization of genes, suggested the involvement of eight genes in their production.[52] However, these gene clusters differed from that involved in the production of BHT-B, revealing variability in the structures of the leaderless bacteriocin gene clusters.

Recently, the genes involved in the secretion and self-immunity of lacticin Q were described.[52] While 11 putative open-reading frames were located in the gene cluster for lacticin Q biosynthesis, only seven had homologues in the gene cluster for the related bacteriocin lacticin Z.[52] The heterologous expression of six of these genes (including the

lacticin Q structural gene) was sufficient for the production and transport of lacticin Q.[52] Two of these encoded proteins, LnqEF, are predicted to form an ABC transporter. Disruption of the *lnqEF* genes indicated that this transporter is the minimal unit for immunity.[53] However, full immunity was only achieved when expression of LnqEF was supplemented with LnqBCD, membrane proteins of unknown function.[53] Furthermore, the extracellular production of lacticin Q required the presence of all of LnqBCDEF.[53] The means by which LnqBCD are involved in both immunity and transport are not yet known.

1.3.3. Mode of action

Aureocin A53 and lacticin Q are the best-characterized leaderless bacteriocins with respect to their modes of action. Studies of these two peptides suggest that they exert an overall similar mode of action, involving membrane permeation followed by leakage of essential metabolites and dissipation of membrane potential.[54-56] Lacticin Q was found to permeabilize liposomes consisting of L-α-phosphatidylcholine and L-α-phosphatidyl-DL-glycerol at lower concentrations than nisin.[54] As discussed above, nisin initially binds to the lipid II in target membranes to facilitate pore formation. The fact that lacticin Q is capable of permeabilizing liposomes at lower concentrations without requiring a docking molecule suggests that it may interact directly with target membranes. The means by which lacticin Q permeabilizes membranes has been suggested to involve the formation of a huge toroidal pore, with a diameter of at least 4.6 nm.[55] A pore this large facilitated the leakage of proteins, a property that had not been previously described for antimicrobial peptides.[55]

Similar to lacticin Q, aureocin A53 acts on both whole cells and artificial liposomes at micromolar levels, suggesting that no specific docking molecules are required.[56] Unusually, aureocin A53 bound more strongly to neutrally charged liposomes than to those containing negatively charged phospholipids, contrasting what is suggested for classical cationic antimicrobial peptides. Unlike lacticin Q, the antimicrobial activity of aureocin A53 is suggested to result from generalized membrane permeabilization as opposed to the formation of discrete pores.[56]

The leaderless bacteriocin LsbB, which has little sequence homology to lacticin Q and aureocin A53, exerts its antimicrobial effects through a different mechanism.[48] The presence of a membrane-bound zinc-dependent metallopeptidase was a requirement for bacterial sensitivity to LsbB.[57] Beyond an interaction with this peptidase, the nature of the antimicrobial mode of action of LsbB (e.g., the means by which the membrane is disrupted) has not yet been reported. However, these results show that different subgroups of leaderless bacteriocins may differ in their particular mode of action.

1.4. Class IIa bacteriocins

1.4.1. Introduction

The class IIa bacteriocins, also referred to as pediocin-type bacteriocins, are noted for their potent antilisterial activity. Peptides of this class range from 37 to 48 amino acids in size, and are classified on the basis of a conserved N-terminal YGNGV sequence and an N-terminal disulfide bridge. The first peptide of this class to be described was leucocin A, isolated from *Leuconostoc gelidum*.[58] Since then, more than 20 other peptides of this class have been discovered.[59] The most well characterized member of this class, pediocin PA-1, has been used commercially for food preservation.[3]

Apart from the conserved YGNGV sequence and N-terminal disulfide bridge, sequence analysis of the class IIa bacteriocins revealed several trends. Residues in the N-terminal halves of these bacteriocins are relatively conserved, while there is great variability with regards to sequence identity and length in the C-terminal halves (Figure 1.6). In addition, several of the longer class IIa bacteriocins such as pediocin PA-1 possess an additional C-terminal disulfide bridge.

```
Piscicolin 126          KYYGNGVSCNKNGCTVDWSKAIGIIGNNAAANLTTGGAAGWNKG
Mundticin               KYYGNGVSCNKKGCSVDWGKAIGIIGNNSAANLATGGAAGWSK
Sakacin P               KYYGNGVHCGKHSCTVDWGTAIGNIGNNAAANWATGWNAGG
Pediocin PA-1           KYYGNGVTCGKHSCSVDWGKATTCIINNGAMAWATGGHQGNHKC
Leucocin A              KYYGNGVHCTKSGCSVNWGEAFSAGVHRLANGGNGFW
Curvacin A            ARSYGNGVYCNNKKCWVNRGEATQSIIGGMISGWASGLAGM
Carnobacteriocin B2     VNYGNGVSCSKTKCSVNWGQAFQERYTAGINSFVSGVASGAGSIGRRP
                          ***** * :  * *: . *
```

Figure 1.6. Sequence alignment of representative class IIa bacteriocins. The conserved YGNGV motif is indicated in red, conserved cysteine residues in green, and (mostly) conserved tryptophan in blue. Conserved residues are indicated with an asterisk, conservative substitutions with a colon, and residues with weakly similar properties with a period.

The structures of several class IIa bacteriocins have been characterized by NMR spectroscopy, including leucocin A,[60] carnobacteriocin B2,[61] sakacin P[62] and curvacin A[63] (Figure 1.7). The structure of leucocin A is divided into two separate halves with an N-terminal antiparallel β-sheet and a C-terminal α-helix, roughly separated by tryptophan-18. The N-terminal region prior to and including Trp-18 corresponds to the highly conserved sequence amongst the class IIa bacteriocins (Figure 1.6), while the C-terminal α-helical region corresponds to the region with greater sequence variability. Excluding carnobacteriocin B2, the N-termini of the other class IIa bacteriocins resemble the β-sheet of leucocin A (Figure 1.7). Despite the sequence variability, the C-termini of these other bacteriocins form amphiphilic α-helices, although the structure of curvacin A

features a kink in this region. The structure of leucocin A is discussed in more detail in subsequent chapters.

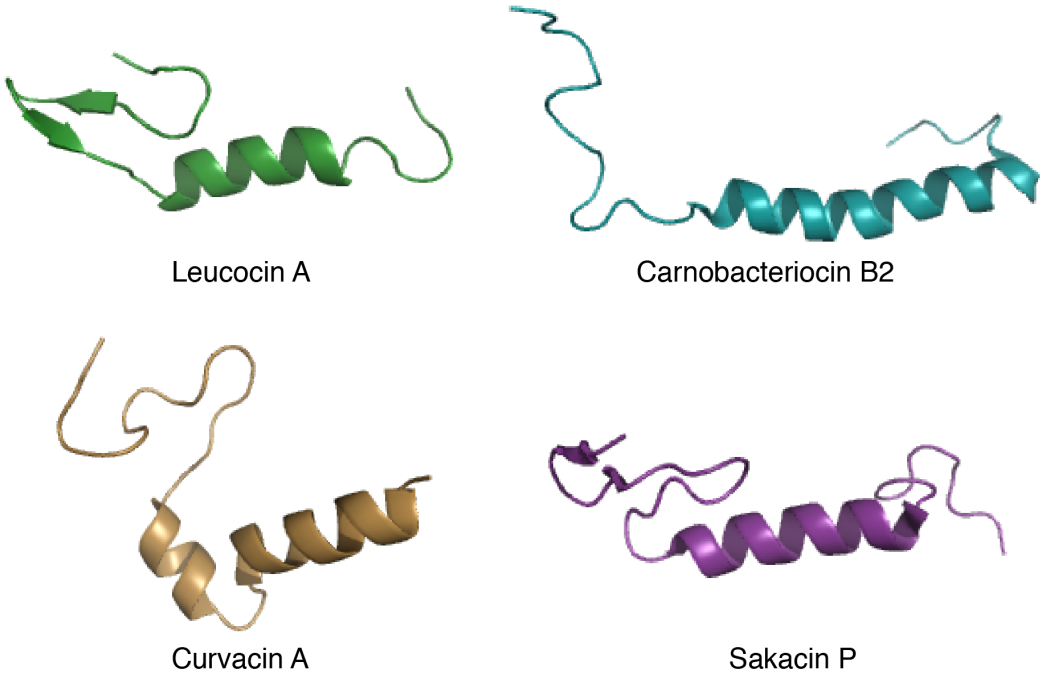

Figure 1.7. Solution structures of class IIa bacteriocins. N-termini are oriented towards the upper left corner.

1.4.2. Biosynthesis

Compared to the lantibiotics, the production of class IIa bacteriocins requires less biosynthetic machinery. In addition to the bacteriocin structural gene, typically at least three other genes are required, encoding an immunity protein, an ATP-binding cassette (ABC) transporter with a protease domain, and an accessory protein of unknown function.[64] There may also be a three-component system involved in regulating the biosynthesis of class IIa bacteriocins, consisting of an induction peptide, a transmembrane histidine protein kinase and a cytosolic response regulator.[64]

The class IIa bacteriocin precursor peptides are expressed with an N-terminal leader sequence.[17] As described above, the presence of the leader peptide serves multiple functions, including modulating the antimicrobial potency of the peptide. Leucocin A and carnobacteriocin B2 with uncleaved leader peptides were less antimicrobially active than the mature peptides.[60,65] Additionally, the leader peptide likely acts as a recognition site for the ABC transporter, facilitating both proteolytic removal of the leader sequence and export of the mature bacteriocin. The proteolytic cleavage typically occurs C-terminal to a conserved double-glycine recognition site immediately N-terminal to the mature bacteriocin sequence.[66] However, several class IIa bacteriocins are exported by the general secretory pathway instead of using a dedicated ABC transporter.[67] The leader sequences of these *sec*-dependent bacteriocins lack the double-glycine motif protease recognition site.[64]

Producers of class IIa bacteriocins are protected against the mature bacteriocins via the production of cytosolic immunity proteins ranging from 81 to 115 amino acids in length.[68,69] Several class IIa bacteriocin immunity proteins have been structurally characterized, such as those associated with carnobacteriocin B2 and piscicolin 126 immunity.[69,70] Although immunity proteins are classified into several groups based on sequence homology, they are largely structurally similar.[68] Immunity proteins are not thought to interact directly with their cognate bacteriocins; no interactions were observed between pisicolin 126 and its cognate immunity protein PisI.[69] Furthermore, addition of both immunity protein and bacteriocin extracellularly to a bacterial culture did not provide any protective effects.[71] Therefore, the intracellular immunity protein appears to

protect the producer organism from extracellular bacteriocins, suggesting that the antimicrobial action of the class IIa bacteriocins may be receptor-mediated.

1.4.3. Mode of action

As with other classes of bacteriocins, the class IIa bacteriocins exert their antimicrobial effects via the membrane disruption of target bacteria. Peptides of this class form pores in target membranes, resulting in the dissipation of membrane potential.[72] This coincided with depletion of intracellular ATP levels, likely consumed while the bacteria attempt to maintain the proton motive force.[59] The pores formed by some class IIa bacteriocins also resulted in the loss of low-molecular weight metabolites such as amino acids.[73]

The class IIa bacteriocins have been demonstrated to require the presence of a receptor molecule in target membranes, namely the IIC and IID subunits of the mannose phosphotransferase (MPT) complex.[74] The heterologous expression of the MPT subunits from a bacteriocin-sensitive strain in a bacteriocin-resistant strain induced sensitivity in this formerly resistant strain.[74,75] Site-directed mutagenesis indicated that an extracellular loop of the IIC MPT subunit was involved in a specific interaction with class IIa bacteriocins.[75] Ten different class IIa bacteriocins, with similar N-termini and different C-termini, all displayed similar specificity towards several hybrid receptors.[75] This may indicate that the bacteriocin N-termini interact directly with the receptor molecule.[68]

The C-termini of the class IIa bacteriocins have been shown to determine target cell specificity. Hybrid bacteriocins were prepared by replacing the C-terminal half of a mature class IIa bacteriocin with that from a different class IIa bacteriocin.[76] These hybrid bacteriocins demonstrated a spectrum of activity consistent with that of the

bacteriocin from which the C-terminal half was derived.[76] Furthermore, C-terminal fragments of class IIa bacteriocin pediocin PA-1 were found to inhibit the antimicrobial activity of the full peptide.[77] These results suggest that there are likely specific interactions between the C-terminus of the bacteriocin and the MPT subunits.[68] While this may appear to contradict the results suggesting an interaction between the bacteriocin N-terminus and MPT, they may instead indicate that the N- and C-termini interact with MPT at different points over the course of receptor recognition and pore formation.[68]

Based on these results, an overall model describing the mode of action of class IIa bacteriocins has been proposed (Figure 1.8).[68] The cationic bacteriocin N-terminus may initially draw the peptide towards the negatively-charged target membrane. The N-terminal β-sheet region may then interact with an extracellular loop of MPT IIC, after which the C-terminal amphiphilic α-helical region inserts into the hydrophobic membrane core in contact with the transmembrane helices of a MPT subunit. This may cause a conformational change in MPT, and could potentially result in pore formation in conjunction with other bacteriocin-MPT complexes. It has been proposed that the class IIa bacteriocin immunity proteins interact with the MPT complex, protecting the producer organism by preventing pore formation.[74] These immunity proteins were found to complex with the components of MPT in the presence of bacteriocin.[74] Presumably once the bacteriocin has bound to the extracellular surface of MPT, a conformation change occurs allowing the immunity protein to then bind to the cytosolic surface of MPT.

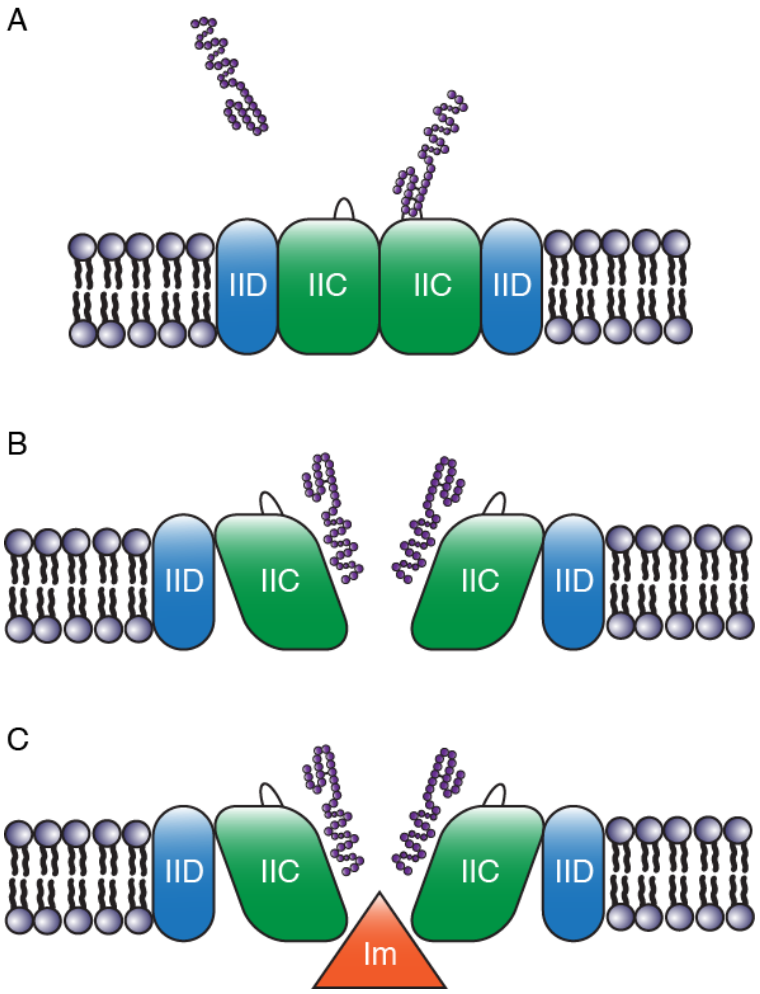

Figure 1.8. Proposed model for the mode of action of class IIa bacteriocins. (A) Initial attraction of the bacteriocin to the bacterial cell, and interaction of the bacteriocin N-terminus with an extracellular loop of MPT IIC. (B) Insertion of the bacteriocin C-terminal α-helix into the hydrophobic membrane core, interacting with the transmembrane helices of MPT IIC and thereby forming a pore. (C) Class IIa immunity protein binding to the bacteriocin-MPT IIC complex and obstructing the pore. Figure adapted from Kjos et al. 2011.[68]

1.5. Antibacterial nonribosomal lipopeptides

1.5.1. Introduction

As mentioned above, bacteria produce numerous nonribosomal peptides with antibacterial properties. NRPS products display broad diversity in structure and mode of action. This is partly due to the incorporation of diverse non-proteinogenic amino acids such as 2,4-diaminobutyrate, ornithine and 2,3-dihydroxybenzoic acid. Furthermore,

epimerase domains may invert the stereochemistry of select amino acids, resulting in peptides containing D-amino acids. Beyond the selection of non-proteinogenic amino acids, the nonribosomal peptide may be further enzymatically modified. While some of these modifications are installed by tailoring enzymes (e.g., glycosylation of vancomycin), domains within the NRPS may also introduce modifications. Some NRPSs contain heterocyclization domains that form oxazole, oxazoline, thiazole and thiazoline rings from serines, threonines and cysteines.[78] Additionally, many nonribosomal peptides feature cyclization of the C-terminus onto a nucleophilic amino acid side chain (e.g., serine, lysine). As a result of all of these biosynthetic possibilities (in addition to numerous others), nonribosomal peptides as a group show a very high degree of structural diversity.

As a result of this diversity, nonribosomal peptides are not as easily grouped into defined classes as are bacteriocins. However, they may be broadly classified according to their chemical structures and the nature of their modifications. Glycopeptide antibiotics such as vancomycin are classified based on the glycosylation of a nonribosomal peptide. A large number of nonribosomal lipopeptides have a lipid chain on the N-terminus, such as polymyxin and surfactin. NRPS products range from highly cationic (e.g., polymyxins) to anionic (e.g., daptomycin), and are often classified on this basis. Others are grouped depending on whether the structure is linear or cyclic. Due to the focus of this thesis, this section will primarily discuss nonribosomal lipopeptides.

The polymyxins are a group of cyclic cationic lipopeptides produced by strains of *Paenibacillus polymyxa* (Figure 1.9). Polymyxins display antimicrobial activity against Gram-negative bacteria, and are considered the last-line of defense against several

multidrug resistant bacterial strains.[7] These peptides consist of ten amino acids, six of which are 2,4-diaminobutyrate (Dab) residues. The polymyxins are cyclized via an amide linkage between the C-terminus and the side-chain of Dab-3. The N-termini of the polymyxins are typically acylated with a fatty acid chain of 8-10 carbons bearing an iso- or anteiso- methyl substituent.[79] The various polymyxins tend to differ based on single amino acid substitutions and the structure of the lipid chain,[79] with polymyxins B and E being the most commonly studied variants.

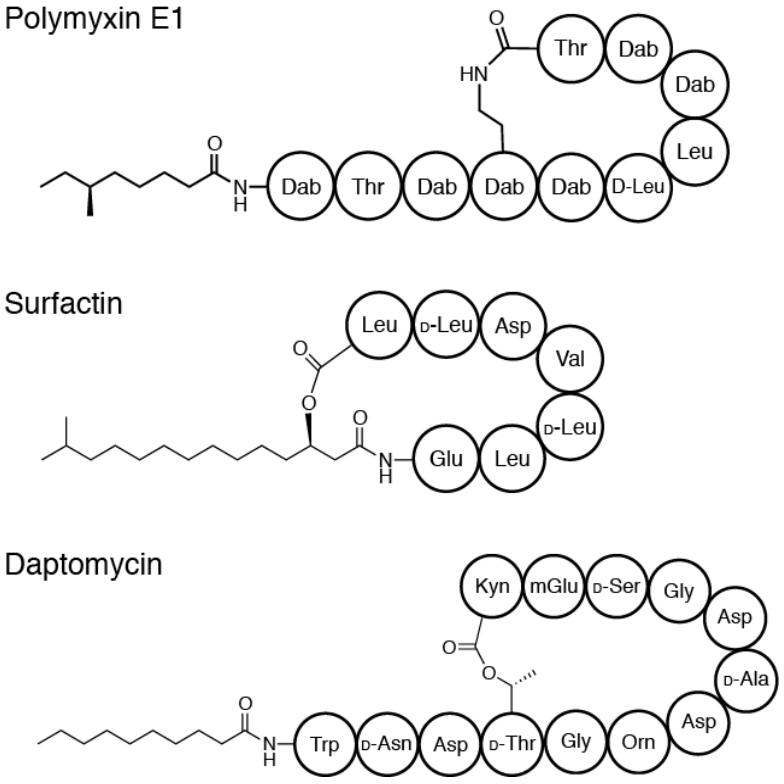

Figure 1.9. Structures of representative lipopeptides. Dab: 2,4-diaminobutryate; Kyn: kynurenine; Orn: ornithine; mGlu: 3-methylglutamate.

The surfactins are cyclic lipopeptides isolated from several different *Bacillus* spp. which act as powerful biosurfactants (Figure 1.9). In addition to antibacterial activity, antiviral, antitumour and hemolytic activities have been attributed to surfactin.[79,80] The

surfactins are relatively small, consisting of seven amino acids. Unlike the polymyxins, surfactins are moderately anionic due to the presence of two acidic residues. The N-terminal glutamate residue is acylated with a β-hydroxy lipid chain ranging from 10-14 carbons in length. These peptides are cyclized via an ester linkage between the C-terminus and the β-hydroxy group of the lipid chain. A large number of surfactin structural variants have been described featuring moderate amino acid substitutions and lipid chains.[79]

Daptomycin is a 13-residue cyclic lipopeptide bearing a decanamide lipid chain on the N-terminus (Figure 1.9). This peptide is noted for its potent activity against multidrug resistant Gram-positive pathogens.[81] Structurally, daptomycin is cyclized through an ester linkage between the C-terminus and the side-chain of a threonine residue. Similar to surfactin, daptomycin is an anionic lipopeptide due to the presence of four acidic residues. Daptomycin also bears unusual amino acids, notably L-kynurenine and L-3-methylglutamic acid.[82]

1.5.2. Biosynthesis

The modular structures of NRPSs consist of a repeating series of domains responsible for the assembly of the peptide chain (Figure 1.10).[83] The primary domains are the adenylation (A), condensation (C), thiolation (T) and thioesterase (TE) domains. The A domain serves to recognize a specific amino acid and activates it as an aminoacyl adenylate through the use of ATP. The activated amino acid is then loaded onto the thiol group of a prosthetic phosphopantetheinyl arm installed on a Ser residue of the T domain, thereby forming a thioester. C domains catalyze the nucleophilic attack of the amino group of an amino acid (covalently bound to a T domain) onto the thioester carbonyl of

the amino acid or peptide chain on an N-terminal T domain. This process occurs repeatedly as the peptide chain gets passed from T-domain to T-domain from the N-terminus to the C-terminus of the NRPS. Once the complete peptide chain is loaded on the final C domain, it is transferred onto the TE domain. This domain off-loads the peptide chain, either by hydrolyzing the peptide from the NRPS (to yield a linear peptide) or by steering a nucleophilic side chain to displace the peptide from the NRPS (to yield a cyclic peptide).

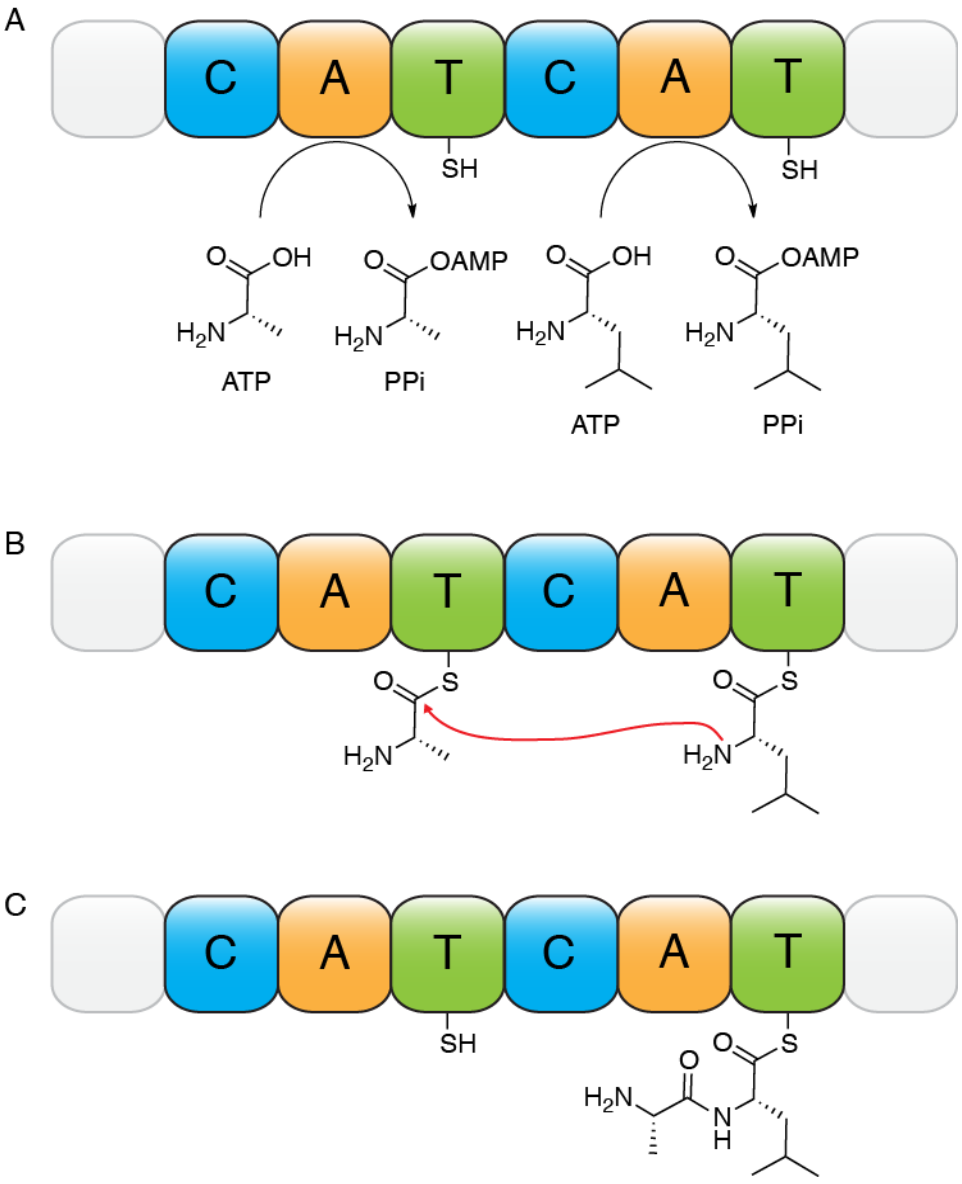

Figure 1.10. General schematic of NRPS-based peptide synthesis. (A) Adenylation domain mediated adenylation of amino acids using ATP. (B) Loading of activated amino acids onto thiolation domain phosphopantetheinyl arms. (C) Condensation domain mediated amide bond formation.

The lipid chains of nonribosomal lipopeptides tend to be introduced by a C domain at the N-terminus of the NRPS initiation module. The first module of surfactin synthetase SrfAA (C – A – T), heterologously expressed in *E. coli*, was shown *in vitro* to transfer a CoA-activated 3-hydroxy fatty acid to the amino group of the glutamic acid residue loaded onto the T domain.[84] Two acyl-CoA ligases were determined to be

responsible for the formation of the activated fatty acid; disruption of their genes impaired surfactin biosynthesis.[84] The NRPS involved in initiating daptomycin biosynthesis possesses a similar N-terminal C domain.[85] Two proteins are involved in activating the lipid chain for incorporation into daptomycin: DptE activates a branched mid- to long-chain fatty acid through the use of ATP, and loads it onto the acyl-carrier protein DptF.[85] Presumably, DptF loaded with the lipid chain then interacts with the NRPS N-terminal C domain, acylating the amino group of L-Glu-1. While the biosynthesis of polymyxin is less studied than those of daptomycin and surfactin, the NRPS initiation module again begins with a C domain.[86] No biosynthetic machinery involved in activating the lipid chain was identified, although the activated lipid could potentially be derived from the fatty acid biosynthetic or catabolism pathways.

1.5.3. Mode of action

The modes of action of several antibacterial nonribosomal lipopeptides have been well studied, including polymyxin, surfactin and daptomycin. As may be expected based on the presence of their lipid tails, these three peptides all act via membrane permeabilization. However, this effect is accomplished through different means as mediated by their different amino acid sequences.

As the polymyxins target Gram-negative bacteria, they must first contend with the outer membrane (OM) to reach and permeabilize the inner membrane. Polymyxins first interact with the lipid A portion of bacterial lipopolysaccharide, a component of the OM. The spectrum of activity of the polymyxins is based on this initial binding step with lipopolysaccharide (LPS).[7] This binding step may displace divalent cations normally involved in stabilizing the outer OM. Then, the polymyxin lipid chain may serve to

disrupt the OM, resulting in the self-promoted uptake of polymyxins into the periplasmic space. From there, the polymyxin may disrupt the integrity of the inner membrane by transient pore formation or by thinning the membrane via straddling the interface between the hydrophilic and hydrophobic portions of the membrane lipids.[7]

As mentioned above, surfactin exerts its antibacterial properties by acting as biosurfactant with a polar amino acid portion and a hydrophobic lipid moiety.[80] Through hydrophobic interactions, surfactin may spontaneously insert into lipid membranes.[87] This insertion is facilitated by Ca^{2+} ions which may neutralize the anionic residues of surfactin, as well as any anionic lipids present in the membrane.[87] At low levels, surfactin is capable of forming cation-conducting pores in artificial lipid membranes.[88] However, at higher concentrations, surfactin may also act through a more detergent-like mechanism.[89]

Like surfactin, daptomycin first inserts into the target bacterial membrane in a Ca^{2+}-facilitated process.[81] Once inserted, daptomycin induces a positive curvature strain in the lipid membrane and may potentially oligomerize. This ultimately results in membrane disruption, leakage of cellular contents and cell death.[81] The impact of daptomycin on membrane architecture influences the distribution of membrane proteins. By affecting the localization of cell division proteins, daptomycin may cause defects in the cell wall and bacterial membrane.[90]

1.6. Applications of bacterial antimicrobial peptides

1.6.1. Food protection

Bacteriocins produced by lactic acid bacteria (LAB) are of great interest for food preservation due to the "generally recognized as safe" status of many of these bacteria.

Furthermore, many bacteria of this class are already associated with the preparation of various food items such as fermented milk products (e.g., cheese and butter). Bacteriocins are antimicrobially active against a variety of food-associated pathogens and spoilage bacteria such as *Listeria monocytogenes*. Nonribosomal peptides have achieved much less interest for their use in food products, in part due to their production by non-GRAS bacterial strains. Furthermore, there are concerns regarding toxicity of several NRPS-derived lipopeptides.

Despite all of the interest in using bacteriocins in food preservation, very few purified bacteriocins are used commercially for this purpose. Only two LAB bacteriocins have attained common usage for food protection, namely the lantibiotic nisin and the class IIa bacteriocin pediocin PA-1.[3] In 1969, a World Health Organization committee assessed that nisin was safe to be used in food. Furthermore, nisin has been approved for certain applications in over 48 countries, including approval by the US Food and Drug Agency (FDA) in 1988. Nisin is active against a wide variety of Gram-positive bacteria including *Clostridium* spp., and has been used to successfully inhibit microbial growth in a variety of food items, including beef, poultry and dairy.[91] ALTA 2431, a fermentate containing pediocin PA-1, has also been commercially marketed. Pediocin PA-1 is antimicrobially active against various spoilage and pathogenic bacteria, such as *L. monocytogenes*, *Enterococcus faecalis* and *Clostridium perfringens*.[92]

1.6.2. Therapeutics

Although most of the focus regarding bacteriocins has been centered on their applications for food protection, there is a growing interest in the potential use of these peptides for therapeutic purposes. Lantibiotics have received a large proportion of this

interest, both for human applications as well as the protection of livestock. Nisin and mersacidin have shown potential in animal models of *Streptococcus pneumoniae* and methicillin-resistant *Staphylococcus aureus* infections, respectively.[93,94] Lacticin 3147 proved capable of decreasing the incidence of bovine mastitis (an inflammation of the udder) caused by *Streptococcus dysgalactiae*.[95] Mouthwash containing nisin decreased the build-up of plaque and development of gingivitis in a canine model.[96]

Several nonribosomal peptides have attained widespread therapeutic usage, including the glycopeptide antibiotics vancomycin and teicoplanin. While several lipopeptides are used, their therapeutic potential is often limited by concerns of toxicity. As indicated above, polymyxins are primarily used as a last resort therapy against multidrug-resistant Gram-negative bacteria such as *Pseudomonas aeruginosa*.[7] However, their use is impeded by their nephrotoxic properties, similar to the cationic aminoglycosides.[97] Attempts have been made to design less toxic polymyxin analogues through a variety of means, such as decreasing the number of cationic amino acids.[98] In the meantime, polymyxins are generally limited to topical applications on the skin, eyes and ears. However, a pro-drug form of polymyxin has found use in the treatment of lung infections in patients with cystic fibrosis.[6]

Daptomycin was FDA approved for the treatment of skin infections in 2003. This agent complements polymyxin, as daptomycin targets Gram-positive pathogens such as methicillin-resistant *S. aureus*, *Streptococcus pyogenes* and *E. faecalis*. Furthermore, daptomycin showed potential in the treatment of *S. aureus* based bacteremia and endocarditis.[99] Compared to the other lipopeptides considered herein (in addition to several other antibiotics prescribed for the treatment of multi-drug resistant Gram-

positive pathogens), daptomycin presents a favourable side-effect profile.[100] However, resistance to daptomycin has emerged during its use for the treatment of vancomycin-resistant enterococci, due to mutations in a regulatory system involved in the cell envelope stress response.[101]

As described above, surfactin displays a broad array of interesting biological properties, but its utility is limited by its hemolytic properties. Despite this undesirable property, surfactin is under consideration for a variety of therapeutic applications.[102] In addition to its antibacterial properties, surfactin can also inhibit lipopolysaccharide activity, thereby preventing an inflammatory response.[103] Furthermore, surfactin was shown to inhibit biofilm formation on urethral catheters by *Salmonella enterica* serovar Typhimurium, *Escherichia coli* and *Proteus mirabilis*, and may potentially be useful for preventing nosocomial infections.[104] There are efforts underway to develop less hemolytic variants of surfactin; synthetic linear analogs retained surface-active properties while not demonstrating significant hemolytic activity.[105] Additionally, the surfactin synthase NRPS was engineered to generate a lipohexapeptide which demonstrated reduced toxicity to erythrocytes but stronger lytic activity against *Bacillus licheniformis*.[106] However, more work needs to be done to fully characterize the therapeutic potential of these surfactin variants.

As described herein, several bacteriocins and nonribosomal lipopeptides have achieved use as therapeutic agents for a variety of applications. Many other peptides from these classes show great potential, therefore deserving further consideration.[79] With the urgent need for new antimicrobial agents due to the ever-increasing prevalence of antibiotic resistance, bacteriocins and lipopeptides represent large reservoirs of diverse

bioactive compounds. Furthermore, many of these peptides have only received a cursory evaluation and may turn out to be of great value after further investigation.

1.7. Overview of projects

The experimental results presented in this thesis focus on the structures and post-translational modifications of diverse bacterial antimicrobial peptides. Chapter 2 describes the structural characterization of lantibiotics and nonribosomal lipopeptides isolated from three different *Paenibacillus* spp.[107,108] These strains were all found to produce variants of tridecaptin, a lipopeptide found to be active against *Campylobacter jejuni*. The highly-cyclized lantibiotic paenicidin A was isolated from a *Paenibacillus* spp., and the connectivity of the Lan and MeLan residues was determined by a novel partial desulfurization strategy. The gene clusters associated with the biosynthesis of these peptides were identified and characterized.

Chapter 3 describes the characterization of carnolysin, a two-component lantibiotic produced by a strain of the lactic acid bacterium *Carnobacterium maltaromaticum* C2.[109] Through mass spectrometry and NMR spectroscopy, the post-translational modifications of carnolysin were determined. In addition to Lan and MeLan residues of unusual stereochemistry, carnolysin was shown to contain D-Ala and D-aminobutyrate residues resulting from enzymatic dehydration and reduction of serines and threonines. Carnolysin was heterologously expressed in *E. coli*, confirming the biosynthetic process and the identity of the reductase involved.

Chapter 4 describes the solution structure of the leaderless bacteriocin enterocin 7A, as determined through NMR spectroscopy.[110] This structure, the first of a bacteriocin

of this class to be solved, unexpectedly resembled the circular bacteriocins. This similarity may have implications regarding the mode of action of these bacteriocins.

Chapter 5 describes the solution structure of a mutant of the class IIa bacteriocin leucocin A, wherein two cysteine residues involved in a disulfide bridge were replaced with leucine residues.[111] Under the conditions used, this modification converted the N-terminal leucocin region from a β-sheet to a short α-helix while still retaining activity. Finally, Chapter 6 describes the materials and methods used for these research projects.

Chapter 2

Structural characterization of antimicrobial peptides produced by *Paenibacillus* spp.

2.1. Background

2.1.1. Bacteriocins and antimicrobial nonribosomal peptides produced by *Bacillus* and *Paenibacillus* spp.

The most well studied bacteriocins tend to come from lactic acid bacteria (LAB) due to their "generally recognized as safe" (GRAS) status and their potential use for food preservation.[112] However, *Bacillus* spp. also produce a wide variety of bacteriocins with diverse structures, and are considered the second most important group of bacteriocin producers after the LAB.[112] While bacilli have historically been used in the preparation of certain foods, certain *Bacillus* spp. have been implicated in food poisoning and spoilage.[112] Unlike the LAB, *Bacillus* spp. have also been found to produce numerous non-ribosomal peptide synthetase (NRPS) products, including several antimicrobial lipopeptides.[79] The production of both bacteriocins and NRPS products provide the producer strains with antimicrobial activity against a broad array of both Gram-positive and Gram-negative bacteria.[108]

The *Paenibacillus* genus was proposed based on the observation that certain former *Bacillus* spp. were phylogenetically distant from other *Bacillus* strains.[113] These *Paenibacillus* spp. could be readily distinguished from *Bacillus* spp. on the basis of phenotypic characteristics and 16S rRNA sequences.[113] Despite these differences, *Paenibacillus* spp. also produce a variety of bacteriocins and NRPS-derived

lipopeptides.[114] However, the antimicrobial peptides produced by *Paenibacillus* spp. tend to structurally differ from those produced by *Bacillus* spp.[79,114]

A large proportion of the bacteriocins produced by *Bacillus* and *Paenibacillus* spp. are lantibiotics. As described in more detail in Chapter 1, lantibiotics are characterized by the presence of the thioether bridged amino acids lanthionine (Lan) and methyllanthionine (MeLan) and the dehydro residues dehydroalanine (Dha) and dehydrobutyrine (Dhb). Lantibiotics from *Bacillus* and *Paenibacillus* spp. show great diversity of structure and Lan/MeLan connectivity patterns. Subtilin, produced by a *Bacillus subtilis* strain, has an N-terminus similar to nisin (Figure 2.1). This region, known as the pyrophosphate cage, binds to the pyrophosphate moiety of lipid II and is essential for the antimicrobial mode of action of many lantibiotics.[14] Mersacidin is a lantibiotic produced by a *Bacillus* sp. with a C-terminal aminovinylcysteine group (Figure 2.1). Mersacidin binds to the carbohydrate-pyrophosphate moiety of lipid II using an arrangement of Lan and MeLan rings different than nisin.[38] Paenibacillin, an unusual N-terminally acetylated lantibiotic isolated from *Paenibacillus polymyxa* OSY-SE, has very different Lan and MeLan ring topologies than other reported lantibiotics.[35] Several two-component lantibiotics have been reported from other bacilli, including haloduracin from *Bacillus halodurans* and lichenicidin from *Bacillus licheniformis*.

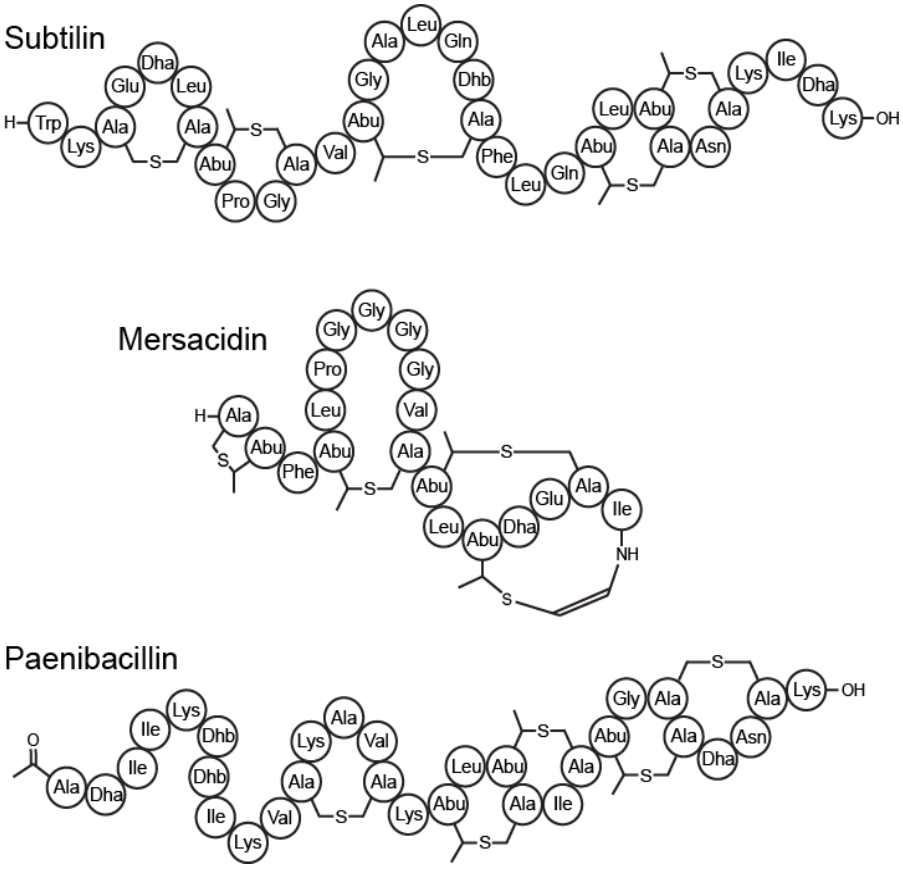

Figure 2.1. Bead structures of representative lantibiotics from *Bacillus* and *Paenibacillus* spp.

Unlike the LAB, *Bacillus* and *Paenibacillus* spp. have been reported to produce very few class IIa (pediocin-like) and class IIb (linear two-component) bacteriocins. However, they produce several types of unusual post-translationally modified bacteriocins not often found in other bacterial genera. The sactibiotics (or sactipeptides) are a growing group of bacteriocins characterized by the presence of a covalent bond formed between a cysteine thiol and the α-carbon of another amino acid. The formation of these linkages has been shown to be mediated by radical SAM enzymes.[115] The first sactibiotic to be characterized, subtilosin A, was isolated from *B. subtilis* (Figure 2.2).[116] This peptide has three sulfur-to-α-carbon bridges in addition to an amide linkage between

the N- and C-termini.[116] Thurincin H, a sactibiotic isolated from *B. thuringiensis*, features four sulfur-to-α-carbon bridges but no backbone cyclization.[117] Another growing class of bacteriocins produced by *Bacillus* spp. are the glycosylated disulfide-rich bacteriocins. Sublancin 168, isolated from *B. subtilis*, was found to bear a glycosylated cysteine residue in addition to two disulfide bridges (Figure 2.2).[118] Another peptide of this class to be recently characterized, thurandacin from *B. thuringiensis* features glycosylation of both cysteine and serine residues.[119]

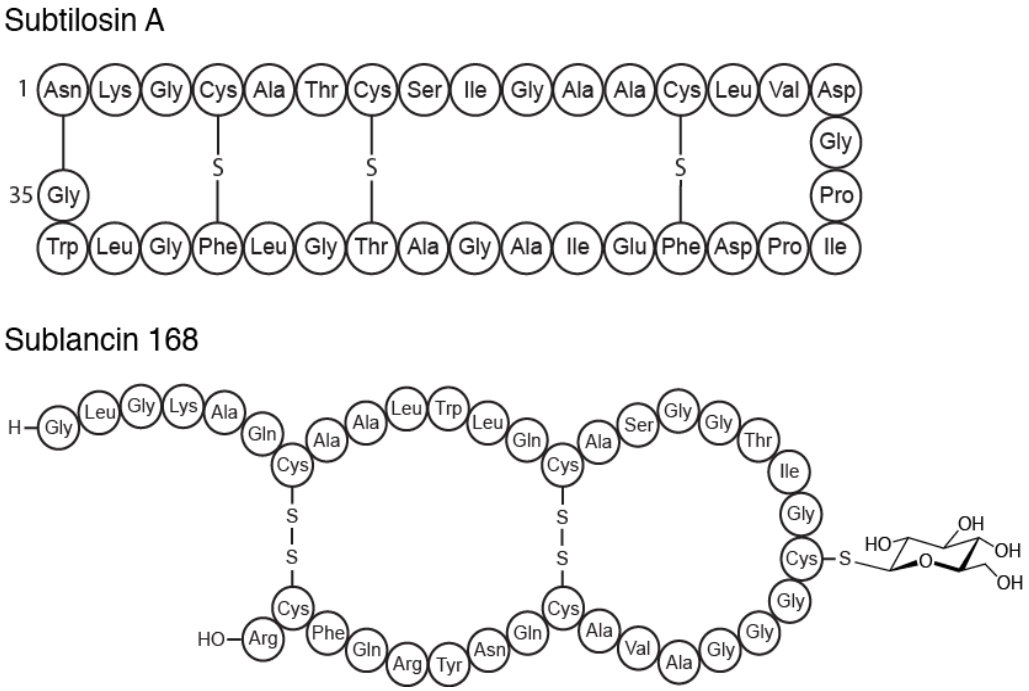

Figure 2.2. Bead structures of subtilosin A and sublancin 168

Apart from the ribosomally-synthesized bacteriocins, *Bacillus* and *Paenibacillus* spp. produce a variety of antimicrobial NRPS-derived peptides. The polymyxins are a group of cyclic NRPS products produced by *Paenibacillus polymyxa* strains bearing a lipid chain on the N-terminus and multiple 2,4-diaminobutyrate residues (Figure 2.3).

Polymyxins have been clinically used for the topical treatment of Gram-negative skin infections, but further use has been sparse due to nephrotoxicity concerns. Surfactin is a highly hydrophobic cyclic NRPS-derived lipopeptide produced by bacilli strains such as *B. subtilis* (Figure 2.3). This peptide exhibits a broad range of biological activities, including antibacterial, antiviral and antifungal properties. However, potential therapeutic usage is limited by the hemolytic properties of surfactin.[79]

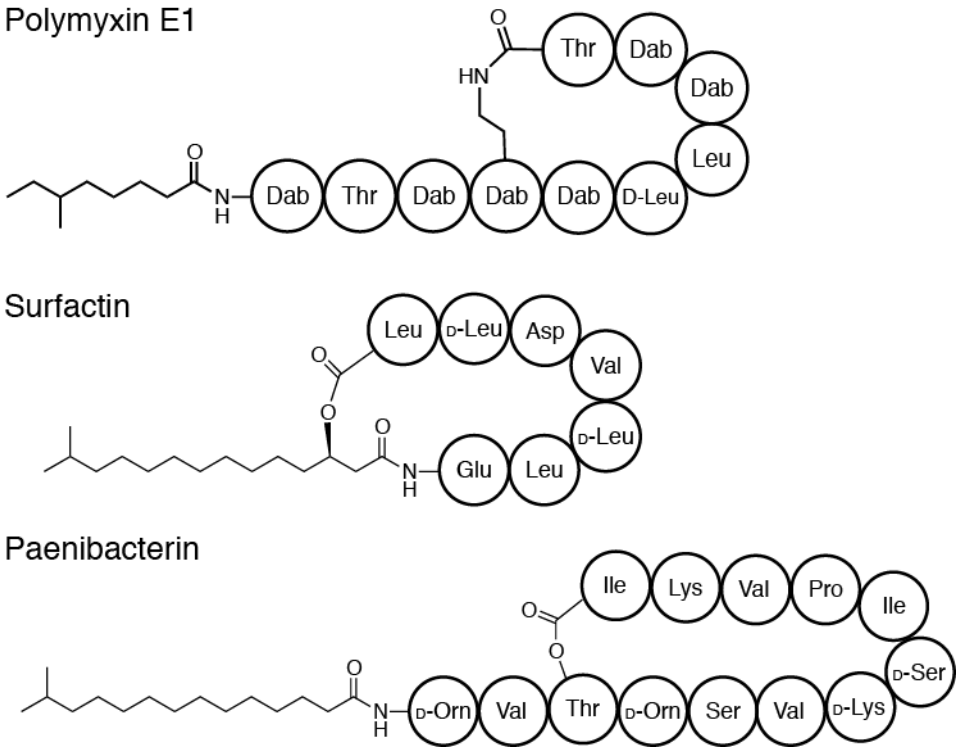

Figure 2.3. Bead structures of polymyxin E1, surfactin and paenibacterin.

Paenibacterin is a cyclic 13-amino acid lipopeptide produced by *Paenibacillus thiaminolyticus* that is antimicrobially active against a variety of Gram-positive and Gram-negative bacteria (Figure 2.3).[120] Furthermore, this peptide significantly improved survival in a murine septic shock model, likely by binding to Gram-negative

endotoxin.[120] Although paenibacterin was only discovered recently, it appears to be a promising candidate for consideration as a therapeutic agent. Despite these examples, relatively few antimicrobial NRPS products from *Bacillus* and *Paenibacillus* spp. have been fully characterized. It is possible that the discovery and re-discovery of antimicrobial peptides produced by these bacteria may yield drug candidates, an essential task due to the increasing prevalence of bacterial resistance.[79]

2.1.2. Control of *Campylobacter jejuni* using antimicrobial peptides

Campylobacter jejuni is one of the major causes of food-borne diarrheal illness, estimated to affect between 0.4 % and 0.9 % of the population annually in the high-income countries studied.[121] Many of these infections result from consumption of poultry products contaminated with *C. jejuni*. Recently, greater levels of antibiotic resistance have been emerging in *Campylobacter* spp.[122] For this reason, there has been great interest in identifying new antimicrobial agents targeting *C. jejuni*. Furthermore, the use of bacterial strains producing antimicrobial peptides to decrease the levels of *C. jejuni* in poultry has also been under investigation. A promising feature of this approach is that only low levels of bacteriocin resistance have been found to develop in *C. jejuni*.[123]

While screening for bacterial isolates antimicrobially active against *C. jejuni*, Svetoch and co-workers obtained three *Paenibacillus polymyxa* strains and a single *Bacillus circulans* strain with this phenotype.[124] They described the isolation of the antimicrobial peptides responsible for this activity, and determined the amino acid sequences of these peptides based on Edman degradation analysis (Table 2.1). The reported sequences were similar to the class IIa bacteriocins, with the conserved YGNGV (or YGNGL) sequence near the N-terminus. However, two of the reported sequences do

not have the two N-terminal Cys residues required for the conserved N-terminal disulfide bridge characteristic of the class IIa bacteriocins. Furthermore, the reported molecular weights of these peptides are not consistent with the masses calculated based on the amino acid sequences (differences of 252 Da, 766 Da and 143 Da for SRCAM 37, 602 and 1580, respectively).

Table 2.1. Reported amino acid sequences and masses of SRCAM 37, 602 and 1580.

Bacteriocin	Primary sequence	MW (Da)
SRCAM 37	FV**YGNGV**TSILVQAQFLVNGQRRFFYTPDK	3214
SRCAM 602	ATY**YGNGL**YCNKQKHYTWVDWNKASREIGKITVNGWVQH	3864
SRCAM 1580	VN**YGNGV**SCSKTKCSVNWGIITHQAFRVTSGVASG	3486

As bacteriocins produced by Gram-positive bacteria do not typically exert antimicrobial activity against Gram-negative bacteria such as *C. jejuni*, the Vederas group became interested in further characterizing the reported SRCAM peptides. Therefore, the four *Paenibacillus* and *Bacillus* strains were obtained from the US Department of Agriculture (USDA) Agricultural Research Service Patent Culture Collection. After culturing these strains and extracting the culture supernatants, Vederas group summer students Maude Giroud and Erika Steels observed antimicrobial activity against both Gram-positive and Gram-negative indicator strains. Furthermore, the activity against Gram-positive and Gram-negative bacteria could be separated, suggesting the presence of more than one antimicrobial peptide. However, after following the reported purification approach, no trace of the SRCAM peptides was found by MALDI-TOF MS. Instead, Maude Giroud obtained a fraction that appeared to contain the lipopeptide polymyxin E1 based on preliminary mass spectrometric characterization.

2.1.3. Project objectives

The primary goal was to identify the antimicrobial components produced by these *Paenibacillus* and *Bacillus* spp. Early experiments suggested that these strains each produced more than one antimicrobial component. It remained to be confirmed in our hands that these strains were antimicrobially active against *Campylobacter* spp. Additionally, it also remained to further examine the reported production of the SRCAM peptides by these strains. Genome sequencing data for the *Paenibacillus* and *Bacillus* spp. would provide information about any genetic determinants for the SRCAM peptides in addition to any other antimicrobial metabolites. Once the antimicrobial isolates were identified, they could be further characterized in terms of structure and activity should they be of interest.

2.2. Results and Discussion

2.2.1 Characterization of *P. polymyxa* NRRL B-30509 and its antimicrobial peptides

2.2.1.1. Genome sequencing and probing for SRCAM 602

To search for potential genetic determinants encoding SRCAM 602 in the genome of *P. polymyxa* NRRL B-30509, genomic DNA was isolated from this strain and sequenced using 454 pyrosequencing. However, no nucleotide sequence encoding the SRCAM 602 amino acid sequence was found. In order to determine if the SRCAM 602 sequence was somehow missed during genome sequencing, Vederas group research associate Dr. Marco van Belkum performed PCR experiments on the genomic DNA using degenerate oligonucleotide primers. These primers were designed to account for the different possible codon usages for the reported amino acid sequence to maximize the chance of amplifying the putative sequence. However, this approach did not yield any

amplicons consistent with a gene encoding SRCAM 602, while amplification of a sequence known to be in the genome using a similar approach yielded a band of the expected size (Figure 2.4).

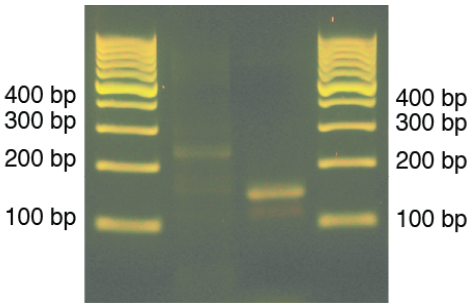

Figure 2.4. Agarose gel showing the attempted PCR amplification of a SRCAM 602 structural gene. Lanes 1 and 4: 100 base pair (bp) ladder. Lane 2: attempted amplification of SRCAM 602 structural gene (expected size: 116 bp). Lane 3: amplification of paenicidin A structural gene (discussed below; expected size: 149 bp).

The genome sequence of *P. polymyxa* NRRL B-30509 resembled those published for other *Paenibacillus* spp. Several biosynthetic gene clusters encoding potential bioactive components were identified. Several non-ribosomal peptide synthetase (NRPS) gene clusters were present, possibly involved in the production of antimicrobial peptides. Furthermore, two potential lantibiotics were also encoded along with the associated biosynthetic proteins.

2.2.1.2. Deferred inhibition assays

As a preliminary means of testing the antimicrobial properties of *P. polymyxa* NRRL B-30509, deferred inhibition assays were performed against an array of indicator organisms, including *Campylobacter jejuni*. Strong inhibition was observed against Gram-positive bacteria including *Bacillus subtilis*, *Lactococcus lactis* and *Listeria monocytogenes*. Furthermore, inhibition of the Gram-negative bacteria *Escherichia coli*,

Salmonella enterica, *Pseudomonas aeruginosa* and *C. jejuni* was observed. Due to the activity observed against *C. jejuni* coupled with the unlikely existence of SRCAM 602, an alternate explanation for this activity was required. Focus shifted to identifying and characterizing the actual antimicrobial compounds responsible for the activity observed against Gram-positive and Gram-negative bacteria.

2.2.1.3. Purification of active components

To isolate the antimicrobial components produced by *P. polymyxa* NRRL B-30509, an activity-guided purification was performed. First, culture supernatant was passed through a hydrophobic Amberlite XAD-16 column, which was then washed with increasing levels of isopropanol in water. These wash fractions were tested for activity against the Gram-positive indicator *Lactococcus lactis* and the Gram-negative indicator *Escherichia coli*. An earlier wash fraction exhibited activity against *L. lactis*, while the last wash step exhibited activity against *E. coli*.

The fraction active against *L. lactis* was further fractionated using a C18 solid-phase extraction cartridge, yielding a single antimicrobially active fraction. This fraction was concentrated and further separated using reversed-phase HPLC. The antimicrobial activity against *L. lactis* was ultimately traced to a component with a strong signal at $[M+H]^+ = 3376.5$ as found by MALDI-TOF MS.

The Amberlite fraction active against *E. coli* was similarly concentrated and fractionated on a C18 solid-phase extraction cartridge. A single antimicrobially active fraction was obtained, which was subjected to reversed-phase HPLC. Antimicrobial testing revealed several active HPLC fractions. Two earlier eluting antimicrobial fractions contained major components with $[M+H]^+ = 1155.8$ and 1169.8. The later

eluting active fraction, containing several related components (major component at $[M+H]^+$ = 1578.9), was also found to be active against *E. coli*.

2.2.1.4. Identification of polymyxins E1 and E2

Using a different approach to purify the antimicrobial components produced by *P. polymyxa* NRRL B-30509, visiting undergraduate student Maude Giroud previously discovered an antimicrobial peptide with the same mass as described above ($[M+H]^+$ = 1169.8). Based on previous high-resolution mass spectrometry and MS/MS, it was suggested that this peptide was the cyclic lipopeptide polymyxin E1. Therefore, the other peptide presently isolated ($[M+H]^+$ = 1155.8) may be polymyxin E2, which differs from polymyxin E1 only in the length of the lipid chain (Figure 2.5). MS/MS data for these isolates were compared to MS/MS data obtained for commercially available polymyxins E1 and E2. The fragmentation patterns of the isolates matched closely with the corresponding commercial polymyxin samples. Further, co-injection of isolated polymyxin E1 with commercial polymyxin E1 by HPLC yielded only a single peak.

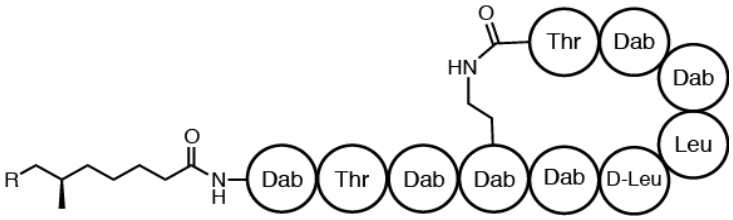

Figure 2.5. Structures of polymyxins E1 and E2. Polymyxin E1: R = CH_3; Polymyxin E2: R = H.

The isolated polymyxins were tested for their antimicrobial activity against an array of Gram-negative indicator organisms including *C. jejuni*. While strains of *E. coli*, *Pseudomonas aeruginosa* and *Salmonella enterica* were inhibited, no inhibition of *C.*

jejuni NCTC 11168 was observed. Furthermore, polymyxins have been used as an ingredient in *Campylobacter*-selective media. Therefore, the antimicrobial activity of *P. polymyxa* NRRL B-30509 against *C. jejuni* must have an alternate source.

2.2.1.5. Isolation and characterization of tridecaptin A_3

The other fraction active against *E. coli* (principal component $[M+H]^+ = 1578.9$), was first characterized by MS/MS. Based on these data, the amino acid sequence of the isolate was consistent with that of the previously described lipopeptide tridecaptin A (Figure 2.6).[125] Structurally, tridecaptin A is 13 residue peptide containing several D-amino acids as well as three 2,4-diaminobutyrate residues. The N-terminus of tridecaptin A is acylated with a 3-hydroxy-6-methyloctanamide group. Based on the MS/MS data, the lipid chain of the tridecaptin isolate appears to be two methylene units longer than the previously described lipid chain. To distinguish this isolate, it was designated tridecaptin A_3.

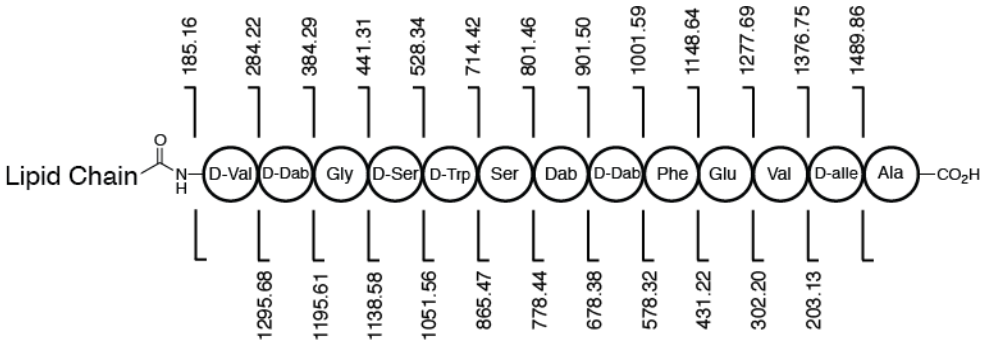

Figure 2.6. Summary of MS/MS fragment ions for tridecaptin A_3.

2.2.1.6. GC-MS analysis of the tridecaptin lipid chain

To determine the structure of the lipid chain of this tridecaptin isolate, GC-MS was used. Presuming that the lipid chain is a 3-hydroxydecanamide derivative, it likely

bears a methyl group on either carbon 8 or 9. It was predicted that the position of the methyl substituent could be distinguished on the basis of EI-MS fragmentation data. Tridecaptin A_3 was isolated and subjected to hydrolysis conditions briefly to minimize the potential dehydration of the lipid chain β-hydroxy group. The hydrolysate was extracted, and the extract was derivatized using trimethylsilyldiazomethane to convert fatty acids to their corresponding methyl esters. The mixture was separated using GC-MS to resolve and identify any derivatized fatty acids. The extracted ion chromatogram revealed a major peak consistent with a β-hydroxy methyl ester, preceded by a smaller peak with a similar fragmentation pattern (Figure 2.7).

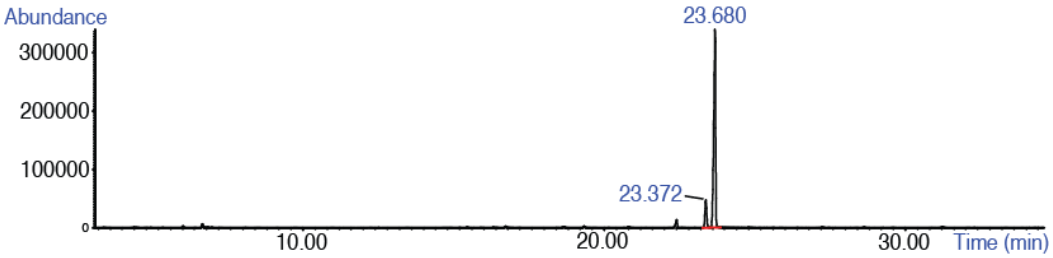

Figure 2.7. GC-MS chromatogram of the derivatized tridecaptin A_3 lipid chains. Extracted ion chromatogram monitoring at 103.0, corresponding to fragmentation between the β- and γ-carbons of a β-hydroxy methyl ester.

The EI-MS data for the two peaks were compared, revealing that the majority of the peaks were the same between the two spectra. However, there were some differences in the spectra at higher m/z values (Figure 2.8). The peak at 23.4 min showed weak ions at 143 and 151, while the peak at 23.7 min showed weak ions at 129 and 137. Based on the typical fragmentation sites for the expected lipid chain functional groups, these differing ions could be related to the differing position of a methyl group on the structure. Based on the data, the fragments of the peak at 23.4 min are consistent with methyl 3-

hydroxy-9-methyldecanoate, while those of the peak at 23.7 min are consistent with methyl 3-hydroxy-8-methyldecanoate. Furthermore, the relative elution order of the iso (9-methyl) and the anteiso (8-methyl) lipid chain forms is consistent with literature precedent.[126] Based on these data, tridecaptin A_3 is primarily acylated with a 3-hydroxy-8-methyldecanamide chain, with smaller amounts 3-hydroxy-9-methyldecanamide acylated peptide present.

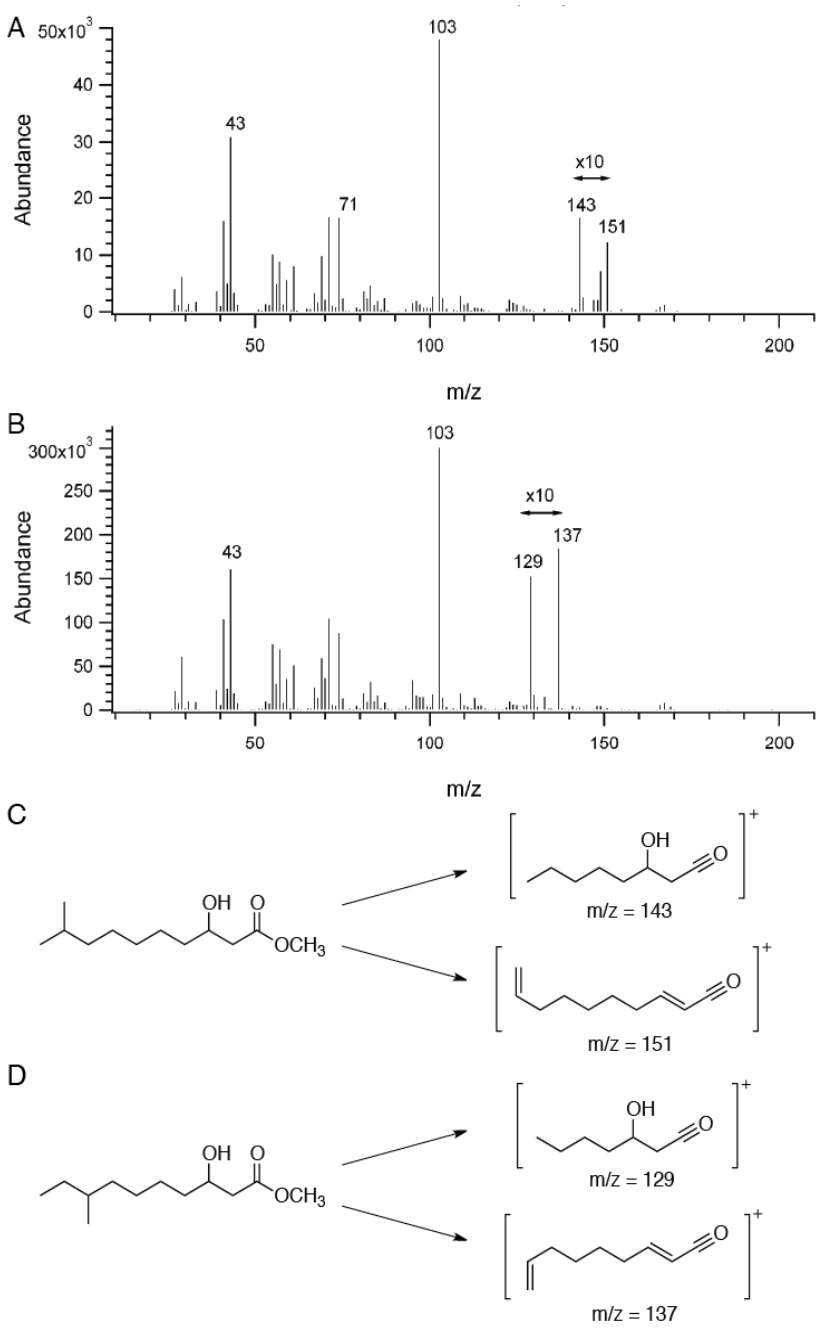

Figure 2.8. EI-MS data for the major tridecaptin lipid chain GC-MS peaks. (A) Fragments observed for the peak at 23.4 min. (B) Fragments observed for the peak at 23.7 min. The intensity of certain regions is increased 10x, as indicated on the figure. (C) Predicted fragments of methyl 3-hydroxy-9-methyldecanoate, corresponding to the peak at 23.4 min. (D) Predicted fragments of methyl 3-hydroxy-8-methyldecanoate, corresponding to the peak at 23.7 min.

2.2.1.7. Tridecaptin A_3 antimicrobial activity against *Campylobacter jejuni*

As polymyxins E1 and E2 were found to be ineffective against *C. jejuni*, the production of tridecaptins offered another explanation for this activity. Indeed, isolated tridecaptin A_3 inhibited the growth of *C. jejuni* NCTC 11168 via spot-on-lawn assay. Therefore, the proposal that SRCAM 602 was responsible for the anti-*Campylobacter* activity of *P. polymyxa* NRRL B-30509 has been further discredited, with tridecaptin A_3 being shown to demonstrate this activity.

2.2.1.8. Initial MS/MS analysis of paenicidin A

The peptide active against *L. lactis* ($[M+H]^+ = 3376.5$), which was given the name paenicidin A, was initially characterized by tandem mass spectrometry in an attempt to obtain sequence information. However, relatively few fragment ions were observed, suggesting full sequence determination through MS/MS was not possible. The lack of fragments corresponding to certain regions of the peptide could be due to the amino acids present in these regions. However, post-translational modifications (e.g., disulfide bridges) could also prevent fragmentations in these regions from being readily observed. Despite this, a partial amino acid sequence was confirmed with both b- and y-ions.

2.2.1.9. Genetic characterization of paenicidin A

From the genome sequence, all of the potential open-reading frames (ORF) of a sufficient size to encode paenicidin A were examined for a nucleotide sequence encoding the partial amino acid sequence obtained from MS/MS. Most of the ORFs were far too large to be bacteriocin structural genes, while others encoded the partial amino acid sequence in a position inconsistent with the MS/MS data. Ultimately, an ORF encoding a 58-residue polypeptide was chosen as a strong candidate as the paenicidin A structural

gene. This gene was grouped with other genes encoding homologues of typical lantibiotic biosynthetic proteins.

A BLAST search of the putative paenicidin A structural gene revealed similarities to structural genes encoding the well-known lantibiotics subtilin and nisin. Alignment of the paenicidin A structural gene with these other lantibiotic structural genes suggested that paenicidin A is produced with a 22-residue leader peptide, which is proteolytically removed to yield the 36-residue mature peptide (Figure 2.9). The paenicidin A core peptide sequence contains six cysteine residues, as well as nine serines and threonines. While the cysteine residues could be involved in disulfide bridges, they are more likely to be modified into lanthionine (Lan) and methyllanthionine (MeLan) residues if paenicidin A is indeed a lantibiotic. This would explain the sparse fragmentation observed by MS/MS, as fragmentation between amino acids contained within Lan and MeLan residues is typically not observed.[127]

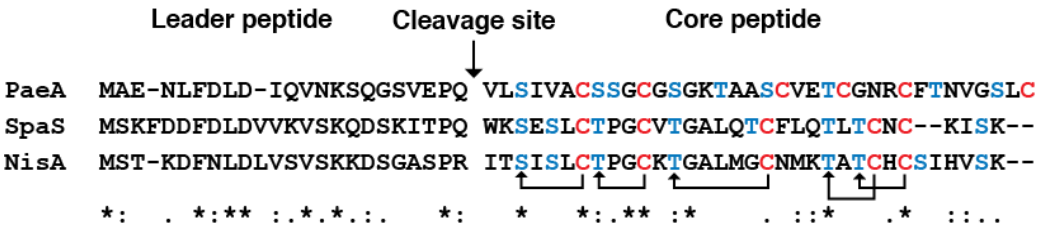

Figure 2.9. Sequence alignment of paenicidin A precursor with other lantibiotics. Paenicidin A (PaeA), subtilin precursor (SpaS) and nisin precursor (NisA). Serines and threonines are indicated in blue, while cysteines are in red. The Lan and MeLan connectivity of subtilin and nisin is indicated below the sequences with arrows. Conserved amino acids are indicated by an asterisk, conservative substitutions with a colon, and amino acids with weakly similar properties with a period.

2.2.1.10. Paenicidin A biosynthetic gene cluster

In addition to the structural gene *paeA*, six other genes were predicted to be involved in the biosynthesis of paenicidin A (Figure 2.10, Table 2.2).[128] Proteins PaeB

and PaeC are homologous to the LanB and LanC-type enzymes involved in Lan and MeLan formation. PaeB is expected to be a dehydratase, dehydrating select serine and threonine residues, forming dehydroalanine (Dha) and dehydrobutyrine (Dhb) respectively. Then, cyclase PaeC likely catalyzes the nucleophilic attack of cysteine thiols onto the β-positions of Dha or Dhb, affording Lan or MeLan respectively. PaeT shows sequence homology to dedicated LanT-type ABC transporters, likely exporting paenicidin A once it has been post-translationally modified. PaeFEG appear to form an ABC transporter that may function to protect the producer organism from the antimicrobial properties of paenicidin A. PaeF is likely a cytosolic ATP-binding protein, while PaeE and PaeG appear to be membrane-spanning subunits of the transporter. No apparent protease was encoded in the biosynthetic gene cluster, raising questions as to how the paenicidin A leader sequence was cleaved once the Lan and MeLan rings had been formed. However, this cleavage could be catalyzed by a protease involved in a different pathway, as has been reported for subtilin.[24] No genes encoding a LanI-type immunity protein were found within the gene cluster.

Figure 2.10. Putative paenicidin A biosynthetic gene cluster.

Table 2.2. Analysis of putative paenicidin A biosynthetic proteins.

Protein	Predicted Function	Size (a.a.)	Size (kDa)
PaeA	Lantibiotic precursor peptide	58	5.9
PaeF	ATP binding protein	242	27.1
PaeE	ABC transporter membrane-bound subunit	266	30.9
PaeG	ABC transporter membrane-bound subunit	255	28.9
PaeB	Lantibiotic dehydratase	1058	122.3
PaeT	ABC transporter	625	71.4
PaeC	Lantibiotic cyclase	460	52.0

2.2.1.11. Analysis of paenicidin A post-translational modifications

With paenicidin A identified as a lantibiotic, it was of interest to characterize the post-translational modifications (PTMs) present in this peptide. In addition to Lan and MeLan residues, mature paenicidin A could also contain Dha and Dhb residues. As the unmodified paenicidin A contains six cysteines and nine serines and threonines, there was the potential for many different combinations of PTMs. As an initial investigation into these modifications, the monoisotopic mass of mature paenicidin A (3375.5 Da) was compared with that calculated for the unmodified amino acid sequence (3483.5 Da). The difference between these masses corresponds to six water molecules, suggesting that the peptide is dehydrated six times during maturation. Therefore, it is likely that this peptide contains six Lan, MeLan, Dha and Dhb residues. Further, three of the serines and threonines are expected to be unmodified in the mature peptide.

It is possible that the six cysteines are all involved in Lan and MeLan formation. The presence of a disulfide bridge was judged to be unlikely based on the mass of paenicidin A; a disulfide bridge would be associated with a 2 Da decrease in mass. To confirm this, former Vederas group graduate student Dr. Zedu Huang treated paenicidin A to reductive alkylating conditions. No increase in the mass of paenicidin A was

observed, indicating that no disulfide bridges were present. Therefore, it is likely that this peptide contains six Lan and MeLan residues, and would therefore have no Dha or Dhb residues.

Analysis of the MS/MS data in combination with the genetically encoded amino acid sequence allowed for the topology of three Lan and MeLan residues to be proposed. The lack of fragmentation observed in certain regions of the peptide was taken as evidence for the presence of Lan or MeLan at these positions (Figure 2.11). Therefore, Lan rings were proposed between Ser-3 and Cys-7 and between Ser-8 and Cys-11, while a MeLan ring was proposed between Thr-30 and Cys-36. However, the connectivity of the three remaining rings could not be proposed based on these MS/MS data. Based on the amino acid sequence, these three Lan and MeLan rings are necessarily interlocking. Therefore, some other approach was required to determine the covalent structure of paenicidin A.

Figure 2.11. Summary of MS/MS data for paenicidin A. Cysteines are in dark blue, while serines and threonines are in light blue.

2.2.1.12. NMR spectroscopic analysis

Perhaps the most common means of determining the bridging patterns of Lan and MeLan residues in lantibiotics is through the use of NMR spectroscopy. Following the assignment of proton chemical shifts, NOE crosspeaks spanning the thioether bridges can be used to support a particular connectivity. Therefore, greater quantities of paenicidin A were isolated for NMR experiments. However, paenicidin A did not prove to be very

soluble in the solvent conditions tested. Regardless, the sample was prepared in a mixture of methanol and water and TOCSY and NOESY datasets were acquired. Based on these data, the majority of the proton chemical shifts could be assigned unambiguously (Table 6.2).

These data supported the post-translational modifications predicted based on the MS/MS data. No distinctive vinyl protons were observed, consistent with the lack of any Dha and Dhb residues. The NMR data also supported the identification of the three serine residues unmodified during lantibiotics maturation. The chemical shifts of the Ser-9, Ser-13 and Ser-34 β-protons were all between 3.8 and 4.1 ppm, higher than that expected for the β-protons of a Lan residue. While the intensity of the NOE crosspeaks in the NOESY spectrum were generally weak, signals supporting three Lan/MeLan bridges were observed. Specifically, these data suggested the presence of Lan and MeLan residues derived from Ser-8 and Cys-11, from Thr-16 and Cys-20, and from Thr-23 and Cys-28. Signals bridging the other Lan and MeLan residues were not observed either due to poor signal intensity or signal overlap. Furthermore, the presence of an NOE crosspeak seemingly bridging a thioether bridge does not guarantee that the two spin systems are covalently linked. As in the region with three interlocking rings, the Lan and MeLan protons may be in close proximity to protons present on other Lan and MeLan residues.

2.2.1.13. Partial desulfurization of paenicidin A

During the course of the characterization of paenicidin A, this peptide was desulfurized in an attempt to gain further information regarding the post-translational modifications. Desulfurization cleaves the thioether bridges of Lan/MeLan residues, allowing for the analysis of the amino acids contained within the rings. Previous reports

have described the full desulfurization of a lantibiotic, followed by analysis using Edman degradation[27] or MS/MS[129] to determine the modified amino acid sequence. For paenicidin A, this would allow for the serine residues incorporated into Lan residues to be distinguished with those that are unmodified.

With former Vederas group member Dr. Zedu Huang, paenicidin A was desulfurized using nickel boride as previously described.[27] MALDI-TOF MS and LC-MS/MS analysis of the resulting sample revealed the presence of a mixture of variably desulfurized states, ranging from the singly desulfurized to the fully desulfurized peptide (Figure 2.12). The full desulfurization of a lantibiotic converts all of the Lan and MeLan residues to Ala and Abu, with no information regarding the connectivity of these residues retained. However, MS/MS analysis of a partially desulfurized lantibiotic could provide additional valuable structural information. Intact Lan/MeLan residues could be mapped due to the lack of fragmentation observed in that region in the MS/MS data. The observation of additional fragmentation in that region following desulfurization would support the cleavage of a Lan/MeLan residue present at that position. For paenicidin A, if one of the three interlocking Lan/MeLan residues were desulfurized, MS/MS data could in theory be used to determine the connectivities of all three rings.

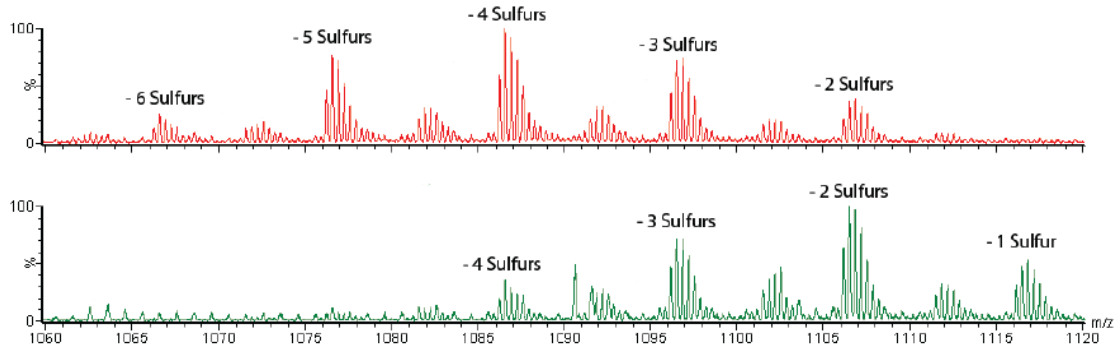

Figure 2.12. Partial desulfurization of paenicidin A. Top: desulfurization after 8 h. Bottom: desulfurization after 0.5 h.

The differentially desulfurized paenicidin A peptides were analyzed using LC-MS/MS (Figure 2.13). Multiple peptides that had been desulfurized to the same extent but which eluted separately during LC were observed. These were predicted to result from the desulfurization of different Lan or MeLan residues. Analysis of the MS/MS data of one of the singly desulfurized paenicidin A peaks revealed additional fragmentation that was not observed for the natural peptide. These fragments occurred within the region corresponding to the predicted Lan residue formed from Ser-8 and Cys-11. Further, the masses of the residues genetically encoded as Ser-8 and Cys-11 were now consistent with alanine residues, indicating that desulfurization was successful. Based on this evidence, a Lan residue between Ser-8 and Cys-11 is heavily supported. Similarly, a different singly desulfurized state of paenicidin A showed fragments consistent with the desulfurization of a N-terminal Lan residue derived from Ser-3 and Cys-7.

The predominant doubly desulfurized paenicidin A peak was found to involve desulfurization of both known N-terminal Lan residues. However, analysis of a triply desulfurized form of paenicidin A proved to be very informative. In this MS/MS dataset, fragmentation was observed within the region originally contained within three Lan and

MeLan rings. These fragments suggested that a Lan residue was formed between Ser-19 and Cys-24. Consequently, this would indicate that MeLan residues were formed from Thr-16 and Cys-20, as well as from Thr-23 and Cys-28. This was supported by the fragmentation pattern observed for a pentadesulfurized state, wherein the only intact Lan or MeLan residue was the MeLan ring formed from Thr-16 and Cys-20. Finally, MS/MS data for the fully desulfurized peptide confirmed which serine residues were unmodified but did not provide any information about the connectivity of the Lan and MeLan residues.

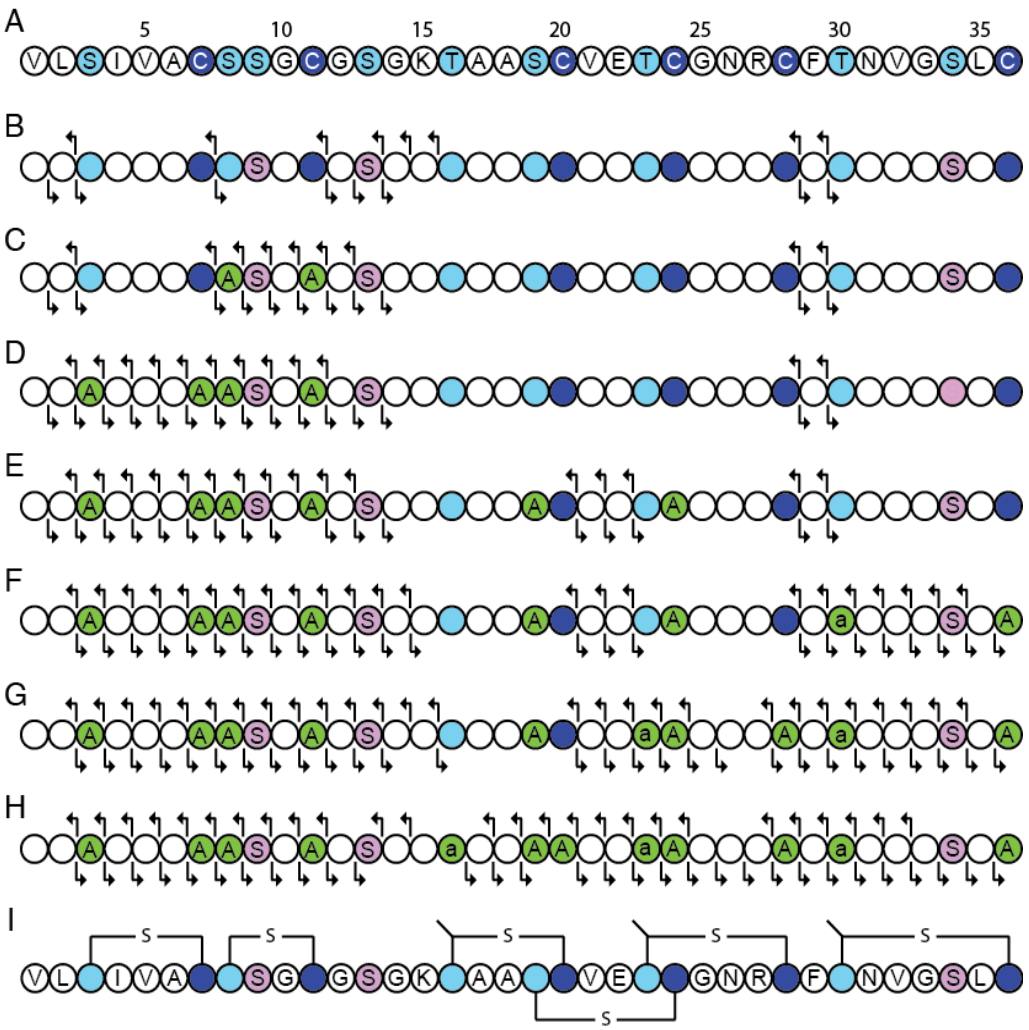

Figure 2.13. Summary of MS/MS data for the variably desulfurized states of paenicidin A. (A) Primary sequence of paenicidin A. Serines and threonines are indicated in light blue, while cysteines are in dark blue. (B) MS/MS fragments observed for mature paenicidin A. MS/MS data for paenicidin desulfurized (C) once, (D) twice, (E) three times, (F) four times, (G) five times and (H) six times. Residues derived from desulfurization are indicated in green, with alanine represented by a capital A and aminobutyrate represented by a lower case a. Observed b-ions are indicated by an arrow above the sequence, and y-ions by an arrow below. Serines that are unmodified during maturation are indicated in purple. (I) Connectivity of Lan and MeLan residues based on desulfurization experiments.

Some trends were noted when examining the differentially desulfurized states of paenicidin A. First, it appeared that Lan residues were desulfurized preferentially over MeLan residues. It may be that the additional methyl group of MeLan sterically hinders the approach of the nickel boride catalyst to the thioether linkage, whereas approach towards Lan is not obstructed. Second, the Lan and MeLan residues near the termini of

the peptide appeared to be desulfurized more quickly than those located at the middle. The terminal residues of paenicidin A may be more surface exposed, while the central residues could be buried within the peptide and as such are less accessible to the catalyst. Alternately, the interlocking nature of the central Lan and MeLan residues could block the approach of the catalyst.

2.2.1.14. Stereochemistry of Lan and MeLan residues

Purified paenicidin A was hydrolyzed, and the constituent amino acids were derivatized as the pentafluoropropanamide methyl esters. The stereochemistry of the Lan and MeLan residues was determined via GC-MS through co-injection experiments with synthetic standards.[130,131] These experiments revealed the exclusive presence of the DL-Lan and DL-MeLan stereoisomers. Until recently, only the DL-Lan and DL-MeLan stereoisomers were found in stereochemically characterized lantibiotics. In 2013, the structure of two-component lantibiotic enterococcal cytolysin was found to contain the unusual LL-Lan and LL-MeLan stereoisomers.[13] These unusual stereoisomers were thought to result from the presence of a dehydro residue as the most N-terminal amino acid contained within the Lan or MeLan ring. While paenicidin A contains three Lan and three MeLan residues, there are no dehydro residues; therefore, the presence of only the DL-Lan and DL-MeLan stereoisomers is as expected.

2.2.1.15. Structure of paenicidin A

Based on NMR and the MS/MS analysis of the partially desulfurized derivatives, the full structure of paenicidin A was proposed (Figure 2.14). The structure bears two N-terminal Lan residues, a C-terminal MeLan residue, and three interlocking Lan and MeLan residues in the center of the peptide. The structure of the N-terminus of

paenicidin A is homologous to many other lantibiotics such as nisin and subtilin. This topology, with a Lan/MeLan residue consisting of five amino acids immediately followed by another Lan/MeLan residue consisting of four amino acids is important for the mode of action of these lantibiotics. This motif has been shown to be responsible for the binding of this group of lantibiotics to lipid II.[14] This binding sequesters the lipid II, preventing its incorporation into peptidoglycan. Once bound, the lantibiotic may insert into the bacterial membrane and form pores, resulting in the leakage of bacterial essential metabolites and electrochemical gradient.[132] Based on the similarity of the N-terminus of paenicidin A to that of nisin, it likely acts initially by binding to lipid II.

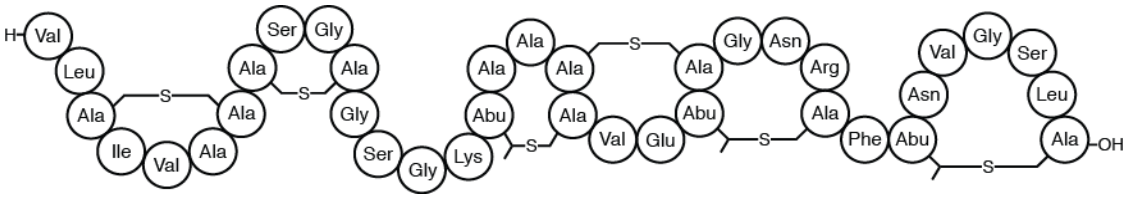

Figure 2.14. Bead structure of paenicidin A.

The central interlocking Lan and MeLan ring system of paenicidin A does not resemble other lantibiotics reported to this point. However, conservation of Lan and MeLan residues in this region may be less important for the overall mode of action of these peptides. The requirements for pore formation may be more dependent on the placement of hydrophilic and hydrophobic surfaces, and not as much the specific amino acid identities or connectivity. However, it is not yet known whether paenicidin A forms pores, or solely acts through inhibition of peptidoglycan biosynthesis.

2.2.1.16. Paenicidin A spectrum of activity

Purified paenicidin A was tested against a variety of Gram-positive and Gram-negative indicator organisms (Table 2.3). As with most lantibiotics, no activity was observed by paenicidin A against the Gram-negative bacteria tested, including *E. coli* and *C. jejuni*. Although paenicidin A inhibited the growth of several of the Gram-positive bacteria tested, it exhibited a relatively narrow spectrum of activity. Strong inhibition of *L. lactis* and *B. subtilis* was observed, while *Enterococcus faecium* and *Listeria monocytogenes* were only weakly inhibited.

Table 2.3. Paenicidin A spectrum of activity

Indicator organism	Extent of Activity[a]
Gram-positive bacteria	
Bacillus subtilis JH642	++
Carnobacterium maltaromaticum UAL26	-
Enterococcus faecium ATCC 19434	+
Lactococcus lactis subsp. *cremoris* HP	++
Listeria monocytogenes ATCC 15313	+
Pediococcus acidilactici PAC 1.0	-
Staphylococcus aureus ATCC 25923	-
Gram-negative bacteria	
Campylobacter jejuni NCTC 11168	-
Escherichia coli DH5α	-
Salmonella enterica serovar Typhimurium ATCC 13311	-
Pseudomonas aeruginosa ATCC 15442	-

[a] Indicates inhibition of indicator strain when tested with a 100 μM solution of paenicidin A using a spot-on-lawn assay. Strength of inhibition: ++, inhibition; +, faint inhibition; -, no inhibition.

2.2.2. *Paenibacillus terrae* NRRL B-30644

2.2.2.1. Genome sequencing and reassignment of species

Bacillus circulans NRRL B-30644 was reported to produce the anti-*Campylobacter* bacteriocin SRCAM 1580.[124] To evaluate the presence of a structural gene encoding this supposed bacteriocin and to gain information regarding other biosynthetic gene clusters, the genome of *B. circulans* NRRL B-30644 was sequenced. However, no genetic determinants for SRCAM 1580 were found in the genome. Instead, several potential NRPS and bacteriocin gene clusters were identified, including one encoding a homolog of paenicidin A.

To determine if the SRCAM 1580 structural gene was missed during genome sequencing, Vederas group research associate Dr. Marco van Belkum employed a strategy similar to that described above for *P. polymyxa* NRRL B-30509. Briefly, PCR using degenerate oligonucleotide primers based on the SRCAM 1580 amino acid sequence did not yield any amplicons of a sequence or size consistent with this peptide. Taken with the unsuccessful attempts to isolate SRCAM 1580, there was no evidence for the production of this peptide by *B. circulans* NRRL B-30644.

During the analysis of the genome sequence, it was noted that many of the genes were highly homologous to those in the published genome of *Paenibacillus terrae* HPL-003.[133] Furthermore, the 16S rRNA sequence of strain NRRL B-30644 more closely resembled that of *P. terrae* HPL-003 than that of any other *Bacillus* or *Paenibacillus* spp. The previous typing of strain NRRL B-30644 as *B. circulans* was based on carbohydrate usage and bacterial morphology, not on genetic data.[124] Therefore, we propose to reclassify this isolate as *P. terrae* NRRL B-30644.

2.2.2.2. Deferred inhibition experiments

The antimicrobial properties of *P. terrae* NRRL B-30644 were tested via deferred inhibition experiments against a variety of bacterial strains. Against the Gram-positive indicators tested, only weak inhibition of *B. subtilis* and *L. lactis* was observed. However, strong growth inhibition of *S. enterica*, *E. coli*, and *C. jejuni* was observed. Of note, this strain did not inhibit the growth of *P. aeruginosa*, contrasting what was observed for *P. polymyxa* NRRL B-30509. Based on the other apparent similarities between these two strains, it was of interest to see if similar antimicrobial peptides were produced and if tridecaptin was again responsible for the activity against *C. jejuni*.

2.2.2.3. Isolation and characterization of tridecaptin A_1

To identify the component(s) responsible for activity against Gram-negative bacteria, an activity-guided purification based on inhibition of *E. coli* was performed. Supernatant from a culture of *P. terrae* NRRL B-30644 was prepared and fractionated over Amberlite XAD-16 resin. The single Amberlite fraction active against *E. coli* was further fractionated using a C18 SPE cartridge, followed by reversed-phase HPLC. Unlike *P. polymyxa* NRRL B-30509, only a single HPLC fraction displayed strong inhibition of *E. coli*. MALDI-TOF MS data obtained for this fraction showed a strong peak ($[M+H]^+$ = 1550.8), differing from tridecaptin A_3 by 28 Da. This peptide was analyzed by MS/MS sequencing, demonstrating a fragmentation pattern consistent with tridecaptin A (Figure 2.15).[125] The predicted mass of the lipid chain was the same as that of the tridecaptin A 3-hydroxy-6-methyloctanamide chain,[125] but the connectivity of the lipid chain was not yet known. Based on these similarities, the tridecaptin isolate from *P. terrae* NRRL B-30644 was named tridecaptin A_1.

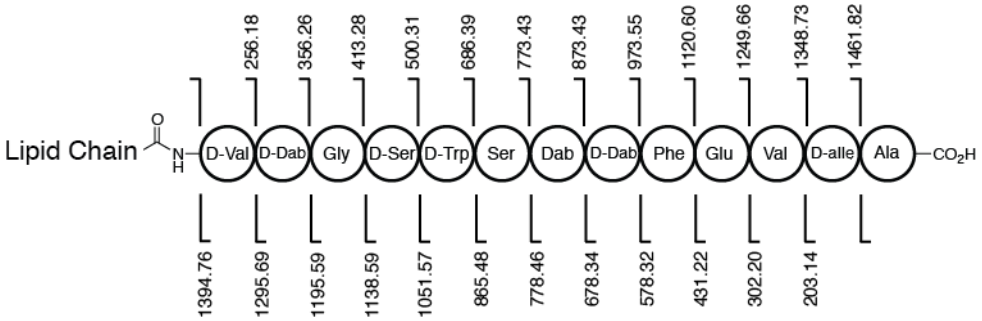

Figure 2.15. Summary of MS/MS fragment ions for tridecaptin A_1.

2.2.2.4. NMR spectroscopy of tridecaptin A_1

Due to the greater levels of tridecaptin A_1 obtained from *P. terrae* NRRL B-30644 (relative to tridecaptin A_3 from *P. polymyxa* NRRL B-30509), obtaining sufficient quantities for NMR spectroscopic characterization was feasible. Purified tridecaptin A_1 was prepared in 10 % D_2O, and TOCSY, ROESY, COSY and ^{13}C-HSQC datasets were acquired. Based on the TOCSY and ROESY data, all of the amino acid proton chemical shifts could be assigned (Figure 2.16, Table 6.3). These data were consistent with the amino acid sequence determined from MS/MS. Furthermore, the chemical shifts of the lipid chain spin system are consistent with a β-hydroxy group. However, it was not possible to distinguish between the different possible methyl substitution patterns.

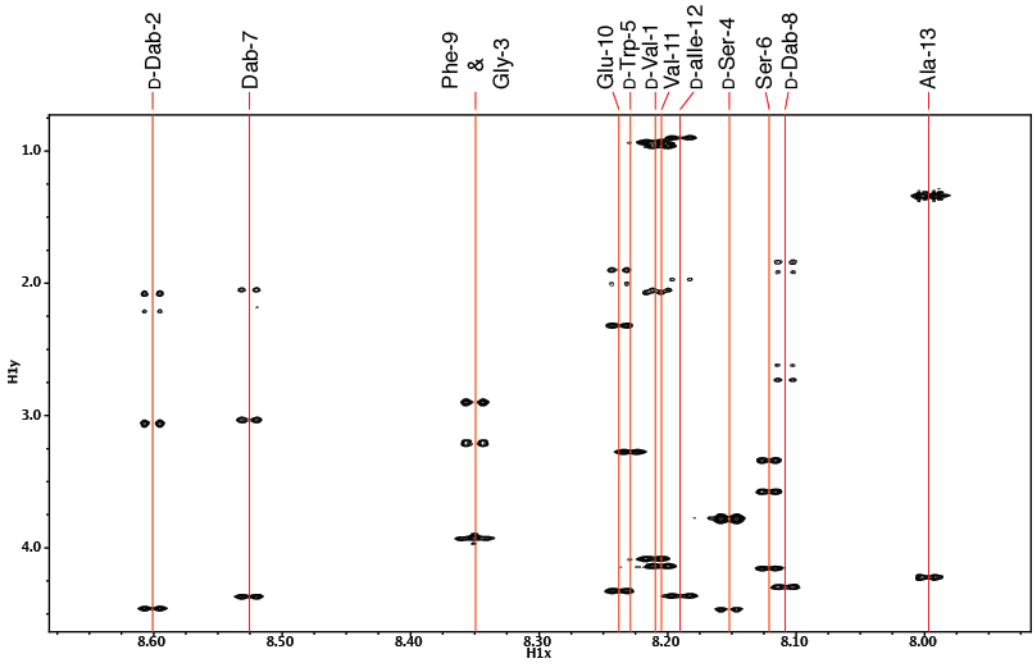

Figure 2.16. TOCSY spectrum of tridecaptin A_1 with spin systems assigned.

2.2.2.5. Tridecaptin A_1 lipid chain structural determination

To determine the position of the methyl group on the lipid chain of tridecaptin A_1, GC-MS was used as described above. Briefly, pure tridecaptin A_1 was hydrolyzed under mild conditions, and the extracted lipid chain was derivatized as the methyl ester. Injection onto GC-MS revealed only a single peak yielding fragment ions consistent with the expected β-hydroxy methyl ester (Figure 2.17). Co-injection of the derivatized tridecaptin A_1 lipid chain with synthetic methyl 3-hydroxy-6-methyloctanoate (prepared by former Vederas group graduate student Dr. Zedu Huang) yielded only a single peak. Furthermore, the EI-MS fragment pattern of the synthetic lipid closely matched that of the natural isolate. Therefore, the lipid chain of tridecaptin A_1 was determined to be 3-hydroxy-6-methyloctanamide.

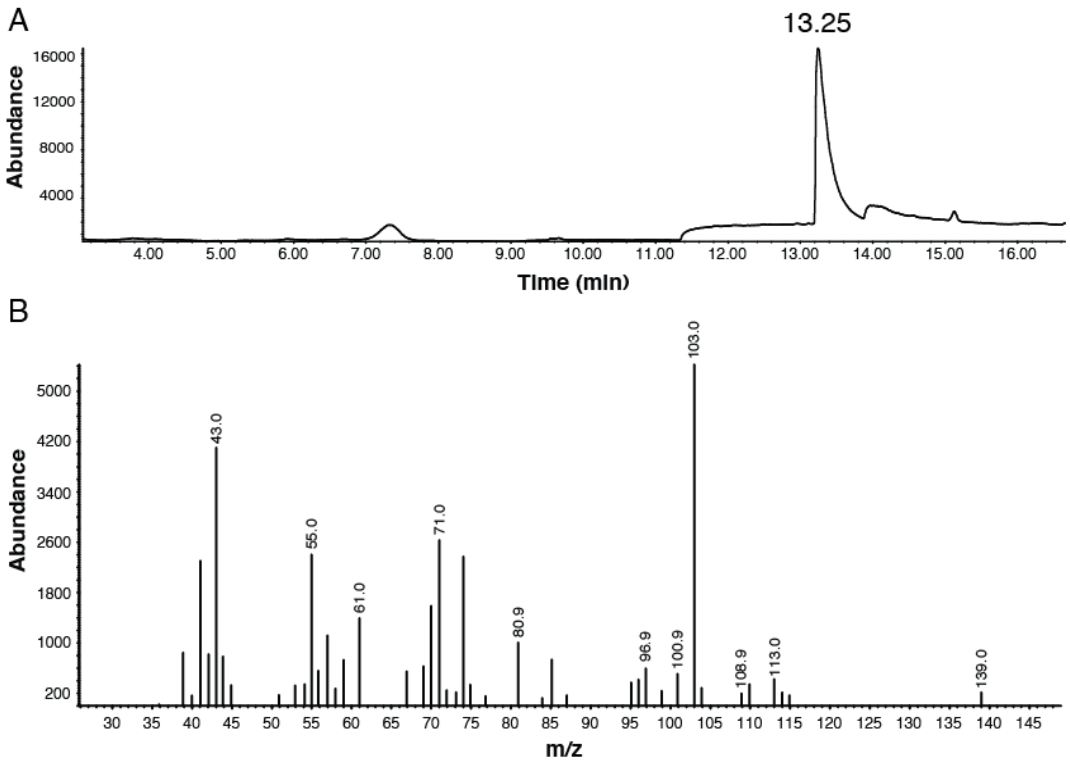

Figure 2.17. GC-MS chromatogram and EI-MS data for the tridecaptin A_1 lipid chain. (A) Extracted ion chromatogram (m/z 103.0) of the derivatized lipid extract from hydrolyzed tridecaptin A_1. (B) EI-MS data for the peak at 13.25 min.

Dr. Zedu Huang and current Vederas group graduate student Stephen Cochrane synthesized tridecaptin A_1 bearing the four possible lipid chain stereoisomers. Through HPLC co-injections, Stephen Cochrane demonstrated that the hydroxyl-bearing carbon had an *R* configuration (i.e., 3*R*). NMR experiments demonstrated that the carbon bearing the methyl group was the *S* stereoisomer (i.e., 6*S*; Figure 2.18A). Therefore, the lipid chain of tridecaptin A_1 is the (3*R*,6*S*)-6-hydroxy-3-methyloctanamide. The stereochemistry of the methyl group suggests that the lipid chain is ultimately derived from L-Ile, which may act as a starter unit during fatty acid synthesis.[134] Such branched fatty acids represent the majority of the lipids found in *Paenibacillus* spp.[135] The configuration of the carbon bearing the hydroxyl group suggests that this stereocenter is

formed during fatty acid biosynthesis.[136] Based on these results, the full stereochemical structure of tridecaptin A_1 was determined (Figure 2.18B).

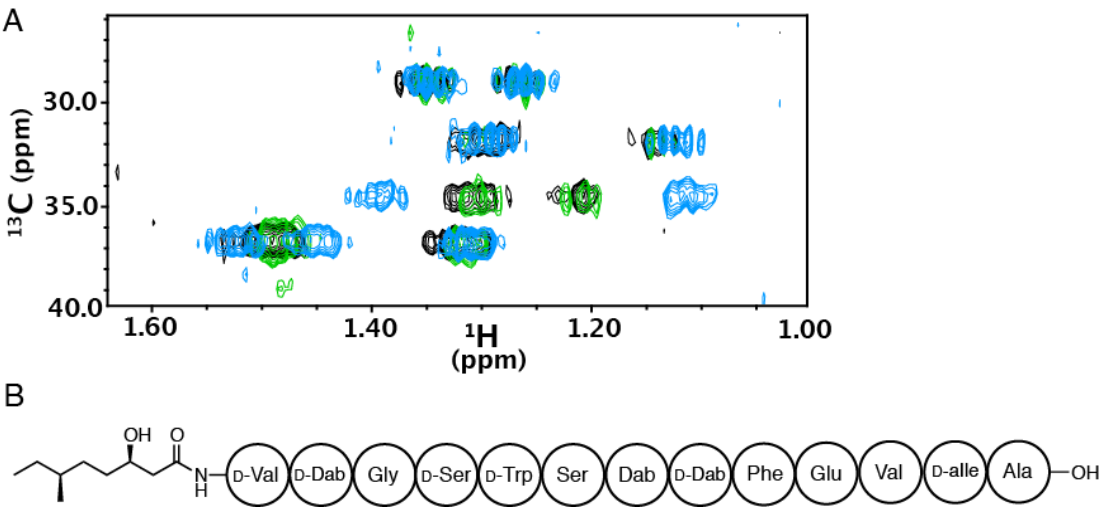

Figure 2.18. Determination of the tridecaptin A_1 lipid chain stereochemistry. (A) Overlap of ^{13}C-HSQC spectra of natural tridecaptin A_1 (green), (3*R*,6*S*)-tridecaptin A_1 (black) and (3*R*,6*R*)-tridecaptin A_1 (blue). The spectra of the (3*R*,6*S*)-stereoisomer closely matched the natural stereoisomer. (B) Full stereochemical structure of tridecaptin A_1.

2.2.2.6. Tridecaptin A_1 antimicrobial activity

As tridecaptin A_3 was shown to be responsible for the anti-*Campylobacter* properties of *P. polymyxa* NRRL B-30509, tridecaptin A_1 was tested against *C. jejuni*. A clear zone of inhibition was observed for tridecaptin A_1 against *C. jejuni* NCTC 11168 via a spot-on-lawn assay. Therefore, tridecaptin A_1 was responsible for the activity against *Campylobacter* spp. instead of SRCAM 1580.

The spectrum of activity of tridecaptin A_1 was tested against a selection of other bacteria (Table 2.4). As had been previously described,[125] tridecaptin A_1 showed antimicrobial activity primarily against Gram-negative indicator organisms, with strong inhibition of *Salmonella enterica* observed. The majority of the Gram-positive indicator

organisms were unaffected, although inhibition of *Bacillus subtilis* and *Staphylococcus aureus* was observed.

Table 2.4. Tridecaptin A_1 spectrum of activity

Indicator organism	MIC (μM)[a]
Gram-positive bacteria	
B. subtilis JH642	50
C. maltaromaticum UAL26	-
E. faecium ATCC 19434	-
L. lactis subsp. *cremoris* HP	-
L. monocytogenes ATCC 15313	-
P. polymyxa NRRL B-30509	-
P. acidilactici PAC 1.0	-
S. aureus ATCC 25923	100
Gram-negative bacteria	
C. jejuni NCTC 11168	100
E. coli DH5α	50
S. enterica serovar Typhimurium ATCC 13311	25
P. aeruginosa ATCC 15442	-

[a] MIC is based on the lowest serial dilution of tridecaptin A_1 at which inhibition of the indicator strain was observed via spot-on-lawn assay. No inhibition at 200 μM is represented by a dash.

2.2.2.7. Tridecaptin A_1 biosynthetic gene cluster

Based on the structure of tridecaptin A_1, it was almost certainly a non-ribosomal peptide synthetase (NRPS) product. The presence of D-amino acids, the non-proteinogenic amino acid 2,4-diaminobutyrate and the N-terminal lipid chain are consistent with an NRPS origin. As described previously, NRPSs are modular proteins consisting of a repeating series of domains.[83] Briefly, adenylation (A) domains activate a particular amino acid, which is loaded onto a thiolation (T) domain. An optional epimerase (E) domain C-terminal to a T domain may catalyze the epimerization of the loaded amino acid. Condensation (C) domains catalyze the formation of peptide bonds

between amino acids loaded on adjacent T domains. Finally, the thioesterase (TE) domain catalyzes the offloading of the peptide chain, most commonly through cyclization or hydrolysis.

A list of all potential open reading frames created from the genome sequence of *P. terrae* NRRL B-30644 was searched for A domains. While a long list of hits was obtained, the majority of these open reading frames were cut off at the edges of contigs. Due to the very high sequence similarity between NRPS domains, the process of assembling sequencing reads was likely unable to connect the different repeating NRPS units. However, putative gene clusters involved in tridecaptin production had been previously reported.[137,138] Further, a likely candidate gene cluster was identified in the genome of *P. polymyxa* NRRL B-30509. Using these similar gene clusters as a template, Vederas group research associate Dr. Marco van Belkum was able to piece together contigs through PCR and sequencing reactions to obtain the putative tridecaptin A_1 biosynthetic gene cluster from *P. terrae* NRRL B-30644 (Figure 2.19).

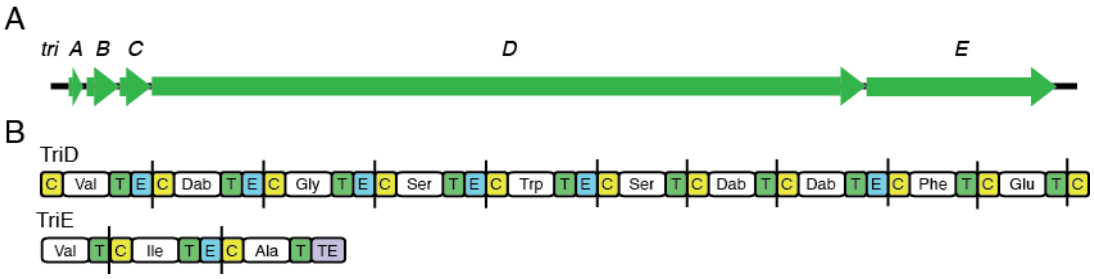

Figure 2.19. Putative tridecaptin A_1 biosynthetic gene cluster and predicted domains of TriD and TriE. (A) Biosynthetic gene cluster. (B) Arrangement of domains in TriD and TriE. Condensation domains in yellow, adenylation domains in white with selected amino acid indicated, thiolation domains in green, epimerase domains in blue, and thioesterase domain in purple.

The tridecaptin A_1 biosynthetic gene cluster is predicted to encode five proteins. The domain architecture of NRPSs TriD and TriE were analyzed using bioinformatic

tools. Together, these two proteins contain thirteen A domains with predicted amino acid specificities consistent with the tridecaptin A_1 amino acid sequence. Further, the positions of E domains were consistent with the positions of the D-amino acids in tridecaptin A_1. The presence of the C domain at the N-terminus of TriD is likely responsible for selecting and loading the lipid chain onto the N-terminal D-Val residue. Based on these characteristics, this gene cluster is a strong candidate for the biosynthesis of tridecaptin A_1.

Situated near *triD* and *triE* are three other genes expected to be involved in tridecaptin production. TriA is expected to be a thioesterase involved in off-loading TriD and/or TriE should they become misacylated.[139] The other two proteins, TriB and TriC, show sequence homology to ABC transporter proteins and are likely involved in the export of tridecaptin A_1. To establish the role of this gene cluster in tridecaptin biosynthesis, attempts were made to knock out TriD. For this purpose, a plasmid unable to replicate in Gram-positive bacteria encoding two regions of *triD* separated by a resistance marker was purchased. It proved possible to prepare electrocompetent cells from *P. terrae* NRRL B-30644, although the transformation efficiency was relatively low. Transformation of electrocompetent cells with the plasmid bearing the resistance marker did not result in any transformants. Ultimately, this strain proved refractory towards recombination-based gene knockouts. Still, based on the bioinformatic analysis of the gene cluster, it is the strongest candidate for tridecaptin biosynthesis.

2.2.2.8. Isolation and characterization of paenicidin B

Following a similar purification approach as described above, an HPLC fraction active against Gram-positive indicator organism *L. lactis* was obtained. By MALDI-TOF

MS, this fraction displayed a strong signal at $[M+H]^+$ = 3290.4. Attempted MS/MS analysis of this peptide demonstrated limited fragmentation, as was seen above with paenicidin A. However, a short amino acid sequence could be determined based on this data. Searching the genome of *P. terrae* NRRL B-30644 for an open-reading frame encoding this sequence yielded a candidate structural gene, which displayed very high sequence homology to paenicidin A. Based on these results, this isolate was given the name paenicidin B.

The structural gene for paenicidin B (*pabA*) was clustered with genes highly similar to those involved in paenicidin A production (Figure 2.20, Table 2.5). PabB and PabC likely act as dehydratases and cyclases, respectively, forming Lan and MeLan residues. PabT is likely the ABC transporter for initial export of paenicidin B, while PabFEG form an ABC transporter that may confer immunity. As before, no dedicated protease was found in the gene cluster, with this function likely being performed by an unrelated protease.

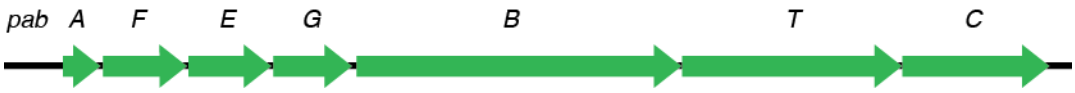

Figure 2.20. Putative paenicidin B biosynthetic gene cluster.

Table 2.5. Analysis of putative paenicidin B biosynthetic proteins.

Protein	Predicted Function	% Amino Acid Identity to Paenicidin A Homolog
PabA	Lantibiotic precursor peptide	93
PabF	ATP binding protein	88
PabE	ABC transporter membrane-bound subunit	71
PabG	ABC transporter membrane-bound subunit	75
PabB	Lantibiotic dehydratase	74
PabT	ABC transporter	84
PabC	Lantibiotic cyclase	80

Sequence alignment of paenicidins A and B revealed that only two amino acids differed in the core peptide (Figure 2.21). None of these altered positions corresponded to the cysteines, serines, and threonines involved in Lan and MeLan residues in paenicidin A. Comparison of the observed molecular weight with that of the molecular weight calculated for the unmodified amino acid sequence suggested that, like paenicidin A, paenicidin B was dehydrated six times during maturation. Furthermore, the MS/MS data for paenicidin B revealed similar fragmentation sites as observed for paenicidin A. Therefore, paenicidin B likely has six Lan and MeLan rings with ring topologies identical to those found in paenicidin A.

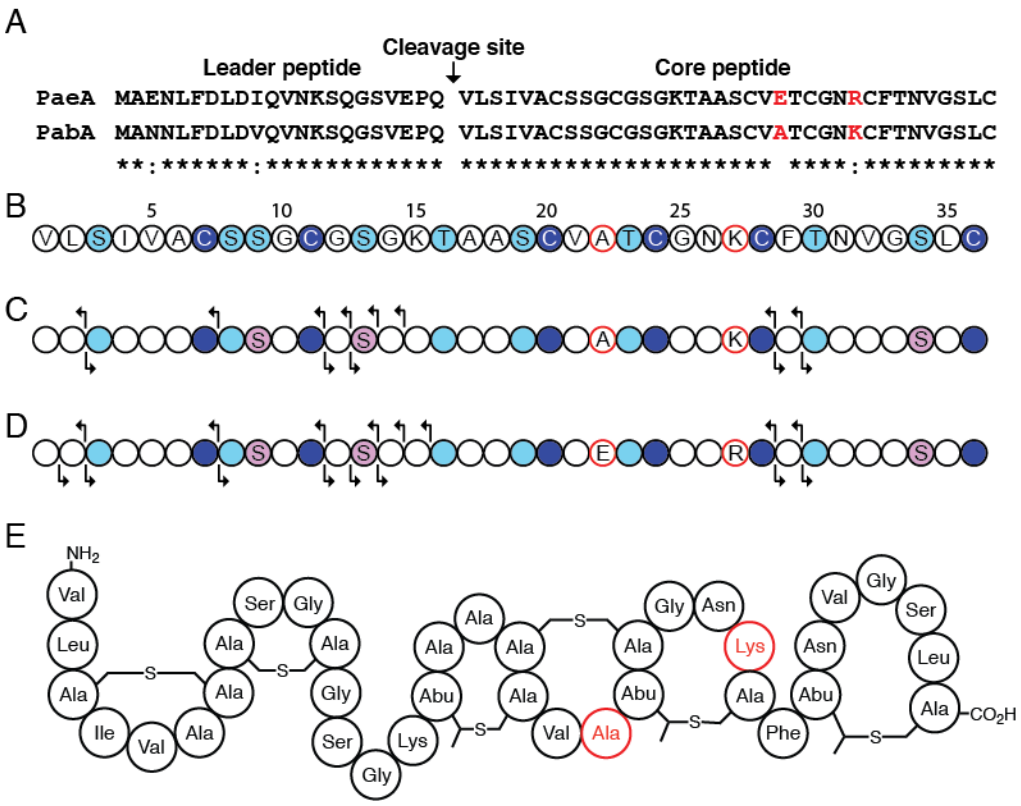

Figure 2.21. Comparison of paenicidin B amino acid sequence and MS/MS data with paenicidin A. (A) Sequence alignment of paenicidin A precursor (PaeA) with paenicidin B precursor (PabA). Conserved residues are indicated with an asterisk and conservative substitutions with a colon. (B) Amino acid sequence of paenicidin B without leader sequence. Summary of MS/MS data for (C) paenicidin B and (D) paenicidin A. Residues genetically encoded as serines and threonines are indicated in light blue, cysteines are in dark blue, and unmodified serines are in purple. (E) Bead structure of paenicidin B with the Lan and MeLan connectivities indicated. Residues indicated in red differ between paenicidins A and B.

As with paenicidin A, paenicidin B is predicted to exert its antimicrobial effects by binding to lipid II. The two N-terminal Lan residues resemble the nisin pyrophosphate cage motif responsible for binding to the lipid II pyrophosphate moiety.[14] The remainder of the peptide is predicted to be involved in pore formation. The variations between paenicidins A and B both occur within the central interlocking ring system, with the conservative substitution of an arginine with lysine, and the more dramatic replacement of a glutamate with an alanine residue. If this region is indeed involved in pore formation, it is difficult to predict the impact of these two differences on activity.

2.2.2.9. Paenicidin B spectrum of activity

Purified paenicidin B was tested against a variety of Gram-positive and Gram-negative indicator strains (Table 2.6). As expected, none of the Gram-negative strains tested were inhibited by paenicidin B. The spectrum of activity of paenicidin B against Gram-positive bacteria was similar to that for paenicidin A, although there were minor differences. Ultimately, both paenicidin peptides exert fairly narrow spectra of activity.

Table 2.6. Paenicidin B spectrum of activity

Indicator organism	MIC (μM)[a]
Gram-positive bacteria	
B. subtilis JH642	50
C. maltaromaticum UAL26	-
E. faecium ATCC 19434	-
L. lactis subsp. *cremoris* HP	12.5
L. monocytogenes ATCC 15313	100
P. polymyxa NRRL B-30509	-
P. acidilactici PAC 1.0	-
S. aureus ATCC 25923	100
Gram-negative bacteria	
C. jejuni NCTC 11168	-
E. coli DH5α	-
S. enterica serovar Typhimurium ATCC 13311	-
P. aeruginosa ATCC 15442	-

[a] MIC is based on the lowest serial dilution of paenicidin B at which inhibition of the indicator strain was observed via spot-on-lawn assay. No inhibition at 200 μM is represented by a dash.

2.2.3. *Paenibacillus polymyxa* NRRL B-30507

2.2.3.1. Genome sequencing

P. polymyxa NRRL B-30507 was reported to produce SRCAM 37, another of the supposed bacteriocins active against *C. jejuni*.[124] To examine for the presence of a structural gene for SRCAM 37, and to obtain information regarding other biosynthetic

gene clusters, the genome of this strain was sequenced. However, no structural gene encoding SRCAM 37 was found. Instead, potential bacteriocin, polyketide synthase, and NRPS gene clusters were identified. The NRPS genes were fragmented over many contigs, so it was not possible to predict their products on the basis of the genomic data. Still, genes encoding homologs of the tridecaptin A_1 biosynthetic proteins TriA, TriB and TriC were identified, suggesting the potential production of tridecaptin by this strain. No structural gene encoding a paenicidin-like lantibiotic was found.

2.2.3.2. Deferred inhibition assays

P. polymyxa NRRL B-30507 was tested for antimicrobial activity against *C. jejuni* using a deferred inhibition assay. As had been reported, this strain did inhibit the growth of *C. jejuni*. Based on similarities to *P. polymyxa* NRRL B-30509 and *P. terrae* NRRL B-30644 and the presence of the tridecaptin biosynthetic gene homologs in the genome, this strain was expected to produce tridecaptin. Antimicrobial activity against other bacterial strains was not tested through deferred inhibition assays.

2.2.3.3. Isolation of antimicrobial components

With internship student Manon Bels (Univ. de Lilles), culture supernatant of *P. polymyxa* NRRL B-30507 was fractionated using hydrophobic Amberlite XAD16 resin. This yielded a single fraction active against the Gram-negative indicator *E. coli*, while no activity was observed against the Gram-positive indicator *L. lactis*. The antimicrobial activity was further purified using a C_{18} solid-phase extraction cartridge, followed by reversed-phase HPLC. Three separate HPLC fractions displayed antimicrobial activity against *E. coli* by spot-on-lawn testing. Using MALDI-TOF MS, the first two fractions to

elute showed strong signals at $[M+H]^+$ = 1189.3 and 1203.4, while the strongest signal of the third fraction appeared at $[M+H]^+$ = 1458.6.

2.2.3.4. Identification of polymyxins B1 and B2

The masses observed in the first two antimicrobial fractions differed from those of polymyxins E1 and E2 by only 34 Da. Comparison of these masses to other known polymyxin variants suggested that they might correspond to polymyxins B1 and B2 (Figure 2.22). Polymyxins B and E differ based on the amino acid in position 6; polymyxin B bears a phenylalanine at this position, while polymyxin E bears a leucine.[79] MS/MS fragmentation data acquired for the isolated polymyxins closely matched MS/MS data acquired for commercial polymyxins B1 and B2. Therefore, it appears that *P. polymyxa* NRRL B-30507 produces polymyxins B1 ($[M+H]^+$ = 1203.4) and B2 ($[M+H]^+$ = 1189.3). However, as with *P. polymyxa* NRRL B-30509, these polymyxins are unlikely to be responsible for the antimicrobial activity against *C. jejuni*.

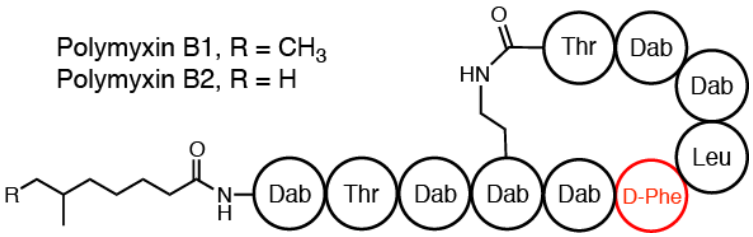

Figure 2.22. Bead structures of polymyxins B1 and B2. The identity of residue 6, indicated in red, is the sole difference between polymyxin B (D-Phe) and polymyxin E (D-Leu).

2.2.3.5. Identification and characterization of tridecaptin B_1

The mass of the major component ($[M+H]^+$ = 1458.6) in the later-eluting antimicrobial fraction was at least 92 Da smaller than the tridecaptin A variants isolated from the two other *Paenibacillus* spp. However, MS/MS analysis of this isolate suggested

a similar amino acid sequence as tridecaptin A, with two major differences (Figure 2.23). First, the data suggested that Phe-9 was replaced with leucine or isoleucine. Furthermore, the combined molecular mass of the N-terminal amino acid and the lipid chain was smaller than that of Val-1 and the β-hydroxy lipid chains found in tridecaptin A_1. No likely signals corresponding to fragmentation between the lipid chain and the presumed first residue were observed, and so this region remained ambiguous. Elemental composition based on high-resolution ESI-MS ($[M+H]^+$ = 1458.8296; calculated 1458.8315) taken with the MS/MS data suggested the absence of a hydroxyl group on the lipid chain of this isolate.

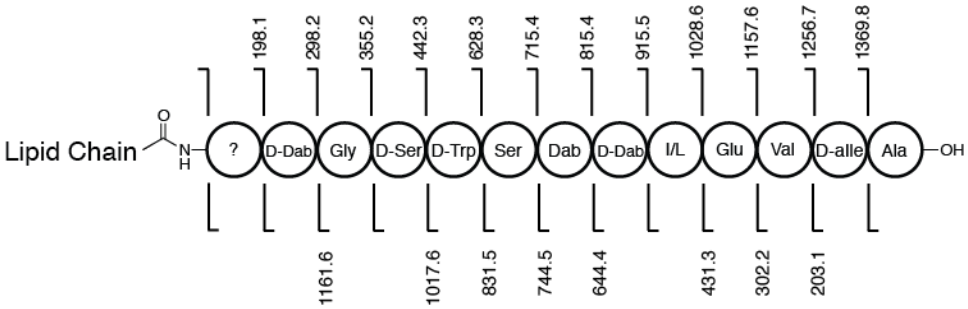

Figure 2.23. Summary of MS/MS fragment ions for tridecaptin isolated from *P. polymyxa* NRRL B-30507.

2.2.3.6. NMR spectroscopic characterization

To identify the lipid chain and the amino acids in positions 1 and 9, TOCSY and NOESY datasets for the tridecaptin isolate were acquired. After the ordering and identification of spin systems (Figure 2.24), the majority of the proton chemical shifts were assigned (Table 6.4). Based on these data, residue 9 was suggested to be isoleucine, while residue 1 was identified as glycine. In combination with the MS/MS and HR-ESI-MS data, the NMR data suggested that the lipid chain consisted of nine carbons.

Furthermore, the chemical shifts corresponding to the lipid chain were consistent with the absence of a hydroxyl group. Based on the branching lipid chains seen for other tridecaptins, this tridecaptin isolate was predicted to be either the 6-methyl or the 7-methyloctanamide.

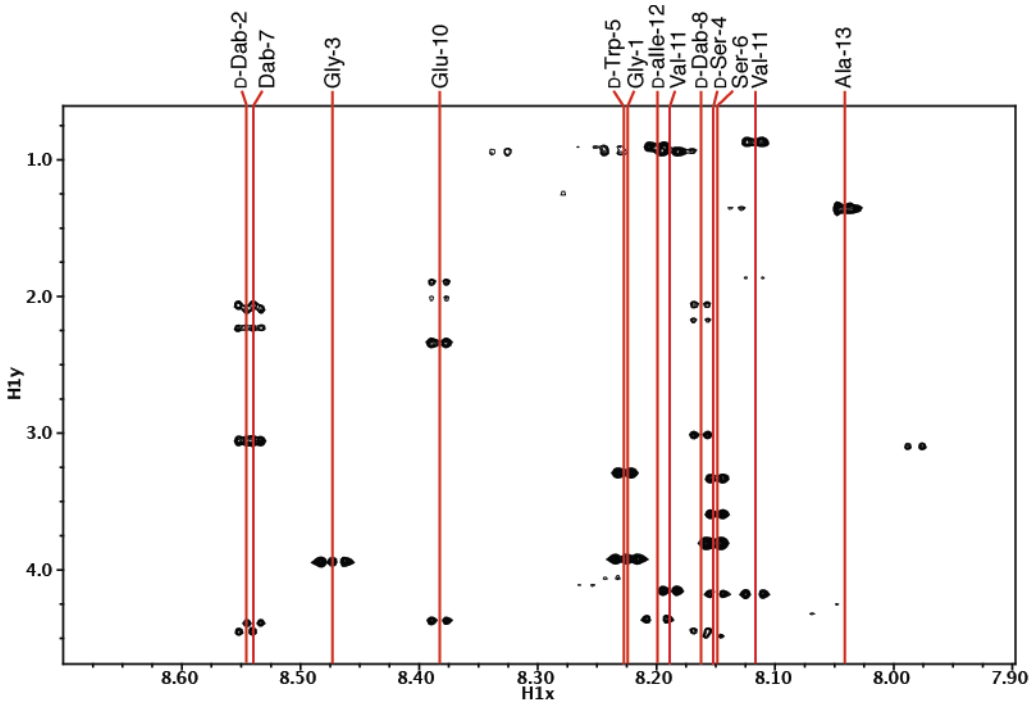

Figure 2.24. Partial TOCSY spectrum of tridecaptin B_1 with assigned spin systems.

The proposed structure of this isolate bears similarity to tridecaptin Bα (Figure 2.25).[140] The four described tridecaptin B variants all bear a 6-methyloctanamide lipid chain, a glycine in position 1, and an isoleucine or valine residue in position 9. However, the C-terminal residue of these tridecaptin B variants is a serine, while the isolate from *P. polymyxa* NRRL B-30507 contains an alanine in this position. Still, based on the overall similarity, this isolate was designated tridecaptin B_1.

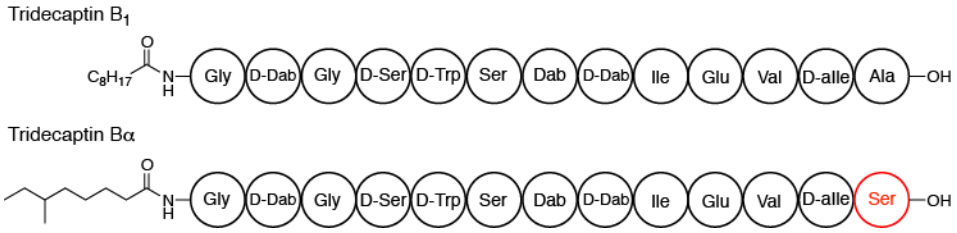

Figure 2.25. Bead structures of tridecaptin B_1 and Bα. The difference between these structures, the identity of residue 13, is highlighted in red.

2.2.3.7. Tridecaptin B_1 variants

By HPLC, several peptides of similar masses co-eluted with tridecaptin B_1. These peptides were analyzed by MS/MS, indicating that they were variants of tridecaptin B_1 with single amino acid substitutions. Other than a derivative of tridecaptin B_1 in which D-Trp-9 was oxidized, two main variants were observed. Tridecaptin B_2 bears D-Val in place of D-allo-Ile-12, while Glu-10 is replaced with Asp in tridecaptin B_3. These variants were attributed to promiscuity of the NRPS adenylation domains involved in tridecaptin biosynthesis. As these variants could not be separated from tridecaptin B_1 by HPLC, the impact of these substitutions on activity could not yet be characterized.

2.2.3.8. Synthesis and characterization of octyl-tridecaptin B_1

The chemical synthesis of tridecaptins B_1, B_2 and B_3 would allow for the production and isolation of a single pure variant, and also serve to support the structural assignments based on NMR and MS/MS. With Manon Bels, the tridecaptin B_1 amino acid sequence was prepared using an automated peptide synthesizer. As the structure of the lipid chain was not yet known, the N-terminus was acylated with an unmethylated octanamide group. The octanamide variant of tridecaptin A_1 had been found to demonstrate a similar extent of activity as natural tridecaptin A_1.[141] Oct-TriB_1 was then fully deprotected, purified by HPLC and lyophilized.

The synthetic Oct-TriB_1 was tested for its activity against *E. coli*. However, Oct-TriB_1 was less potent than Oct-TriA_1, with an MIC value 16x higher. Comparison of TOCSY spectra for natural tridecaptin B_1 and the synthetic Oct-TriB_1 mostly showed very good overlap of signals. As expected, the signals corresponding to the lipid chain were different. However, the amide proton of Ala-13 also differed by 0.04 ppm. Although the lipid chain and Ala-13 are at opposite termini, it is possible that the use of the unmethylated octanamide lipid chain was responsible for this shift. Efforts are underway to identify the structure of the natural tridecaptin B_1 lipid chain via the synthesis of the different possible isomers.

2.3. Conclusions and future directions

These studies have described the range of antimicrobial peptides produced by three *Paenibacillus* spp. Instead of the anti-*Campylobacter* SRCAM peptides reportedly produced by these strains, this activity was instead attributed to the production of several variants of the lipopeptide tridecaptin. The tridecaptin variants show diversity of amino acid sequence and lipid chain length and functionalization. The tridecaptin biosynthetic gene cluster in *P. terrae* NRRL B-30644 was identified and characterized, containing two NRPSs responsible for selecting all 13 amino acids. In addition to tridecaptins, two of these strains were found to produce the cyclic lipopeptides polymyxins B and E.

Study of these strains has also resulted in the discovery of two novel lantibiotics, paenicidin A and B. Both paenicidins are highly cyclized, containing six Lan and MeLan residues. Elucidation of the Lan and MeLan connectivity of paenicidin A required the development of a new approach wherein the lantibiotic is partially desulfurized and

analyzed by MS/MS. Paenicidins A and B demonstrate relatively narrow spectra of antimicrobial activity against Gram-positive bacteria.

It is of interest to determine if the combination of paenicidin, polymyxin and/or tridecaptin demonstrates any synergistic antimicrobial activity. The combination of nisin and polymyxin[142] and of lacticin 3147 and polymyxin[143] results in stronger activity against both Gram-positive and Gram-negative bacteria. However, these reports involve peptides produced by two different bacterial strains. The potential for one bacterial strain to produce multiple antimicrobial peptides that exert synergistic activity deserves further investigation. While this likely provides the producer strain with a competitive advantage in its ecological niche, it may also provide it with desirable properties for use in food preservation and livestock protection. Furthermore, the synergistic properties may decrease the levels of toxic biomolecules (e.g., the potentially nephrotoxic polymyxins) required to effect the desired inhibition of pathogenic bacteria.

While the modes of action of the polymyxins and several lantibiotics have been well studied, nothing is known about the mode of action of tridecaptins. Due to the broad structural similarities of tridecaptins and polymyxins, both being cationic lipopeptides, they might be expected to exert their antimicrobial effects through similar means. However, the differences in target spectrum (e.g., tridecaptin targets *C. jejuni*, polymyxin does not) suggest that they may act differently. Work is underway by Vederas group graduate student Stephen Cochrane to elucidate the antimicrobial mode of action of tridecaptin.

With the structures and activities of the antimicrobial peptides produced by these *Paenibacillus* strains better understood, the potential application of these strains and their

products to food preservation and livestock protection may be undertaken. Due to the association of several of these *Paenibacillus* strains with poultry, these strains may prove efficacious at decreasing the levels of *C. jejuni* in poultry-derived food products. Alternately, the isolated tridecaptin peptides could prove useful for a similar purpose. These *Paenibacillus* strains and their products are also currently under consideration for their use against a variety of fish pathogens. These peptides could potentially be used to prevent bacterial infections at commercial salmon farms, preventing the use of large quantities of antibiotics and the associated development of bacterial resistance.

Although there has been much interest in the use of bacteriocins and other antimicrobial peptides to control *Campylobacter jejuni*, few of these peptides have been well characterized. The results described herein demonstrate that tridecaptin is active against *C. jejuni*, and that the reported SRCAM peptides are not produced by these strains. This raises questions regarding further work done by the same group wherein the SRCAM peptides were shown to control *C. jejuni* in a chicken model.[144] The full characterization of the determinants of antimicrobial activity is a crucial foundation for further applications. While the work indicating that a product of *P. polymyxa* NRRL B-30509 successfully controlled *C. jejuni in vivo* may be valid, the misattribution of this activity casts significant doubt on what may otherwise be an important or useful discovery. With the anti-*Campylobacter* activity of tridecaptin established, its use for food protection and livestock protection can begin in earnest.

Chapter 3

Structural and biosynthetic studies of carnolysin

3.1. Background

3.1.1. Enterococcal cytolysin

Enterococci are a group of Gram-positive facultative anaerobic bacteria representing a principal component of the human commensal intestinal microbiota.[145] Currently, enterococci are one of the most prevalent causes of multidrug resistant nosocomial infections worldwide.[146] The majority of these infections are caused by two enterococcal species, *E. faecalis* and *E. faecium*. Isolates of *E. faecalis* have been found to exhibit a hemolytic phenotype when grown on blood agar. Furthermore, these hemolytic strains also demonstrated antimicrobial properties against other Gram-positive bacteria.

Mutational analysis using UV irradiation demonstrated that the hemolytic and antibacterial properties are related.[147] This hemolytic and bactericidal component, enterococcal cytolysin, was associated with increased toxicity of enterococcal infections. In a mouse intraperitoneal infection model, the production of cytolysin was related to a much greater mortality rate than that of cytolysin-negative enterococci.[148]

Enterococcal cytolysin consists of two components: a larger peptide encoded by the gene $cylL_L$ and a smaller peptide encoded by the gene $cylL_S$.[149] The biosynthetic gene cluster responsible for the production of cytolysin may be encoded within chromosome-associated pathogenicity islands or on pheromone responsive-plasmids.[146] Genetic evidence suggested that cytolysin is a lantibiotic, as the structural genes were grouped

with other genes encoding homologues of lantibiotic biosynthetic enzymes. Additionally, amino acid analysis of both cytolysin peptides indicated the presence of lanthionine (Lan) and/or methyllanthionine (MeLan) (Figure 3.1).[150]

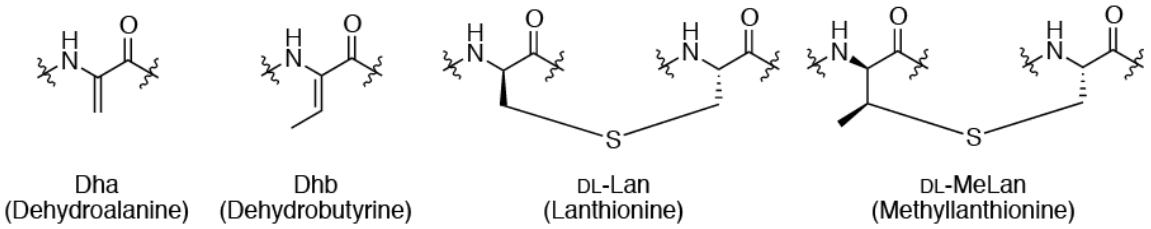

Figure 3.1. Structures of dehydroalanine, dehydrobutyrine, lanthionine and methyllanthionine.

Apart from the two structural genes, six other genes were implicated in the biosynthesis of cytolysin (Figure 3.2).[151] Genes *cylR1* and *cylR2* encode a two-component regulator involved in controlling cytolysin production. Derepression of CylR1 and CylR2 occurs via a quorum-sensing mechanism, wherein cytolysin production is autoinduced once one of the cytolysin peptides reaches a threshold concentration.[152] CylM shows sequence homology to known LanM-type lantibiotic synthetases, and is involved in the formation of dehydroalanine (Dha), dehydrobutyrine (Dhb), Lan and MeLan residues (Figure 3.1). CylB is homologous to lantibiotic transporter proteins. Like these homologues, CylB contains both an ATP binding cassette (ABC)-transporter domain and a protease domain. The sequence of CylA resembles known serine proteases, while the presence of an N-terminal signal peptide sequence indicates that this protease acts extracellularly. Finally, CylI acts as an immunity protein, protecting the producer strain from the antimicrobial properties of cytolysin.[153]

Figure 3.2. Enterococcal cytolysin biosynthetic gene cluster.

$CylL_L$ and $CylL_S$ are first expressed as precursor peptides of 68 and 63 amino acids, respectively (Figure 3.3). Modification by CylM yields the post-translationally modified $CylL_L^*$ and $CylL_S^*$ peptides. Thereafter, CylB cleaves a portion of the $CylL_L^*$ and $CylL_S^*$ leader peptide sequences yielding $CylL_L'$ and $CylL_S'$, respectively, and exports these peptides. Extracellular protease CylA performs another proteolytic cleavage, yielding the fully mature, doubly-cleaved, $CylL_L''$ and $CylL_S''$ peptides.

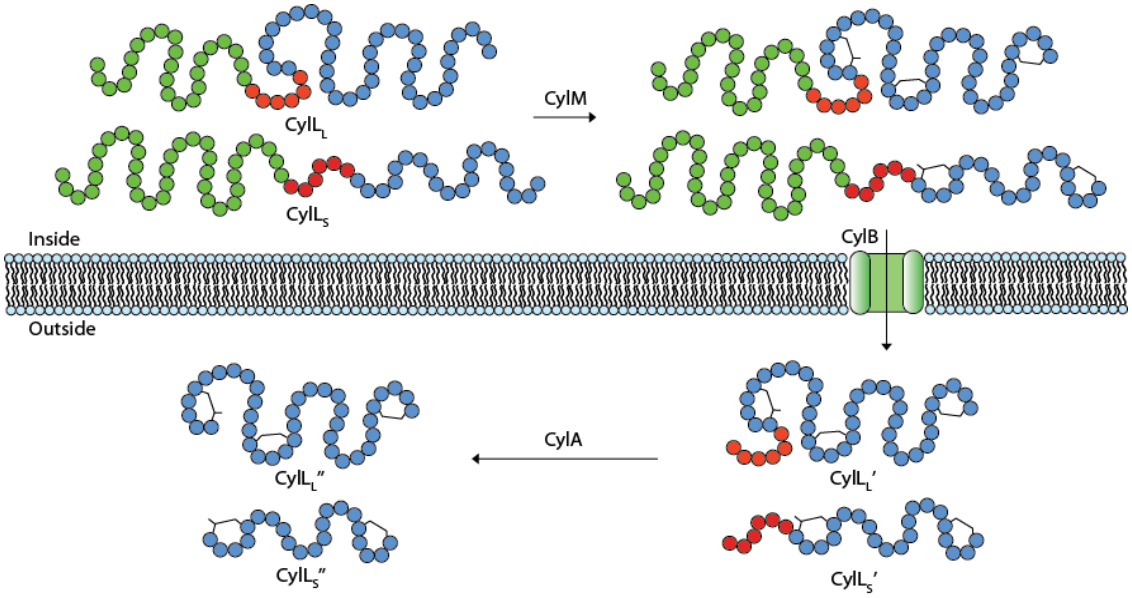

Figure 3.3. Biosynthetic pathway for cytolysin. Green circles represent the leader sequence removed by transporter CylB, red circles are the leader sequence removed by protease CylA, while blue circles are the amino acids that make up the mature peptide.

Recently, the post-translational modifications of $CylL_L''$ and $CylL_S''$ were fully characterized by Tang and van der Donk.[13] Due to the low levels of production by

cytolysin-positive enterococci, the biosynthetic genes were expressed in *E. coli*. Specifically, the cytolysin structural genes were co-expressed with *cylM*, and the post-translationally modified peptides (with N-terminal hexahistidine tags) were purified by Ni^{2+}-affinity chromatography. Site-directed mutagenesis was used to place a lysine residue immediately N-terminal to the predicted CylA cleavage sites, allowing for the use of trypsin to obtain mature $CylL_L''$ and $CylL_S''$. The structures of the enterococcal cytolysin peptides were characterized using MS/MS and NMR. Based on these data, the primary structures of these peptides were determined (Figure 3.4).

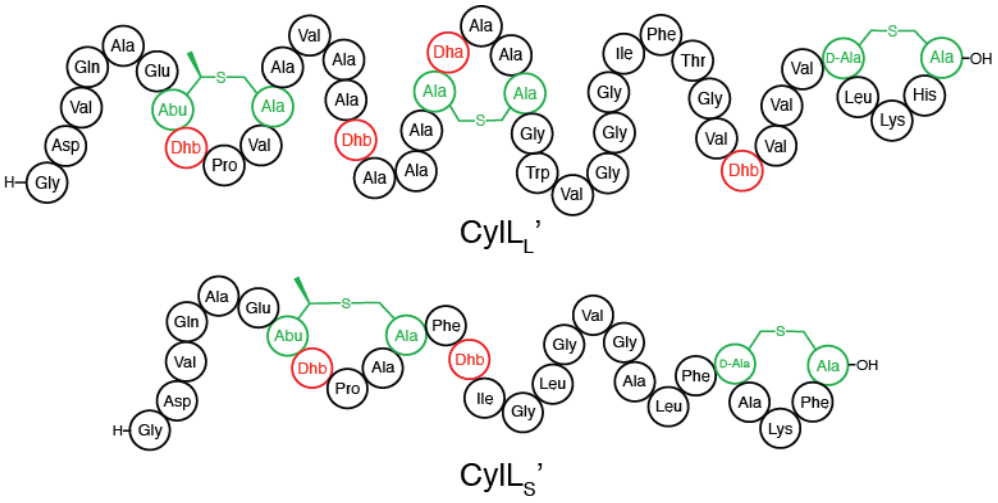

Figure 3.4. Bead structures of cytolysin L_L' and cytolysin L_S'. Dha and Dhb are indicated in red, while Lan and MeLan are in green.

The stereochemistry of the cytolysin Lan and MeLan residues were characterized using chiral GC-MS.[13] Previously, the stereochemistry of Lan and MeLan residues in all stereochemically defined lantibiotics were exclusively the DL-stereoisomers.[13] However, cytolysin was found to contain the unusual LL-Lan and LL-MeLan stereoisomers, in addition to the more typical DL-Lan. Through the creation of mutants, the positions of the

LL-Lan and DL-Lan residues were identified in $CylL_L'$. It was noted that the unusual LL-Lan and LL-MeLan residues all contained a Dha or Dhb residue as the most N-terminal amino acid contained with the ring. It was suggested that the presence of this dehydro residue altered the trajectory of the cysteine thiol during Lan/MeLan formation, resulting in the different stereochemistry. Investigation of Lan and MeLan stereochemistry of the β-peptide of two-component lantibiotic haloduracin revealed the presence of a LL-MeLan residue, also containing an N-terminal dehydro residue within the rings.[13] The stereochemistry of Lan and MeLan residues is often an essential factor for biological activity; varying the stereochemistry of the Lan/MeLan residues in the lantibiotic lacticin 481 was found to abolish antimicrobial activity.[154]

3.1.2. *Carnobacterium* spp. and their bacteriocins

One of the primary areas of interest related to bacteriocins and the bacteria that produce them is for the purpose of food preservation.[3] Many bacteriocins produced by Gram-positive bacteria demonstrate potent inhibition of important food pathogens, such as *Listeria* and *Clostridium* spp. Additionally, many bacteriocin producers are naturally associated with foods. A major group of Gram-positive bacteriocin producers associated with food are the lactic-acid bacteria (LAB). LAB have been used for thousands of years in the preparation of fermented milk products, including cheese, butter and yogurt. Bacteriocin-producing LAB of note belong to several genera, including *Lactobacillus* spp., *Lactococcus* spp., *Pediococcus* spp., and *Carnobacterium* spp. While bacteriocin-producers have seen wide-spread use in food preparation, very few purified or extracted bacteriocins have been used industrially for food preservation. Nisin, a lantibiotic produced by strains of *Lactococcus lactis*, has been used as a food preservative for

several decades. Pediocin PA-1, a class IIa bacteriocin produced by strains of *Pediococcus acidilactici*, has also been developed for food biopreservation.[3]

Carnobacterium spp. have been found to produce a diverse array of bacteriocins, and many strains produce more than one bacteriocin. Primarily, class IIa bacteriocins with similarities to pediocin PA-1 have been isolated from these strains. For example, *C. piscicola* LV17B (now *C. maltaromaticum*) produces class IIa bacteriocins carnobacteriocin BM1 (CbnBM1) and carnobacteriocin B2 (CbnB2).[155] In addition to CbnBM1, *C. maltaromaticum* UAL26 produces class IIa bacteriocin piscicolin 126.[156] Other types of bacteriocins have also been described from *Carnobacterium* spp. The circular bacteriocin carnocyclin A is produced by *C. maltaromaticum* UAL307, a strain that also produces CbnBM1 and piscicolin 126.[157] The partially-characterized lantibiotic carnocin UI49 was isolated from a strain of *C. piscicola*.[158] The production of multiple bacteriocins by these strains offers several advantages, including a broader antimicrobial spectrum.

3.1.3. Prior characterization of *Carnobacterium maltaromaticum* C2

Carnobacterium maltaromaticum C2 was originally isolated from vacuum-packed fillets of surubim fish, and was identified due to its potent inhibition of *Listeria monocytogenes*. Our collaborators Fabricio Tulini and Prof. Elaine De Martinis isolated the major component responsible for this activity, and characterized it using MALDI-TOF MS and MS/MS.[109] This revealed that this strain produces the well-known class IIa bacteriocin CbnBM1, and its oxidized form CbnB1. Further investigation revealed other peptides that exhibited lower levels of antimicrobial activity. MS/MS analysis of one of these fractions indicated an amino acid sequence consistent with carnobacteriocin X

(CbnX), a peptide whose genetic determinants had been previously described but which had not otherwise been observed.

3.2. Results and Discussion

3.2.1. Genome sequencing of *Carnobacterium maltaromaticum* C2

As a means of better understanding *C. maltaromaticum* C2 and its potential application for food preservation, the genome of this strain was sequenced. Towards this end, genomic DNA was isolated from a culture of *C. maltaromaticum* C2 and sequenced with 454 pyrosequencing technology.[159] Based on the contig sequences, the size of the genome (and potentially plasmids) was approximately 3.6 Mbp. The GC content and 16S rRNA sequence resembled known *Carnobacterium* genome sequences.[160]

Within the genome, a small gene cluster containing the CbnBM1 structural gene and a gene for the cognate immunity protein CbiBM1 was identified.[161] Additionally, the gene cluster associated with the production of carnobacteriocin X and a variant of carnobacteriocin B2 was identified. While this gene cluster was distributed over several contigs, the genes were in a similar overall order and orientation as reported for *C. piscicola* LV17B.[161]

3.2.2. Activity-guided purification of antimicrobial peptides

Working with visiting collaborator Fabricio Tulini, an alternative purification approach was developed to isolate the antimicrobial peptides produced by *C. maltaromaticum* C2. Previously, an adsorption-desorption approach had been used, wherein manipulations of pH were used to control the binding of bacteriocins to bacterial cells.[162] Briefly, the new approach began with fractionating culture supernatant using Amberlite XAD16 resin. The resin was washed with increasingly hydrophobic aqueous

organic solvents, and the antimicrobial activity of the fractions was determined against the indicator strain *C. maltaromaticum* A9b-. The active fractions were further fractionated using a C_{18} solid-phase extraction cartridge, and the activity was followed as before. Finally, the antimicrobial components were purified by reverse-phased HPLC. The active fractions were examined using MALDI-TOF MS, indicating the presence of CbnBM1, CbnB1 and CbnX as before (Figure 3.5).

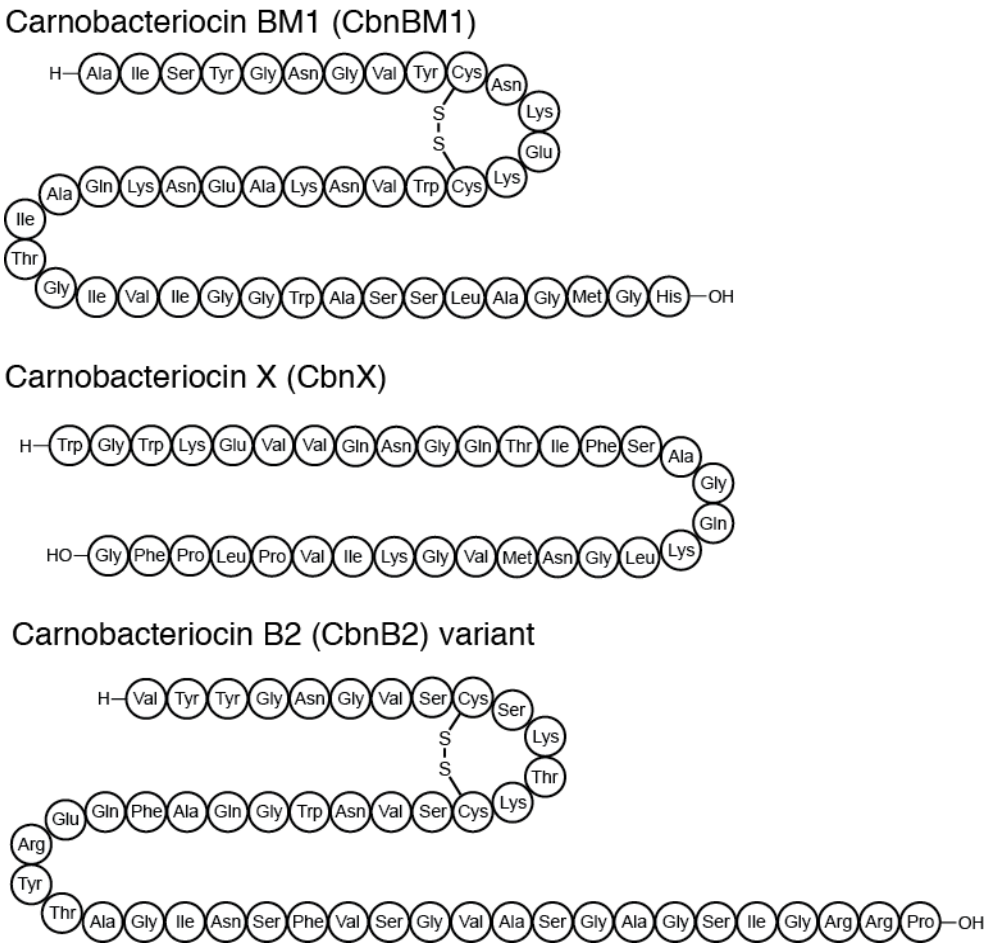

Figure 3.5. Bead structures of carnobacteriocin BM1, carnobacteriocin X and a variant of carnobacteriocin B2.

3.2.3. Identification of a carnobacteriocin B2 variant

After the departure of collaborator Fabricio Tulini, the antimicrobial peptides produced by this strain were further characterized. Following the modified purification approach, an HPLC fraction which displayed activity against indicator organism *Lactococcus lactis* showed a strong signal at $[M+H]^+$ = 5018.9 by MALDI-TOF MS. This closely matched the molecular weight of the predicted mature peptide encoded by the structural gene of the carnobacteriocin B2 variant seen during genome analysis. MS/MS confirmed this assignment, revealing that *C. maltaromaticum* C2 indeed produces a variant of CbnB2 (Figure 3.5). Compared with CbnB2, this variant bears a tyrosine residue in position 2 in place of an asparagine.

3.2.4. Initial isolation and MS/MS characterization of carnolysin

MALDI-TOF MS spectra of a later-eluting HPLC fraction obtained during the isolation of the other characterized bacteriocins revealed the presence of two major components ($[M+H]^+$ = 3050.5 and 4178.1). As these masses are within a range commonly observed for bacteriocins, the isolates were further characterized by MS/MS. From these data, partial amino acid sequences were obtained for both peptides. It was also observed that there were several regions of these peptides wherein no discernable fragmentation occurred. Within the partial sequences, the presence of amino acids such as Dha, Dhb, and potentially aminobutyrate (Abu) were suggested.

Dha and Dhb are commonly observed in lantibiotics, resulting from the dehydration of Ser and Thr, respectively. Furthermore, the absence of fragmentation in certain regions may sometimes be attributed to the presence of Lan and MeLan rings, as found in lantibiotics.[127] If the partial sequence containing Abu is accurate, the presence of

this amino acid is highly unusual, as it has not been observed in any lantibiotics to date. However, its presence may be explained by comparison to the lantibiotics lacticin 3147 and lactocin S. These peptides contain D-Ala residues that are derived from serines through a two-step process (Figure 3.6).[15,33] Following the dehydration of a serine residue to Dha, a reductase catalyzes its reduction to D-Ala. The presence of Abu could be analogously explained through the dehydration and reduction of a threonine residue (Figure 3.6).

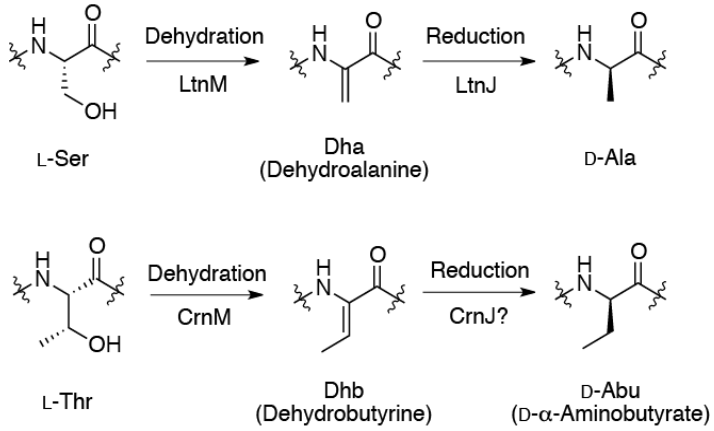

Figure 3.6. Proposed formation of α-aminobutyrate via reduction of dehydrobutyrine.

3.2.5. Identification of the carnolysin structural genes

Taking into consideration the amino acids from which the post-translationally modified residues were likely derived, the genome sequence was searched for the partial amino acid sequences obtained for both peptides. Candidate structural genes were identified for both peptides on different contigs in the genome. BLAST analyses of the two putative precursor peptides revealed sequence homology with the two-component lantibiotic enterococcal cytolysin. For this reason, the isolates from *C. maltaromaticum*

C2 were named carnolysin A1 and A2, and are encoded by the genes *crnA1* and *crnA2*. Carnolysin A1 is homologous to cytolysin L_L, while carnolysin A2 is homologous to cytolysin L_S (Figure 3.7). The open reading frames clustered with the carnolysin structural genes are homologous to the cytolysin biosynthetic genes. During the maturation of cytolysin, two proteolytic cleavages occur. The extent of proteolytic processing of cytolysin is indicated by a single quote or a double quote; $CylL_L'$ and $CylL_S'$ are singly cleaved, while $CylL_L''$ and $CylL_S''$ are doubly cleaved. The carnolysin peptides described above are cleaved at an analogous position to the first cleavage of the cytolysin peptides. For this reason, they were given the names CrnA1′ and CrnA2′.

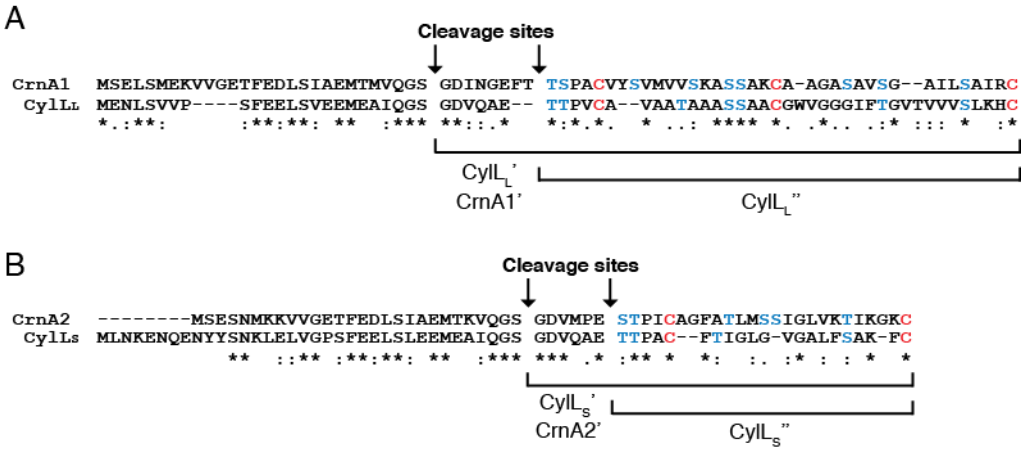

Figure 3.7. Sequence alignments of carnolysin with cytolysin. (A) Alignment of carnolysin A1 (CrnA1) with cytolysin L_L ($CylL_L$). (B) Alignment of carnolysin A2 (CrnA2) with cytolysin L_S ($CylL_S$). Conserved residues are indicated with an asterisk, conservative substitutions are indicated with a colon, and residues with weakly similar properties with a period. Serines and threonines are indicated in blue, while cysteines are in red. The regions corresponding to the proteolytically cleaved products are indicated below the sequences.

The partial amino acid sequences obtained from MS/MS of the isolated carnolysins were compared with the predicted gene products. This comparison suggested that the Abu residue is indeed derived from threonine. Additionally, several alanines

observed by MS/MS were in positions genetically encoded as serine residues. This represents further evidence that these peptides possess similar post-translational modifications as lacticin 3147 and lactocin S.

3.2.6. Assembly and description of the carnolysin gene cluster

While the cytolysin biosynthetic genes are clustered together, the two carnolysin structural genes were found on two separate small contigs in the genome. However, both of these contigs contain a partial open reading frame (ORF) with homology to *cylB*, the ABC transporter involved in cytolysin export. Some sequence of the contig containing *crnA1* was homologous to the 5' section of *cylB*, while the *crnA2* contig contained a sequence homologous to the 3' region of *cylB*. Therefore, the contigs encoding CrnA1 and CrnA2 are likely adjacent in the actual bacterial genome, and are fragmented in the center of an ORF. Comparison of the other genes on these contigs with the cytolysin gene cluster revealed that a large portion of a *cylM* homolog was missing at the edge of a contig, and no *cylI* homolog was detected. BLAST searches of the other contigs did not allow for the detection of these missing proteins. Therefore, it was necessary to determine the missing sequences at both ends of these contigs to obtain the full carnolysin biosynthetic gene cluster.

Using genomic DNA isolated from *C. maltaromaticum* C2, a fosmid library was prepared. Hybridization experiments using a labeled probe allowed for the identification of fosmids bearing the carnolysin gene cluster. Sequencing experiments were used to determine the sequences on either side of the known carnolysin gene cluster until the neighbouring contigs were identified. The gap in the *cylB* homolog was amplified by PCR and similarly sequenced.

Figure 3.8. Putative carnolysin biosynthetic gene cluster.

Analysis of the genes clustered with the carnolysin structural genes suggested that a total of seven genes are involved in carnolysin biosynthesis (Figure 3.8; Table 3.1). The carnolysin A1 structural gene (*crnA1*) encodes a peptide of 73 amino acids, while the carnolysin A2 structural gene (*crnA2*) encodes a peptide of 59 amino acids. The gene product of *crnM* is homologous to LanM-type lantibiotic synthetases such as CylM. This CrnM is most likely involved in the formation of Lan, MeLan, Dha and Dhb residues, forming CrnA1* and CrnA2*. A homologue of the dual ABC-transporter and protease CylB is encoded by *crnT*. The protease domain of CrnT is likely responsible for the first proteolytic cleavage involved in carnolysin maturation, forming CrnA1′ and CrnA2′. The gene *crnP* encodes a serine protease with homology to CylA. In cytolysin biosynthesis, CylA removes a conserved N-terminal hexapeptide sequence from $CylL_L'$ and $CylL_S'$, thereby forming Cyl_LL'' and $CylL_S''$.[150] However, the N-terminal amino acid sequences of CrnA1′ and CrnA2′ are not identical (Figure 3.7), and so it is not clear if CrnP cleaves one or both of these peptides.

Table 3.1. Description of putative carnolysin biosynthetic gene cluster.

Protein	Predicted Product or Function	Cytolysin Homolog	Size (a.a.)	Size (kDa)
CrnM	Lantibiotic synthetase	CylM	1003	117.3
CrnA1	Lantibiotic precursor peptide	$CylL_L$	73	7.4
CrnJ	Reductase	None	240	27.6
CrnT	ABC transporter	CylB	696	76.9
CrnP	Protease	CylA	454	50.8
CrnA2	Lantibiotic precursor peptide	$CylL_S$	59	6.2
CrnY	Transcriptional regulator	None	122	13.9

No homolog of *crnJ*, a putative reductase, is found in the cytolysin biosynthetic gene cluster. However, CrnJ shows sequence homology to LtnJ, the reductase involved in the biosynthesis of lacticin 3147.[33] Therefore, the presence of this gene is consistent with the observation of Ala and Abu residues in positions genetically encoded as Ser and Thr, respectively. As the biosynthesis of D-Ala in lacticin 3147 involves dehydration followed by reduction, CrnJ is most likely involved in the analogous transformation in carnolysin biosynthesis. The last gene, *crnY*, is similar to helix-turn-helix transcriptional regulators involved in modulating the biosynthesis of other lantibiotics. This differs from the regulation of cytolysin biosynthesis, which involves a two-protein quorum-sensing system.[152] Notably, no homologue of the cytolysin immunity protein *cylI* was found in the carnolysin gene cluster. This raises questions regarding how *C. maltaromaticum* C2 protects itself from any antimicrobial properties associated with carnolysin.

3.2.7. Attempted purification of CrnA1″ and CrnA2″

Spot-on-lawn testing of a mixture of CrnA1′ and CrnA2′ did not result in any observable antimicrobial activity. In the analogous cytolysin system, no hemolytic

activity was observed for a mixture of $CylL_L'$ and $CylL_S'$.[150] Only when a high concentration of $CylL_L'$ is mixed with the doubly cleaved $CylL_S''$ was a small amount of activity observed. When both peptides are doubly cleaved (i.e., $CylL_L''$ and $CylL_S''$), the strongest hemolytic activity was observed. Therefore, it was predicted that further proteolytic processing of CrnA1′ or CrnA2′ was required to obtain the predicted antimicrobial activity. As indicated above, the N-terminal differences between CrnA1′ and CrnA2′ make it unclear whether both sequences are cleavable by the same enzyme (i.e., CrnP), or whether cleavage of both peptides is necessary for activity.

The same purification approach was attempted as above, and all of the HPLC fractions were collected. These fractions were all examined by MALDI-TOF MS in an attempt to detect the putative CrnA1″ and CrnA2″ peptides. However, no masses consistent with these doubly-cleaved peptides were observed. *C. maltaromaticum* C2 was grown in several different liquid media with different growth times, but there was no indication of the hypothetical CrnA1″ and CrnA2″ peptides.

There are several possible explanations for the lack of the doubly-cleaved carnolysins. One possibility is that these doubly-cleaved peptides simply do not exist. However, the presence of a *cylA* homolog, *crnP*, in the gene cluster supports the possibility of a second cleavage step. It is possible that CrnP is inactive or not produced under the culture conditions used. Another potential explanation is that something happens to the doubly-cleaved peptides after their production, precluding their purification and observation by MS. Over time, a mixture of $CylL_L''$ and $CylL_S''$ formed stable aggregates (ranging from 132 kDa to greater than 216 kDa) which were resistant to boiling in 0.5 % sodium dodecyl sulfate.[163] If an analogous process occurs for carnolysin,

the absence of the doubly-cleaved peptides could simply be a result of this aggregation. Much of the work with cytolysin used mutant strains of *E. faecalis* expressing only one of the subunit peptides, as the separate cytolysin subunits did not appear to aggregate.[163]

3.2.8. Purification of CrnA1′ and CrnA2′

While the screening for CrnA1″ and CrnA2″ was ultimately unsuccessful, the testing of different media and growth times revealed the best conditions for the production of CrnA1′ and CrnA2′. The highest production levels were observed following growth in a semidefined CAA media for 3 to 5 days. Therefore, cultures were grown in this manner, and CrnA1′ and CrnA2′ were purified as before. However, the masses of CrnA1′ and CrnA2′ obtained by this approach were inconsistent with those observed previously. The masses of both peptides were lower than expected, with unusually broad isotope distributions (Figure 3.9A). MS/MS data acquired for these peptides revealed that Dha and Dhb were not being reduced to Ala and Abu to the full extent as had been seen before.

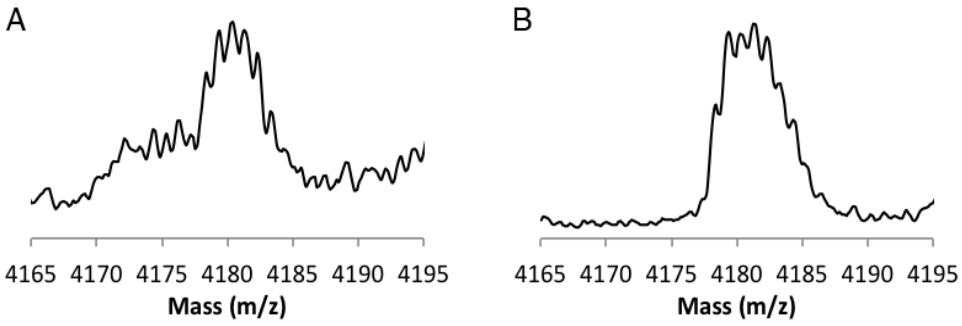

Figure 3.9. MALDI-TOF MS spectra showing the effect of a vitamin supplement on the mass of CrnA1′. CrnA1′ purified from a culture (A) without and (B) with a vitamin supplement.

Based on the elevated levels of carnolysin produced in the culture conditions used, it was possible that the levels of any necessary cofactors (e.g., NADPH, FADH) were being exhausted by the bacteria. To compensate for this, a sterile multivitamin solution was prepared and added to the large-scale culture prior to inoculation. After culturing and purifying CrnA1′ and CrnA2′ as before, MALDI-TOF MS revealed masses consistent with the fully reduced peptides (Figure 3.9).

3.2.9. Structural characterization of carnolysin A1′

With the optimal culture conditions determined, the focus shifted to the characterization of the carnolysin post-translational modifications (PTM). Based on sequence homology, it was expected that the topologies of the Lan and MeLan residues would likely be similar between carnolysin and cytolysin. Further, it was of interest to determine if carnolysin bears the unusual LL-Lan and LL-MeLan stereoisomers. Finally, the presence and stereochemistry of Ala and Abu residues derived from serine and threonine in CrnA1′ and CrnA2′ remained to be fully characterized.

3.2.9.1. Mass spectrometry

First, the mass of CrnA1′ was compared to that of the theoretical unmodified amino acid sequence to determine the extent of post-translational modification. The monoisotopic ion of CrnA1′ from ESI-qTOF MS was $[M+H]^+$ = 4178.08, while the corresponding amino acid sequence without PTMs was calculated to appear at $[M+H]^+$ = 4350.12. After considering different combinations of dehydration and reduction, the most likely scenario appeared to involve 10 dehydrations and four reductions.

To determine the positions of these PTMs, the MS/MS data obtained for CrnA1′ was fully analyzed and compared to the amino acid sequence encoded by the structural

gene (Figure 3.10). As mentioned previously, MS/MS fragmentation is not typically observed in regions contained with Lan and MeLan rings. No fragmentation was observed in three different regions of CrnA1′, which corresponded to the positions of the three Lan and MeLan rings found in $CylL_L$″. Further, three alanines derived from serines could be identified from these data. However, certain structural ambiguities could not be resolved from these data. The central region contains three serines, which are modified to alanine, Dha, and Lan; the MS/MS data could not be used to conclusively determine which serine was modified to each of these residues. Furthermore, although the data suggest a MeLan residue between Thr-9 and Cys-13, the possibility that a Lan residue was formed between Ser-10 and Cys-13 could not be excluded.

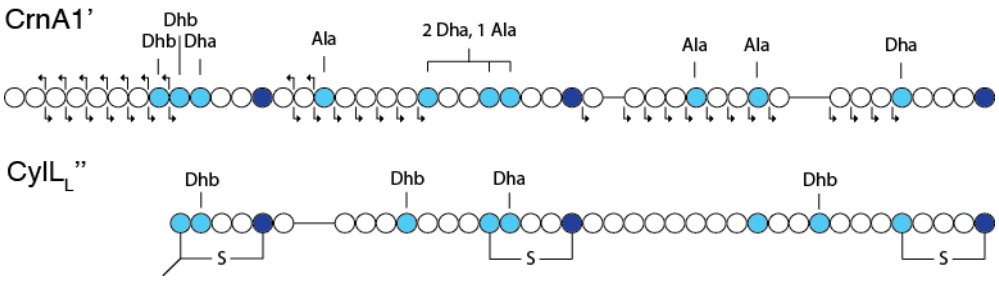

Figure 3.10. Summary of MS/MS data obtained for CrnA1′ and comparison of post-translational modifications to $CylL_L$″. Residues genetically encoded as serines and threonines are indicated in light blue, while cysteines are indicated in dark blue. The arrows above the structure represent b-ions, while those below represent y-ions.

3.2.9.2. NMR spectroscopy

To resolve these ambiguities and support the PTMs suggested from MS/MS, further structural characterization was performed using NMR spectroscopy. CrnA1′ was purified from a 4 L culture of *C. maltaromaticum* C2, and prepared in 10 % D_2O. TOCSY and NOESY datasets were acquired for this peptide, revealing a good dispersion of amide proton chemical shifts. Based on these data, the majority of the CrnA1′ proton

chemical shifts could be assigned (Table 6.5).[164] The chemical shifts of the different spin systems were diagnostic of the extent of post-translational modification at different positions.

Three dehydro residues were easily recognizable due to the high amide proton chemical shift, the lack of an α-proton, and the distinctive vinyl protons. These were identified as Dhb-8, Dha-10 and Dha-26 (Figure 3.11). Additionally, the four serine residues (Ser-16, Ser-21, Ser-33 and Ser-36) modified into alanine residues were identified. Furthermore, the chemical shifts of the β-protons of the residues derived from Thr-9, Ser-24 and Ser-41 were consistent with their incorporation into Lan and MeLan residues. NOE crosspeaks were supportive of the formation of a MeLan residue between Thr-9 and Cys-13, a Lan residue between Ser-24 and Cys-28, and a second Lan residue between Ser-41 and Cys-45.

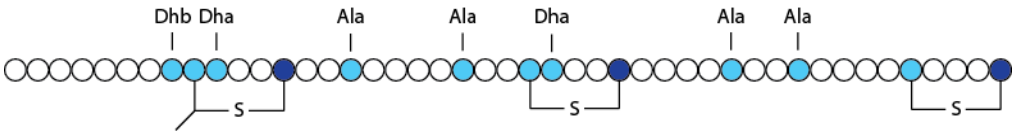

Figure 3.11. Covalent structure of CrnA1′ based on NMR spectroscopy, detailing the post-translational modifications. Residues genetically encoded as serines and threonines are indicated in light blue, while cysteines are indicated in dark blue.

3.2.9.3. GC-MS stereochemical analysis of carnolysin A1′

Due to the presence of the unusual LL-Lan and LL-MeLan stereoisomers in enterococcal cytolysin, it was of interest to determine the stereochemistry of the Lan and MeLan residues in the carnolysins. Based on the presence of Dha or Dhb immediately C-terminal to the Ser or Thr-derived residues in the N-terminal and central Lan and MeLan rings, these were expected to be the LL-Lan and LL-MeLan stereoisomers. CrnA1′ likely

also contains a DL-Lan near the C-terminus, based on the lack of a dehydro residue in this ring. Furthermore, it was expected that CrnA1′ contains four D-Ala residues derived from serine residues.

To determine the stereochemistries of these residues, both achiral and chiral GC-MS was used. Purified CrnA1′ was hydrolyzed into its constituent amino acids and derivatized as pentafluoropropanamide methyl esters. The stereochemistry of the single MeLan residue was determined using an achiral ZB5MS GC column. The derivatized MeLan from CrnA1′ was co-injected with synthetic DL-MeLan, D-allo-L-MeLan, LL-MeLan and L-allo-L-MeLan standards (Figure 3.12).[131] Co-injection with DL-MeLan and D-allo-L-MeLan yielded two distinct peaks, while co-injection with L-allo-L-MeLan resulted in a broad peak. Only co-injection with LL-MeLan resulted in a single narrow peak. Small peaks corresponding to partial epimerization of the threonine-derived alpha-carbon were observed for both synthetic and natural samples. The minor epimerized MeLan peak from CrnA1′ eluted with a retention time consistent with DL-MeLan, further suggesting that CrnA1′ contains LL-MeLan.

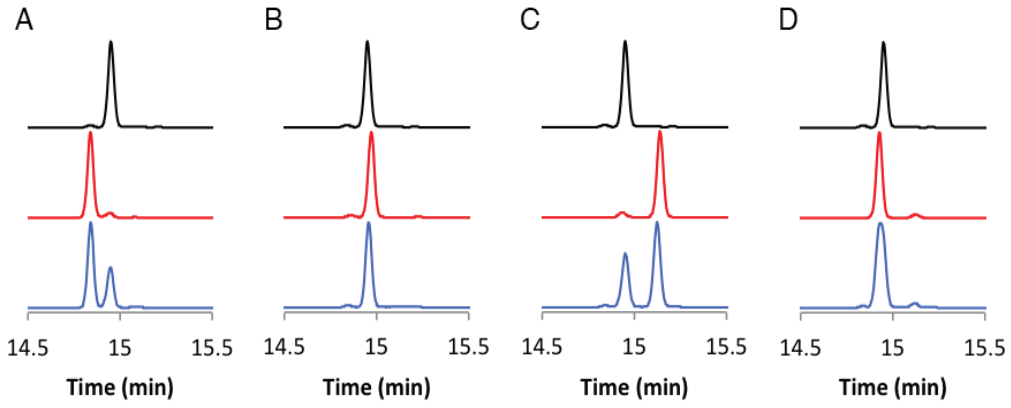

Figure 3.12. GC-MS co-injection experiments to determine the CrnA1′ MeLan stereochemistry. Co-injections with (A) DL-MeLan, (B) LL-MeLan, (C) D-allo-L-MeLan and (D) L-allo-L-MeLan. Derivatized CrnA1′ in black, synthetic standard in red, and co-injection of the two in blue.

As described above, it was predicted that the central Lan of CrnA1′ is LL-Lan, while the C-terminal Lan is the DL-stereoisomer. Co-injection of the derivatized CrnA1′ Lan residues with LL-Lan and DL-Lan on a Chirasil L-Val column revealed that this peptide does indeed contain both stereoisomers (Figure 3.13). To determine the position of the different stereoisomers within the peptide, some means of cleaving CrnA1′ between the two Lan residues was required. However, the amino acid sequence between the Lan residues did not appear to have any common protease cleavage sites, consisting mostly of alanine and glycine residues. Therefore, a partial hydrolysis approach was used in an attempt to obtain fragments containing only a single Lan residue.

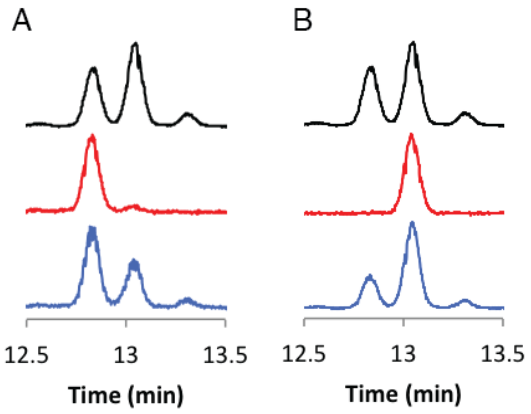

Figure 3.13. GC-MS co-injection experiments to determine the stereochemistry of the CrnA1′ Lan residues. Co-injections of hydrolyzed and derivatized CrnA1′ with (A) DL-Lan and (B) LL-Lan. Derivatized CrnA1′ in black, synthetic standard in red, and co-injection in blue.

CrnA1′ was treated to mild hydrolysis conditions, resulting in the almost complete loss of CrnA1′ as judged by MALDI-TOF MS. Additionally, several ions corresponding to C-terminal fragments of CrnA1′ were observed. Most of these fragments resulted from hydrolysis of the amide bonds of alanine and glycine residues, with cleavage C-terminal to Gly-37 and Ala-38 appearing to be favoured. By HPLC, several of these C-terminal

fragments eluted as a single peak (Figure 3.14). These C-terminal fragments were isolated by HPLC, fully hydrolyzed, and the constituent amino acids were derivatized as before. Then, the derivatized sample was co-injected with LL-Lan and DL-Lan synthetic standards on the Chirasil L-Val GC column (Figure 3.14). Based on these chromatograms, the C-terminal Lan residue is the DL-stereoisomer. Therefore, the middle Lan residue is the LL-stereoisomer, as expected based on the presence of Dha-25 in this ring.

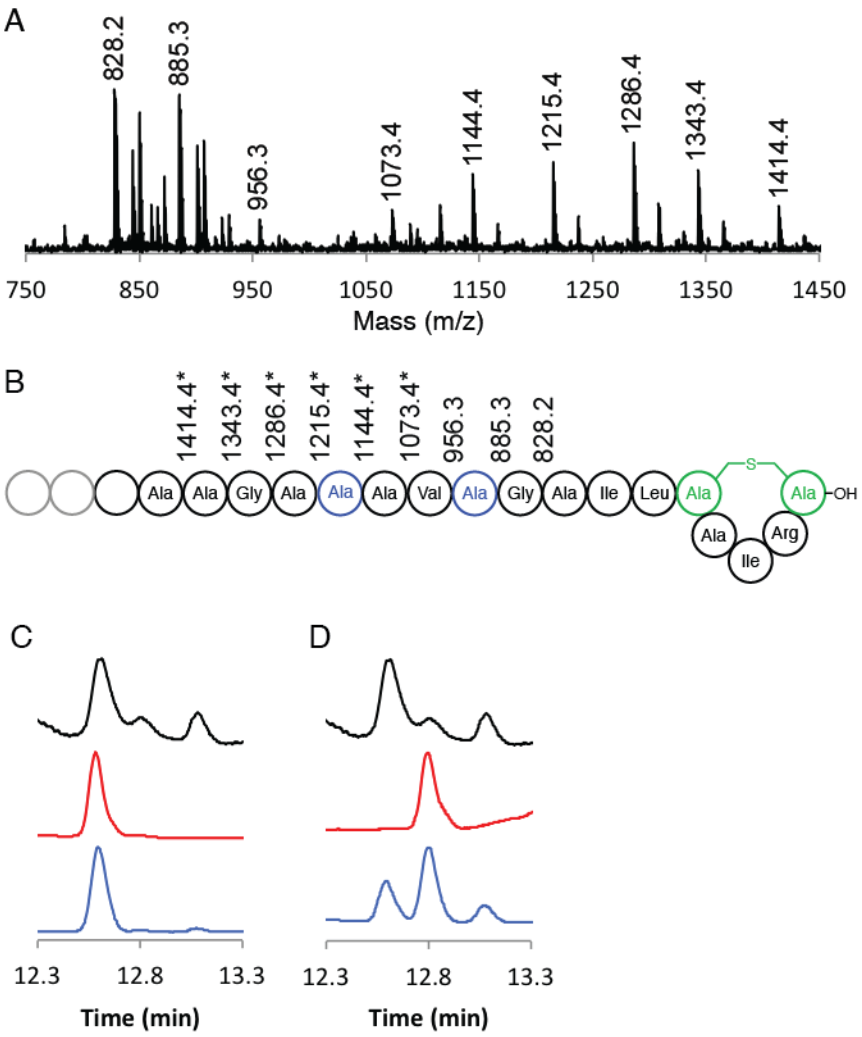

Figure 3.14. Partial hydrolysis of CrnA1′ to separate the Lan stereoisomers and GC-MS analysis. (A) MALDI-TOF MS spectrum of an HPLC fraction from the partial hydrolysate. (B) Sites of peptide bond cleavages on CrnA1′ corresponding to the ions observed by MALDI-TOF MS. Masses indicated with an asterisk are 18 Da greater than expected, likely due to hydrolysis occurring within the Lan ring. GC-MS co-injection of the hydrolyzed and derivatized C-terminal fragment of CrnA1′ with (C) DL-Lan and (D) LL-Lan.

With the Lan and MeLan stereochemistries established, the configuration of the Ala residues was examined. However, the intensity of the derivatized Ala peak was greatly diminished as compared to the earlier runs with the same sample. It was thought that much of the derivatized alanine was lost during the evaporation of the solvent for the purpose of storage. In order to decrease the volatility of the derivatized alanine residues,

the amino acids of CrnA1′ were derivatized as the pentafluoropropanamide isopropyl esters instead of the methyl esters. Injection of this sample on the Chirasil L-Val GC column revealed the presence of two peaks with fragment peaks consistent with alanine. Co-injection with L-Ala and D-Ala standards confirmed the presence of both stereoisomers in CrnA1′ (Figure 3.15). Further, integration of these peaks suggested a ratio of 4 D-Ala : 9 L-Ala. Based on NMR and MS/MS, CrnA1′ contains four alanine residues resulting from dehydration and reduction of serine residues, in addition to nine genetically encoded alanines. Therefore, all four alanine residues derived from serine residues have a D configuration.

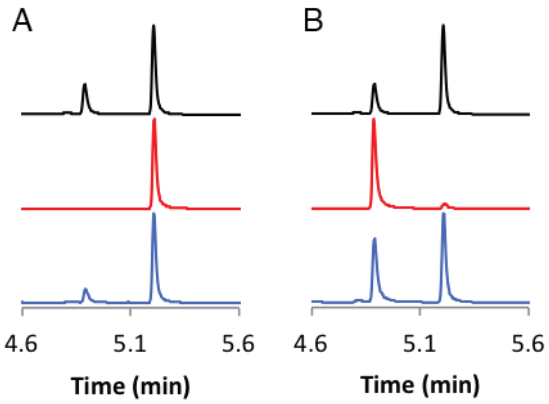

Figure 3.15. GC-MS co-injection experiments to determine the stereochemistry of the CrnA1′ alanine residues. Co-injections of hydrolyzed and derivatized CrnA1′ with (A) L-Ala and (B) D-Ala. Derivatized CrnA1′ in black, synthetic standards in red, and co-injection experiments in blue.

3.2.9.4. Overview of CrnA1′ structure and comparison to CylL$_L$′

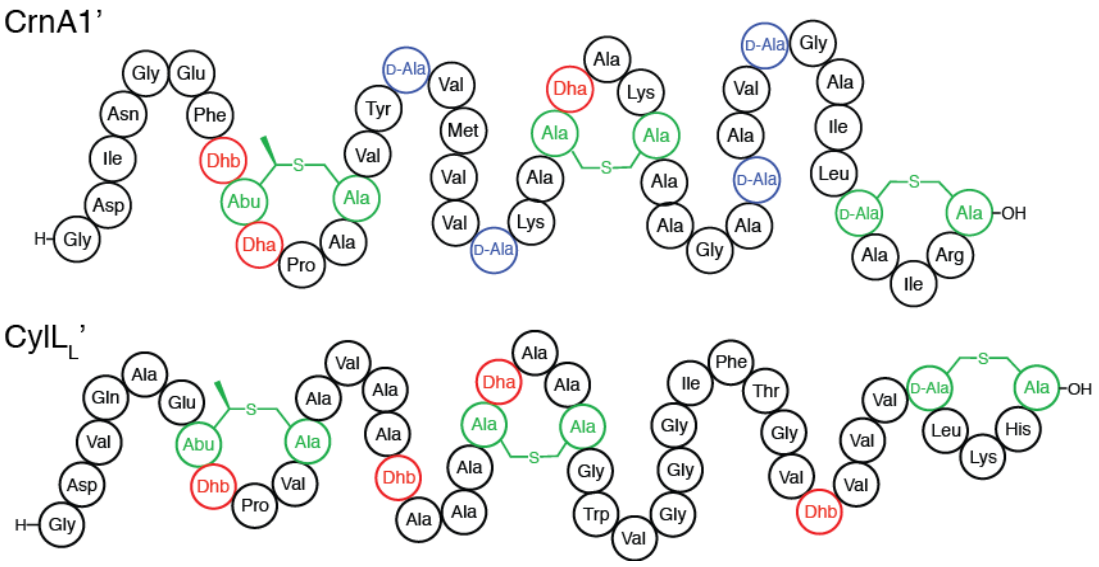

Figure 3.16. Covalent structure and stereochemistry of CrnA1′ compared to CylL$_L$′.

Compared to CylL$_L$′, the most notable aspect of the structure of CrnA1′ is the presence of four D-Ala residues (Figure 3.16). These D-Ala residues are situated in the linear portions of CrnA1′, distributed evenly between the Lan and MeLan residues. In addition, CrnA1′ contains three Dha and Dhb residues, which are directly adjacent to Lan and MeLan residues. This placement may make them inaccessible to the putative reductase CrnJ. While both peptides bear conserved dehydro residues within the LL-Lan and LL-Melan rings, the other dehydro residues differ. CrnA1′ has an additional Dhb residue immediately N-terminal to the LL-MeLan residue, while CylL$_L$′ has a Glu residue at this position. Elsewhere, CylL$_L$′ contains two other dehydro residues which are not found in CrnA1′.

The overall placements and sizes of Lan and MeLan residues are highly similar between CrnA1′ and CylL$_L$′. Both peptides bear an N-terminal LL-MeLan residue, a

central LL-Lan residue and a C-terminal DL-Lan residue. The number of amino acids between these Lan and MeLan residues is slightly different, as the N-terminal and central Lan/MeLan are farther apart for carnolysin, while the central and C-terminal Lan residues are farther apart for cytolysin.

3.2.10. Structural characterization of carnolysin A2′

3.2.10.1. Mass spectrometry

As with CrnA1′, the mass of mature CrnA2′ was compared to the mass of the theoretical unmodified amino acid sequence. CrnA2′ has a monoisotopic ion at $[M+H]^+$ = 3050.53, while the unmodified peptide was calculated to have a theoretical ion at $[M+H]^+$ = 3154.59. Comparison of these values with consideration of the amino acid sequence suggests that six dehydrations and two reductions occur during maturation. MS/MS suggested the presence of Lan/MeLan residues in the same positions as for $CylL_S′$ (Figure 3.17). Additionally, the presence of an Abu residue was supported by both the b- and y-series of ions. It was not possible to distinguish between the two residues in positions 19 and 20. While both are genetically encoded as serines, one is modified to dehydroalanine and the other to alanine.

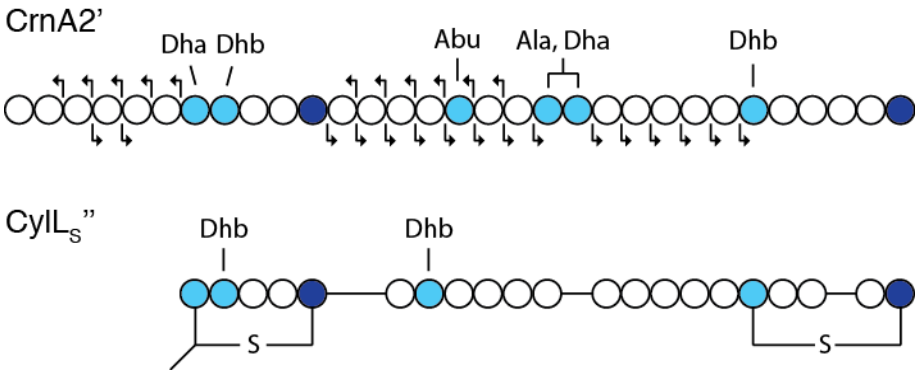

Figure 3.17. Summary of MS/MS data obtained for CrnA2′ and comparison of the post-translational modifications to CylL$_S$″. Residues genetically encoded as serines and threonines are indicated in light blue, while cysteines are indicated in dark blue. The arrows above the structure represent b-ions, while those below are y-ions.

3.2.10.2. NMR spectroscopy

NMR characterization of CrnA2′ was used to resolve the structural ambiguities remaining following the analysis of MS/MS data. To obtain sufficient material for NMR, CrnA2′ was purified from a 20 L culture of *C. maltaromaticum* C2. Pure CrnA2′ was prepared in a methanol-water solution, and TOCSY and NOESY datasets were acquired. Based on these data, the majority of the CrnA2′ proton chemical shifts were assigned (Table 6.6).

The NMR data clarified the post-translational modifications of Ser-19 and Ser-20, indicating that Ser-19 is converted into Ala-19 and Ser-20 is converted into Dha-20 (Figure 3.18). Further, these data confirmed the modification of Thr-16 into Abu-16. In addition to Dha-20, Thr-8 was shown to be dehydrated into Dhb-8. The topologies of the Lan and MeLan rings were also confirmed by the NMR data based on the presence of NOE crosspeaks spanning the thioether bridges. These data show that a Lan ring is formed from Ser-7 and Cys-11, while a MeLan ring is formed from Thr-26 and Cys-31.

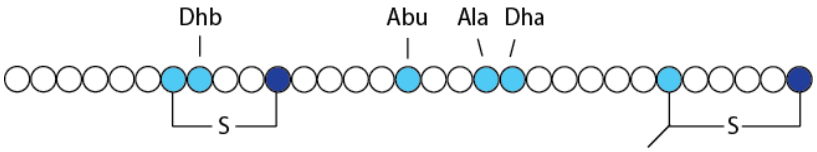

Figure 3.18. Covalent structure of CrnA2′ based on NMR spectroscopy. Residues genetically encoded as serines and threonines are indicated in light blue, while cysteines are indicated in dark blue.

3.2.10.3. Stereochemical analysis of carnolysin A2′

From the NMR data, CrnA2′ contains one Lan residue and one MeLan residue. The N-terminal Lan ring contains Dhb-9 immediately C-terminal to the serine-derived portion of the Lan residue, suggesting that it likely has an LL-configuration. The C-terminal MeLan ring, containing no dehydro residues, likely exists in the DL-configuration. CrnA2′ contains one Ala residue and one Abu residue derived from the dehydration and reduction of Ser and Thr residues, respectively. Based on the results obtained for CrnA1′, it is likely that these residues are both the D-stereoisomers.

Purified CrnA2′ was hydrolyzed and derivatized as pentafluoropropanamide methyl esters. To avoid the undesired evaporation of derivatized Ala and Abu residues, the derivatized sample was divided into two fractions and carefully dried under a stream of argon. Injection of this sample on GC confirmed the presence of derivatized Lan, MeLan, Ala and Abu.

As with CrnA1′, the stereochemistry of the MeLan residue was determined through co-injection experiments with synthetic standards (Figure 3.19). Co-injection with LL-MeLan, L-allo-L-MeLan and D-allo-L-MeLan all resulted in two distinct MeLan peaks. Co-injection with DL-MeLan yielded a single peak, confirming that the MeLan stereochemistry was as expected.

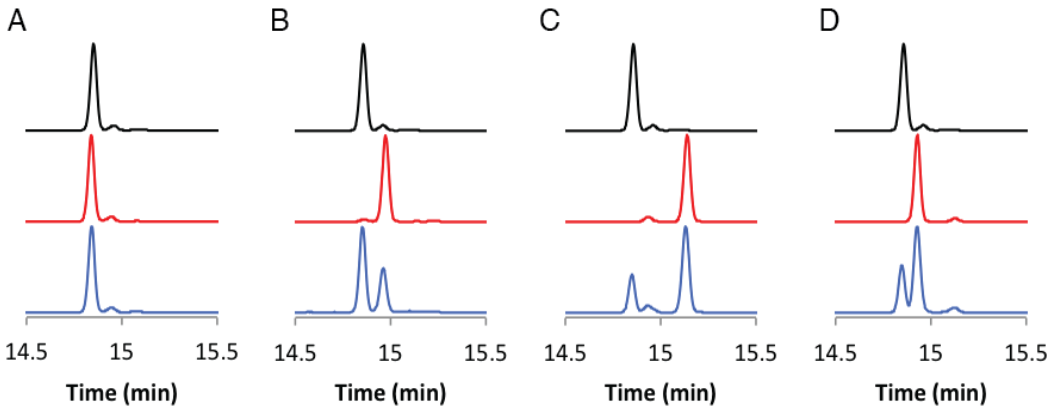

Figure 3.19. GC-MS co-injection experiments to determine the stereochemistry of the CrnA2′ MeLan residue. Co-injections of hydrolyzed and derivatized CrnA2′ with (A) DL-MeLan, (B) LL-MeLan, (C) D-allo-L-MeLan and (D) L-allo-L-MeLan. Derivatized CrnA2′ in black, synthetic standards in red, and co-injection experiments in blue.

A Chirasil L-Val column was used to determine the stereochemistry of the Lan, Ala and Abu residues. Co-injection with DL-Lan resulted in two Lan peaks, while co-injection with LL-Lan resulted in only one (Figure 3.20). Therefore, CrnA2′ contains the unusual LL-Lan stereoisomer, as may be predicted on the basis of the Dhb residue contained with this ring.

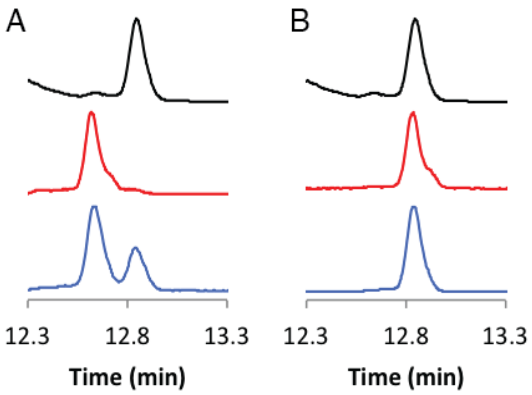

Figure 3.20. GC-MS co-injection experiments to determine the stereochemistry of the CrnA2′ Lan residue. Co-injections of hydrolyzed and derivatized CrnA2′ with (A) DL-Lan and (B) LL-Lan. Derivatized CrnA2′ in black, synthetic standards in red, and co-injection experiments in blue.

In the derivatized CrnA2′ sample, only a single peak was observed for Abu, while two peaks were observed for Ala. Co-injection with a synthetic L-Abu standard resulted in two distinct Abu peaks, while co-injection with D-Abu only resulted in a single peak (Figure 3.21). Further, co-injection with L-Ala and D-Ala standards indicated the presence of both stereoisomers in CrnA2′ (Figure 3.21). Integration of these peaks suggested a ratio of 3-4 L-Ala to 1 D-Ala. However, based on the sequence and modifications of CrnA2′, a ratio of only 2 L-Ala to 1 D-Ala was expected. The excess of L-Ala may arise from contamination of the CrnA2′ sample with low levels of other peptides or proteins. Based on previous NMR experiments, the CrnA2′ sample used was of good purity without major signals corresponding to undesired contaminants.

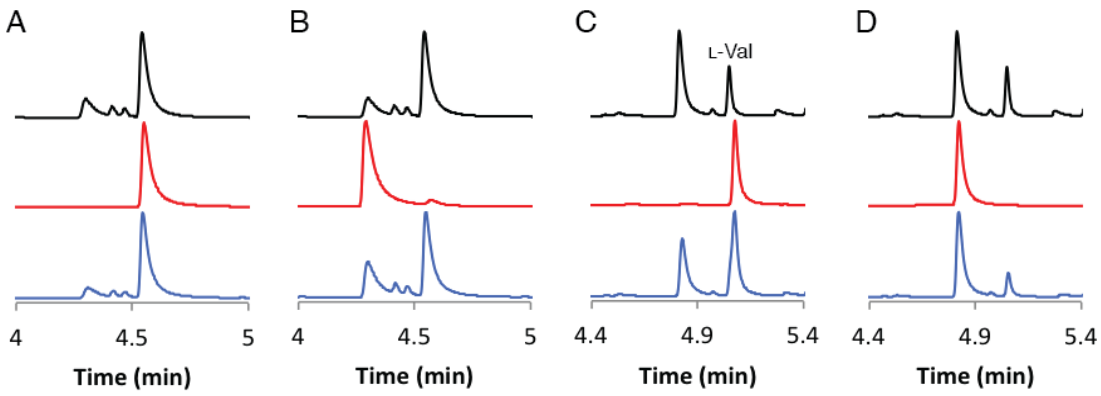

Figure 3.21. GC-MS co-injection experiments to determine the stereochemistry of the CrnA2′ Ala and Abu residues. Co-injections of hydrolyzed and derivatized CrnA2′ with (A) L-Ala, (B) D-Ala, (C) L-Abu and (D) D-Abu. Derivatized CrnA2′ in black, synthetic standards in red, and co-injection experiments in blue. L-Abu elutes closely with L-Val in section C.

3.2.10.4. Summary of CrnA2′ structure and comparison to CylL$_S$′

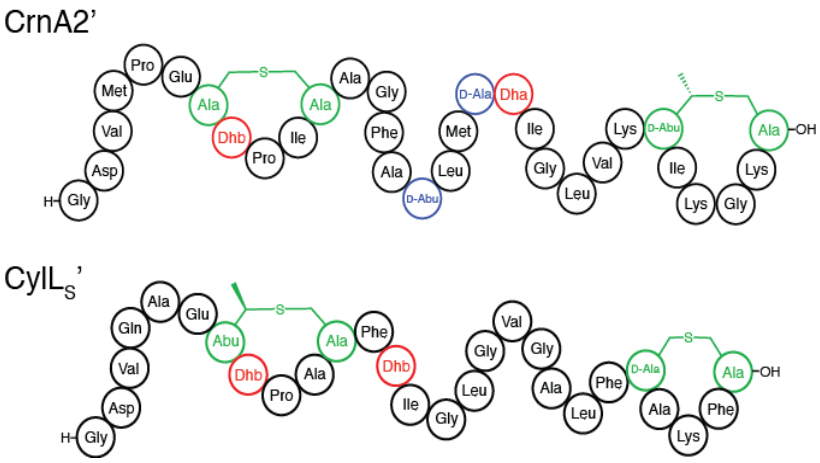

Figure 3.22. Covalent structures and stereochemistries of CrnA2′ and CylL$_S$′.

As with CrnA1′ and CylL$_L$′, the primary difference between CrnA2′ and CylL$_S$′ is the presence of D-Ala and D-Abu in the former (Figure 3.22). Like CrnA1′, both D-amino acids are situated in the linear region of the peptide. In the mature CrnA2′ peptide, two dehydro residues remain unreduced. Similar to CrnA1′, the Dhb residue contained within the N-terminal LL-Lan ring is not modified by CrnJ. However, the Dha residue situated in the linear region between the Lan and MeLan residues is also not reduced. This may be explained by the presence of a D-Ala residue immediately N-terminal to this Dha. Possibly, putative reductase CrnJ recognizes the stereochemistry of the amino acid N-terminal to the Dha/Dhb residue, requiring it to be the L-stereoisomer for reduction to occur. Furthermore, this may provide some insight into the directionality displayed by CrnJ. If CrnJ catalyzes reduction from the N-terminus to the C-terminus of the CrnA2 precursor, Dha-19 would be encountered before Dha-20. Alternately, CrnJ could be

inhibited by the presence of a dehydro residue N-terminal to the dehydro residue to be reduced.

Overall, CrnA2′ is four amino acids larger than $CylL_S$′. The positions of the Lan and MeLan residues are similar between CrnA2′ and $CylL_S$′, although the N-terminal MeLan residue of $CylL_S$′ is replaced with a Lan residue in CrnA2′ and the C-terminal Lan residue of $CylL_S$′ is replaced with a MeLan residue in CrnA2′. The N-terminal rings are of similar size between the two peptides, while the C-terminal DL-Lan ring of $CylL_S$′ is one residue smaller than the corresponding DL-MeLan residue of CrnA1′. In addition to the conserved dehydro residue within the N-terminal Lan/MeLan residue, both peptides contain another dehydro residue; however, the position of this residue is not conserved.

3.2.11. Antimicrobial activity of carnolysins

A mixture of CrnA1′ and CrnA2′ did not demonstrate antimicrobial activity when tested against indicator organisms *Lactococcus lactis* and *Carnobacterium maltaromaticum*. As described previously, enterococcal cytolysin only demonstrated strong cytolytic activity when both $CylL_S$ and $CylL_L$ were cleaved twice. It was predicted that further proteolytic processing of CrnA1′ and CrnA2′ was necessary to obtain antimicrobial activity, if the analogy to cytolysin holds. Therefore, methods of proteolytically removing the N-terminal extensions of CrnA1′ and CrnA2′ were explored.

3.2.11.1. Attempted expression and purification of CrnP

Within the carnolysin biosynthetic gene cluster, putative protease CrnP shows homology to CylA, the protease responsible for the second cleavage in cytolysin maturation. Therefore, CrnP is predicted to fulfill a similar role, cleaving CrnA1′ and/or CrnA2′. The six N-terminal amino acids of $CylL_L$′ and $CylL_S$′ are identical, and so their

processing by a single protease is not unexpected. However, the N-termini of CrnA1′ and CrnA2′ are more variable with regards to length and amino acid identity. Therefore, it is unclear if both CrnA1′ and CrnA2′ undergo further proteolytic processing, and if this would be performed by the same protease. Furthermore, it is also unclear if CrnP is active *in vivo*, as only singly cleaved CrnA1′ and CrnA2′ could be purified from *C. maltaromaticum* C2.

Initially, CrnP was expressed with an N-terminal His_6-tag. However, attempted purification of this construct failed: either the protein expressed insolubly, or the His-tag was removed with the N-terminal signal sequence by a signal peptidase prior to purification. A different construct expressing CrnP with a C-terminal His-tag was then constructed. This too yielded no soluble protein following Ni^{2+}-affinity chromatography. A third construct was prepared, wherein the predicted signal peptide sequence was replaced with an N-terminal His-tag. This protein also appeared to express insolubly. Attempts were made to refold the insoluble protein, however this did not yield an active protease, assuming it cleaves CrnA1′ and/or CrnA2′.

3.2.11.2. Cleavage of CrnA1′ and CrnA2′ by endoproteinase GluC

Due to the lack of success expressing CrnP, alternative approaches were considered. Notably, CrnA2′ bears a glutamic acid residue immediately N-terminal to the N-terminal LL-MeLan ring. Cleaving C-terminal to this Glu residue would correspond to the second cleavage required in the maturation of cytolysin L_S, yielding CrnA2″. Furthermore, cleavage following the Glu residue in position 6 of CrnA1′ would yield a peptide closer in length to $CylL_L$″, with two remaining amino acids N-terminal to the MeLan ring.

The cleavage of CrnA1′ and CrnA2′ with GluC, an endoproteinase cleaving selectively C-terminal to Glu residues, was attempted. MALDI-TOF MS analysis of test cleavages revealed the presence of small amounts of CrnA1″(7-45) and CrnA2″, and mostly undigested CrnA1′ and CrnA2′ (Figure 3.23). The slow conversion was rationalized by the sterically congested cleavage sites, as the Glu-6 residue of CrnA1′ is N-terminal to Phe-7, and Glu-6 of CrnA2′ is situated between Pro-5 and the N-terminal Lan residue.

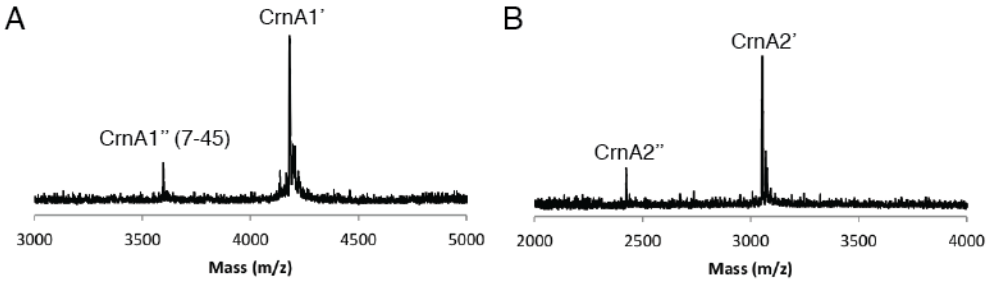

Figure 3.23. MALDI-TOF MS spectra of carnolysin GluC digests. Digest of (A) CrnA1′ yielding fragment CrnA1″(7-45) and (B) CrnA2′ yielding CrnA2″.

3.2.11.3. Antimicrobial testing of GluC-digested carnolysin

The antimicrobial properties of the crude GluC-cleaved carnolysin peptides were tested against indicator organism *L. lactis* (Figure 3.24). An overnight GluC digest of a mixture of CrnA1′ and CrnA2′ showed a strong zone of inhibition using a spot-on-lawn assay. Unexpectedly, GluC-digested CrnA1′ was antimicrobially active by itself, although not to the same extent as in combination with digested CrnA2′. Control experiments indicated that GluC-digested CrnA2′ was not active in combination with undigested CrnA1′ at the levels tested.

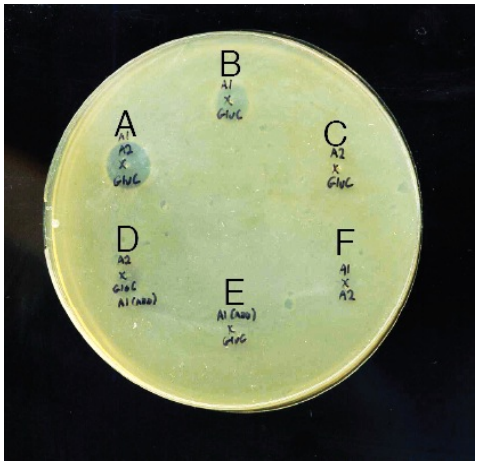

Figure 3.24. Antimicrobial testing of GluC-digested carnolysins against *Lactococcus lactis*. Spot-on-lawn assay of (A) CrnA1′ and CrnA2′ digested overnight with GluC, (B) CrnA1′ digested overnight with GluC, (C) CrnA2′ digested overnight with GluC, (D) CrnA2′ digested overnight with GluC; CrnA1′ added immediately before antimicrobial testing, (E) GluC incubated overnight; CrnA1′ added immediately before antimicrobial testing, and (F) undigested CrnA1′ and CrnA2′. The concentrations of the digested peptides were not determined.

3.2.11.4. Spectrum of activity of carnolysin

With the activity of the GluC-digested carnolysin established against *L. lactis*, their spectrum of activity was explored (Table 3.2). The digest was tested for activity against an array of Gram-positive and Gram-negative indicator organisms. As expected, the Gram-negative indicators tested were not susceptible to digested carnolysin; lantibiotics typically target only Gram-positive bacteria. Against the Gram-positive indicators tested, carnolysin displayed a relatively broad spectrum of activity. Growth inhibition was observed of all Gram-positive indicators tested, with the exception of *Staphylococcus aureus* and *Paenibacillus polymyxa*. Particularly potent inhibition was observed of *Enterococcus faecium* and *C. maltaromaticum* A9b-, in addition to *L. lactis*.

Due to the hemolytic properties associated with cytolysin, the carnolysin GluC digest was tested against sheep blood. However, no hemolysis was observed at concentrations sufficient to observe strong antibacterial activity. Not a great deal is

known about the mode of action of enterococcal cytolysin against red blood cells or bacteria. It may be possible that some combination of amino acid sequence, post-translational modifications (i.e., the D-amino acids), concentration, and proteolytic processing render carnolysin antibacterial but not hemolytic, unlike cytolysin.

Table 3.2. **Spectrum of activity of GluC-digested CrnA1′ and CrnA2′**

Indicator Strain	**Activity Test Result**[a]
Gram-Positive Bacteria	
Lactococcus lactis subsp. *cremoris* HP	++
Bacillus subtilis JH642	+
Staphylococcus aureus ATCC 13311	-
Carnobacterium maltaromaticum A9b-	++
Pediococcus acidilactici PAC 1.0	++
Lactobacillus sakei UAL1218	+
Paenibacillus polymyxa NRRL B-30507	-
Enterococcus faecium BFE 900	++
Listeria monocytogenes ATCC 15313	+
Gram-Negative Bacteria	
Escherichia coli DH5α	-
Pseudomonas aeruginosa ATCC 15442	-
Salmonella enterica serovar Typhimurium ATCC 13311	-

[a] Inhibition of the indicator organism from a spot-on-lawn assay using a GluC digest of CrnA1′ and CrnA2′. Extent of activity indicated by: ++, inhibition; +, faint inhibition; -, no inhibition. Concentrations of digested carnolysin peptides not determined.

3.2.12. Expression of carnolysin in *E. coli*

3.2.12.1. Cloning and expression of *crnM*, *crnJ*, *crnA1* and *crnA2*

The co-expression of lantibiotic precursor peptides with their associated biosynthetic machinery in *E. coli* has been used to successfully install PTMs found in several lantibiotics, such as cytolysin.[13] Due to the similarities between cytolysin and carnolysin, the approach used for production of carnolysin was modeled after that used

for cytolysin. Putative reductase CrnJ was included in this system to establish its role in the reduction of Dha and Dhb. After purchasing the nucleotide sequences encoding *crnM*, *crnJ*, *crnA1* and *crnA1* with codon optimization for *E. coli*, these genes were cloned into the appropriate plasmids. Briefly, plasmids pRSFDuet-crnM-crnA1, pRSFDuet-crnM-crnA2 and pETDuet-crnJ were prepared following standard molecular biology techniques.[165] The plasmids were prepared such that CrnA1 and CrnA2 would be produced with an N-terminal His_6-tag to facilitate purification.

E. coli BL21(DE3) was co-transformed with pETDuet-crnJ and either pRSFDuet-crnM-crnA1 and pRSFDuet-crnM-crnA2. Following growth and induction of expression, the cultures were lysed and the His-tagged carnolysin precursors were purified by Ni^{2+}-affinity chromatography. After determining which fractions contained the peptides of interest by MALDI-TOF MS, the mixtures were further fractionated by HPLC. Finally, peptides of the predicted masses were obtained (Figure 3.25). Considering the addition of the His_6-tag, a linker sequence, and the removal of Met-1, the observed masses were consistent with the expected extent of post-translational modification. Partial MS/MS sequencing confirmed the identities of these isolates as well as some of the PTMs.

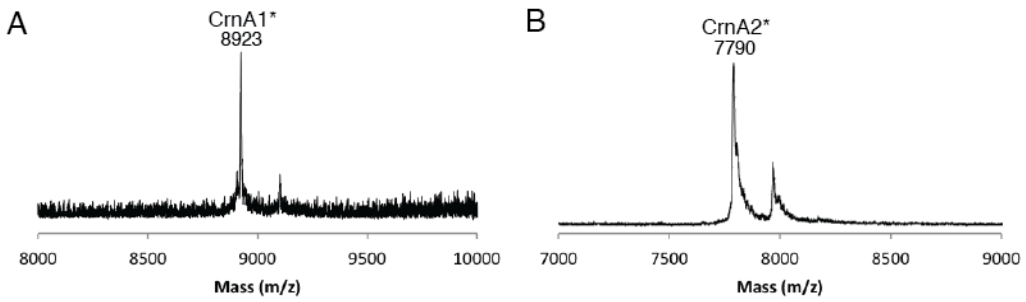

Figure 3.25. Heterologously-produced CrnA1* and CrnA2*. MALDI-TOF MS spectra of HPLC-purified (A) CrnA1* and (B) CrnA2*.

3.2.12.2. Production and activity of protease CrnT-150

To confirm that the modifications installed by CrnM and CrnJ in *E. coli* are consistent with those of the natural producer, some means of comparing the heterologously produced peptides with the natural isolate was required. Cleavage of the primary N-terminal leader sequences of CrnA1* and CrnA2* would theoretically yield CrnA1′ and CrnA2′. Based on analogy with other lantibiotic biosynthetic systems, the N-terminal protease domain of transporter CrnT was predicted to perform this role *in vivo*. The expression of a lantibiotic protease domain separate from the transmembrane domains has been previously described. The N-terminal 150 amino acids of transporters LctT (involved in lacticin 481 biosynthesis) and BovT (involved in bovicin HJ50 biosynthesis) were capable of removing the leader sequences from the corresponding lantibiotic precursors.[22,37]

Using genomic DNA isolated from *C. maltaromaticum* C2, the first 450 base pairs encoding CrnT were amplified and cloned into pET28 with an N-terminal His-tag. Following transformation of this construct into *E. coli* BL21(DE3), a culture was grown from a transformant and protein expression was induced. Ni^{2+}-affinity chromatography of the cell lysate revealed the successful expression and purification of CrnT-150 (Figure 3.26).

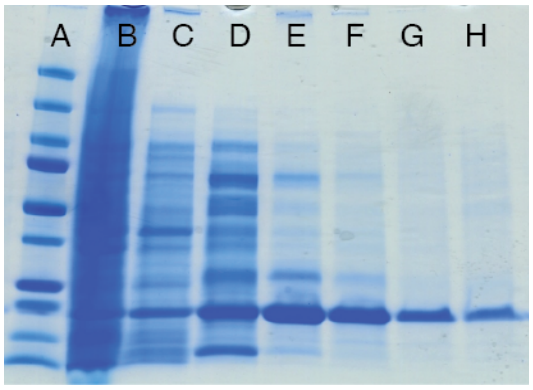

Figure 3.26. SDS-PAGE of CrnT-150 Ni^{2+}-affinity chromatography fractions. (A) Ladder, (B) flow-through, and washes with buffer supplemented with (C) 0 mM imidazole, (D) 50 mM imidazole, (E) 100 mM imidazole, (F) 250 mM imidazole, (G) 500 mM imidazole, and (H) 1 M imidazole.

After testing several conditions, CrnT-150 was found to successfully cleave the leader sequences of CrnA1* and CrnA2* obtained from heterologous expression in *E. coli*. Digestion of CrnA1* with CrnT-150 resulted in a peak consistent with CrnA1′ based on MALDI-TOF MS and LC-MS/MS (Figure 3.27). Co-injection on LC-MS of CrnA1′ obtained from *E. coli* with CrnA1′ obtained from *C. maltaromaticum* C2 resulted in only a single peak. Under the reaction conditions, CrnT-150 digestion of CrnA2* did not result in a peak consistent with CrnA2′. However, two peaks of the same mass were noted by LC-MS/MS, which were both 251 Da greater than CrnA2′. Based on MS/MS data, this is predicted to result from the attack of tris(2-carboxyethyl)phosphine (TCEP) onto Dha-20 of CrnA2′, yielding two different stereoisomers (Figure 3.27). Based on these results, the post-translational modifications of carnolysin produced in *E. coli* appear to be consistent with those of carnolysins isolated from *C. maltaromaticum* C2.

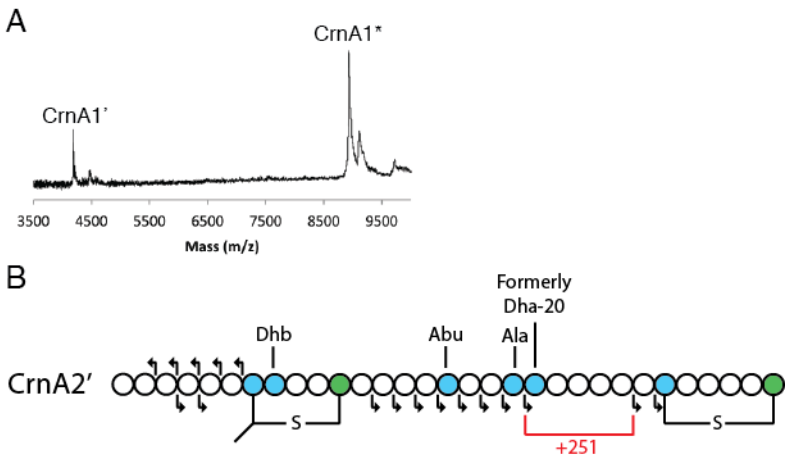

Figure 3.27. MS data for CrnT-150 cleaved CrnA1* and CrnA2*. (A) MALDI-TOF MS spectrum of CrnA1′ obtained via CrnT-150 digest of CrnA1*. (B) Summary of MS/MS data for a putative TCEP adduct of CrnA2′, obtained via CrnT-150 mediated digest of CrnA2*.

3.3. Conclusions and future directions

Through the characterization of the antimicrobial peptides produced by *C. maltaromaticum* C2, a novel two-component lantibiotic with sequence homology to enterococcal cytolysin was discovered. However, the two components of this lantibiotic, named carnolysin, were not antimicrobially active as isolated. After identification of the lantibiotic structural genes, the carnolysin biosynthetic gene cluster was identified in the genome of *C. maltaromaticum* C2. The biosynthetic genes were homologous to those involved in cytolysin biosynthesis, with the additional presence of a reductase enzyme, CrnJ.

After optimizing culture conditions, CrnA1′ and CrnA2′ were purified and analyzed by LC-MS/MS, NMR and GC-MS. Structurally, the carnolysin peptides were found to be similar to cytolysin. The presence of the unusual LL-Lan and LL-MeLan stereoisomers was found in both peptides, similar to cytolysin. However, carnolysin also contains rare D-Ala and unprecedented D-Abu residues, which are not found in cytolysin.

The role of reductase CrnJ in the formation of D-Ala and D-Abu was confirmed via the heterologous expression of carnolysin biosynthetic proteins in *E. coli*. This approach yielded peptides post-translationally modified to the same extent as those purified from *C. maltaromaticum* C2. Protease CrnT-150, expressed in *E. coli*, cleaved the primary leader sequence of the carnolysin precursors, producing CrnA1′ and CrnA2′.

Antimicrobially active products of carnolysin were obtained after cleavage of both components with the endoproteinase GluC. Carnolysin, while demonstrating antimicrobial activity, was not hemolytic at the levels tested. This contrasts cytolysin, which possesses both of these activities. Mutational analysis of the cytolysin peptides revealed certain amino acid substitutions that impacted hemolytic activity while not affecting the bacteriocin activity, and vice versa.[166] This suggests that the two activities are, to some extent, separable. Comparison of the structures of carnolysin and cytolysin may provide further perspective regarding the basis of the cytolysin hemolytic activity.

With the function of CrnJ confirmed, it would be of interest to fully characterize this enzyme. A similar reductase, LtnJ, has been demonstrated to be involved in the biosynthesis of lacticin 3147, but it has not been studied *in vitro*. During the characterization of LtnJ, one of the lacticin 3147 serine residues (ultimately modified to D-Ala) was mutated to a threonine residue.[33] While this threonine residue was successfully dehydrated to Dhb, it was not reduced to D-Abu. Therefore, it appears that CrnJ may be more promiscuous as to which residues it reduces. To see if this is generally true, other carnolysin serine residues (i.e., those which are converted to D-Ala) could be mutated to threonines to observe the impact on reduction, as well as on antimicrobial activity. It is also of interest to explore the promiscuity of CrnJ further, and see if it could

reduce other dehydro residues (i.e., the conversion of dehydrovaline to D-Val). Furthermore, the reliance of CrnJ on the leader sequence could be explored. Potentially, fusion of the carnolysin leader sequences to other bacteriocins or peptides could yield a variety of bioengineered variants containing D-Ala and D-Abu residues.

Chapter 4

Structure and activity of the leaderless bacteriocin enterocin 7A

4.1. Background

4.1.1. Solution structures of bacteriocins

Nuclear magnetic resonance (NMR) spectroscopic data has been used to calculate the solution structures of numerous bacteriocins. Bacteriocins tend to be of a size where complete chemical shift assignment is feasible and sufficient spectral dispersion allows for the use of distance restraints derived from NOE crosspeaks. The use of X-ray crystallography for bacteriocins is often not feasible, due to the difficulty associated with crystallizing hydrophobic peptides of this size. Furthermore, NMR allows the dynamic conformation of a peptide in solution to be observed, compared to the static nature of an X-ray crystal structure. NMR solution structures of representative members of most classes of bacteriocins have been solved. These structures provide insight into their antimicrobial mode of action, and reveal some commonalities between otherwise diverse bacteriocins.

Linear bacteriocins not bearing any post-translational modifications tend to exist as a random coil in aqueous conditions. As most of these bacteriocins are thought to exert their antimicrobial effects through membrane permeabilization, they are predicted to undergo conformational changes upon interacting with a target membrane.[60] Therefore, mixed lipophilic and aqueous conditions, such as aqueous trifluoroethanol (TFE)

solutions or lipid micelles, have been commonly used to induce structure in these peptides for NMR studies.

The structure of class IIa bacteriocin leucocin A (LeuA), a 37 residue peptide produced by *Leuconostoc gelidum*, was characterized in both 90 % TFE and dodecylphosphocholine (DPC) micelles (Figure 4.1). In both conditions, the structure consisted of an N-terminal three-strand antiparallel β-sheet stabilized by a disulfide bridge, and a C-terminal amphiphilic α-helix.[60] The relative orientation of these two motifs differed depending on the choice of solvent. The structure of carnobacteriocin B2 (CbnB2), a 48 residue class IIa bacteriocin isolated from *Carnobacterium maltaromaticum*, showed similarities to LeuA in the central amphiphilic α-helical region (Figure 4.1). However, despite the high sequence similarity between the N-termini of these two peptides, the structures of this region differ greatly. While the leucocin A N-terminus formed a β-sheet, the N-terminus of CbnB2 was largely unstructured. Class IIa bacteriocins exert their antimicrobial effects through membrane permeabilization. First, these peptides bind to the mannose phosphotransferase complex situated in the target membrane.[64] Then, the amphiphilic α-helical region inserts into and disrupts the target membrane, resulting in the loss of essential metabolites.

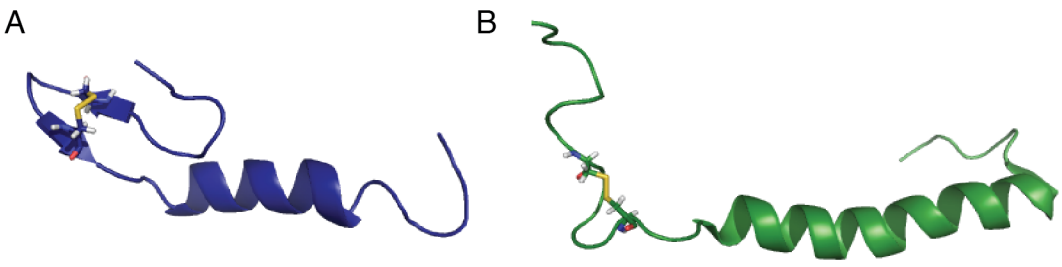

Figure 4.1. Solution structures of class IIa bacteriocins. Cartoon representations of (A) leucocin A TFE (B) carnobacteriocin B2, both in aqueous TFE. Disulfide bridges are represented in stick form.

Solvent choice has a similar effect on the structure of class IIb bacteriocins (i.e., two-peptide bacteriocins biosynthesized with leader sequences) as on the class IIa bacteriocins. The two peptides of plantaricin EF were unstructured in aqueous conditions, but developed α-helicity in DPC micelles;[167] similar behavior was observed for lactococcin G.[168] The NMR solution structures of several of these bacteriocins consist largely of amphiphilic α-helices in structure-inducing conditions (Figure 4.2), consistent with their antimicrobial action via membrane permeabilization.[169] Recently, several bacteriocins of this class were found to interact with UppP, an undecaprenyl pyrophosphate phosphatase involved in peptidoglycan biosynthesis.[169] Once bound to UppP situated in the target membrane, the amphiphilic α-helices may insert into the target membrane thereby resulting in pore formation.

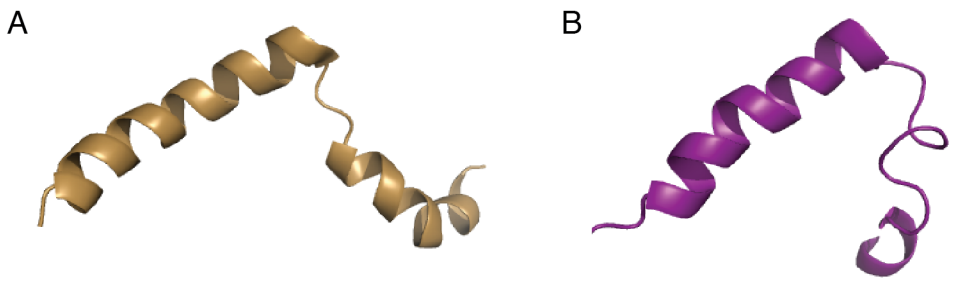

Figure 4.2. Solution structures of class IIb bacteriocin lactococcin G. Cartoon representations of (A) LcnG - α and (B) LcnG - β prepared in DPC micelles.

Some classes of bacteriocins do not require the use of structure-inducing conditions to exhibit defined structure. However, these bacteriocins tend to be post-translational modified, effectively limiting their structural flexibility. Circular bacteriocins carnocyclin A[170] and AS-48,[171] which feature an amide bond between the N- and C-termini, are highly structured in aqueous conditions. The structures of these peptides are highly α-helical, consisting of four or five amphiphilic α-helices (Figure 4.3). Like most other bacteriocins, circular bacteriocins exert their antimicrobial action by permeabilizing the membrane of target bacteria. However, unlike the class IIa and IIb bacteriocins, circular bacteriocin carnocyclin A does not appear to require a docking molecule in target membranes.[172] Carnocyclin A has been found to act by forming anion-selective pores,[172] while AS-48 forms non-selective pores.[173]

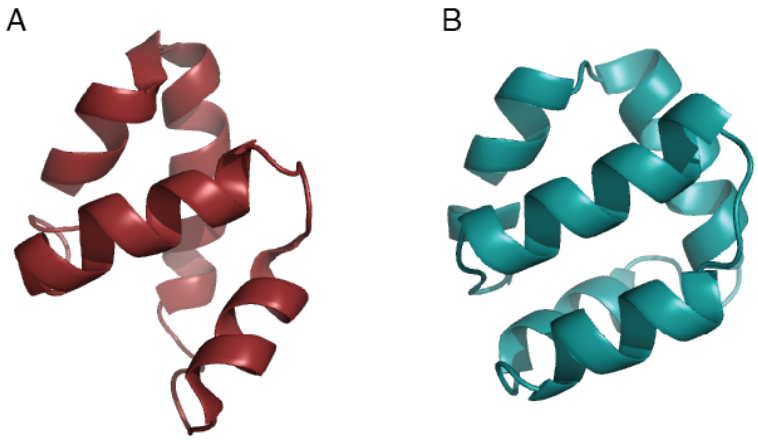

Figure 4.3. Solution structures of circular bacteriocins. Cartoon representations of (A) carnocyclin A and (B) AS-48.

The leaderless bacteriocins, introduced in Chapter 1, are less well characterized than most other groups of bacteriocins. Until the presently described work,[110] there had been no reported solution structure of a leaderless bacteriocin. Structural predictions have been made regarding these peptides on the basis of experimental techniques other than NMR spectroscopy, primarily using circular dichroism (CD) spectroscopy. CD spectra of leaderless bacteriocins aureocin A53 and lacticin Q suggested a high degree of α-helicity in aqueous conditions.[46,54] Sequence analysis suggested that these α-helical regions are likely amphiphilic, similar to the class IIa, IIb and circular bacteriocins.[46,54] Furthermore, aureocin A53 and lacticin Q were found to act by permeabilizing target cell membranes.[55,56] Like carnocyclin A, lacticin Q does not require a docking molecule for this permeabilization activity.[55] Therefore, the extent to which the solution structures of the leaderless bacteriocins resemble other classes of bacteriocins is of interest, and may allow the mode of action of these peptides to be rationalized.

4.1.2. Leaderless bacteriocins enterocin 7A and 7B

Enterococcus faecalis 710C was found to demonstrate a broad spectrum of antimicrobial activity, inhibiting the growth of Gram-positive food pathogens such as *Listeria monocytogenes*, *Clostridium* spp., and methicillin-resistant *Staphylococcus aureus* (MRSA).[174] This antimicrobial activity was traced to the production of two bacteriocins, which were named enterocins 7A and 7B. The molecular masses of enterocins 7A and 7B were noted to be very similar to those of leaderless bacteriocins enterocins MR10A and MR10B.[45] MS/MS confirmed that the amino acid sequences of these isolates were indeed the same as enterocins MR10A and MR10B. High-resolution mass spectrometry demonstrated the presence of a formyl group on the N-terminus, as had been suggested for other leaderless bacteriocins.[174] The primary structures of enterocins 7A and 7B are highly similar, with 74 % conservation of amino acid identity between the two peptides (Figure 4.4). While the N-termini of the two peptides are almost identical, the C-termini are more diverse.

```
Ent7A  MGAIAKLVAKFGWPIVKKYYKQIMQFIGEGWAINKIIDWIKKHI
Ent7B  MGAIAKLVAKFGWPFIKKFYKQIMQFIGQGWTIDQIEKWLKRH-
       ***************::**:*********:**:*::* .*:*:*
```

Figure 4.4. Sequence alignment of enterocins 7A and 7B. Conserved residues are indicated with an asterisk, conservative substitutions with a colon, and residues with weakly similar properties with a period.

4.2. Results and Discussion

4.2.1. Isolation of enterocin 7A

Enterocin 7A was purified from a culture of *E. faecalis* 710C using a modified approach based on a literature report.[174] Briefly, culture supernatant was passed through strong cation-exchange chromatographic resin, to which enterocin 7A bound strongly.

After a wash step, the desired peptide was eluted using elevated salt concentrations. The elution fraction was desalted using a reverse-phased solid-phase extraction cartridge, and eluted using an 80 % isopropanol solution. Finally, enterocin 7A was purified to homogeneity using reversed-phase HPLC. Enterocin 7B was purified by an identical approach, eluting before enterocin 7A by HPLC.

4.2.2. Circular dichroism spectroscopy

The impact of solvent on the structure of enterocin 7A was examined through CD spectroscopy. CD spectra were obtained in milli-Q water, in phosphate buffer and in 50 % TFE. In all three solvent conditions, the spectra demonstrated minima and maxima consistent with α-helicity (Figure 4.5). The 50 % TFE solution was calculated to have 66 % α-helicity, while the buffered and unbuffered solutions were 39 % and 29 % α-helical, respectively.

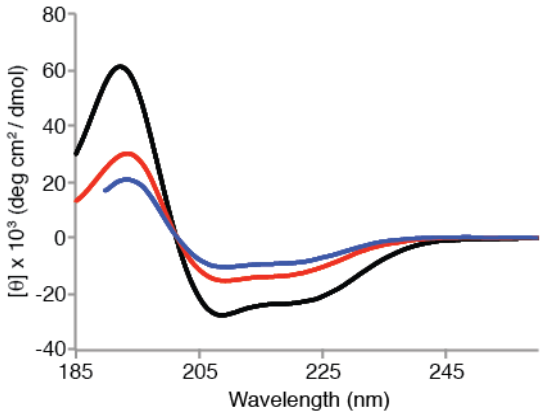

Figure 4.5. Circular dichroism data for enterocin 7A. Black: 50 % trifluoroethanol; red: 20 mM sodium phosphate, pH 7.0; blue: unbuffered water.

As mentioned in the introduction, this structuring in aqueous solution without requiring micelles or organic co-solvents contrasts what is observed for many other linear

bacteriocins. The CD data resemble previous reports describing leaderless bacteriocins aureocin A53 and lacticin Q. CD spectra suggested that aureocin A53 was α-helical in both unbuffered and phosphate-buffered water.[46] Similarly, the CD spectrum of lacticin Q in a tris-buffered solution suggested extensive α-helicity.[54] While the spectral data for lacticin Q in small unilamellar vesicles suggested a similar extent of α-helicity based on the minima at 220 nm, the minima peak at 207 nm was more pronounced.[54] This may suggest that lacticin Q is folded differently in aqueous solution and lipid environments, although both structures are likely to be primarily α-helical.

4.2.3. Enterocin 7A NMR spectroscopy

To simplify chemical shift assignment and structure calculation, attempts were made to isotopically label enterocin 7A with carbon-13 and nitrogen-15. However, *E. faecalis* 710C grew poorly in unlabeled Celtone media, a complex media previously used for the isotopic labeling of other bacteriocins. Although this strain grew marginally better if the Celtone was supplemented with all-purpose tween (APT) broth, only minimal amounts of enterocin 7A were produced. While other means of labeling this peptide were under consideration, such as the expression as a fusion protein in *Escherichia coli*, preliminary NMR data was obtained for unlabeled enterocin 7A.

A one-dimensional proton NMR spectrum for enterocin 7A prepared in 10 % D_2O was acquired. This revealed a good distribution of backbone amide protons with minimal overlap in aqueous conditions, consistent with the CD results. This peptide showed other indications of being highly structured, such as the presence of a peak at -0.13 ppm. Based on these spectral data, chemical shift assignment using unlabeled peptide appeared to be feasible. Therefore, TOCSY, NOESY, COSY and ^{15}N-HSQC datasets were acquired for

unlabeled enterocin 7A. The ^{15}N-HSQC spectrum showed excellent resolution of signals (Figure 4.6). Apart from the signals attributed to tryptophan, asparagine and glutamine side chains, almost all of the backbone amide signals were distinguishable. Only eight of the signals corresponding to the 44 amino acids of Ent7A overlapped in this spectrum.

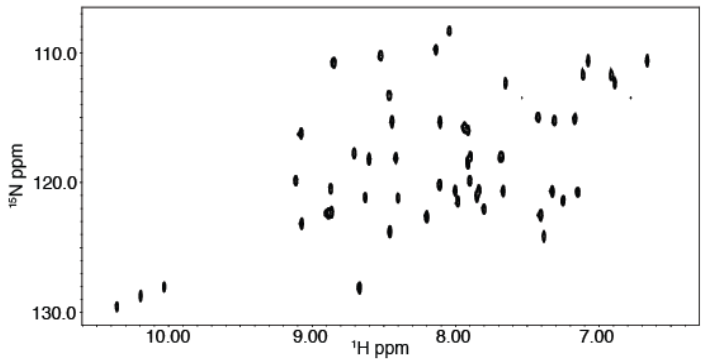

Figure 4.6. ^{15}N-HSQC spectrum for enterocin 7A

Similarly, almost all of the amino acid spin systems were distinguishable in the TOCSY spectrum. Only a few of these spin systems could not be fully resolved due to spectral overlap. Using the NOESY and TOCSY spectra, the amino acid spin systems were put in order based on αH-NH(i, i + 1) and NH-NH(i, i + 1) NOE crosspeaks.[164] Once the order was determined, the majority of the proton chemical shifts could be assigned based on the TOCSY and COSY datasets (Table 6.7). Consistent with the CD data, numerous NOE crosspeaks characteristic of α-helicity such as αH-NH(i, i + 3) were observed. The chemical shift assignments were analyzed using the chemical shift index functionality of NMRView, suggesting three major α-helical regions (Figure 4.7).[175]

Figure 4.7. Chemical shift index analysis of enterocin 7A. Red circles are regions predicted to be α-helical, blue are β-sheet regions, and grey are neither.

4.2.4. Enterocin 7A structure calculation

Automated structure calculation of enterocin 7A was performed using CYANA 2.1.[176] Along with chemical shift assignments, CYANA was provided with a list of NOE crosspeaks as distance restraints. With this input, CYANA was used to calculate 20 structures representative of enterocin 7A. After some minor manual assignment of NOE crosspeaks, the 20 calculated structures overlapped well with a root-mean-square deviation (RMSD) of 0.48 ± 0.15 Å for backbone atoms (Figure 4.8, Table 4.1).

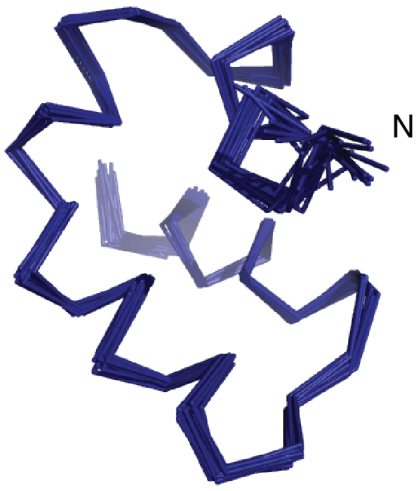

Figure 4.8. Overlay of 20 structures calculated by CYANA for enterocin 7A. N-terminus indicated by the letter N.

Table 4.1. Enterocin 7A structure calculation statistics

Total number of NOE assignments	1481
Short ($\| i - j \| \leq 1$)	373
Medium ($1 < \| i - j \| < 5$)	212
Long ($\| i - j \| \geq 5$)	166
Average target function value	0.40
RMSD for full peptide	
Backbone atoms (Å)	0.48 ± 0.15
Heavy atoms (Å)	0.92 ± 0.11

4.2.5. Description of enterocin 7A solution structure

The structure of enterocin 7A is primarily composed of three α-helices: one at the N-terminus, one at the C-terminus, and a kinked α-helix in the central region (Figure 4.9). The N-terminal α-helix extends from residues 4 to 10, followed by a turn. The central kinked α-helix extends from residues 14 to 29, with the kink occurring at residue 19. Finally, the C-terminal α-helix extends from residue 33 to the C-terminus. These α-helical ranges are consistent with the chemical shift index analysis (Figure 4.7). All three α-helical regions are amphiphilic, with the hydrophobic residues buried in the core of the peptide. The structure is highly compact, with extensive contact between the three α-helices. Numerous long-range NOEs were observed between hydrophobic residues from different α-helices. The signal at -0.13 ppm was explained by this hydrophobic packing, resulting from the orientation of an Ile-40 methyl group above the aromatic side chain of Phe-11.

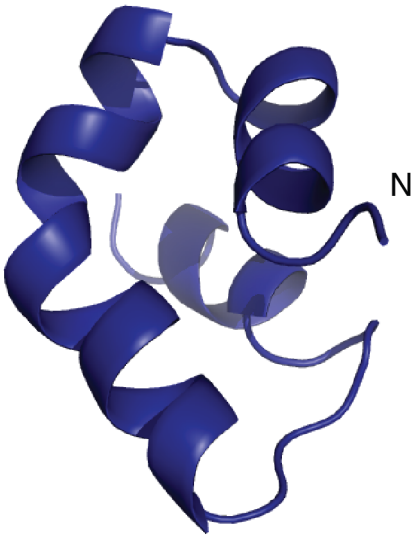

Figure 4.9. Solution structure of enterocin 7A. N-terminus is indicated by the letter N.

As may be expected due to the high number of lysine residues, the surface of enterocin 7A is highly cationic (Figure 4.10). The lysines are relatively dispersed through the enterocin 7A primary sequence, except for a region just C-terminal to the middle of the peptide sequence. The two anionic residues, Glu-29 and Asp-38, are situated on opposite sides of the structure. The highly cationic surface likely has implications for the mode of action of enterocin 7A, potentially drawing this peptide to the negatively-charged membrane surface of target bacteria. However, the similarly cationic leaderless bacteriocin aureocin A53 was found to bind more strongly to neutrally charged membranes than to negatively charged membranes.[46]

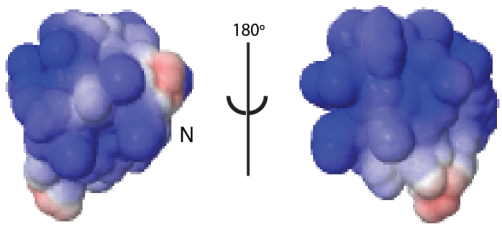

Figure 4.10. Electrostatic potential maps of enterocin 7A. Calculated using the APBS implementation of the PDB2PQR online pipeline.[177] Cationic regions indicated in blue, anionic regions in red, and neutral regions in white. N-terminus is indicated with the letter N.

The surface of enterocin 7A is mostly hydrophilic, due to the nature of the amphiphilic α-helices (Figure 4.11). However, there is also a hydrophobic patch that extends from one face of the peptide to the other. If the cationic surface of enterocin 7A draws the peptide to the bacterial surface, this hydrophobic strip may then be responsible for insertion into the membrane, resulting in any subsequent membrane disruption. The structure of aureocin A53 was predicted to feature surface-exposed hydrophobic tryptophan residues, based on fluorescence results.[46] The structure of enterocin 7A is similar, as all three tryptophan side-chains are exposed on the peptide surface.

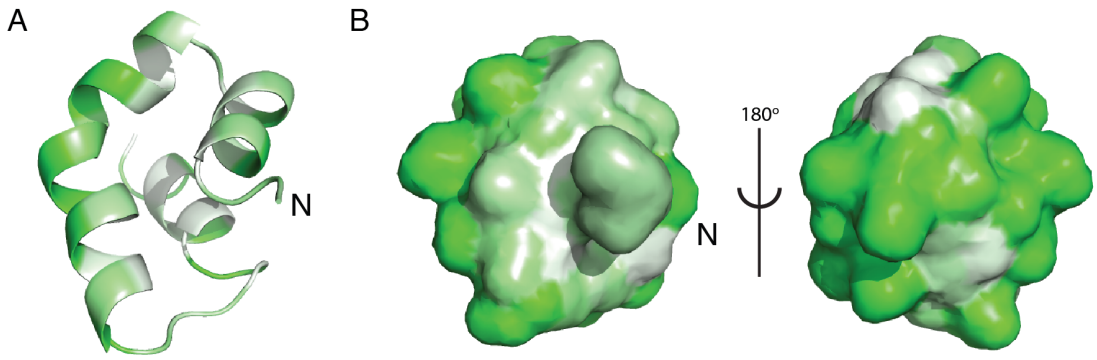

Figure 4.11. Hydrophobic surface maps of enterocin 7A. (A) Cartoon representation and (B) surface structure. Hydrophilic residues indicated in green, and hydrophobic residues in white. N-terminus is indicated with the letter N.

4.2.6. Comparison to enterocin 7B

The solution structure of enterocin 7B was solved by Vederas group graduate student Kaitlyn Towle. The overall conformation was highly similar to that of enterocin 7A, consisting of the same three α-helical regions. The two structures aligned well, with an RMSD of 1.46 Å over 507 atoms (Figure 4.12). Based on the high sequence similarity between these peptides, this conservation of structure was expected. The electrostatic potential and hydrophobic surface maps for enterocin 7B were similar but not identical to those of enterocin 7A.

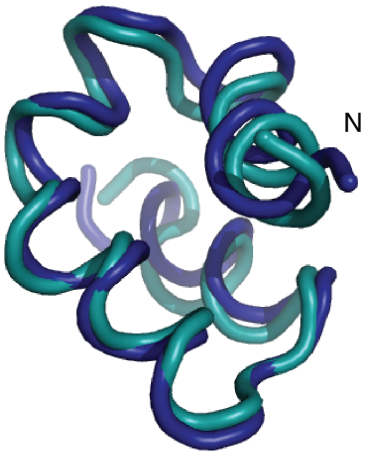

Figure 4.12. Overlay of structures of enterocins 7A and 7B. Enterocin 7A indicated in dark blue, while enterocin 7B is in light blue. The N-termini are indicated with the letter N.

4.2.7. Synergism

The initial report describing enterocins 7A and 7B indicated that no synergism was observed between these peptides against indicator organism *Lactobacillus sakei* DSM 20017.[174] This contrasts what was described for enterocins L50A and L50B and for enterocins MR10A and MR10B, which displayed significant synergistic activity.[44,45] Therefore, enterocins 7A and 7B were tested both individually and together against a selection of Gram-positive indicator organisms. These peptides displayed synergistic activity (with up to a four-fold increase in potency) against several indicator organisms, including *Lactococcus lactis*, *Brochothrix campestris* and the *Lactobacillus sakei* strain against which no synergism had been observed previously. This may be due to the use of different methodology for the testing of synergistic activity; the previously used methodology was not described.

4.2.8. Testing for interactions between enterocins 7A and 7B

To examine if the synergistic activity observed between enterocins 7A and 7B resulted from physical interactions between these peptides, NMR spectra were collected for these peptides both individually and together. The ^{15}N-HSQC spectrum of a mixture of enterocins 7A and 7B was overlaid with ^{15}N-HSQC spectra acquired for enterocin 7A and 7B individually (Figure 4.13). This overlay revealed only minimal changes in the proton and ^{15}N chemical shifts of these peptides upon mixing. Furthermore, isothermal calorimetry did not demonstrate any endothermic or exothermic interactions upon the mixing of enterocins 7A and 7B. Based on these data, there appears to be no structural changes representing a binding interaction between these peptides in solution. However, it is also possible that binding interactions occur only in a membrane environment or upon binding to a receptor protein.

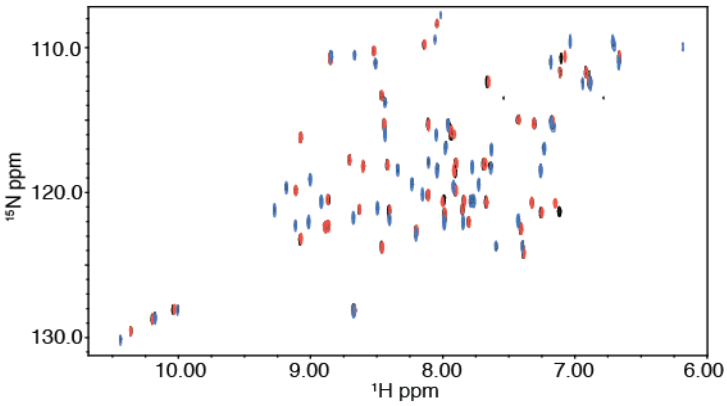

Figure 4.13. Overlay of ^{15}N-HSQC data for enterocin 7A and enterocin 7B individually and as a mixture. Data for enterocin 7A in red, for enterocin 7B in blue, and for the mixture in black.

4.2.9. Structural similarity to circular bacteriocin carnocyclin A

Carnocyclin A is a circular bacteriocin produced by *Carnobacterium maltaromaticum* UAL307.[157] This peptide consists of 60 amino acids, and is cyclized through an amide linkage between the N- and C-termini. The NMR solution structure of carnocyclin A was solved, showing it to be primarily composed of four α-helices.[170] The relative orientation of the α-helices in enterocin 7A and 7B were noted to resemble those of carnocyclin A. Alignment of the structures revealed a similar structural motif (Figure 4.14). The C-terminal α-helix and the C-terminal portion of the central kinked α-helix of enterocin 7A aligned with α-helices α1 and α2 of carnocyclin with an RMSD of 2.68 Å over 232 atoms. The corresponding region of enterocin 7B aligned better with carnocyclin A, with an rmsd of 1.21 Å over 169 atoms.

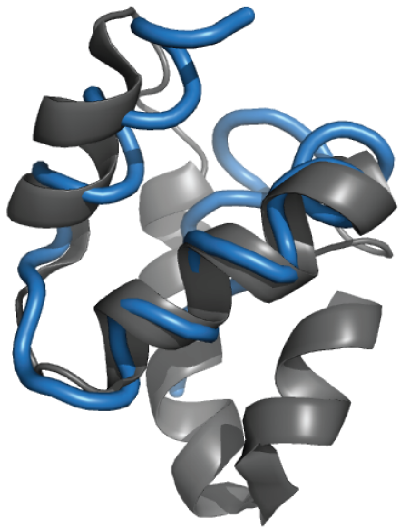

Figure 4.14. Overlay of enterocin 7A and carnocyclin A. Enterocin 7A indicated in blue, while carnocyclin A is in grey.

This structural similarity may explain the similar mode of action of leaderless bacteriocins and circular bacteriocins. Both carnocyclin A and the leaderless bacteriocin

lacticin Q are capable of permeabilizing membranes without requiring a particular receptor molecule.[55,172] However, the specific means by which they permeabilize the membrane differs; while lacticin Q forms huge toroidal pores in the target membrane, carnocyclin A forms anion-selective channels. Based on sequence similarity to lacticin Q and aureocin A53, enterocins 7A and 7B are expected to also act through membrane permeabilization. Therefore, this conserved structural motif may be necessary for both leaderless and circular bacteriocins to insert into the membrane. Once inserted, the other regions of these peptides may be responsible for the different types of pore formation and membrane disruption.

4.3. Conclusions and future directions

The solution structure of the leaderless bacteriocin enterocin 7A was characterized using NMR spectroscopy. Unlike most other linear bacteriocins, enterocin 7A is highly structured in aqueous solvents without lipid vesicles or organic co-solvents. CD spectroscopy suggested a high degree of α-helicity in water. The solution structure of enterocin 7A was solved using CYANA with distance constraints derived from NOESY experiments. This structure, which is highly similar to that of enterocin 7B, is principally α-helical. Three main α-helical regions were observed: at the N-terminus, the C-terminus, and a kinked α-helix in between. Enterocins 7A and 7B were confirmed to exert synergistic activity, although there did not appear to be a physical basis for this interaction in aqueous solution. Structural similarities to carnocyclin A revealed that leaderless bacteriocins and circular bacteriocins possess unexpected structural homology, which may be responsible for their similar modes of action.

As enterocins 7A and 7B likely insert into the target bacterial membrane, their structures in lipid micelles may be of interest. The CD spectra of lacticin Q differed between aqueous conditions and lipid vesicles although α-helicity appeared to be maintained.[54] In aqueous conditions, the hydrophobic residues of the enterocins are largely buried in the peptide core. However, in a more hydrophobic environment, the α-helices of these peptides may unpack and adopt a conformation more relevant to their mode of action. Intermolecular interactions between the unpacked peptides could also develop under these conditions, potentially forming pores or other complexes.

As described before, the mode of action of leaderless bacteriocins lacticin Q and aureocin A53 has been described. The antimicrobial activity of these two bacteriocins has been attributed to the disruption of the target bacterial membrane, resulting in the loss of essential metabolites and membrane depolarization. Lacticin Q forms huge toroidal pores in bacterial membranes of a size large enough to allow for the leakage of proteins, a property not previously associated with bacteriocins.[55] However, the mode of action of aureocin A53 was significantly different than that of lacticin Q. There was no evidence that aureocin A53 formed discrete pores in the target bacterial membrane; instead, it was found to act through generalized membrane permeabilization.[56] That these similar peptides can have such variable effects on the bacterial membrane brings up questions regarding the mode of action of enterocin 7A and 7B. Only conjecture based on the structures is possible at this point. Investigation into their particular mode of action would allow rationalization of the structure activity relationship of these peptides.

As the modes of action of lacticin Q and aureocin A53 have been studied, it would be of interest to determine the solution structures of these peptides. With these

structures, it may be possible to rationalize their differing means of permeabilizing bacterial membranes. Moreover, their structures could be compared to enterocins 7A and 7B, carnocyclin A, and AS-48. If the solution structures of lacticin Q and aureocin A53 contain the same relative orientation of α-helices as are conserved between enterocins 7A/7B and carnocyclin A, this would further support the hypothesis that this structural motif is implicated in membrane permeabilization.

The basis of the synergistic activity observed between enterocin 7A and 7B deserves further consideration. The majority of two-component bacteriocins feature structurally different subunits. The components of class IIb bacteriocins (i.e., two-component bacteriocins that are biosynthesized with a leader sequence) such as plantaricin E/F and plantaricin J/K show very little sequence homology.[167] The same is true for two-component lantibiotics and sactibiotics, such as lacticin 3147 and thuricin CD.[27,178] Many of these two-component bacteriocins require the presence of both components to display strong activity. However, enterocins 7A and 7B are strongly active individually. That two such similar peptides, in terms of both sequence and structure, demonstrate synergistic activity is unusual. Potentially, one could imagine that pores formed from both peptides may be more stable and long-lived, thereby more effectively disrupting a bacterial membrane. Mechanistic studies of the enterocins individually and together may reveal the cause of the synergistic activity, as well as reveal similarities to other leaderless and circular bacteriocins.

Chapter 5

Solution structure of a leucocin A mutant

5.1. Background

5.1.1. Introduction

The class IIa bacteriocins are a group of antilisterial peptides characterized by the presence of a conserved N-terminal YGNGV sequence and N-terminal disulfide bridge. The biosynthesis and mode of action of these bacteriocins is discussed in detail in Chapter 1. Leucocin A, a 37 residue bacteriocin produced by *Leuconostoc gelidum*, was the first member of this class to be identified (Figure 5.1).[58] However, much of the focus on these bacteriocins has centered on pediocin PA-1/AcH, produced by *Pediococcus acidilactici*. Extracts containing pediocin have found widespread use for the purpose of food preservation.[3]

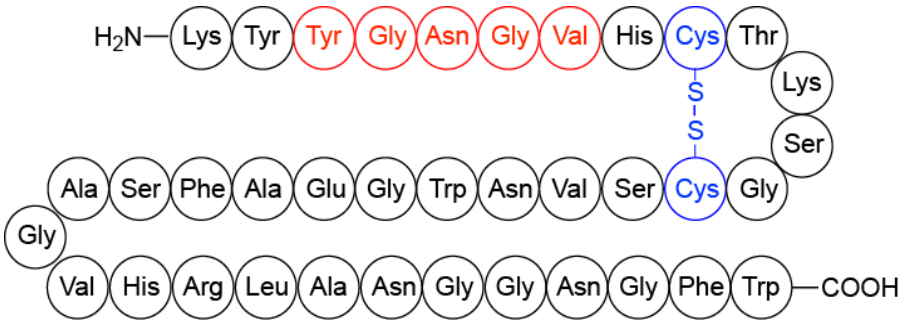

Figure 5.1. Bead structure of leucocin A. Conserved YGNGV motif indicated in red, conserved N-terminal disulfide bond indicated in blue.

The solution structures of several class IIa bacteriocins have been determined using NMR spectroscopy, as mentioned in Chapter 4. Bacteriocins of this class tend to

exist as random coils in aqueous conditions, based on circular dichroism (CD) spectroscopy.[60] The use of organic co-solvents (e.g., trifluoroethanol) or lipid micelles (e.g., dodecylphosphocholine) induces structure formation in these bacteriocins.[60,63] The structures of leucocin A,[60] carnobacteriocin B2,[61] curvacin A[63] and sakacin P[62] have all been elucidated using NMR spectroscopy.

The structure of leucocin A was solved in a mixture of trifluoroethanol and water, as well as in dodecylphosphocholine micelles, with well-defined conformations under both conditions (Figure 5.2).[60,61] The N-terminus exists as a three-strand antiparallel β-sheet stabilized by a disulfide bridge between cysteines 9 and 14. The conserved YGNGV sequence occurs in the N-terminal portion of this β-sheet structure. A C-terminal amphiphilic α-helix exists between residues 19 and 30, occurring after the tryptophan-18 hinge position. The C-terminal tail (residues 33-37) folds back towards the α-helix region.

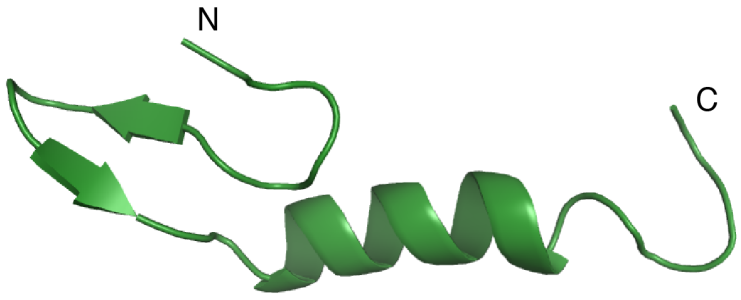

Figure 5.2. NMR solution structure of leucocin A. Termini indicated with N and C. Structure determined in aqueous trifluoroethanol.[61]

As described in Chapter 1, class IIa bacteriocins act by permeabilizing the membrane of target bacteria, resulting in depletion of ATP and loss of proton motive force.[59] The cationic N-terminus is thought to initially attract the peptide to the negatively-charged target membrane.[179] Bacterial sensitivity to the class IIa bacteriocins has been shown to be dependent on the presence of the transmembrane mannose phosphotransferase (MPT) complex. An extracellular loop of the IIC MPT subunit is a determinant of target recognition for these bacteriocins.[75] Presumably after interacting with a MPT subunit, the amphiphilic C-terminal α-helix may insert into the target membrane. This C-terminal α-helix is responsible for determining the spectrum of activity of these bacteriocins, likely interacting directly with the transmembrane helices of MPT.[68,76] The formation of this MPT bacteriocin complex may result in pore formation, ultimately killing the target bacteria.[68]

The conserved N-terminal disulfide bridge found in the class IIa bacteriocins is generally very important for activity. Acetamidomethylation of the cysteine residues involved in disulfide formation of mesentericin Y105 resulted in a great loss in antimicrobial potency.[180] Similarly, a mutant of this peptide wherein Cys-9 and Cys-14 were replaced with serine residues was 20,000 times less active than the natural peptide.[180]

During structure-activity relationship studies of leucocin A, the impact of replacing the conserved disulfide bridge with a carbocycle was explored.[181] For this purpose, a leucocin A analogue with cysteines 9 and 14 replaced with allylglycine residues was synthesized. Ring-closing metathesis was used to form the carbocycle, yielding carba-LeuA (Figure 5.3A). Antimicrobial testing of this derivative indicated that

it was approximately eight-fold less active than natural leucocin A. However, the uncyclized double allylglycine variant was as antimicrobially active as natural leucocin A (Figure 5.3B). Similar to mesentericin Y105, replacement of both leucocin A cysteine residues with serines resulted in an antimicrobially inactive analogue.[181]

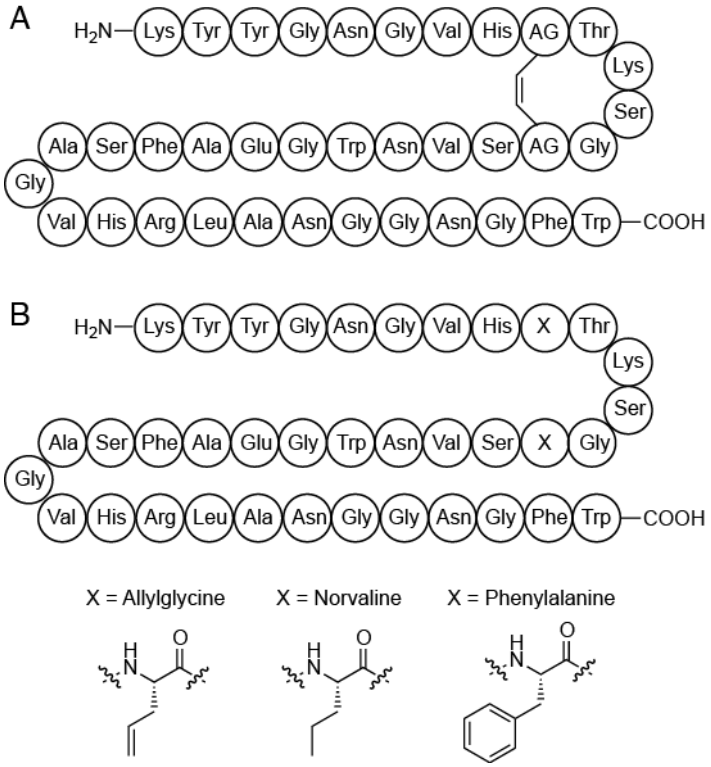

Figure 5.3. Bead structures of leucocin A variants. (A) Carba-LeuA and (B) diallylglycine LeuA. AG represents residues derived from allylglycine.

Hydrophobic interactions between the two allylglycine residues were suggested to maintain the leucocin A mutant peptide in a similar conformation as the wild type peptide. To explore this possibility, other leucocin A analogues were synthesized bearing norvaline or phenylalanine residues in place of the cysteine residues.[182] These variants were all as active as wild-type leucocin A against a selection of bacterial indicator organisms. Therefore, the replacement of the two leucocin A cysteine residues with

hydrophobic residues appears to generally yield active variants. Based on these results, it was of interest to examine the impact of these substitutions on the conformations of these variants and see if the N-terminal three-strand β-sheet of leucocin A is maintained.

5.1.2. Project objectives

The impact of replacing the disulfide bridge of leucocin A with other residues was to be explored by determining the solution structures of three leucocin A mutants. For this purpose, the active C9F,C14F mutant and the inactive C9S,C14S mutant would be studied by Vederas group graduate students Chantel Campbell and Clarissa Sit, respectively. The characterization of a new C9L,C14L mutant is described herein. Comparison of the structures of these three peptides may provide insight into the basis for the retention of antimicrobial activity by the hydrophobic mutants.

5.2. Results and Discussion

5.2.1. Cloning, expression and purification of MBP-(C9L,C14L)-leucocin A

While the leucocin A analogues were previously obtained through chemical synthesis, some means of isotopically labeling these peptides with carbon-13 and nitrogen-15 was desired to simplify the interpretation of NMR data. The heterologous expression of a class IIa bacteriocin as a maltose-binding protein (MBP) fusion in *Escherichia coli* was previously described for the purpose of isotopically labeling precarnobacteriocin B2.[183] Additionally, this approach results in a more hydrophilic protein species, avoiding complications associated with expressing small peptides in *E. coli*,[184] and simplifying the purification of the resulting fusion protein.

With Vederas group research associate Dr. Marco van Belkum, synthetic oligonucleotide primers encoding the mutant structural gene were used to create the

desired nucleotide sequence for cloning purposes. The mutant sequence was cloned into commercial plasmid pMAL-c2X in frame with the *malE* gene. This construct would yield a fusion protein with the MBP sequence N-terminal to the leucocin A mutant. These two domains were separated by the recognition sequence for serine protease Factor Xa, allowing subsequent cleavage to provide the (C9L,C14L)-leucocin A mutant with no additional amino acids.

E. coli BL21(DE3) was transformed with the constructed plasmid for protein expression. Following the culturing of a transformant to an OD_{600} of 0.5, protein expression was induced through the addition of 0.3 mM isopropyl-β-D-thiogalactopyranoside (IPTG). After lysing the induced cells via a passage through a cell disruptor, the lysate was clarified through centrifugation. The lysate supernatant was passed through a column of amylose resin, to which the fusion protein bound. After washing off unbound proteins, the desired protein was eluted using running buffer containing maltose. Elution was monitored by UV, and fractions containing the desired fusion protein were confirmed by SDS-PAGE. The fractions containing MBP-(C9L,C14L)-LeuA were dialyzed against milli-Q water and lyophilized.

5.2.2. Factor Xa cleavage and purification of (C9L,C14L)-leucocin A

The lyophilized fusion protein was dissolved in lysis buffer, and pilot cleavage studies were conducted with protease Factor Xa. The extent of cleavage was monitored using both MALDI-TOF MS and SDS-PAGE (Figure 5.4). After 3 h, cleavage of the fusion protein was judged to be complete based on the absence of the full fusion protein. Longer digests resulted in the appearance of other masses by MALDI-TOF MS, likely due to non-specific proteolytic cleavage catalyzed by Factor Xa.

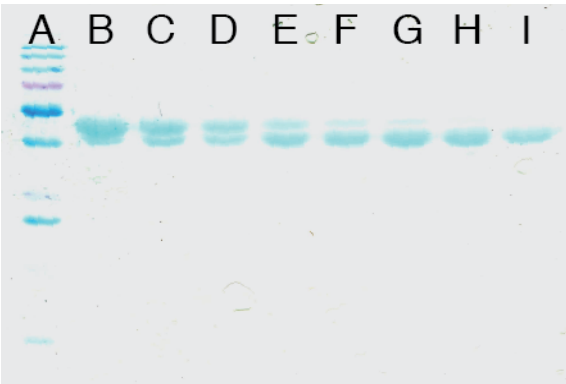

Figure 5.4. SDS-PAGE of (C9L,C14L)-LeuA Factor Xa digests. (A) Protein ladder. Digests after (B) 0 h, (C) 0.5 h, (D) 1.0 h, (E) 1.5 h, (F) 2.0 h, (G) 2.5 h, (H) 3.0 h and (I) 3.5 h. The top band corresponds to MBP-(C9L,C14L)-LeuA, while the bottom band corresponds to MBP.

With the cleavage protocol established, the final step was to purify (C9L,C14L)-leucocin A. To separate the desired peptide from the protease buffer components, Factor Xa and MBP, the scaled-up digest was fractionated using reverse-phase HPLC. The leucocin A mutant eluted as a single peak, separate from the other contaminants as judged by MALDI-TOF MS. The HPLC-purified (C9L,C14L)-leucocin A was concentrated and lyophilized.

5.2.3. Antimicrobial activity

As the double leucine leucocin A mutant had not been previously characterized, its potency relative to the wild-type leucocin A remained to be determined. Serial dilutions of mutant and wild-type leucocin A were tested using a spot-on-lawn assay against indicator organism *Carnobacterium maltaromaticum* UAL26. The lowest concentration of mutant peptide that displayed antimicrobial activity was 25 μM, while wild-type leucocin A was active down to 3.13 μM. However, this is in contrast to the extent of activity observed for the double allylglycine, norvaline and phenylalanine

mutants, which were as active as wild-type leucocin A against *C. maltaromaticum* UAL26.[182]

5.2.4. Isotopic labeling

With the purification protocol established and the activity of the double leucine mutant confirmed, the next step was to isotopically label this peptide for NMR studies. *E. coli* bearing the desired plasmid was grown in M9 minimal media containing uniformly ^{13}C-labeled glucose and ^{15}N-labeled ammonium sulfate as the primary carbon and nitrogen sources, respectively. The remainder of the purification protocol was performed in the same manner as for the unlabeled peptide. The extent of isotopic labeling was evaluated by MALDI-TOF MS, which demonstrated that ^{13}C,^{15}N-incorporation was almost complete (expected average $[M+H]^+$ = 4183.6, observed $[M+H]^+$ = 4176.5) (Figure 5.5).

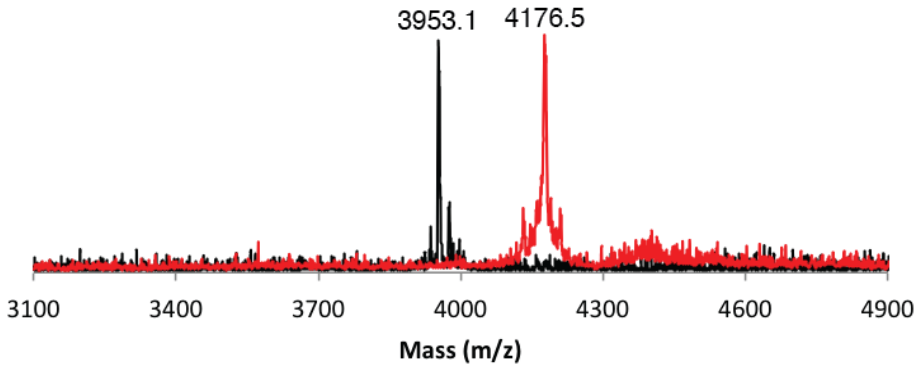

Figure 5.5. MALDI-TOF MS spectra of unlabeled and labeled (C9L,C14L)-leucocin A. Unlabeled peptide indicated in black, labeled peptide indicated in red.

5.2.5. NMR spectroscopy of ^{13}C,^{15}N-labeled (C9L,C14L)-leucocin A

^{13}C,^{15}N-labeled (C9L,C14L)-leucocin A was dissolved in 90 % trifluoroethanol for NMR. As with wild-type leucocin A, trifluoroethanol was used to induce structuring,

otherwise the peptide would likely exist as a random coil.[60] A ^{15}N-HSQC dataset for this peptide showed good dispersion of backbone amide nitrogen and proton signals, suggestive of structure (Figure 5.6). Therefore, a suite of two- and three-dimensional heteronuclear NMR datasets were acquired.

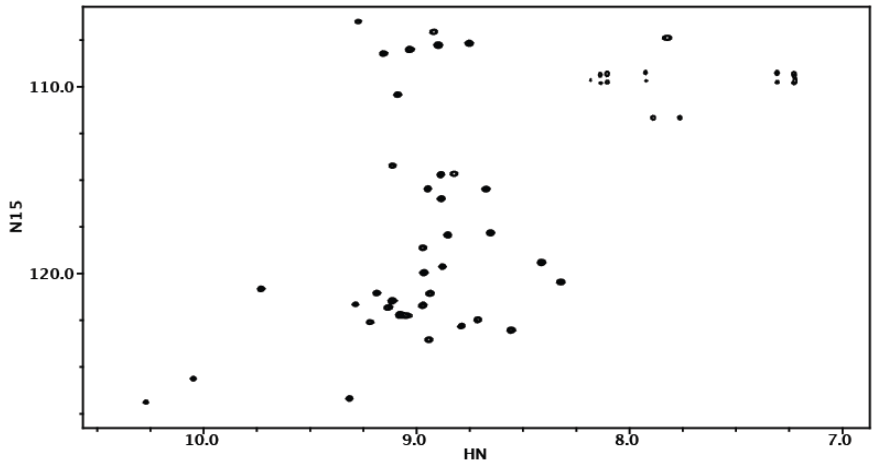

Figure 5.6. ^{15}N-HSQC spectrum of (C9L,C14L)-leucocin A.

The sequential order of the signals corresponding to the backbone amide nitrogens and protons was determined on the basis of HNCACB and CBCA(CO)NH experiments.[164] Once each amide proton signal was attributed to a particular amino acid, the amino acid side chain chemical shifts were determined primarily using the ^{15}N-TOCSYHSQC and HCCH-TOCSY datasets. Based on these datasets, the majority of the ^{1}H, ^{13}C and ^{15}N chemical shifts were assigned (Table 6.9, 6.10).

5.2.6. (C9L,C14L)-Leucocin A structure calculations

Automated structure calculation of (C9L,C14L)-leucocin A was performed using CYANA.[176] CYANA was provided with a list of NOE crosspeaks derived from ^{15}N-NOESYHSQC and ^{13}C-NOESYHSQC experiments to act as distance restraints.

Backbone angle restraints were derived from an HNHA dataset and the output of TALOS. Comparison of the intensity of diagonal peaks to cross-peaks in the HNHA dataset provided *J* couplings for the corresponding amide proton and α-proton.[185] TALOS compared the mutant amino acid sequence and chemical shift assignments to a database of proteins of known structure to provide predicted backbone φ and ψ angles.[186]

Automated NOE assignment was performed by providing CYANA with the chemical shift assignments for (C9L,C14L)-leucocin A and a list of NOE crosspeaks. Based on these data, CYANA calculated 20 different representative structures (Table 5.1). Following the manual assignment of select NOEs, a series of closely overlapping structures were generated with no distance, angle and steric constraint violations (Figure 5.7). While the positions of the termini were highly variable, the α-helical regions and the turn connecting them overlapped well.

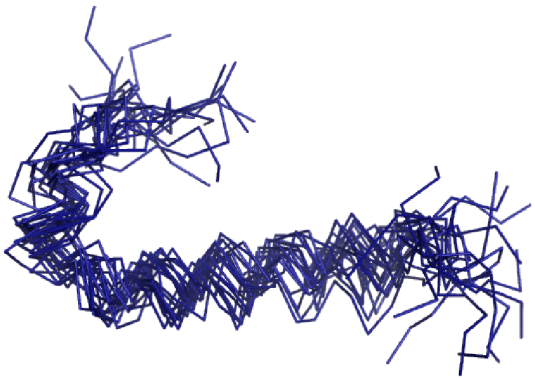

Figure 5.7. Overlay of 20 structures calculated by CYANA for (C9L,C14L)-leucocin A.

Table 5.1. (C9L,C14L)-leucocin A structure calculation statistics

Distance and angle restraints	
Total NOE crosspeak assignments	385
Short ($\|i-j\| \leq 1$)	331
Medium ($1 < \|i-j\| < 5$)	52
Long ($\|i-j\| \geq 5$)	2
Number of φ angles	21
Average target function value	0.02
RMSD (Å) for residues 1 – 36	
Backbone	2.53 ± 0.48
Heavy atoms	3.37 ± 0.47
RMSD (Å) for residues 14 – 30	
Backbone	0.46 ± 0.17
Heavy atoms	1.09 ± 0.21

5.2.7. Description of the (C9L,C14L)-leucocin A solution structure

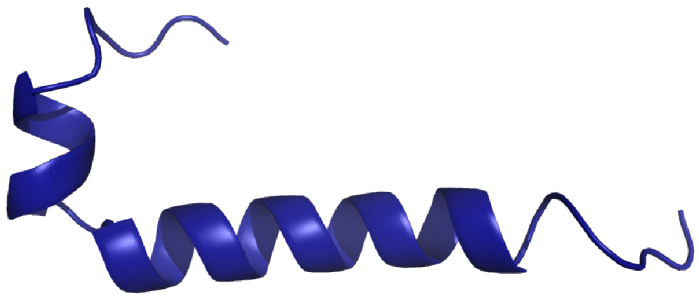

Figure 5.8. Solution structure of (C9L,C14L)-leucocin A.

The most noteworthy feature of (C9L,C14L)-leucocin A is the presence of a short α-helical region near the N-terminus (Figure 5.8, 5.9). This contrasts the three-strand β-sheet found in the structure of wild-type leucocin A. While one possibility was that the hydrophobic interactions between the two leucine residues would hold the N-terminus in

a similar β-sheet structure, this does not appear to be the case. Based on this, it appears that the disulfide bridge is indeed essential for maintaining the β-sheet conformation of the leucocin N-terminus. The C-terminal α-helical region of the mutant extends much closer to the N-terminus, reaching residue 14, whereas the α-helical region of the wild-type peptide only reaches Trp-18 (Figure 5.9). However, the α-helices both extend towards the C-terminus to the same extent, ending at Leu-29.

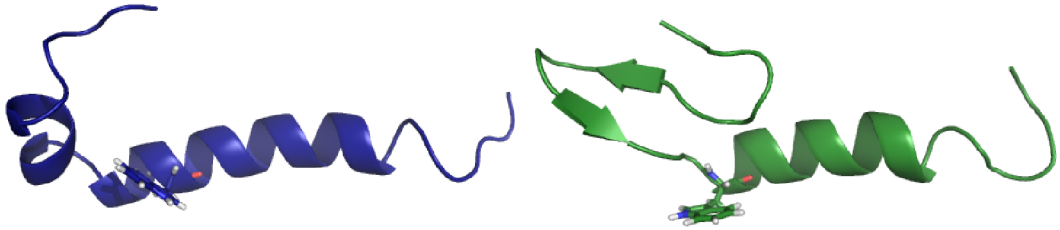

Figure 5.9. Comparison of (C9L,C14L)-LeuA and wild-type LeuA. (C9L,C14L)-LeuA indicated in blue, wild-type LeuA in green. Tryptophan-18 is shown in a stick representation.

While the N-termini of wild-type leucocin A and (C9L,C14L)-LeuA have the same number of cationic residues, these residues were less grouped together in the mutant structure than in that of the wild-type peptide (Figure 5.10A). The only anionic regions present on the surface are due to a glutamic acid residue in the α-helix and the C-terminus. A hydrophobic surface map of the mutant structure demonstrates the amphiphilic nature of the α-helix, with a strip of hydrophobic residues present on one face (Figure 5.10B). Consistent with its cationic nature, the N-terminus is largely hydrophilic, while the C-terminal tail consists largely of hydrophobic residues.

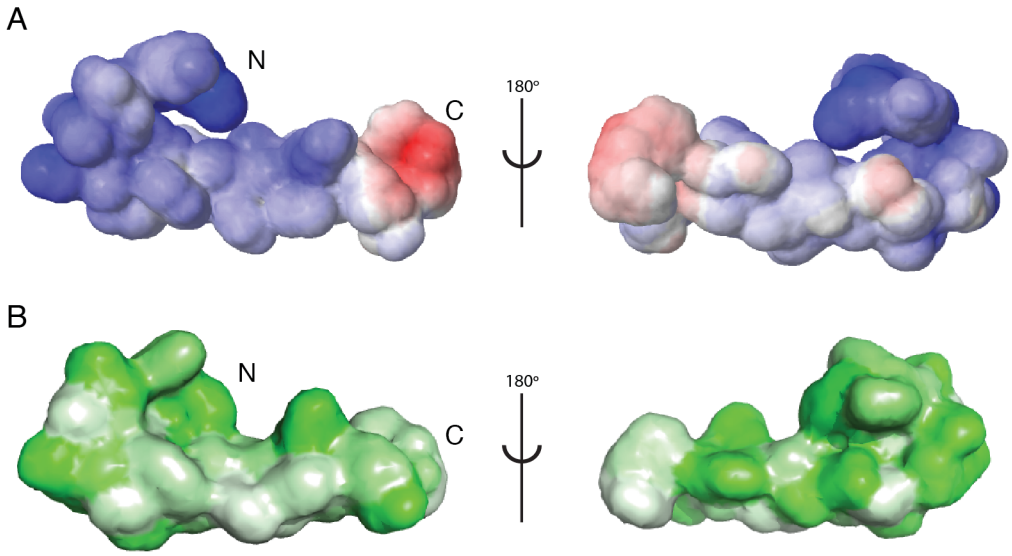

Figure 5.10. Electrostatic potential and hydrophobic solvent accessible surface maps of (C9L,C14L)-leucocin A. (A) Electrostatic surface potential calculated using the APBS implementation of the PDB2PQR online pipeline.[177] Cationic regions are indicated in blue, anionic regions in red, and neutral regions in white. (B) Hydrophobic surface map, with hydrophilic residues indicated in green, and hydrophobic residues in white.

While the two leucine residues did not mimic the disulfide bridge of the wild-type leucocin A, NOE crosspeaks were observed between the δ-protons of Leu-9 and the α- and β-protons of Leu-14 suggesting that these two residues were close in space (Figure 5.11). Leu-9 was situated in the middle of the N-terminal α-helix, while the C-terminal α-helix started at Leu-14. It is possible that the presence of these two hydrophobic residues affects the relative orientation of the two α-helices as mediated through hydrophobic interactions.

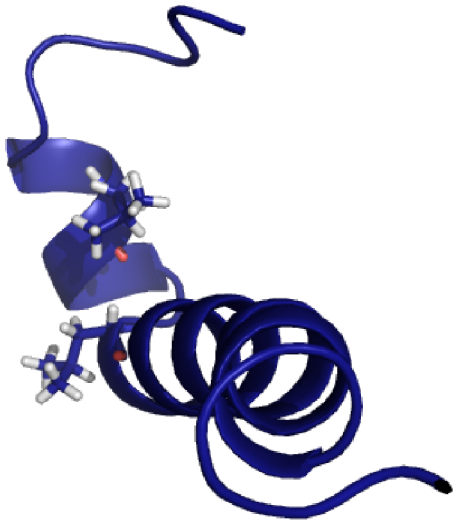

Figure 5.11. Possible hydrophobic interactions between Leu-9 and Leu-14.

5.2.8. Comparison to (C9S,C14S)-leucocin A

The solution structure of the inactive C9S,C14S mutant of leucocin A was solved by former Vederas group graduate student Dr. Clarissa Sit (Figure 5.12). As expected, this peptide did not bear the N-terminal β-sheet found in wild-type leucocin A. However, the N-terminus also differed greatly from that of the double leucine mutant, existing largely as an unstructured coil. The C-terminal α-helical region of the double serine mutant resembled that of the double leucine mutant, reaching closer to the N-terminus than in the wild-type peptide. The α-helices of both mutants extended up to residue 14, whereas that of leucocin A extended to Trp-18.

The impact of the amino acid substitution on the N-terminal structures of these peptides may be due to a variety of factors. Relative to serine, leucine residues have a higher propensity to be involved in α-helices.[187] Hydrophobic interactions between the two introduced leucine residues could stabilize the α-helical region. Alternately,

hydrogen bonding interactions of the two serine residues could stabilize a different conformation in (C9S,C14S)-LeuA.

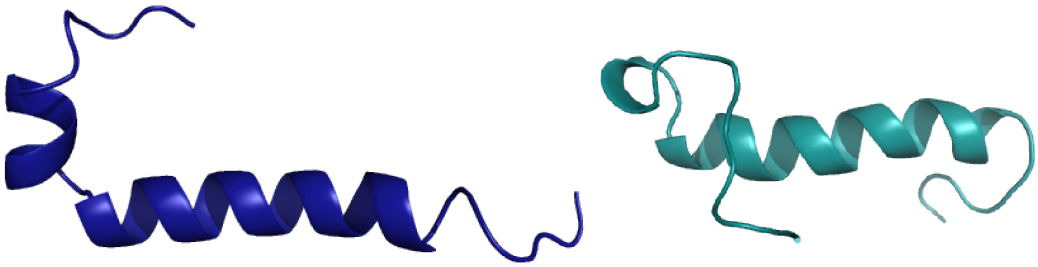

Figure 5.12. Comparison of (C9L,C14L)-LeuA and (C9S,C14S)-LeuA. The double leucine mutant is indicated in dark blue, while the double serine mutant is in teal.

Structural characterization of the double phenylalanine leucocin A mutant is still in progress. Depending on the relatedness of this structure to (C9L,C14L)-LeuA, some conclusions relating structure to activity may be possible.

5.2.9. Implications of structure and mode of action

An important consideration regarding these structures is the choice of solvent. As trifluoroethanol is noted for its tendency to induce structuring in peptides,[188] the fact that the N-terminus of the double leucine mutant becomes α-helical in these conditions is not necessarily noteworthy. The solvent conditions are used to approximate the membrane environment wherein the bacteriocins interact with their target bacteria. However, the N-termini of class IIa bacteriocins are thought to act away from the membrane core,[59] as the amphiphilic α-helix inserts into the membrane. Potentially, the conformation of the N-terminus of the double leucine mutant would better mimic the disulfide bridge found in the wild-type peptide in a different solvent environment. The exposure of the two

hydrophobic leucine residues on the surface of the peptide may not be significant, given the use of an aqueous trifluoroethanol solution.

The interpretation of the structure depends on a consideration of the mode of action of bacteriocins of this class. The conformation of the bacteriocin N-terminus may be involved in orienting the cationic residues to facilitate an initial electrostatic attraction. The N-terminal cationic residues of wild-type leucocin A are clustered on the surface, while those of the double leucine mutant are relatively dispersed. Similarly, the cationic residues of the double serine mutant are oriented in different directions. However, as mentioned above, the N-terminal conformations of the mutants may not be representative of the peptide structure in the conditions wherein the bacteriocins encounter target bacteria. Based on a comparison of the mutant structures, it is not clear why the double leucine mutant is active but the double serine mutant is not. This is compounded by the lack of understanding regarding the interaction between class IIa bacteriocins and the transmembrane MPT complex of target bacteria.

5.3. Conclusions and Future Directions

As was seen for other variants, replacement of the two cysteine residues of leucocin A with leucine residues yielded an antimicrobially active peptide, although there was a loss of potency with this substitution. Structural characterization of this mutant peptide revealed a short α-helix in place of the β-sheet of wild-type leucocin A. Under the solvent conditions tested (i.e., aqueous TFE), the two leucine residues did not form a hydrophobic bridge mimicking the disulfide bridge as had been hypothesized. However, there was evidence for an interaction between the two leucine residues, potentially affecting the relative orientation of the two α-helices.

The use of aqueous trifluoroethanol likely biases the structure of the N-terminus, as the expected mode of action does not position the N-terminal region directly in a membrane environment. Therefore, determination of the solution structure of (C9L,C14L)-LeuA in lipid micelles may be more representative of the actual biological system. Presumably, the amphiphilic C-terminal α-helix would insert into the micelles to the extent where tryptophan-18 is situated at the membrane-solution interface.[59,189] This may allow the N-terminus to adopt a different conformation than if it were fully immersed in aqueous trifluoroethanol.

The precise role of the N-termini of class IIa bacteriocins in their mode of action is not fully understood. These bacteriocins are known to interact with a subunit of the MPT complex of the target bacterial strain. Although there is evidence that the bacteriocin C-terminal α-helix interacts with an MPT subunit,[59] there could potentially be an interaction between the bacteriocin N-terminus and an extracellular portion of this same subunit. To gain insight into the nature of the interaction between bacteriocin and MPT permease, structural studies must be done. However, there is currently no experimental structural data for the MPT subunits, complicated by the transmembrane nature of these proteins.

With the advances in determining the X-ray crystal structures of transmembrane proteins, efforts should be made to determine the structure of the MPT subunits, either individually or together. As the extracellular loop region of the MPT IIC subunit responsible for susceptibility is known.[75] Inferences regarding the interaction with a bacteriocin could be made based on this structure. Alternately, if it could be obtained, an X-ray crystal structure of a bacteriocin complexed to the MPT subunit would be

extremely valuable for characterizing the interaction. Alternately, NMR studies using isotopically labeled samples could provide some preliminary structural information about any binding interactions. With these data, the role of the bacteriocin N-terminus in its antimicrobial action would become more clear. Until then, only speculation regarding the role of the leucocin A disulfide bridge can be made.

Chapter 6

Experimental procedures

6.1. General experimental details

6.1.1. General techniques for microbiological work

6.1.1.1. Media

Unless otherwise indicated, all pre-prepared media and media components were purchased from Becton Dickinson and Company (BD, Franklin Lakes, NJ, USA). Liquid media was prepared according to the manufacturer's instructions. Soft agar tubes (0.75 % agar) were prepared by first boiling the desired amount of agar in the appropriate liquid media. The molten solution was aliquoted into screw-cap tubes in 10 mL portions and autoclaved. Agar plates (1.5 % agar) were prepared by first boiling the desired amount of agar in the appropriate liquid media. The agar solution was autoclaved and allowed to cool to 55 °C prior to the addition of any antibiotic solutions. The agar solution was poured into 10 cm Petri dishes (20 mL per plate) in a laminar flow cabinet and allowed to cool. The poured plates were stored at 4 – 8 °C until used.

6.1.1.2. Glycerol stocks

Bacterial strains were maintained as glycerol stocks. Sterile 60 % glycerol (333 μL) was mixed with fresh bacterial culture (667 μL), for a final concentration of 20 % glycerol. These stocks were maintained at -80 °C, and the amount of time exposed to room temperature during inoculation was minimized. Cultures were inoculated using the

glycerol stocks by aseptically transferring a small amount of the frozen mixture into liquid media using a sterile pipette tip.

6.1.2. Antimicrobial testing

6.1.2.1. Deferred inhibition assays

A sterile toothpick was dipped into a fully-grown culture of the bacteria of interest and stabbed into an agar plate supplemented with media appropriate for this organism. The stabbed plate was then incubated overnight at a temperature appropriate for the bacterial strain. A 5 mL tube of molten soft agar was inoculated (1 %) with a fully-grown liquid culture of the indicator organism, vortexed, and poured over the stabbed agar plate. To prepare a liquid culture of *C. jejuni*, cells from a confluent plate were suspended in Mueller-Hinton broth, which was used to inoculate molten soft agar as above. The overlaid plate was incubated overnight at an appropriate temperature for the indicator organism.

6.1.2.2. Spot-on-lawn assays

Tubes of molten medium-supplemented soft agar were inoculated (1 %) with a fully-grown overnight liquid culture of the indicator organism, vortexed, and poured over an agar plate (20 mL; 1.5 % agar) of the same medium. Suspensions of *C. jejuni* were prepared and used as described above. After the molten soft agar had solidified, samples were pipetted onto the surface (10 μL once, or 2 μL five times) and allowed to evaporate. Plates were incubated overnight at an appropriate temperature for the indicator organism, and activity was judged based on the presence and magnitude of zones of clearing.

6.1.2.3. MIC testing

Minimal inhibitory concentration (MIC) values were tested using a modified broth microdilution method.[190] A culture of the indicator organism was streaked onto an agar plate and incubated overnight at the appropriate temperature for the indicator organism. Approximately four isolated colonies were suspended in 1 mL of Mueller-Hinton Broth (MHB), and the OD_{600} was measured. Based on the absorbance, the cell suspension was diluted in 12 mL of MHB to a predicted OD_{600} of 0.001.

In a 96-well plate, 100 μL of the diluted bacterial suspension was added to the appropriate number of wells for testing each desired serial dilution (either in duplicate or triplicate). To the first column of wells containing bacterial cells, 100 μL of the antimicrobial solution was added and mixed. Then, 100 μL of this resulting solution was added to the second column of wells, mixed, and so on until all of the desired serial dilutions had been prepared. The plate was then incubated overnight at a temperature appropriate for the indicator organism.

6.1.2.4. Indicator organism culture conditions

Table 6.1. Indicator organisms

Indicator strain	Media[b]	Conditions
Bacillus subtilis JH642	APT	30 °C, 0 rpm
Brochothrix campestris ATCC 43754	APT	RT, 0 rpm
Campylobacter jejuni NCTC 11168	MHB	37 °C, 0 rpm[a]
Carnobacterium maltaromaticum A9b-	APT	RT, 0 rpm
Carnobacterium maltaromaticum UAL26	APT	RT, 0 rpm
Enterococcus faecium ATCC 19434	APT	RT, 0 rpm
E. faecium BFE900	APT	RT, 0 rpm
Escherichia coli DH5α	LB	37 °C, 225 rpm
Lactobacillus sakei DSM 20017	APT	RT, 0 rpm
Lactococcus lactis subsp. *cremoris* HP	APT	RT, 0 rpm
Listeria monocytogenes ATCC 15313	APT	RT, 0 rpm
Paenibacillus polymyxa NRRL B-30509	Brucella	37 °C, 225 rpm
Pseudomonas aeruginosa ATCC 15442	LB	37 °C, 225 rpm
Pediococcus acidilactici PAC 1.0	APT	30 °C, 0 rpm
Salmonella enterica serovar Typhimurium ATCC 13311	LB	37 °C, 225 rpm
Staphylococcus aureus ATCC 25923	LB	30 °C, 0 rpm

[a] Grown on solid media under 10 % CO_2, 5 % O_2 and the remainder N_2. [b]APT: all-purpose tween, MHB: Mueller-Hinton broth, LB: Luria-Bertani broth.

6.1.3. General chromatographic purification of peptides and proteins

6.1.3.1. Amberlite XAD-16 hydrophobic interactions chromatography

The desired amount of Amberlite XAD-16 resin (Sigma-Aldrich, St. Louis, MO, USA; usually 20-30 g per liter of culture supernatant) was soaked in isopropanol for 15-30 min. The resin slurry was poured into a glass column fitted at the base with Miracloth (EMD Millipore, Billerica, MA, USA), and the isopropanol was passed through the resin without letting the column run dry. The resin was then washed at 10 mL/min with 250 mL of 0.1 % trifluoroacetic acid (TFA) in water per 30 g resin. The column was stored

under a volume of 0.1 % TFA until use. The solvent conditions and flow rates used are described later.

6.1.3.2. C18 solid-phase extraction cartridges

Both Strata C18-E (Phenomenex, Torrance, CA, USA) and Megabond C18 (Agilent, Santa Clara, CA, USA) solid-phase extraction (SPE) cartridges were used interchangeably. These cartridges were pre-conditioned at 10 mL/min with 50 mL of methanol followed with 100 mL of Milli-Q water. Flow rates were controlled using either a peristaltic pump or by attaching the cartridge to the house vacuum line.

6.1.3.3. HPLC

High-pressure liquid chromatography (HPLC) was used as the final purification step for all of the isolations described herein. Separations were performed on Beckman System Gold chromatographs (analytical and preparative), a Varian Prostar Model 210 systems (analytical and preparative) and a Gilson system with a model 322 HPLC pump (preparative). HPLC grade solvents were all passed through a Millipore filter under vacuum prior to use. The appropriate solvent gradients and HPLC columns used are described later in the appropriate sections of this Chapter.

6.1.4. General molecular biology procedures

6.1.4.1. Plasmid isolation

A culture of *E. coli* DH5α bearing the plasmid of interest (inoculated from a single colony or glycerol stock) was grown overnight in 10 - 50 mL LB broth (supplemented with any relevant antibiotics) at 37 °C, 225 rpm. Plasmids were isolated from these cultures using either GeneJET Plasmid Miniprep Kit (Thermo Scientific, Waltham, MA, USA) or the QIAprep Spin Miniprep Kit (Qiagen, Mississauga, ON,

Canada) according to the manufacturer's instructions. Plasmids were eluted using the provided Tris-ethylenediaminetetraacetic acid (EDTA; TE) buffer solutions.

6.1.4.2. Restriction enzyme digests

FastDigest restriction enzymes from Thermo Scientific were used exclusively. Single and double digests were performed according to the manufacturer's instructions. Digests were typically incubated at 37 °C for 1 h. Restriction enzymes and buffers were removed using a QIAquick PCR Purification Kit (Qiagen) or through a gel extraction protocol.

6.1.4.3. Agarose gel electrophoresis

Agarose gels (1 – 2 % w/v) were prepared using Ultra-Pure Agarose (Invitrogen, Carlsbad, CA, USA) and either Tris-acetate-EDTA (TAE) or Tris-borate-EDTA (TBE) buffer. SYBR® Safe DNA gel stain (Life Technologies; 1/10,000 dilution in DMSO) was added to the gel before casting. DNA samples were prepared using 6 X sample buffer (Thermo Scientific). Gels were generally run at 85 V for 45 min, and visualized using a Dark Reader Transilluminator (Clare Chemical Research, Dolores, CO, USA) or an ImageQuant RT ECL imager (GE Healthcare Life Sciences, Little Chalfont, Buckinghamshire, UK).

6.1.4.4. DNA quantification

DNA concentrations were measured spectrophotometrically based on absorbance at 260 nm. Larger sample volumes were measured using a BioMate 3 Spectrophotometer with a 100 μL quartz cuvette. Smaller volumes were analyzed using a NanoDrop ND-1000 Spectrophotometer (Thermo Scientific). Purity from protein contaminants was estimated based on the ratio of absorbance at 260 nm and 280 nm.

6.1.4.5. Ligation reactions

T4 DNA ligase (Invitrogen) was used for all ligation reactions according to the manufacturer's instructions. A total of 200 ng of DNA (plasmid and insert combined) was used in each ligation reaction, with a ratio of three insert molecules to one plasmid molecule. Ligation reactions were incubated at room temperature for 1 h and were directly transformed. If no transformants were obtained, the remaining ligation reaction was ethanol precipitated and re-transformed.

6.1.4.6. Transformation of chemically competent *Escherichia coli*

Frozen tubes of chemically competent *E. coli* cells (prepared according to Hanahan[191] or purchased from New England Biolabs (Ipswich, MA, USA)) were thawed gently on ice bath and aliquoted into 50 μL portions. The DNA sample to be transformed (1 – 5 μL) was added to the thawed *E. coli* cells, gently stirred with a pipette tip, and incubated on ice for 30 min. The tubes were heat-shocked at 42 °C for 20 s, and then placed back on ice for 2 min. Pre-warmed LB broth (950 μL) was added to each tube, and the transformant solution was incubated at 37 °C, 225 rpm for 1 h. The transformant cultures were centrifuged (13 krpm, 2 min on a benchtop microcentrifuge) and approximately 900 μL of the supernatant was decanted. The cell pellets were gently resuspended in the remaining 100 μL, spread on LB agar plates supplemented with the appropriate antibiotic, and incubated overnight at 37 °C.

6.1.4.7. Ethanol precipitation

To the DNA sample, 0.1 volume of 3 M sodium acetate (pH 5.2) and 2.5 volumes of ice-cold 95 % ethanol were added. The mixture was vortexed, briefly spun down, and incubated at -20 °C for 15 – 60 min. The precipitated DNA was centrifuged (13 krpm, 15

min) and the supernatant was carefully removed using a gel-loading pipette tip. A 70 % ethanol solution (180 μL) was added to the pellet and the mixture was briefly vortexed. Once again, the mixture was centrifuged (13 krpm, 15 min), and the supernatant was removed as before. The DNA pellets were allowed to air-dry for 30 – 60 min.

6.1.4.8. Sanger sequencing

A BigDye Terminator v3.1 Cycle Sequencing Kit (Applied Biosystems, Foster City, CA, USA) was used for Sanger sequencing. Sequencing reactions (10 μL scale) were subjected to 30 cycles of (1) denaturing at 96 °C for 30 s, (2) annealing at 50 °C for 15 s and (3) extending at 60 °C for 60 s. The sequencing products were diluted with 10 μL of Milli-Q water, 2 μL of a sodium acetate/EDTA premix, and 80 μL of 95 % ice-cold ethanol. The remainder of the ethanol precipitation protocol was performed as described above. Following ethanol precipitation, the sample was analyzed by the University of Alberta Molecular Biology Service Unit on an ABI 3730 DNA Analyzer (Applied Biosystems).

6.1.5. Bioinformatics

The predicted products of open reading frames were analyzed using the NCBI Basic Local Alignment Search Tool (BLAST; http://blast.ncbi.nlm.nih.gov/Blast.cgi). Nucleotide and amino acid sequences were aligned using ClustalW and Clustal Omega.[192] The domains of non-ribosomal peptide synthetases (NRPS) were analyzed using the SBSPKS NRPS-PKS prediction tool.[193] The specificities of NRPS adenylation domains were predicted using NRPSpredictor2.[194]

6.1.6. Heterologous expression of proteins

6.1.6.1. Cell lysis

Bacterial cells were lysed using a TS series benchtop cell disruptor (Constant Systems Ltd, Low March, UK). The system was prepared by first passing through 20 mL of the desired lysis buffer at 5 kpsi. Then, the bacterial suspension in lysis buffer was passed through the system at 25 kpsi, collecting the lysate. Another 20 mL of lysis buffer was passed through the system at 25 kpsi and combined with the lysate.

6.1.6.2. SDS-PAGE

The protein content in samples was analyzed using SDS-PAGE, either with a 10 % resolving gel topped with a 4 % stacking gel, or using a commercial 4 – 20 % Mini-PROTEAN TGX precast gel (Bio-Rad, Hercules, CA, USA). Protein samples were prepared in 2 X Laemmli Sample Buffer (Bio-Rad) and boiled at 100 °C for 10 min. Samples run on a PAGE gel containing a stacking gel were run at a voltage of 50 V for 30 min and then 180 V until the dye front reached the bottom of the gel. The 4 – 20 % commercial gels were run at 180 V until the dye front reached the bottom. Gels were rinsed for 3 x 5 min in fresh Milli-Q water, and then submerged and shaken in GelCode Blue Stain reagent (Pierce, Rockford, IL, USA) for 60 min. After decanting the stain, the gel was left in Milli-Q water overnight and scanned.

6.1.7. Hydrolysis and derivatization of peptides for GC-MS analysis of amino acids

Purified peptide (ranging from 0.1 to 1 mg) was dissolved in 3 mL of 6 M HCl and heated at 110 °C for 16 h with stirring in a sealed thick-walled glass tube. Once cooled, the solution was evaporated to dryness *in vacuo*. To 5 mL of methanol or isopropanol (depending if methyl or isopropyl esters were desired) in an ice-water bath,

1.5 mL of acetyl chloride was added dropwise. The hydrolysate was dissolved in this mixture, and the solution was heated at 110 °C for 45 min with stirring in a sealed thick-walled glass tube. After cooling, solvent was removed using a rotary evaporator. In an ice-water bath, 1 mL of pentafluoropropionic anhydride was added to 3 mL of freshly distilled dichloromethane. The amino acid residue was dissolved in this mixture, and then heated at 110 °C for 15 min with stirring in a sealed thick-walled tube. After cooling, the solution was transferred to a clean vial and evaporated to dryness under a stream of argon. Derivatized amino acid samples were stored as solids under argon at -20 °C.

6.1.8. Mass spectrometry

6.1.8.1. MALDI-TOF MS

Matrix-assisted laser desorption ionization-time of flight mass spectrometry (MALDI-TOF MS) was performed on an AB Sciex Voyager Elite system (Foster City, CA, USA) and a Bruker 9.4T Apex-Qe FTICR (Billerica, MA, USA). Matrices 3,5-dimethoxy-4-hydroxycinnamic acid (sinapinic acid) and 4-hydroxy-α-cyanocinnamic acid (HCCA) were used with a two-layer sample preparation method.[195] The AB Sciex Voyager Elite system was operated in positive reflectron mode with delayed extraction.

6.1.8.2. LC-MS/MS

Liquid chromatography-tandem mass spectrometry (LC-MS/MS) experiments were conducted on a Q-Tof Premier mass spectrometer (Waters, Milford, MA, USA) coupled with a Waters nanoAcquity UPLC system. Samples (5 μL) were first passed through a Waters Symmetry® C18 nanoAcquity nano trap column (180 μm x 20 mm) followed by a Waters Atlantis dC18 nanoAcquity nano analytical column (75 μm x 150 mm). The peptide trap was flushed with aqueous 1 % acetonitrile and 0.1 % formic acid

at a flow rate of 10 μL/min for 5 min to desalt the sample. Then, samples were resolved using a gradient from 1 to 60 % of solvent B (acetonitrile with 0.1 % formic acid) over the span of 45 – 55 min using a flow rate of 350 nL/min.

6.1.8.3. MALDI-TOF/TOF

Fragmentation data for tridecaptin B variants were collected on a Bruker Ultraflextreme matrix-assisted laser desorption ionization-tandem mass spectrometer (MALDI-TOF/TOF; Billerica, MA, USA). 4-Hydroxy-α-cyanocinnamic acid was used as the matrix for sample preparation.

6.1.8.4. HR-ESI MS

High-resolution electrospray ionization mass spectrometry (HR-ESI MS) was performed on an Agilent Technologies 6220 oaTOF (Santa Clara, CA, USA). Samples were ionized via ESI and monitored in positive mode.

6.1.9. NMR spectroscopy

Spectral data were collected on several different nuclear magnetic resonance (NMR) spectrometers. At the University of Alberta Department of Chemistry, a Varian Inova 600 MHz spectrometer (equipped with a triple-resonance HCN cold probe) and a Varian VNMRS 700 MHz spectrometer (equipped with a triple-resonance HCN probe and Z-axis pulsed-field gradients) were used. Data were also acquired at the National High Field Nuclear Magnetic Resonance Centre (NANUC) on a Varian Inova 800 MHz spectrometer equipped with a triple-resonance HCN cold probe and Z-axis pulsed-field gradients.

6.2. Experimental procedures for the characterization of *Paenibacillus* spp. and their antimicrobial peptides

6.2.1. Genome sequencing

Genomic DNA from *Paenibacillus polymyxa* NRRL B-30509, *Paenibacillus terrae* NRRL B-30644 and *P. polymyxa* NRRL B-30507 were isolated using the DNEasy Blood and Tissue Kit (Qiagen) according to the manufacturer's instructions. The genomes of *P. polymyxa* NRRL B-30509 and *P. terrae* NRRL B-30644 were sequenced at GenoSeq (UCLA Genotyping and Sequencing Core, Los Angeles, CA, USA). Sequencing reads were acquired on a Roche GS FLX Titanium system, and were assembled using the GS De Novo Assembler software (Roche). The genome of *P. polymyxa* NRRL B-30507 was sequenced at the University of Illinois at Urbana-Champaign (UIUC) Roy J. Carver Biotechnology Center. Sequence reads were acquired on an Illumina HiSeq 2500 system, and were processed using a Velvet assembler at UIUC. Artemis was used to browse the contigs produced by the assembly process.[196]

6.2.2. Genetic probing for SRCAM 602 and 1580

Genomic DNA from *P. polymyxa* NRRL B-30509 and *P. terrae* NRRL B-30644 was isolated as described above. The genome sequence of *P. polymyxa* NRRL B-30509 was probed using degenerate primers MVB212 (5' – GCN CAN TAY TAY GGN AAY GG – 3') and MVB213 (5' – TGY TGN ACC CAN CCR TTN AC – 3'). Primers MVB224 (5' – TTY GAY CTN GAY ATH CAR GT – 3') and MVB225 (5' – CCN ACR TTN GTR AAR CAN CG – 3') were used to amplify a known sequence (paenicidin A structural gene). The genome sequence of *P. terrae* NRRL B-30644 was probed using degenerate primers MVB214 (5' – GTN AAY TAY GGN AAY GGN GT –

3') and MVB215 (5' – GTN CAN CKR AAN GCY TGR TG – 3'). Primers MVB222 (5' – CTN GAY GTN CAR GTN AAY AA – 3') and MVB223 (5' – CCN ACR TTN GTR AAR CAY TT – 3') were used to amplify a known sequence (paenicidin B structural gene). PCR amplification consisted of 30 cycles of: (1) denaturing at 94 °C for 60 s, (2) annealing at 45 °C for 30 s, and (3) extension at 68 °C for 15 s. HiFi Platinum Taq Polymerase (Invitrogen) was used according to the manufacturer's instructions.

6.2.3. Derivatization of the tridecaptin A_1 and A_3 lipid chains

The derivatization of tridecaptin lipid chains for GC-MS was based on a literature protocol.[125] Tridecaptin A_1 (up to 1 mg), or tridecaptin A_3 (too little to weigh) were dissolved in 4 mL of 6 M HCl and heated at 110 °C for 2 h with stirring in a sealed thick-walled reaction vessel. After cooling, the hydrolysate was extracted with 5 mL of diethyl ether. The ether layer was dried with anhydrous sodium sulfate and filtered. To the filtered ether, 2 mL of methanol and 50 μL of 2 M trimethylsilyldiazomethane in hexanes were added. The mixture was stirred for 30 min at room temperature, and quenched by the addition of 50 μL of 2 M acetic acid. The sample was then dried under a stream of argon.

6.2.4. GC-MS of tridecaptin lipid chains

The derivatized lipid chain extracts were dissolved in dichloromethane and analyzed using a 7890A GC system with a 5975C VL MSD (Agilent Technologies, Santa Clara, CA, USA). A Phenomenex Zebron ZB-5MS (30 m length, 0.25 mm i.d., 0.25 μm film thickness) capillary column was used. Sample (1 μL) was injected onto the column via pulsed splitless injection. Elution was monitored using both full scan and single-ion monitoring modes (SIM ions: 103.0, 43.0 and 29.0). For tridecaptin A_3 and A_4, the

temperature programme started at 70 °C, was immediately ramped up to 250 °C at 3 °C/min, and held at 250 °C for 5 min. For tridecaptin A_1, the temperature programme started at 70 °C, and was increased to 120 °C at a rate of 3 °C/min.

6.2.5. *Paenibacillus polymyxa* NRRL B-30509

6.2.5.1. Purification of polymyxins E1 and E2

A preculture of *P. polymyxa* NRRL B-30509, inoculated from a 20 % glycerol stock, was grown in 10 mL BBL™ Brucella broth for 16 h at 34 °C and 225 rpm. BBL Brucella broth (1 L) was inoculated (0.1 %) using the overnight culture, and incubated for 40 h at 34 °C and 225 rpm. The culture was centrifuged (10,000 g, 10 min, 4 °C) and the supernatant collected. To the supernatant, ammonium sulfate was added to 80 % saturation, and the mixture was stirred at 10 °C for 16 h. The mixture was then centrifuged (10,000 g, 10 min, 4 °C) and the supernatant disposed of.

The pellets were re-dissolved in 100 mL of Milli-Q water, and the resulting solution was passed through a 20 mL CM-Sephadex C-25 column (GE Healthcare) equilibrated with 50 mM sodium phosphate, pH 7.8 at 1 mL/min. The column was washed with 100 mL of 50 mM sodium phosphate, pH 7.8, and polymyxins were eluted with 100 mL of 50 mM sodium phosphate, pH 7.8 with 500 mM NaCl. This elution fraction was then passed through a 4 g column of Amberlite XAD-16 resin (Sigma-Aldrich) at 2 mL/min The Amberlite resin was washed with 100 mL of Milli-Q water, and the polymyxins were eluted with 100 mL of 80 % isopropanol with 0.1 % TFA. This fraction was concentrated *in vacuo* to remove the organic solvents. Finally, polymyxins E1 and E2 were purified using reversed-phase HPLC with a C18 column (VYDAC® 218TP54; 4.6 mm x 250 mm, 5 μm particle diameter, 300 Å pore diameter). Mobile

phases A (water with 0.1 % TFA) and B (acetonitrile with 0.1% TFA) were used at an overall flow rate of 1 mL/min, with detection at 220 nm. The solvent gradient started held at 20 % B for 5 min, and was then ramped up to 45 % B over 40 min. Polymyxins E2 and E1 were collected at 18 min and 21 min, respectively. The identities of the isolated polymyxins E1 and E2 ($[M+H]^+$ = 1169.8 and 1155.8, respectively) were confirmed by MALDI-TOF MS and LC-MS/MS. Commercial polymyxins E1 and E2 (Sigma-Aldrich) were purified via the same HPLC method.

6.2.5.2. Purification of tridecaptin A_3

The culture supernatant of *P. polymyxa* NRRL B-30509, prepared as described above, was passed through a 40 g column of Amberlite XAD-16 resin (Sigma-Aldrich) at 10 mL/min. This column was then washed at 10 mL/min with 250 mL of: (1) water, (2) 20 % isopropanol, (3) 40 % isopropanol, (4) 60 % isopropanol, and (5) 80 % isopropanol with 0.1 % TFA. The 60 % isopropanol and 80 % isopropanol 0.1 % TFA fractions were concentrated using a rotary evaporator to a total volume of 50 mL. The concentrated Amberlite XAD-16 fractions were passed through the preconditioned Strata SPE C18-E cartridge (Phenomenex) at 3 mL/min. The cartridge was then washed at 5 mL/min with 50 mL of: (1) 30 % ethanol, (2) 30 % acetonitrile, (3) 40 % isopropanol and (4) 80 % isopropanol 0.1 % TFA. The 80 % isopropanol 0.1 % TFA SPE fraction was concentrated using a rotary evaporator to 10 mL. The tridecaptins in this concentrated extract were purified by HPLC using the same conditions as described for the polymyxin isolation above. The different tridecaptin variants eluted over a range from 36 to 41 min. The identity of the isolated tridecaptin A_3 ($[M+H]^+$ = 1578.9) was confirmed by MALDI-TOF MS.

6.2.5.3. Purification of paenicidin A

The 40 % isopropanol Amberlite XAD-16 wash described above was concentrated to 50 mL using a rotary evaporator. The concentrated fraction was passed through a preconditioned Strata SPE C18-E cartridge (Phenomenex) at 3 mL/min. This cartridge was washed at 5 mL/min with 50 mL of: (1) 30 % ethanol, (2) 30 % acetonitrile, (3) 40 % isopropanol and (4) 80 % isopropanol with 0.1 % TFA. The 80 % isopropanol 0.1 % TFA was concentrated using a rotary evaporator to 10 mL. Paenicidin A was then purified by HPLC using the same conditions as described for the polymyxin isolation above, eluting at 26 min. The identity of the isolated paenicidin A ($[M+H]^+$ = 3376.5) was confirmed by MALDI-TOF MS.

6.2.5.4. Reductive alkylation of paenicidin A

Purified paenicidin A (0.1 mg) was prepared in 50 μL of 100 mM NH_4HCO_3. DTT (5 μL, 100 mM) was added to the paenicidin solution and the mixture was heated at 50 °C for 20 min. Iodoacetamide (5 μL, 200 mM) was added, and the mixture was incubated in the dark for 20 min. The extent of alkylation was analyzed using MALDI-TOF MS, indicating no increase in the molecular mass of paenicidin A.

6.2.5.5. Reductive desulfurization of paenicidin A

Purified paenicidin A (0.5 mg) was suspended in 2 mL of a 1:1 mixture of CH_3OH and H_2O and transferred to a thick-walled reaction vessel. To this, 10 mg of $NiCl_2$ and 10 mg of $NaBH_4$ were added. This mixture was stirred under H_2 (1 atm) at room temperature. Aliquots were removed after 30 min and 8.5 h. These aliquots were centrifuged (10 min, 13 krpm on a benchtop centrifuge) and the supernatant was collected. To the pellets, 2 mL of a 1:1 mixture of CH_3OH and H_2O were added, and the

suspensions were sonicated for 15 min. The suspensions were centrifuged as before, and the supernatants were collected. After removing the methanol *in vacuo*, the supernatants were analyzed by MALDI-TOF MS and LC-MS/MS.

6.2.5.6. NMR spectroscopy

Paenicidin A was dissolved in 500 μL of a 4:1 mixture of H_2O and CD_3OH to a concentration of 0.6 mM and transferred to a standard 5 mm NMR tube. 2,2-Dimethyl-2-silapentane-5-sulfonic acid (DSS; 0.01 %) was added to the sample for referencing. TOCSY (mixing time 100 ms) and NOESY (mixing time 200 ms) datasets were acquired at 27 °C on a Varian VNMRS 700 MHz spectrometer. The water signal was suppressed by transmitter presaturation. Proton chemical shifts were assigned on the basis of the standard analysis of homonuclear TOCSY and NOESY data (Table 6.2).[164] NMR spectra were processed using NMRPipe[197] and analyzed using NMRViewJ.[175]

Table 6.2. Chemical shift assignments for paenicidin A

	HN	Hα	Hβ	others
Val 1		3.78	2.18	γCH_3 1.03
Leu 2	8.68	4.51		
Ala(S) 3	8.58	4.54	2.98, 3.12	
Ile 4	8.11	4.04	2.02	γCH 1.16, δCH_3 0.82, 0.94
Val 5	7.88	4.19	2.08	γCH_3 0.93, 0.96
Ala 6	8.67	4.11	1.40	
Ala(S) 7	8.21	4.53	2.95, 3.00	
Ala(S) 8	9.01	5.00	3.09	
Ser 9	8.50	4.34	3.91, 3.96	
Gly 10	9.02	3.88, 4.21		
Ala(S) 11	7.58	4.10	2.93, 3.54	
Gly 12	8.62	3.97		
Ser 13	8.19	4.45	3.86, 3.88	
Gly 14	8.45	3.97		
Lys 15	8.22	4.34		
Abu(S) 16	8.86	4.76	3.56	γCH_3 1.32
Ala 17	8.07	4.27	1.41	
Ala 18	7.82	4.55	1.35	
Ala(S) 19	8.47	4.58	2.85, 3.26	
Ala(S) 20	8.57		3.03, 3.34	
Val 21	7.55	4.43	2.17	γCH_3 0.86, 0.93
Glu 22	8.50	4.26		
Abu(S) 23	8.59	4.68	3.67	γCH_3 1.29
Ala(S) 24	8.01	4.62	3.08, 3.18	
Gly 25	8.65	4.04, 4.14		
Asn 26	8.58	4.38	2.81, 2.85	
Arg 27	8.36	4.20		
Ala(S) 28	7.52	4.40	2.88, 2.94	
Phe 29	8.28	4.44	3.07, 3.17	
Abu(S) 30	8.20	4.57	4.12	γCH_3 1.24
Asn 31	8.18	4.55	3.42	
Val 32	8.41	3.99	2.05	γCH_3 0.95, 1.01
Gly 33	8.72	3.81, 4.20		
Ser 34	8.17	4.51	3.84, 4.03	
Leu 35	8.29			
Ala(S) 36	7.58			

6.2.5.7. GC-MS analysis of paenicidin A

Purified paenicidin A was hydrolyzed and the constituent amino acids were derivatized as the pentafluoropropanamide methyl esters as described above. GC-MS analyses were performed on a 7890A GC system with a 5975C VL MSD (Agilent Technologies). Methyllanthionine (MeLan) stereochemistry was examined using a Phenomenex Zebron ZB-5MS capillary column (30 m x 0.25 mm, 0.25 μm film thickness). Sample (1 μL) was injected onto the column via pulsed splitless injection, and the chromatography was monitored using both full scan and SIM modes (SIM detection at m/z 379.0, 248.0). The temperature programme started at 70 °C, was increased to 190 °C at 10 °C/min, and was then increased to 205 °C at 1 °C/min. Lanthionine (Lan) stereochemistry was examined using a Phenomenex Zebron ZB-1701 capillary column (30 m x 0.25 mm, 0.25 μm film thickness). Sample (1 μL) was injected onto the column using a 10:1 split, and the chromatography was monitored using both full scan and SIM modes (SIM detection at m/z 365.0, 248.0). The temperature programme started at 70 °C, was increased to 170 °C at 10 °C/min, increased to 200 °C at 3 °C/min, and then increased to 300 °C at 10 °C/min.

6.2.6. *Paenibacillus terrae* NRRL B-30644

6.2.6.1. Isolation of tridecaptin A_1

A preculture of *P. terrae* NRRL B-30644 was grown from a glycerol stock overnight in 10 mL BBL Brucella broth at 34 °C, 225 rpm for 16 h. This was used to inoculate (0.1 %) 1 L of BBL Brucella broth, which was incubated for 40 h at 34 °C, 225 rpm. The bacterial cells were pelleted by centrifugation (5,000 x g, 10 min, 4 °C) and the supernatant was collected. The culture supernatant was passed through a 30 g Amberlite

XAD-16 column (Sigma-Aldrich) at 10 mL/min. The column was then washed with 250 mL of: (1) water, (2) 20 % isopropanol, (3) 40 % isopropanol, (4) 60 % isopropanol, and (5) 80 % isopropanol with 0.1% TFA. The 80 % isopropanol 0.1 % TFA fraction was concentrated to 50 mL using a rotary evaporator, and passed through a Strata SPE C18-E cartridge (Phenomenex) at 3 mL/min. The cartridge was then washed with 50 mL of: (1) 30 % ethanol, (2) 30 % acetonitrile, (3) 40 % isopropanol and (4) 80 % isopropanol with 0.1 % TFA. The 80 % isopropanol 0.1 % TFA fraction was concentrated to 5 mL using a rotary evaporator, and further purified by reverse-phase HPLC. A C18 HPLC column was used (VYDAC® 218TP54; 4.6 mm x 250 mm, 5 μm particle diameter, 300 Å pore diameter) with mobile phases A (water with 0.1 % TFA) and B (acetonitrile with 0.1 % TFA). An overall flow rate of 1 mL/min was used, and elution was monitored at 220 nm. The solvent gradient started at 20 % B for 5 min, and was increased to 45 % B over the course of 40 min. Tridecaptin A_1 eluted between 30 and 35 min. The identity of the isolated tridecaptin A_1 was confirmed by MALDI-TOF MS ($[M+H]^+$ = 1550.8) and HR-ESI MS ($[M+H]^+$ *m/z* = 1550.8551, calc'd 1550.8577).

6.2.6.2. NMR spectroscopy

Tridecaptin A_1 was dissolved in 500 μL of 10 % D_2O, 90 % H_2O to a concentration of 2 mM and transferred to a standard 5 mm NMR tube. DSS (0.01 %) was added to the sample for referencing. TOCSY, NOESY, ROESY and ^{13}C-HSQC datasets were acquired at 25 °C on Varian 600 MHz and 800 MHz spectrometers. The water signal was suppressed using transmitter presaturation. NMR spectra were processed using NMRPipe[197] and analyzed using NMRViewJ.[175] Proton chemical shifts were assigned based on the TOCSY and NOESY datasets (Table 6.3).[164]

Table 6.3. Chemical shift assignments for tridecaptin A_1

	HN	Hα	Hβ	others
Lipid		2.49, 2.45	3.98	γCH_2 1.49, δCH_2 1.31, 1.21, εCH 1.32, ζCH_2 1.29, 1.14, ζCH_3 0.82, ηCH_3 0.82
D-Val 1	8.21	4.09	2.07	γCH_3 0.94
D-Dab 2	8.61	4.46	2.22, 2.09	γCH_2 3.07
Gly 3	8.35	3.93		
D-Ser 4	8.16	4.47	3.79	
D-Trp 5	8.23	4.65	3.28	10.14, 7.24, 7.60, 7.50, 7.24, 7.14
Ser 6	8.12	4.16	3.58, 3.34	
Dab 7	8.53	4.37	2.18, 2.06	γCH_2 3.04
D-Dab 8	8.11	4.30	1.92, 1.84	γCH_2 2.74, 2.62
Phe 9	8.35	4.69	3.21, 2.90	7.34, 7.30, 7.23
Glu 10	8.24	4.33	1.90	γCH_2 2.32, 2.01
Val 11	8.21	4.14	2.06	γCH_3 0.97
D-aIle 12	8.19	4.37	1.98	γCH_2 1.34, 1.25, γCH_3 0.90, δCH_3 0.88
Ala 13	8.00	4.23	1.34	

6.2.6.3. Isolation of paenicidin B

The 40 % isopropanol Amberlite XAD-16 fraction obtained during the tridecaptin purification was concentrated to 50 mL using a rotary evaporator. This sample was then passed through a preconditioned Strata SPE C18-E cartridge (Phenomenex) at 3 mL/min. The cartridge was washed at 5 mL/min with (1) 30 % ethanol, (2) 30 % acetonitrile, (3) 40 % isopropanol and (4) 80 % isopropanol with 0.1 % TFA. The 80 % isopropanol 0.1 % TFA fraction was concentrated to 5 mL using a rotary evaporator. The sample was then further separated using reverse-phase HPLC using identical conditions to those used for the isolation of tridecaptin A_1, with paenicidin B eluting at 34 min. The identity of the isolated paenicidin B ($[M+H]^+$ = 3290.4) was confirmed by MALDI-TOF MS.

6.2.7. *Paenbacillus polymyxa* NRRL B-30507

6.2.7.1. Isolation of polymyxins B1 and B2

A preculture of *P. polymyxa* NRRL B-30507 was grown in 10 mL BBL Brucella broth at 37 °C, 225 rpm for 16 h. This culture was used to inoculate (0.1 %) 1 L of BBL Brucella broth, which was incubated at 37 °C, 225 rpm for 40 h. The grown culture was centrifuged (5,000 g, 10 min, 4 °C), and the supernatant was collected. The culture supernatant was passed through a 30 g Amberlite XAD16 (Sigma-Aldrich) column at a flow rate of 10 mL/min. The Amberlite column was washed at 10 mL/min with 250 mL of: (1) water, (2) 20 % isopropanol, (3) 40 % isopropanol and (4) 80 % isopropanol with 0.1 % TFA. The 80 % isopropanol 0.1 % TFA fraction was concentrated to 50 mL using a rotary evaporator. This concentrated fraction was passed through a preconditioned Strata SPE C18-E cartridge (Phenomenex) at a flow rate of 3 mL/min. The cartridge was then washed at 5 mL/min with 50 mL of: (1) 30 % ethanol, (2) 30 % acetonitrile, (3) 40 % isopropanol, and (4) 80 % isopropanol with 0.1 % TFA. The 80 % isopropanol 0.1 % TFA SPE fraction was concentrated to approximately 5 mL using a rotary evaporator. Samples were then further purified by reverse-phase HPLC using a C18 analytical column (VYDAC® 218TP54; 4.6 mm x 250 mm, 5 μm particle diameter, 300 Å pore diameter) with mobile phases A (water with 0.1 % TFA) and B (acetonitrile with 0.1 % TFA). An overall flow rate of 1 mL/min was used, and detection was monitored at 220 nm. The solvent gradient started at 20 % B for 5 min, then increased to 45 % B over the course of 40 min. Polymyxins B2 and B1 eluted after 18 and 22 min, respectively. The identities of the isolated polymyxins B1 and B2 ($[M+H]^+$ = 1203.4 and 1189.3, respectively) were confirmed by MALDI-TOF MS.

6.2.7.2. Isolation of tridecaptin B_1

The protocol used to isolate tridecaptin B_1 was identical to that used for the isolation of polymyxins B1 and B2 described above. Using the same HPLC conditions, tridecaptin B_1 eluted after 32 min. Several other tridecaptin variants eluted over the range of 29 to 34 min. The identity of isolated tridecaptin B_1 was confirmed by MALDI-TOF MS ($[M+H]^+$ = 1458.6) and HR-ESI MS ($[M+H]^+$ *m/z* = 1458.8296, calc'd 1458.8315).

6.2.7.3. NMR spectroscopy

Natural tridecaptin B_1 was dissolved in 600 μL of 10 % D_2O, 90 % H_2O to a concentration of 1 mM and transferred to a standard 5 mm NMR tube. DSS (0.01 %) was added to the sample for referencing. TOCSY, NOESY, ROESY and ^{13}C-HSQC datasets were acquired at 25 °C on a Varian VNMRS three-channel 600 MHz spectrometer. The water signal was suppressed using transmitter presaturation. NMR spectra were processed using NMRPipe[197] and analyzed using NMRViewJ.[175] Proton chemical shifts were assigned based on the TOCSY and NOESY datasets (Table 6.4).[164]

Table 6.4. Chemical shift assignments for tridecaptin B_1

	HN	Hα	Hβ	others
Lipid		2.28	1.53	1.25, 1.07, 0.79
Gly 1	8.22	3.92		
D-Dab 2	8.55	4.46	2.23, 2.06	γCH_2 3.06
Gly 3	8.47	3.94		
D-Ser 4	8.15	4.18	3.81	
D-Trp 5	8.23	4.65	3.29	10.14, 7.60, 7.51, 7.25, 7.24, 7.14
Ser 6	8.12	4.16	3.59, 3.33	
Dab 7	8.54	4.39	2.23, 2.09	γCH_2 3.06
D-Dab 8	8.16	4.45	2.17, 2.06	γCH_2 3.01
Ile-9	8.12	4.18	1.86	γCH_2 1.39, 1.15, γCH_3 0.87, δCH_3 0.87
Glu 10	8.38	4.37	1.90	γCH_2 2.30, 2.01
Val 11	8.19	4.15	2.04	γCH_3 0.94
D-aIle 12	8.20	4.36	1.98	γCH_2 1.33, 1.25, γCH_3 0.90, δCH_3 0.88
Ala 13	8.04	4.26	1.36	

6.2.7.4. Synthesis of octyl-tridecaptin B_1

A CEM Liberty 1 Microwave Peptide Synthesizer (Matthews, NC, USA) was used for the automated Fmoc-chemistry solid-phase peptide synthesis of tridecaptin B_1. A 0.1 mmol scale of Fmoc-L-Ala pre-loaded 2-chlorotrityl resin was used. Solutions (0.2 M) of commercially available protected amino acids were prepared in DMF. Coupling reactions used 2-(1H-7-azabenzotriazol-1-yl)-1,1,3,3-tetramethyluronium hexafluorophosphate (HATU) as the activating agent, and were heated at 70 °C for 5 min coupling time. A 20 % solution of piperidine in DMF was used for the deprotection of Fmoc groups, and the deprotection progress was monitored by the UV detection (301 nm) of the formation of a dibenzofulvene-piperidine adduct.

The synthetic product was examined by shaking a small amount of resin in 1 mL of trifluoroacetic acid/triisopropylsilane/water (95 : 2.5 : 2.5) for 30 min. After removing

the resin via filtration, the filtrate was concentrated *in vacuo* and the peptide was precipitated using cold ether. A peptide of the expected mass was observed ($[M+H]^+$ = 1458.8) by MALDI-TOF MS. HATU-activated octanoic acid was added to approximately one quarter of the resin-bound peptide and the mixture was shaken at room temperature under argon. The resin-bound material was filtered, washed five times with 5 mL CH_2Cl_2, and dried under vacuum for 5 min. Cleavage of the peptide from the resin and the removal of side-chain protecting groups, filtration and trituration were performed as above. Oct-TriB_1 was purified by reverse-phase HPLC on a C18 preparative scale (Phenomenex Luna®; 21.2 mm x 250 mm, 5 μm particle diameter, 100 Å pore diameter) using the same HPLC conditions as for the isolation of tridecaptin A_1, eluting at 34 min. The identity of the isolated octyl-tridecaptin B_1 was confirmed by MALDI-TOF MS.

6.3. Experimental procedures for the characterization of carnolysins A1 and A2 and their producer organism *Carnobacterium maltaromaticum* C2

6.3.1. Genome sequencing

Genomic DNA from a culture of *Carnobacterium maltaromaticum* C2 grown in APT broth was isolated using the DNEasy Blood and Tissue Kit (Qiagen) according to the manufacturer's instructions. The genome was sequenced at GenoSeq (UCLA Genotyping and Sequencing Core, Los Angeles, CA, USA). Sequencing reads were acquired on a Roche GS FLX Titanium system, and assembled using the GS De Novo Assembler software (Roche). Artemis was used to browse the assembled contigs.[196]

6.3.2. Fosmid library production and sequencing

A fosmid library was created from isolated *C. maltaromaticum* C2 genomic DNA using an Epicentre CopyControl™ Fosmid Library Production Kit according to the manufacturer's instructions. Screening of fosmids was performed using probes prepared with the AlkPhos Direct Labeling Kit (Amersham Biosciences), and hybridization was detected using the CDP-Star reagent (Amersham Biosciences), all according to the manufacturer's instructions. Fosmids containing the desired gene cluster were sequenced using the BigDye Terminator v3.1 Cycle Sequencing Kit (Applied Biosystems). The sequencing products were ethanol precipitated and analyzed at the University of Alberta Molecular Biology Service Unit on an ABI 3730 DNA Analyzer (Applied Biosystems).

6.3.3. Isolation of carnolysin A1′ and A2′

A pre-culture of *C. maltaromaticum* C2 was grown in 10 mL APT broth overnight at 25 °C without shaking. This was used to inoculate (0.2 %) 50 mL of a semidefined casamino acid media (per liter: 15 g casamino acids, 5 g yeast extract, 2 g disodium phosphate, 2 g glucose, 5 g sodium chloride, 5 g sodium citrate, 0.1 g magnesium sulfate and 0.05 g manganese sulfate), which was incubated overnight at 25 °C without shaking. A vitamin solution was prepared by mixing a single multivitamin tablet (Quest Super Once a Day) in 50 mL of water, which was centrifuged (5 min, 13 krpm on a benchtop centrifuge) and filter sterilized. After autoclaving larger volumes of the semidefined casamino acid media, 1 mL of vitamin solution was added per liter media. This supplemented media was inoculated (1 %) with the overnight culture grown in casamino acid-based media, and incubated at 25 °C for 3 – 4 days without shaking.

The culture was then centrifuged (5,000 g, 10 min, 4 °C) and the supernatant collected. The culture supernatant was loaded onto an Amberlite XAD-16 column (Sigma-Aldrich; 20 g resin per liter of culture) at a flow rate of 10 mL/min. The column was then washed at a flow rate of 10 mL/min with 250 mL (per 20 g of resin) of: (1) water, (2) 20 % isopropanol, (3) 40 % isopropanol and (4) 80 % isopropanol with 0.1 % TFA. The organic solvents were removed from the 80 % isopropanol 0.1 % TFA fraction using a rotary evaporator. This concentrated fraction was passed through a preconditioned Strata SPE C18-E cartridge (Phenomenex) at a flow rate of 3 mL/min; approximately one cartridge was used for every 5 L of culture. The cartridge was washed at 5 mL/min with 50 mL of (1) 30 % ethanol, (2) 40 % isopropanol and (3) 80 % isopropanol with 0.1 % TFA. The organic solvent was removed from the 80 % isopropanol 0.1 % TFA fraction using a rotary evaporator.

CrnA1′ and CrnA2′ were then purified by two rounds of reversed-phase HPLC. The concentrated SPE sample was first injected onto a C8 semi-preparative scale HPLC column (VYDAC® 208TP1010; 10 mm x 250 mm, 10 μm particle size). Mobile phases A (water with 0.1 % TFA) and B (acetonitrile with 0.1 % TFA) were used with an overall flow rate of 3 mL/min, and the detector was set to monitor at 220 nm and 280 nm. The solvent gradient started at 20 % B for 5 min, then increased to 60 % B over the course of 40 min. The retention time of CrnA1′ was 32 min, while CrnA2′ eluted after 37 min.

Both peptides were further purified via injection onto a C18 analytical HPLC column (VYDAC® 218TP54; 4.6 mm x 250 mm, 5 μm particle size, 300 Å pore diameter). The same mobile phases were used as above, at an overall flow rate of 1 mL/min and with detection at 220 nm. The method for purifying CrnA1′ started held at

30 % B for 5 min, and was increased to 70 % B over 40 min, with CrnA1′ eluting after 36 min. The gradient used for CrnA2′ started at 35 % B, was immediately ramped up to 60 % B over 15 min, with CrnA2′ eluting after 12 min. The identities of the isolated CrnA1′ ($[M+H]^+$ = 4178.1) and CrnA2′ ($[M+H]^+$ = 3050.5) were confirmed by MALDI-TOF MS. The organic solvent was removed from fractions containing pure CrnA1′ and CrnA2′ using a rotary evaporator, and the samples were lyophilized. Purified peptides were stored at -20 °C under argon.

6.3.4. Partial hydrolysis of CrnA1′

Approximately 4 mg of CrnA1′ was dissolved in 8 mL of 0.1 M HCl, and was heated at 110 °C for 4 h with stirring in a thick-walled reaction vessel. Once the hydrolysate had cooled, the HCl was neutralized with ammonium bicarbonate. The peptide fragments were separated via reverse-phase HPLC on a C18 analytical column (VYDAC® 218TP54; 4.6 mm x 250 mm, 5 μm particle size, 300 Å pore size). Mobile phases A (water with 0.1 % TFA) and B (acetonitrile with 0.1 % TFA) were used at an overall flow rate of 1 mL/min with detection at 220 nm. The solvent gradient was held at 5 % B for 5 min, then increased to 60 % B over 40 min. Once the desired fraction had been fully collected from the hydrolysate, the acetonitrile and TFA were removed using a rotary evaporator. Concentrated HCl was added to a final concentration of 6 M, and the mixture was fully hydrolyzed and derivatized for GC-MS as described above.

6.3.5. GC-MS analysis of carnolysin amino acids

GC-MS characterization of the amino acids from CrnA1′ and CrnA2′ (derivatized as pentafluoropropanamide methyl or isopropyl esters, as described previously) was performed on a Bruker SCION TQ EI-MS coupled with a 456 GC. Pulsed splitless

injections were used to load 1 μL of sample, while elution was monitored using full scan and single-ion monitoring (SIM) modes. Derivatized MeLan stereochemistry was tested on a Zebron ZB-5MS capillary column (30 m, 0.25 mm i.d., 0.25 μm film thickness). The temperature programme for derivatized MeLan residues started at 70 °C, was increased to 190 °C at a rate of 10 °C/min, and was held at 190 °C for 5 min. SIM mode ion detection was set to monitor at m/z 379 and 248.

Derivatized Lan, Ala and 2-aminobutyrate (Abu) stereoisomers were characterized on an Agilent CP-Chirasil L-Val column (25 m, 0.25 mm i.d., 0.12 μm film thickness). The temperature programme used for Lan residues started at 160 °C for 5 min, was increased to 180 °C at a rate of 3 °C/min, and was held at 180 °C for 6 min. SIM mode ion detection was set to monitor at m/z 365, 248 and 234. The temperature programme used for Ala and Abu residues started at 30 °C, then immediately increased to 180 °C at a rate of 15 °C/min. SIM mode ion detection was set to monitor at m/z 119 and 190 for Ala and m/z 119 and 204 for Abu.

6.3.6. NMR spectroscopy

CrnA1′ was dissolved in 400 μL of 10 % D_2O, 90 % H_2O to a concentration of 1 mM and transferred to a 5 mm Shigemi tube matched to the magnetic susceptibility of D_2O. CrnA2′ was dissolved in a 600 μL mixture of 33 % CD_3OD, 6.2 % D_2O and 60.8 % H_2O and transferred to a standard 5 mm NMR tube. DSS (0.01 %) was added to these samples for referencing. TOCSY and NOESY datasets were acquired at 27 °C on a Varian VNMRS 700 MHz spectrometer. The water signal was suppressed using transmitter presaturation. Proton chemical shifts were assigned on the based on TOCSY

and NOESY datasets (Table 6.5, 6.6).[164] NMR spectra were processed using NMRPipe[197] and analyzed using NMRViewJ.[175]

Table 6.5. Chemical shift assignments for carnolysin A1′

	HN	Hα	Hβ	others
Gly-1		3.84		
Asp-2	8.64	4.71	2.76, 2.66	
Ile-3	8.32	4.18	1.88	γCH_3 0.88, γCH_2 1.44, δCH_3 0.86
Asn-4	8.49	4.71	2.82, 2.78	δNH_2 7.63, 6.91
Gly-5	8.25	3.91		
Glu-6	8.15	4.31	1.96, 1.90	γCH_2 2.26, 2.20
Phe-7	8.37		3.28, 3.13	δCH 7.31, εCH and ζCH 7.33, 7.30
Dhb-8	9.46		6.56	γCH_3 1.61
Abu(S)-9	7.73		3.47	γCH_3 1.33
Dha-10	9.61		5.41, 5.21	
Pro-11		4.41	2.36, 2.11	γCH_2 2.00, δCH_2 3.95, 3.75
Ala-12	7.91	4.48	1.54	
Ala(S)-13	7.78	4.97	3.34, 2.52	
Val-14	7.53		1.94	γCH_3 0.87, 0.76
Tyr-15	8.21	4.47	3.02, 2.95	δCH 7.09, εCH 6.82
Ala-16	7.88	4.17	1.16	
Val-17	7.83	4.07	2.06	γCH_3 0.89
Met-18	8.34	4.49	2.01	γCH_2 2.56, 2.48
Val-19	8.13	4.12	2.01	γCH_3 0.89
Val-20	8.11	4.12	2.04	γCH_3 0.91
Ala-21	8.44	4.34	1.39	
Lys-22	8.39	4.26	1.87, 1.76	γCH_2 1.43, δCH_2 1.67, εCH_2 2.98
Ala-23	8.36	4.31	1.44	
Ala(S)-24	8.16	4.46	3.22, 2.95	
Dha-25	9.43		5.48, 5.44	
Ala-26	9.11	4.20	1.51	
Lys-27	8.28	4.21	1.98	γCH_2 1.56, 1.47, δCH_2 1.71, εCH_2 3.00
Ala(S)-28	7.77	4.42	2.99	
Ala-29	7.98	4.29	1.43	
Ala-30	7.99	4.28	1.43	
Gly-31	8.09	3.92		
Ala-32	7.97	4.29	1.39	
Ala-33	8.21	4.26	1.39	
Ala-34	8.05	4.35	1.32	
Val-35	8.08	4.12	2.07	γCH_3 0.94
Ala-36	8.54	4.31	1.40	
Gly-37	8.38	3.91		
Ala-38	8.00	4.36	1.38	
Ile-39	7.98	4.12	1.84	γCH_3 0.88, γCH_2 1.45, δCH_3 0.86
Leu-40	8.34	4.47	1.64	γCH 2.07, δCH_3 0.95, 0.94
Ala(S)-41	8.93	4.58	3.25, 2.88	
Ala-42	7.99	4.27	1.43	
Ile-43	7.85	4.18	1.90	γCH_3 0.90, γCH_2 1.46, 1.14, δCH_3 0.88
Arg-44	8.31	4.23	1.92, 1.80	γCH_2 3.21, 1.61, δNH 7.24
Ala(S)-45	8.18	4.47	3.11, 2.93	

Table 6.6. Chemical shift assignments for carnolysin A2′

	HN	Hα	Hβ	others
Gly-1		3.82		
Asp-2	8.65	4.74	2.78, 2.64	
Val-3	8.21	4.12	2.05	γCH_3 0.91
Met-4	8.40		2.05, 1.97	γCH_2 2.62, 2.54
Pro-5		4.43	1.98	γCH_2 2.31, δCH_2 3.82, 3.71
Glu-6	8.66	4.29	2.04	γCH_2 2.48, 2.17
Ala(S)-7	8.01	4.59	3.34, 3.04	
Dhb-8	9.38		5.84	γCH_3 1.80
Pro-9		4.36	2.35, 2.04	γCH_2 2.12, 1.97, δCH_2 3.98, 3.74
Ile-10	7.44	4.05	2.17	γCH_3 0.96, γCH_2 1.57, 1.32, δCH_3 0.90
Ala(S)-11	7.48	4.38	3.07, 2.85	
Ala-12	7.81	4.15	1.36	
Gly-13	7.92	3.86		
Phe-14	7.82	4.57	3.19, 3.02	δCH 7.22, εCH and ζCH 7.31, 7.27
Ala-15	7.98	4.26	1.37	
Abu-16	7.93	4.10	1.84, 1.75	γCH_3 0.92
Leu-17	8.19	4.34	1.64	γCH 1.58, δCH_3 0.84
Met-18	8.25	4.40	2.04	γCH_2 2.57, 2.47
Ala-19	8.22	4.31	1.41	
Dha-20	9.61		5.70, 5.60	
Ile-21	8.07	4.14	1.94	γCH_3 0.94, γCH_2 1.52, 1.25, δCH_3 0.86
Gly-22	8.35	3.90		
Leu-23	7.81	4.34	1.60, 1.56	γCH 1.57, δCH_3 0.85
Val-24	7.83	4.08	2.08	γCH_3 0.94
Lys-25	8.23	4.38	1.80	
Abu(S)-26	8.32	4.42	3.51	γCH_3 1.30
Ile-27	7.84	4.01	1.85	γCH_3 0.93, γCH_2 1.47, δCH_3 0.86
Lys-28	8.38	4.12	1.49	γCH_2 1.78, 1.41, δCH_2 1.68, εCH_2 2.98
Gly-29	8.64	4.23, 3.73		
Lys-30	8.27	4.54	1.77	γCH_2 1.96, 1.40, δCH_2 1.67, 1.35, εCH_2 2.98
Ala(S)-31	7.86	4.34	3.18, 2.92	

6.3.7. GluC digest of carnolysin A1′ and A2′

Lyophilized endoproteinase GluC (New England Biolabs) was dissolved in Milli-Q water to a final concentration of 1 μg/μL. Digests consisted of 10 μL of 2X GluC

buffer, 8 μL of purified CrnA1′ or CrnA2′ (approximately 1 mg/mL) and 2 μL of GluC. Digests were incubated at 37 °C for 16 h.

6.3.8. Construction of pRSFDuet-crnM-crnA1 and pRSFDuet-crnM-crnA2

Synthetic genes *crnM*, *crnA1*, *crnA2* and *crnJ* were purchased (BioBasic Canada Inc., Markham, ON, Canada) with codon optimization for expression in *E. coli*. The synthetic constructs pUC57-crnM and pUC57-crnJ were designed with NdeI and XhoI cleavage sites, while pUC57-crnA1 and pUC57-crnA2 were designed with EcoRI and HindIII cleavage sites. Chemically competent *E. coli* DH5α was transformed with these plasmids, and transformants were selected for ampicillin resistance. Colonies were screened through culturing, plasmid isolation, restriction enzyme digestion, and analysis by agarose gel electrophoresis. Glycerol stocks (20 % glycerol) were prepared of the positive hits.

pUC57-crnM was isolated from an overnight culture of transformed *E. coli* DH5α using the QIAprep Spin Miniprep Kit (Qiagen). Isolated pUC57-crnM was digested with FastDigest NdeI and XhoI (Thermo Scientific). The digest was cleaned up using the QIAquick PCR Purification Kit (Qiagen) and ethanol precipitated. Plasmid pRSFDuet-1 was digested under the same conditions, and the digest was run on an agarose gel. The cut plasmid was extracted from the gel using the QIAquick Gel Extraction Kit (Qiagen). A ligation reaction was set up between the cut pUC57-crnM and pRSFDuet-1 using T4 DNA Ligase (Life Technologies). The ligation mixture was transformed into chemically competent *E. coli* DH5α, and transformants were screened for the desired pRSFDuet-crnM plasmid.

Isolated plasmid pUC57-crnA1 was digested with FastDigest EcoRI and HindIII (Thermo Scientific), cleaned up with the QIAquick PCR Purification Kit (Qiagen) and ethanol precipitated. Isolated plasmid pRSFDuet-crnM was digested under the same conditions, run on an agarose gel, and gel extracted using the QIAquick Gel Extraction Kit (Qiagen). A ligation reaction was set up between cut pUC57-crnA1 and cut pRSFDuet-crnM using T4 DNA Ligase (Life Technologies). Chemically competent *E. coli* DH5α was transformed with the ligation mixture, and transformants were screened for the pRSFDuet-crnM-crnA1 plasmid. A similar approach was used to obtain pRSFDuet-crnM-crnA2.

6.3.9. Construction of pETDuet-crnJ

Plasmids pETDuet-1 and pUC57-crnJ were digested using FastDigest NdeI and XhoI (Thermo Scientific). The digests were separated by agarose gel electrophoresis and the desired bands extracted using the QIAquick Gel Extraction Kit (Qiagen). A ligation reaction was set up between the digested and gel-extracted pETDuet-1 and *crnJ* insert using T4 DNA Ligase (Life Technologies). The ligation mixture was transformed into chemically competent *E. coli* DH5α, and transformants were screened for the desired pETDuet-crnJ plasmid.

6.3.10. Production and purification of CrnA1* and CrnA2*

The approach used to produce and purify post-translationally modified carnolysin in *E. coli* was based on the protocol reported for the production of enterococcal cytolysin.[13] Chemically competent *E. coli* BL21(DE3) was co-transformed with pETDuet-crnJ and either pRSFDuet-crnM-crnA1 or pRSFDuet-crnM-crnA2. LB broth (50 mL) with 50 μg/mL kanamycin (Kan) and 100 μg/mL ampicillin (Amp) was

inoculated with a single transformant colony and grown at 37 °C, 225 rpm for 16 h. This overnight culture was used to inoculate (1 %) 1 L of LB broth (with 50 μg/mL Kan, 100 μg/mL Amp), which was incubated at 37 °C, 225 rpm until the OD_{600} of the culture reached 0.5. The culture was put on ice for 30 min, IPTG was added to a concentration of 0.1 mM, and the induced culture was incubated at 18 °C, 225 rpm for 20 h.

The induced culture was then centrifuged (5,000 g, 10 min, 4 °C) and the supernatant decanted. The cell pellets were resuspended in 20 mL of LanA start buffer (20 mM NaH_2PO_4, pH 7.5, 500 mM NaCl, 0.5 mM imidazole, 20 % glycerol), and lysed by a single passage through a TS Series benchtop cell disruptor set at 25 kpsi. The lysate was centrifuged (23,700 g, 30 min, 4 °C), and the supernatant was collected. The lysate pellet was resuspended in 10 mL of LanA buffer 1 (6 M guanidine hydrochloride, 20 mM NaH_2PO_4, pH 7.5, 500 mM NaCl, 0.5 mM imidazole). The suspension was re-centrifuged (23,700 g, 30 min, 4 °C), and the supernatant collected. The two supernatants were combined, and 1 mL of PerfectPro Ni-NTA Superflow resin slurry (5PRIME, Gaithersburg, MD, USA) was added. The mixture was mixed at 50 rpm for 60 min at 8 °C. The mixture was run through a fritted plastic column connected to a peristaltic pump at 1 mL/min. The Ni-NTA resin was washed with 30 mL of LanA buffer 1, 15 mL of LanA buffer 2 (4 M guanidine hydrochloride, 20 mM NaH_2PO_4, pH 7.5, 300 mM NaCl and 30 mM imidazole), and 30 mL of LanA elution buffer (4 M guanidine hydrochloride, 20 mM Tris, pH 7.5, 100 mM NaCl and 1 M imidazole).

Small fractions of the wash and elution steps were desalted using C_{18} ZipTips (EMD Millipore) according to the manufacturer's instructions. The desalted elution fraction was concentrated *in vacuo* and analyzed using MALDI-TOF MS. The MS data

revealed the presence of peaks corresponding to CrnA1* and CrnA2* (i.e., His_6-CrnA1 and His_6-CrnA2 with the expected post-translational modifications) in both the LanA buffer 2 and LanA elution buffer solutions.

Both CrnA1* and CrnA2* were purified by reversed-phase HPLC using a C_{18} analytical column (VYDAC® 218TP54; 4.6 mm x 250 mm, 5 μm particle size, 300 Å pore diameter). Mobile phases A (water with 0.1 % TFA) and B (acetonitrile with 0.1 % TFA) were used with an overall flow rate of 1 mL/min and elution was monitored at 220 nm. CrnA1* was purified with a gradient initially held at 38 % B for 5 min, then increased to 50 % B over 20 min, eluting after 22.5 min. CrnA2* was purified with a gradient initially held at 30 % B for 5 min, then increased to 60 % B over 40 min, eluting after 28.3 min. This method yielded approximately 0.5 mg of pure CrnA1* and CrnA2* per liter of culture. The identities of the isolated CrnA1* ($[M+H]^+$ = 8922.8) and CrnA2* ($[M+H]^+$ = 7788.7) were confirmed by MALDI-TOF MS.

6.3.11. Construction of pET-28a-crnT150

The 450 bp sequence encoding the CrnT N-terminal protease domain was amplified from *C. maltaromaticum* C2 genomic DNA by PCR. Primers CTL60 (5' – ATA TAC ATA TGA AAA TAC GGT TTC AAC AAC AAA GTG – 3') and CTL61 (5' – ATA TAC TCG AGT TAA TTT TTA ACT AAT TCT TTT AAA ACT GGA TTT AAT TTA G – 3'), designed with NdeI and XhoI cleavage sites respectively, were used. The PCR reaction consisted of: 8 μL *C. maltaromaticum* C2 genomic DNA (25 ng/μL), 1 μL primer CTL60 (10 μM), 1 μL primer CTL61 (10 μM), 2 μL $MgSO_4$, 5 μL 10X PCR buffer, 1 μL dNTP mix, 0.2 μL Platinum *Taq* High Fidelity DNA Polymerase (Life Technologies) and 31.8 μL H_2O. The thermocycler conditions used were (1) one cycle at

95 °C for 2:00, (2) 30 cycles of: 95 °C for 0:20, 50 °C for 0:20, 68 °C for 1:30, (3) one cycle at 72 °C for 3:00. PCR yielded one band of the desired size by agarose gel electrophoresis. The PCR product was extracted from the gel using QIAquick Gel Extraction Kit (Qiagen).

The gel-extracted DNA was ligated into plasmid pJET 1.2 using the CloneJET PCR Cloning Kit (Thermo Scientific) according to the manufacturer's instructions. pJET-crnT150, confirmed via sequencing, was digested using FastDigest NdeI and XhoI (Thermo Scientific). The digest was cleaned up using the QIAquick PCR Purification Kit (Qiagen), ethanol precipitated and redissolved in TE buffer. pET28 was similarly digested, gel extracted, ethanol precipitated and redissolved in TE. T4 DNA Ligase was used to ligate crnT150 insert into pET28, in frame with the upstream hexahistidine-encoding sequence. *E. coli* DH5α was transformed with the ligation mixture, and transformants were screened for the desired plasmid.

6.3.12. Expression and purification of CrnT-150

A starter culture of *E. coli* BL21(DE3) transformed with pET-28a-crnT150 was grown in LB medium (with 50 μg/mL Kan) at 37 °C and 225 rpm for 16 h. This was used to inoculate (1 %) 1 L of LB medium (with 50 μg/mL Kan), which was incubated at 37 °C, 225 rpm. Once the OD_{600} reached 0.5, the culture was put on ice for 30 min and induced with 0.1 mM IPTG, and incubated at 18 °C, 225 rpm for 16 h.

The induced culture was then centrifuged (5,000 g, 10 min, 4 °C) and the supernatant removed. Cell pellets were resuspended in 20 mL of lysis buffer (50 mM sodium phosphate, pH 7.5, 500 mM NaCl), and lysed using a TS Series benchtop cell disruptor at 25 kpsi. The lysate was centrifuged (23,700 x g, 30 min, 4 °C) and the

supernatant was collected. PerfectPro Ni-NTA FastFlow resin slurry (1 mL) was added to the supernatant, which was then mixed at 50 rpm, 8 °C for 1 h.

The resin-lysate mixture was poured into a plastic fritted column and the flow-through was collected by gravity. The nickel column was washed with 3 mL fractions of lysis buffer supplemented with: 0 mM, 50 mM, 100 mM, 250 mM, 500 mM and 1000 mM imidazole. The presence and purity of CrnT150 in the wash fractions was determined by SDS-PAGE.

6.3.13. CrnT-150 activity assays

Due to the tendency of CrnT-150 to precipitate at higher temperatures, protease cleavage assays were set up on ice. Further, cooler temperatures seemed to slow the formation of tris(2-carboxyethyl)phosphine-lantibiotic adducts. Reaction mixtures consisted of 10 μL CrnT-150 (50 mM Na_2HPO_4, pH 7.5, 50 mM Na_2SO_4, 10 % glycerol), 10 μL of CrnA1* or CrnA2* (approximately 0.5 mg/mL), and 2 μL of 10 mM TCEP. Reaction mixtures were mixed, briefly centrifuged, and incubated at 10 °C for 5 h. Aliquots of the reaction were desalted using a C_{18} ZipTip (Millipore) and eluted in 60 % acetonitrile 0.1 % formic acid. The organic solvents from the ZipTip elution fraction were removed *in vacuo* and the mixture was analyzed by MALDI-TOF MS and LC-MS/MS.

6.4. Experimental procedures for the structural characterization of the leaderless bacteriocin enterocin 7A

6.4.1. Isolation of enterocin 7A

The purification scheme used to purify enterocin 7A was based on a previously reported protocol, with some modifications.[174] A preculture of *Enterococcus faecalis* 710C was grown in 100 mL of APT broth at 37 °C without shaking. This was used to inoculate (5 %) 1 L of APT broth, which was incubated at 37 °C without shaking for 22 h. The culture was centrifuged (5,000 g, 10 min, 4 °C), and the supernatant was collected. The culture supernatant was passed, at 1 mL/min, through a 20 mL SP Sepharose Fast Flow (Sigma-Aldrich) column pre-equilibrated with 20 mM sodium phosphate, pH 6.9. The column was washed with 100 mL of: (1) 20 mM sodium phosphate, pH 6.9, (2) 20 mM sodium phosphate, pH 6.9, with 0.2 M NaCl, and (3) 20 mM sodium phosphate, pH 6.9, with 1.0 M NaCl.

The fraction containing 1.0 M NaCl was desalted using a preconditioned Bond Elut C18 solid-phase extraction cartridge (Agilent; 10 g, 60 mL). After passing the 1.0 M NaCl fraction through the cartridge at 3 mL/min, it was washed with 50 mL of: (1) 30 % ethanol, (2) 30 % acetonitrile, (3) 40 % isopropanol, and (4) 80 % isopropanol with 0.1 % TFA. The 80 % isopropanol with 0.1 % TFA fraction was concentrated on a rotary evaporator down to 10 mL and further fractionated using reverse-phase HPLC. A C18 analytical scale HPLC column was used (VYDAC® 218TP54; 4.6 mm x 250 mm, 5 μm particle size, 300 Å pore diameter) with mobile phases A (water with 0.1 % TFA) and B (acetonitrile with 0.1 % TFA) at a flow rate of 1 mL/min, and detection at 220 nm. The solvent gradient started at 30 % B for 5 min, then increased to 71 % B over the course of

26 min. Enterocin 7A eluted after 27 min using this method, while enterocin 7B eluted after 25 min. The identity of the isolated enterocin 7A ($[M+H]^+$ = 5201.8) was confirmed by MALDI-TOF MS.

6.4.2. Circular dichroism

Circular dichroism (CD) spectra were acquired on an Olis DSM 17 CD spectrophotometer. Samples were analyzed in a 0.2 mm quartz cuvette. Solutions of enterocin 7A (100 μL; 0.8 mg/mL) were prepared in unbuffered water, in 20 mM sodium phosphate (pH 7.0), and in 50 % trifluoroethanol. Enterocin 7A showed α-helicity in all the solvent conditions assayed.

6.4.3. NMR spectroscopy

Enterocin 7A was dissolved in 300 μL of 10 % D_2O, 90 % H_2O to a concentration of 0.8 mM and transferred to a 5 mm Shigemi tube matched to the magnetic susceptibility of D_2O. A 600 μL mixture of enterocin 7A and 7B was prepared in the same solvent conditions to a concentration of 0.8 mM for each peptide and transferred to a standard 5 mm NMR tube. DSS (0.01 %) was added to these samples for referencing. TOCSY, NOESY, and natural abundance ^{13}C-HSQC and ^{15}N-HSQC datasets were acquired for both samples at 27 °C on a Varian VNMRS 700 MHz spectrometer. The water signal was suppressed via transmitter presaturation. NMR spectra were processed using NMRPipe[197] and analyzed using NMRViewJ.[175] Proton chemical shifts were assigned based on TOCSY and NOESY datasets (Table 6.7).[164] Chemical shift assignments were deposited in the BioMagResBank (accession number 19094).

Table 6.7. Chemical shift assignments for enterocin 7A

	HN	Hα	Hβ	others
Formyl				8.24
Met 1	8.67	4.52	2.15, 2.10	γCH_2 2.74, 2.62, εCH_3
Gly 2	8.85	4.01		
Ala 3	8.20	4.08	1.44	
Ile 4	7.93	3.69	2.21	γCH_3 1.00, γCH_2 1.57, δCH_3 0.75
Ala 5	7.98	3.98	1.49	
Lys 6	7.69	4.08	2.02, 1.83	
Leu 7	8.11	4.16	2.23, 1.38	γCH 2.14, δCH_3 0.99, 0.94
Val 8	8.86	3.12	1.79	γCH_3 0.38, 0.17
Ala 9	7.80	4.06	1.46	
Lys 10	7.17	4.07	1.58, 1.30	γCH_2 0.59, 0.56, δCH_2 1.42, 1.32, εCH_2 2.80, 2.64
Phe 11	8.46	4.83	3.42, 2.79	δCH 7.45, εCH 7.32, ζCH 7.49
Gly 12	8.52	4.68, 3.98		
Trp 13	9.11	4.67	3.39, 3.31	$\delta_1 CH$ 7.32, $\varepsilon_1 NH$ 10.19, $\zeta_2 CH$ 7.47, $\eta_2 CH$ 7.13, $\zeta_3 CH$ 6.91, $\varepsilon_3 CH$ 7.63
Pro 14		4.13	2.35, 1.95	γCH_2 2.28, 2.04, δCH_2 4.12, 3.93
Ile 15	7.90	3.83	1.88	γCH_3 0.77, γCH_2 1.80, 1.46, δCH_3 1.08
Val 16	7.33	3.43	2.09	γCH_3 1.00, 0.91
Lys 17	9.08	3.84	1.61, 1.41	γCH_2 1.55, 1.34, δCH_2 1.55, εCH_2 2.75
Lys 18	7.68	3.88	1.74, 1.69	γCH_2 1.02, 0.37, δCH_2 1.49, 1.36, εCH_2 2.83
Tyr 19	7.42	5.22	3.65, 2.51	δCH 7.28, εCH 6.78
Tyr 20	7.39	3.84	3.62, 2.90	δCH 7.00, εCH 6.82
Lys 21	8.44	3.75	1.79, 1.64	γCH_2 1.52, 1.32, δCH_2 1.66, εCH_2 2.97
Gln 22	7.90	3.22	1.76, 0.87	γCH_2 2.21, εNH_2 7.11, 6.91
Ile 23	8.42	3.07	1.65	γCH_3 0.67, γCH_2 1.74, δCH_3 0.94
Met 24	8.11	4.14	1.87, 1.73	γCH_2 2.31
Gln 25	7.40	3.83	1.74, 1.62	γCH_2 2.25, 1.90, εNH_2 7.07, 6.66
Phe 26	7.84	3.60	2.55, 2.31	δCH 5.73, εCH 5.63, ζCH 5.36
Ile 27	8.63	3.77	1.82	γCH_3 0.90
Gly 28	8.14	3.94		
Glu 29	7.68	4.44	2.14	γCH_2 2.58, 2.42
Gly 30	8.04	4.26, 3.93		
Trp 31	8.40	4.45	3.02, 2.74	$\delta_1 CH$ 7.03, $\varepsilon_1 NH$ 10.03, $\zeta_2 CH$ 7.18, $\eta_2 CH$ 6.54, $\zeta_3 CH$ 5.88, $\varepsilon_3 CH$ 6.51
Ala 32	8.46	4.43	1.57	
Ile 33	8.88	3.94	2.05	γCH_3 1.01, γCH_2 1.56, 1.47, δCH_3 1.01
Asn 34	8.71	4.43	2.82, 2.80	δNH_2 7.65, 6.89
Lys 35	7.25	4.13	1.79	γCH_2 1.20, 0.89, δCH_2 1.42, 0.65, εCH_2 1.96
Ile 36	7.85	3.82	2.24	γCH_3 1.12
Ile 37	8.87	3.78	2.09	γCH_3 1.12
Asp 38	7.92	4.43	2.85, 2.73	
Trp 39	8.00	4.12	3.68, 3.41	$\delta_1 CH$ 7.45, $\varepsilon_1 NH$ 10.36, $\zeta_2 CH$ 7.13, $\eta_2 CH$ 6.60, $\zeta_3 CH$ 5.99, $\varepsilon_3 CH$ 7.05
Ile 40	9.07	3.18	1.76	γCH_3 -0.13, γCH_2 2.16, 0.94, δCH_3 0.76
Lys 41	8.60	3.91	2.09, 2.00	γCH_2 1.69, δCH_2 1.86, 1.80, εCH_2 3.06, 3.00
Lys 42	7.31	4.08	1.50, 1.35	γCH_2 1.44, 1.35, δCH_2 1.53, εCH_2 2.89
His 43	7.91	4.29	3.23, 1.94	$\delta_2 CH$ 6.91, $\varepsilon_1 CH$ 7.13
Ile 44	7.15	4.36	2.08	γCH_3 0.99, γCH_2 1.50, 1.38, δCH_3 0.98

6.4.4. Structure calculations

CYANA 2.1 was used for the structural calculations of enterocin 7A.[176] Automated NOE crosspeak assignment was performed by CYANA, supplemented with select manual assignments. NOE distance restraints were generated in CYANA based on signal intensity. Seven rounds of calculation were performed, consisting of 10,000 steps per round. The final structure calculation used 1481 NOE crosspeaks, of which 166 were long-range, 212 were medium-range and 373 were short-range. Coordinates for the final structure were deposited in the Protein Data Bank (accession number 2m5z).

6.5. Experimental procedures for the structural characterization of a (C9L,C14L)-leucocin A mutant

6.5.1. Cloning of pMAL-c2x-leuA-C9L,C14L

A nucleotide sequence encoding the C9L,C14L-leucocin A mutant was constructed by PCR using long oligonucleotide primers MVB195 and MVB196, which possessed complementary sequences at the 3' end. PCR was set up using 36.5 μL of H_2O, 5 μL of 10 X PCR buffer, 2.5 μL of primer MVB195 (20 pmol/μL), 2.5 μL of MVB196 (20 pmol/μL), 2 μL of 50 mM $MgSO_4$, 1 μL of a 10 mM dNTP mixture and 0.5 μL of Platinum *Taq* High Fidelity polymerase (Invitrogen). The thermocycler was programmed for 20 cycles consisting of holding at (1) 94 °C for 30 s, (2) 56 °C for 30 s and (3) 68 °C for 30 s. After the first five cycles, 1 μL of primer MVB191 (200 pmol/μL), 1 μL of primer MVB192 (200 pmol/μL) and 1 μL of water was added to the PCR mixture, and thermocycling was allowed to continue. After thermocycling was complete, the PCR product was cleaned up using a QIAquick PCR Purification Kit (Qiagen).

Table 6.8. Oligonucleotide primer sequences

Primer name	Sequence
MVB195	5' – AAT ATG AGC TCG AAC AAC AAC AAC AAT AAC AAT AAC AAC AAC CTC GGG ATC GAG GGA AGG AAA TAC TAC GGT AAC GGC GTT CAC CTG ACC AAA TCT GGT CTG TCC G – 3'
MVB196	5' – TAT ATG GAT CCT TAC CAG AAA CCG TTG CCA CCG TTC GCC AGA CGG TGC ACG CCA GCA GAG AAC GCT TCA CCC CAG TTA ACG GAC AGA CCA GAT TTG GTC AGG TGA A – 3'
MVB191	5' – AAT ATG AGC TCG AAC AAC AAC AA – 3'
MVB192	5' – TAT ATG GAT CCT TAC CAG AAA C – 3'
MVB35	5' – TTT CCC AGT CAC GAC GTT GT – 3'
MVB36	5' – TCA ACG CCG CCA GCG GTC – 3'

The PCR product was digested with FastDigest restriction enzymes SacI and BamHI (Thermo Scientific), cleaned up with a QIAquick PCR Purification Kit (Qiagen) and ethanol precipitated. Plasmid pMAL-c2X (New England Biolabs) was digested and cleaned up in the same manner. T4 DNA Ligase (Invitrogen) was used to ligate the digested insert and plasmid. After 2.5 h, the ligation mixture was transformed into electrocompetent *E. coli* JM109 (prepared according to Inoue et al.)[198] and the transformants were plated on LB agar supplemented with ampicillin (150 μg/mL). Plasmids were isolated from cultures of selected transformants, and the presence of the desired insert was examined via PCR (using primers MVB191 and MVB192) and sequencing reactions (using primers MVB35 and MVB36). The pMAL-c2x-leuA-C9L,C14L plasmid construct was transformed into chemically competent *E. coli* BL21(DE3) cells.

6.5.2. Expression and purification of MBP-(C9L,C14L)-LeuA

A pre-culture of *E. coli* BL21(DE3) containing the pMAL-c2x-leuA-C9L,C14L plasmid was grown in 50 mL of LB broth (with 100 μg/mL ampicillin) at 37 °C, 200 rpm. This was used to inoculate (0.1 %) 1 L of LB broth (for the unlabeled peptide) or 1 L of labeled M9 minimal media (for the ^{13}C,^{15}N-labeled peptide). For the preparation of M9 minimal media, 200 mL of a 5X M9 salt solution (0.043 M NaCl, 0.11 M KH_2PO_4, 0.25 M $Na_2HPO_4 \bullet 7H_2O$) was diluted with 785 mL of Milli-Q water and autoclaved. To the sterile salt solution, filter-sterilized solutions of 20 % [U-^{13}C]-D-glucose (10 mL), 20 % $(^{15}NH_4)_2SO_4$ (2.5 mL), 1 M $MgSO_4$ (2 mL), 0.1 M $CaCl_2$ (1 mL), 10 mM $FeSO_4$ (100 μL) and 10 mg/mL thiamine (100 μL) were added. The inoculated culture was incubated at 37 °C, 200 rpm until an OD_{600} of 0.5 was reached. IPTG was added to a final concentration of 0.3 mM, and the culture was incubated for 3 h at 37 °C and 200 rpm.

The induced culture was centrifuged (10,000 g, 10 min, 4 °C) and the supernatant removed. The cell pellets were resuspended in 50 mL of cold amylose column buffer (20 mM Tris-HCl, pH 7.4, 100 mM NaCl, 1 mM EDTA, 1 mM NaN_3, 1 mM dithiothreitiol (DTT)). A Cφmplete EDTA-free protease inhibitor cocktail tablet (Roche) was added to the suspension prior to lysis to prevent digestion of the fusion protein. Bacterial cells were lysed by a single passage through a TS Series benchtop cell disruptor set at 25 kpsi. The lysate was centrifuged (27,200 g, 30 min, 4 °C) and the supernatant was collected. The lysate supernatant was diluted to 300 mL using amylose column buffer and passed through a 40 mL amylose resin column (New England Biolabs) at 1 mL/min. Unbound material was removed by washing the column with 800 mL of amylose column buffer. The fusion protein was eluted from the column by washing with amylose column buffer

supplemented with 10 mM maltose, while monitoring by UV at 280 nm. Protein fractions were analyzed by SDS-PAGE to confirm the presence of MBP-(C9L,C14L)-LeuA. The fractions containing the desired protein were pooled in dialysis tubing (6–8 kDa molecular-weight cutoff) and dialyzed against 4 L of Milli-Q water at 4 °C for 16 h (replacing the water twice). The dialyzed sample was then frozen on dry ice and lyophilized.

6.5.3. Factor Xa cleavage of MBP-(C9L,C14L)-LeuA

The lyophilized MBP-(C9L,C14L)-leucocin A fusion protein was dissolved (2.5 mg/mL) in Factor Xa buffer (20 mM Tris-HCl, pH 8.0, 100 mM NaCl, 2 mM $CaCl_2$). Factor Xa (New England Biolabs) was added (0.0125 mg/mL) to the fusion protein, and the mixture was incubated at room temperature for 3 h. The cleavage reaction was terminated by adding 4-(2-aminoethyl)benzenesulfonyl fluoride (AEBSF) to a final concentration of 0.1 mM. The progress of the reaction was monitored by MALDI-TOF MS and SDS-PAGE.

6.5.4. Purification of (C9L,C14L)-LeuA

The (C9L,C14L)-LeuA peptide obtained from cleavage of the fusion protein was purified by reverse-phase HPLC. The digest was injected onto a preparative scale C18 HPLC column (Phenomenex Luna®; 21.2 mm x 250 mm, 5 μm particle diameter, 100 Å pore diameter). Mobile phases A (water with 0.1 % TFA) and B (acetonitrile with 0.1 % TFA) were used with an overall flow rate of 10 mL/min, and elution was monitored at 220 nm. The solvent gradient started at 25 % B for 5 min, then increased to 55 % B over the course of 20 min. (C9L,C14L)-leucocin A eluted after 21.6 min using this method.

The identity of the isolated peptide (unlabeled: $[M+H]^+$ = 3953.1, isotopically labeled: $[M+H]^+$ = 4176.5) was confirmed by MALDI-TOF MS.

6.5.5. NMR spectroscopy

Purified ^{13}C,^{15}N-labeled (C9L,C14L)-LeuA was prepared in 90 % TFE-d_3 in H_2O to a concentration of approximately 0.5 mM and transferred to a standard 5 mm NMR tube. DSS was added to a final concentration of 100 μM as a reference. Two- and three-dimensional NMR datasets (^{13}C-HSQC, ^{15}N-HSQC, HNHA, CBCA(CO)NH, HCCH-TOCSY, HNCO, HNCACB, ^{13}C-NOESYHSQC, ^{15}N-NOESYHSQC and ^{15}N-TOCSYHSQC) were all acquired at 27 °C on a Varian VNMRS 700 MHz spectrometer. Spectra were processed using NMRPipe[197] and analyzed using NMRViewJ.[175] The sequence of spin systems relative to the peptide primary sequence was determined based on HNCACB and CBCA(CO)NH datasets. Side-chain chemical shift assignments were made based on ^{15}N-TOCSYHSQC and HCCH-TOCSY datasets (Table 6.9, 6.10). Chemical shift assignments were deposited into the BioMagResBank (accession number 17958).

Table 6.9. Proton chemical shift assignments for (C9L,C14L)-leucocin A

	HN	Hα	Hβ	others
Lys 1		3.95	1.83	γCH_2 1.37, 1.34, δCH_2 1.71, εCH_2 2.99
Tyr 2	8.20	4.59	3.05, 2.92	
Tyr 3	7.68	4.52	3.10, 2.87	
Gly 4	6.94	3.93, 3.79		
Asn 5	7.97	4.73	2.91	
Gly 6	8.28	4.01, 3.95		
Val 7	7.84	3.84	2.16	γCH_3 1.02, 0.95
His 8	8.09	4.52	3.36	
Leu 9	8.26	4.24	1.84, 1.72	γCH 1.73, δCH_3 0.96, 0.93
Thr 10	8.01	4.20	4.38	γCH_3 1.32
Lys 11	8.31	4.19	1.95	γCH_2 1.63, 1.48, δCH_2 1.72, εCH_2 2.98
Ser 12	8.07	4.32	4.08, 3.96	
Gly 13	8.22	3.95		
Leu 14	8.17	4.31	1.86, 1.60	γCH 1.82, δCH_3 0.96, 0.94
Ser 15	7.95	4.39	4.16, 4.01	
Val 16	7.91	3.99	2.17	γCH_3 1.09, 0.94
Asn 17	8.00	4.65	2.94, 2.89	
Trp 18	8.41	4.47	3.45	
Gly 19	8.40	3.97, 3.84		
Glu 20	8.35	4.16	2.35, 2.19	γCH_2 2.69, 2.53
Ala 21	8.07	4.11	1.52	
Phe 22	8.86	4.16	2.91, 2.68	
Ser 23	8.24	4.11	4.15, 4.05	
Ala 24	8.44	4.16	1.56	
Gly 25	8.04	3.92, 3.79		
Val 26	8.09	3.65	1.93	γCH_3 0.79, 0.72
His 27	8.01	4.23	3.29	
Arg 28	8.09	4.15	2.29, 2.03	
Leu 29	8.06	4.16	1.87, 1.64	γCH 1.79, δCH_3 0.91, 0.89
Ala 30	8.24	4.20	1.45	
Asn 31	7.80	4.76	2.97, 2.82	
Gly 32	8.02	3.93		
Gly 33	8.16	4.02, 3.85		
Asn 34	7.78	4.74	2.84	
Gly 35	7.88	3.83, 3.72		
Phe 36	7.54	4.58	3.05, 2.94	
Trp 37	7.45	4.79	3.39, 3.31	

Table 6.10. ^{13}C and ^{15}N chemical shift assignments for (C9L,C14L)-leucocin A

	N	Cα	Cβ	others
Lys 1		55.90	32.98	Cγ 23.83, Cδ 28.72, Cε 42.04
Tyr 2	121.31	58.19	38.67	
Tyr 3	122.15	58.07	38.57	
Gly 4	106.50	45.60		
Asn 5	117.06	54.14	38.04	
Gly 6	107.27	46.42		
Val 7	121.57	65.53	31.60	Cγ 20.95, 20.26
His 8	117.75	57.72	28.17	
Leu 9	120.85	57.57	42.17	Cγ 27.07, Cδ 23.60, 23.03
Thr 10	113.78	65.93	69.57	Cγ 20.89
Lys 11	120.19	58.84	32.11	Cγ 25.19, Cδ 28.97, Cε 42.40
Ser 12	114.59	61.08	63.06	
Gly 13	109.55	46.48		
Leu 14	121.35	57.39	41.94	Cγ 26.91, Cδ 24.28
Ser 15	113.76	61.14	63.24	
Val 16	121.90	65.13	32.09	Cγ 21.25, 20.43
Asn 17	118.74	55.72	38.50	
Trp 18	120.77	60.56	28.74	
Gly 19	105.60	47.11		
Glu 20	121.73	58.97	27.78	Cγ 32.66
Ala 21	122.68	55.22	17.34	
Phe 22	119.95	60.96	38.91	
Ser 23	113.34	61.62	63.01	
Ala 24	125.82	55.44	17.28	
Gly 25	106.19	46.96		
Val 26	120.84	66.24	31.41	Cγ 21.75, 20.26
His 27	115.10	59.49	27.43	
Arg 28	119.05	58.95	29.64	Cγ 27.40, Cδ 43.15
Leu 29	120.21	57.34	41.92	Cγ 27.00, Cδ 24.01, 22.71
Ala 30	120.59	53.72	17.72	
Asn 31	114.61	53.36	38.89	
Gly 32	106.87	45.80		
Gly 33	107.13	45.28		
Asn 34	116.91	52.89	38.67	
Gly 35	106.80	44.95		
Phe 36	118.50	57.84	39.41	
Trp 37	119.59	55.95	29.24	

6.5.6. Structure calculations

The structure of (C9L,C14L)-leucocin A was calculated using CYANA 2.1.[176] CYANA was used for automated NOE crosspeak assignment based on the provided chemical shift assignments, which were supplemented with several manually assigned NOE crosspeaks. Distance restraints were derived from NOE crosspeak intensity using CYANA. Backbone angle restraints were derived from HNHA data and TALOS. NMRViewJ[175] was used to compare the relative intensities of diagonal peaks and cross-peaks in the HNHA dataset, calculating the *J* coupling values between the corresponding amide protons and α-protons.[185] TALOS provided predicted backbone φ and ψ angles based on the comparison of the primary sequence and chemical shifts to a database of structurally characterized proteins.[186] Seven rounds of structure calculations were performed with 10,000 steps in each round. The final structure calculation used 385 NOE crosspeaks, of which 2 were long-range, 52 were medium range and 331 were short-range. The coordinates for the final (C9L,C14L)-leucocin A structure were deposited in the Protein Data Bank (accession number 2ljt).

References

1. **Li JW, Vederas JC.** 2009. Drug discovery and natural products: end of an era or an endless frontier? Science **325**:161-165.
2. **Cotter PD, Ross RP, Hill C.** 2013. Bacteriocins - a viable alternative to antibiotics? Nat. Rev. Microbiol. **11**:95-105.
3. **Cotter PD, Hill C, Ross RP.** 2005. Bacteriocins: developing innate immunity for food. Nat. Rev. Microbiol. **3**:777-788.
4. **Jack RW, Tagg JR, Ray B.** 1995. Bacteriocins of gram-positive bacteria. Microbiol. Rev. **59**:171-200.
5. **Lohans CT, Vederas JC.** 2012. Development of class IIa bacteriocins as therapeutic agents. Int. J. Microbiol. **2012**:386410.
6. **Marr AK, Gooderham WJ, Hancock RE.** 2006. Antibacterial peptides for therapeutic use: obstacles and realistic outlook. Curr. Opin. Pharmacol. **6**:468-472.
7. **Velkov T, Thompson PE, Nation RL, Li J.** 2010. Structure--activity relationships of polymyxin antibiotics. J. Med. Chem. **53**:1898-1916.
8. **Knerr PJ, van der Donk WA.** 2012. Discovery, biosynthesis, and engineering of lantipeptides. Annu. Rev. Biochem. **81**:479-505.
9. **Piper C, Cotter PD, Ross RP, Hill C.** 2009. Discovery of medically significant lantibiotics. Curr. Drug Discov. Technol. **6**:1-18.
10. **Bierbaum G, Sahl H-G.** 2009. Lantibiotics: mode of action, biosynthesis and bioengineering. Curr. Pharm. Biotechnol. **10**:2-18.

11. **Crowther GS, Baines SD, Todhunter SL, Freeman J, Chilton CH, Wilcox MH.** 2013. Evaluation of NVB302 versus vancomycin activity in an in vitro human gut model of *Clostridium difficile* infection. J. Antimicrob. Chemother. **68**:168-176.

12. **Piper C, Casey PG, Hill C, Cotter PD, Ross RP.** 2012. The lantibiotic lacticin 3147 prevents systemic spread of *Staphylococcus aureus* in a murine infection model. Int. J. Microbiol. **2012**:806230.

13. **Tang W, van der Donk WA.** 2013. The sequence of the enterococcal cytolysin imparts unusual lanthionine stereochemistry. Nat. Chem. Biol. **9**:157-159.

14. **Hsu ST, Breukink E, Tischenko E, Lutters MA, de Kruijff B, Kaptein R, Bonvin AM, van Nuland NA.** 2004. The nisin-lipid II complex reveals a pyrophosphate cage that provides a blueprint for novel antibiotics. Nat. Struct. Mol. Biol. **11**:963-967.

15. **Skaugen M, Nissen-Meyer J, Jung G, Stevanovic S, Sletten K, Inger C, Abildgaard M, Nes IF.** 1994. In vivo conversion of L-serine to D-alanine in a ribosomally synthesized polypeptide. J. Biol. Chem. **269**:27183-27185.

16. **McClerren AL, Cooper LE, Quan C, Thomas PM, Kelleher NL, van der Donk WA.** 2006. Discovery and in vitro biosynthesis of haloduracin, a two-component lantibiotic. Proc. Natl. Acad. Sci. U. S. A. **103**:17243-17248.

17. **Oman TJ, van der Donk WA.** 2010. Follow the leader: the use of leader peptides to guide natural product biosynthesis. Nat. Chem. Biol. **6**:9-18.

18. **Garg N, Salazar-Ocampo LM, van der Donk WA.** 2013. In vitro activity of the nisin dehydratase NisB. Proc. Natl. Acad. Sci. U. S. A. **110**:7258-7263.

19. **Xie L, Miller LM, Chatterjee C, Averin O, Kelleher NL, van der Donk WA.** 2004. Lacticin 481: in vitro reconstitution of lantibiotic synthetase activity. Science **303**:679-681.

20. **Chatterjee C, Miller LM, Leung YL, Xie L, Yi M, Kelleher NL, van der Donk WA.** 2005. Lacticin 481 synthetase phosphorylates its substrate during lantibiotic production. J. Am. Chem. Soc. **127**:15332-15333.

21. **McAuliffe O, Ross RP, Hill C.** 2001. Lantibiotics: structure, biosynthesis and mode of action. FEMS Microbiol. Rev. **25**:285-308.

22. **Furgerson Ihnken LA, Chatterjee C, van der Donk WA.** 2008. In vitro reconstitution and substrate specificity of a lantibiotic protease. Biochemistry **47**:7352-7363.

23. **van der Meer JR, Polman J, Beerthuyzen MM, Siezen RJ, Kuipers OP, De Vos WM.** 1993. Characterization of the *Lactococcus lactis* nisin A operon genes nisP, encoding a subtilisin-like serine protease involved in precursor processing, and nisR, encoding a regulatory protein involved in nisin biosynthesis. J. Bacteriol. **175**:2578-2588.

24. **Corvey C, Stein T, Dusterhus S, Karas M, Entian KD.** 2003. Activation of subtilin precursors by *Bacillus subtilis* extracellular serine proteases subtilisin (AprE), WprA, and Vpr. Biochem. Biophys. Res. Commun. **304**:48-54.

25. **Draper LA, Ross RP, Hill C, Cotter PD.** 2008. Lantibiotic immunity. Curr. Protein Pept. Sci. **9**:39-49.

26. **Stein T, Heinzmann S, Solovieva I, Entian KD.** 2003. Function of *Lactococcus lactis* nisin immunity genes nisI and nisFEG after coordinated expression in the surrogate host *Bacillus subtilis*. J. Biol. Chem. **278**:89-94.

27. **Martin NI, Sprules T, Carpenter MR, Cotter PD, Hill C, Ross RP, Vederas JC.** 2004. Structural characterization of lacticin 3147, a two-peptide lantibiotic with synergistic activity. Biochemistry **43**:3049-3056.

28. **Velasquez JE, Zhang X, van der Donk WA.** 2011. Biosynthesis of the antimicrobial peptide epilancin 15X and its N-terminal lactate. Chem. Biol. **18**:857-867.

29. **Sit CS, Yoganathan S, Vederas JC.** 2011. Biosynthesis of aminovinyl-cysteine-containing peptides and its application in the production of potential drug candidates. Acc. Chem. Res. **44**:261-268.

30. **Kupke T, Kempter C, Jung G, Gotz F.** 1995. Oxidative decarboxylation of peptides catalyzed by flavoprotein EpiD. Determination of substrate specificity using peptide libraries and neutral loss mass spectrometry. J. Biol. Chem. **270**:11282-11289.

31. **Ryan MP, Jack RW, Josten M, Sahl HG, Jung G, Ross RP, Hill C.** 1999. Extensive post-translational modification, including serine to D-alanine conversion, in the two-component lantibiotic, lacticin 3147. J. Biol. Chem. **274**:37544-37550.

32. **Ollivaux C, Soyez D, Toullec JY.** 2014. Biogenesis of D-amino acid containing peptides/proteins: where, when and how? J. Pept. Sci. **20**:595-612.

33. **Cotter PD, O'Connor PM, Draper LA, Lawton EM, Deegan LH, Hill C, Ross RP.** 2005. Posttranslational conversion of L-serines to D-alanines is vital for

optimal production and activity of the lantibiotic lacticin 3147. Proc. Natl. Acad. Sci. U. S. A. **102**:18584-18589.

34. **Suda S, Lawton EM, Wistuba D, Cotter PD, Hill C, Ross RP.** 2012. Homologues and bioengineered derivatives of LtnJ vary in ability to form D-alanine in the lantibiotic lacticin 3147. J. Bacteriol. **194**:708-714.
35. **He Z, Yuan C, Zhang L, Yousef AE.** 2008. N-terminal acetylation in paenibacillin, a novel lantibiotic. FEBS Lett. **582**:2787-2792.
36. **Foulston LC, Bibb MJ.** 2010. Microbisporicin gene cluster reveals unusual features of lantibiotic biosynthesis in actinomycetes. Proc. Natl. Acad. Sci. U. S. A. **107**:13461-13466.
37. **Lin Y, Teng K, Huan L, Zhong J.** 2011. Dissection of the bridging pattern of bovicin HJ50, a lantibiotic containing a characteristic disulfide bridge. Microbiol. Res. **166**:146-154.
38. **Brotz H, Bierbaum G, Leopold K, Reynolds PE, Sahl H-G.** 1998. The lantibiotic mersacidin inhibits peptidoglycan synthesis by targeting lipid II. Antimicrob. Agents Chemother. **42**:154-160.
39. **Hasper HE, Kramer NE, Smith JL, Hillman JD, Zachariah C, Kuipers OP, de Kruijff B, Breukink E.** 2006. An alternative bactericidal mechanism of action for lantibiotic peptides that target lipid II. Science **313**:1636-1637.
40. **Breukink E, Wiedemann I, van Kraaij C, Kuipers OP, Sahl H-G, de Kruijff B.** 1999. Use of the cell wall precursor lipid II by a pore-forming peptide antibiotic. Science **286**:2361-2364.

41. **Hasper HE, de Kruijff B, Breukink E.** 2004. Assembly and stability of nisin-lipid II pores. Biochemistry **43**:11567-11575.

42. **Wiedemann I, Bottiger T, Bonelli RR, Wiese A, Hagge SO, Gutsmann T, Seydel U, Deegan L, Hill C, Ross P, Sahl HG.** 2006. The mode of action of the lantibiotic lacticin 3147--a complex mechanism involving specific interaction of two peptides and the cell wall precursor lipid II. Mol. Microbiol. **61**:285-296.

43. **Oman TJ, van der Donk WA.** 2009. Insights into the mode of action of the two-peptide lantibiotic haloduracin. ACS Chem. Biol. **4**:865-874.

44. **Cintas LM, Casaus P, Holo H, Hernandez PE, Nes IF, Havarstein LS.** 1998. Enterocins L50A and L50B, two novel bacteriocins from *Enterococcus faecium* L50, are related to staphylococcal hemolysins. J. Bacteriol. **180**:1988-1994.

45. **Martin-Platero AM, Valdivia E, Ruiz-Rodriguez M, Soler JJ, Martin-Vivaldi M, Maqueda M, Martinez-Bueno M.** 2006. Characterization of antimicrobial substances produced by *Enterococcus faecalis* MRR 10-3, isolated from the uropygial gland of the hoopoe (*Upupa epops*). Appl. Environ. Microbiol. **72**:4245-4249.

46. **Netz DJ, Pohl R, Beck-Sickinger AG, Selmer T, Pierik AJ, Bastos Mdo C, Sahl HG.** 2002. Biochemical characterisation and genetic analysis of aureocin A53, a new, atypical bacteriocin from *Staphylococcus aureus*. J. Mol. Biol. **319**:745-756.

47. **Fujita K, Ichimasa S, Zendo T, Koga S, Yoneyama F, Nakayama J, Sonomoto K.** 2007. Structural analysis and characterization of lacticin Q, a novel bacteriocin belonging to a new family of unmodified bacteriocins of gram-positive bacteria. Appl. Environ. Microbiol. **73**:2871-2877.

48. **Gajic O, Buist G, Kojic M, Topisirovic L, Kuipers OP, Kok J.** 2003. Novel mechanism of bacteriocin secretion and immunity carried out by lactococcal multidrug resistance proteins. J. Biol. Chem. **278**:34291-34298.

49. **Netz DJ, Sahl HG, Marcelino R, dos Santos Nascimento J, de Oliveira SS, Soares MB, do Carmo de Freire Bastos M.** 2001. Molecular characterisation of aureocin A70, a multi-peptide bacteriocin isolated from *Staphylococcus aureus*. J. Mol. Biol. **311**:939-949.

50. **Sandiford S, Upton M.** 2012. Identification, characterization, and recombinant expression of epidermicin NI01, a novel unmodified bacteriocin produced by Staphylococcus epidermidis that displays potent activity against Staphylococci. Antimicrob. Agents Chemother. **56**:1539-1547.

51. **Hyink O, Balakrishnan M, Tagg JR.** 2005. *Streptococcus rattus* strain BHT produces both a class I two-component lantibiotic and a class II bacteriocin. FEMS Microbiol. Lett. **252**:235-241.

52. **Iwatani S, Yoneyama F, Miyashita S, Zendo T, Nakayama J, Sonomoto K.** 2012. Identification of the genes involved in the secretion and self-immunity of lacticin Q, an unmodified leaderless bacteriocin from *Lactococcus lactis* QU 5. Microbiology **158**:2927-2935.

53. **Iwatani S, Horikiri Y, Zendo T, Nakayama J, Sonomoto K.** 2013. Bifunctional gene cluster, lnqBCDEF, mediates bacteriocin production and immunity with differential genetic requirements. Appl. Environ. Microbiol. **79**:2446-2449.

54. **Yoneyama F, Imura Y, Ichimasa S, Fujita K, Zendo T, Nakayama J, Matsuzaki K, Sonomoto K.** 2009. Lacticin Q, a lactococcal bacteriocin, causes

high-level membrane permeability in the absence of specific receptors. Appl. Environ. Microbiol. **75**:538-541.

55. **Yoneyama F, Imura Y, Ohno K, Zendo T, Nakayama J, Matsuzaki K, Sonomoto K.** 2009. Peptide-lipid huge toroidal pore, a new antimicrobial mechanism mediated by a lactococcal bacteriocin, lacticin Q. Antimicrob. Agents Chemother. **53**:3211-3217.

56. **Netz DJ, Bastos Mdo C, Sahl HG.** 2002. Mode of action of the antimicrobial peptide aureocin A53 from *Staphylococcus aureus*. Appl. Environ. Microbiol. **68**:5274-5280.

57. **Uzelac G, Kojic M, Lozo J, Aleksandrzak-Piekarczyk T, Gabrielsen C, Kristensen T, Nes IF, Diep DB, Topisirovic L.** 2013. A Zn-dependent metallopeptidase is responsible for sensitivity to LsbB, a class II leaderless bacteriocin of *Lactococcus lactis* subsp. *lactis* BGMN1-5. J. Bacteriol. **195**:5614-5621.

58. **Hastings JW, Sailer M, Johnson K, Roy KL, Vederas JC, Stiles ME.** 1991. Characterization of leucocin A-UAL 187 and cloning of the bacteriocin gene from *Leuconostoc gelidum*. J. Bacteriol. **173**:7491-7500.

59. **Nissen-Meyer J, Rogne P, Oppegard C, Haugen HS, Kristiansen PE.** 2009. Structure-function relationships of the non-lanthionine-containing peptide (class II) bacteriocins produced by gram-positive bacteria. Curr. Pharm. Biotechnol. **10**:19-37.

60. **Fregeau Gallagher NL, Sailer M, Niemczura WP, Nakashima TT, Stiles ME, Vederas JC.** 1997. Three-dimensional structure of leucocin A in trifluoroethanol

and dodecylphosphocholine micelles: spatial location of residues critical for biological activity in type IIa bacteriocins from lactic acid bacteria. Biochemistry **36**:15062-15072.

61. **Wang Y, Henz ME, Gallagher NL, Chai S, Gibbs AC, Yan LZ, Stiles ME, Wishart DS, Vederas JC.** 1999. Solution structure of carnobacteriocin B2 and implications for structure-activity relationships among type IIa bacteriocins from lactic acid bacteria. Biochemistry **38**:15438-15447.
62. **Uteng M, Hauge HH, Markwick PR, Fimland G, Mantzilas D, Nissen-Meyer J, Muhle-Goll C.** 2003. Three-dimensional structure in lipid micelles of the pediocin-like antimicrobial peptide sakacin P and a sakacin P variant that is structurally stabilized by an inserted C-terminal disulfide bridge. Biochemistry **42**:11417-11426.
63. **Haugen HS, Fimland G, Nissen-Meyer J, Kristiansen PE.** 2005. Three-dimensional structure in lipid micelles of the pediocin-like antimicrobial peptide curvacin A. Biochemistry **44**:16149-16157.
64. **Drider D, Fimland G, Hechard Y, McMullen LM, Prevost H.** 2006. The continuing story of class IIa bacteriocins. Microbiol. Mol. Biol. Rev. **70**:564-582.
65. **Quadri LE, Yan LZ, Stiles ME, Vederas JC.** 1997. Effect of amino acid substitutions on the activity of carnobacteriocin B2. Overproduction of the antimicrobial peptide, its engineered variants, and its precursor in *Escherichia coli*. J. Biol. Chem. **272**:3384-3388.

66. **van Belkum MJ, Worobo RW, Stiles ME.** 1997. Double-glycine-type leader peptides direct secretion of bacteriocins by ABC transporters: colicin V secretion in *Lactococcus lactis*. Mol. Microbiol. **23**:1293-1301.

67. **Cintas LM, Casaus P, Havarstein LS, Hernandez PE, Nes IF.** 1997. Biochemical and genetic characterization of enterocin P, a novel sec-dependent bacteriocin from *Enterococcus faecium* P13 with a broad antimicrobial spectrum. Appl. Environ. Microbiol. **63**:4321-4330.

68. **Kjos M, Borrero J, Opsata M, Birri DJ, Holo H, Cintas LM, Snipen L, Hernandez PE, Nes IF, Diep DB.** 2011. Target recognition, resistance, immunity and genome mining of class II bacteriocins from Gram-positive bacteria. Microbiology **157**:3256-3267.

69. **Martin-Visscher LA, Sprules T, Gursky LJ, Vederas JC.** 2008. Nuclear magnetic resonance solution structure of PisI, a group B immunity protein that provides protection against the type IIa bacteriocin piscicolin 126, PisA. Biochemistry **47**:6427-6436.

70. **Sprules T, Kawulka KE, Vederas JC.** 2004. NMR solution structure of ImB2, a protein conferring immunity to antimicrobial activity of the type IIa bacteriocin, carnobacteriocin B2. Biochemistry **43**:11740-11749.

71. **Quadri LE, Sailer M, Terebiznik MR, Roy KL, Vederas JC, Stiles ME.** 1995. Characterization of the protein conferring immunity to the antimicrobial peptide carnobacteriocin B2 and expression of carnobacteriocins B2 and BM1. J. Bacteriol. **177**:1144-1151.

72. **Hechard Y, Sahl HG.** 2002. Mode of action of modified and unmodified bacteriocins from Gram-positive bacteria. Biochimie **84**:545-557.

73. **Chikindas ML, Garcia-Garcera MJ, Driessen AJ, Ledeboer AM, Nissen-Meyer J, Nes IF, Abee T, Konings WN, Venema G.** 1993. Pediocin PA-1, a bacteriocin from *Pediococcus acidilactici* PAC1.0, forms hydrophilic pores in the cytoplasmic membrane of target cells. Appl. Environ. Microbiol. **59**:3577-3584.

74. **Diep DB, Skaugen M, Salehian Z, Holo H, Nes IF.** 2007. Common mechanisms of target cell recognition and immunity for class II bacteriocins. Proc. Natl. Acad. Sci. U. S. A. **104**:2384-2389.

75. **Kjos M, Salehian Z, Nes IF, Diep DB.** 2010. An extracellular loop of the mannose phosphotransferase system component IIC is responsible for specific targeting by class IIa bacteriocins. J. Bacteriol. **192**:5906-5913.

76. **Johnsen L, Fimland G, Nissen-Meyer J.** 2005. The C-terminal domain of pediocin-like antimicrobial peptides (class IIa bacteriocins) is involved in specific recognition of the C-terminal part of cognate immunity proteins and in determining the antimicrobial spectrum. J. Biol. Chem. **280**:9243-9250.

77. **Fimland G, Jack R, Jung G, Nes IF, Nissen-Meyer J.** 1998. The bactericidal activity of pediocin PA-1 is specifically inhibited by a 15-mer fragment that spans the bacteriocin from the center toward the C terminus. Appl. Environ. Microbiol. **64**:5057-5060.

78. **Schwarzer D, Finking R, Marahiel MA.** 2003. Nonribosomal peptides: from genes to products. Nat. Prod. Rep. **20**:275-287.

79. **Cochrane SA, Vederas JC.** 2014. Lipopeptides from *Bacillus* and *Paenibacillus* spp.: a gold mine of antibiotic candidates. Med. Res. Rev. DOI: 10.1002/med.21321.

80. **Grau A, Gomez Fernandez JC, Peypoux F, Ortiz A.** 1999. A study on the interactions of surfactin with phospholipid vesicles. Biochim. Biophys. Acta **1418**:307-319.

81. **Straus SK, Hancock RE.** 2006. Mode of action of the new antibiotic for Gram-positive pathogens daptomycin: comparison with cationic antimicrobial peptides and lipopeptides. Biochim. Biophys. Acta **1758**:1215-1223.

82. **Miao V, Coeffet-Legal MF, Brian P, Brost R, Penn J, Whiting A, Martin S, Ford R, Parr I, Bouchard M, Silva CJ, Wrigley SK, Baltz RH.** 2005. Daptomycin biosynthesis in *Streptomyces roseosporus*: cloning and analysis of the gene cluster and revision of peptide stereochemistry. Microbiology **151**:1507-1523.

83. **Finking R, Marahiel MA.** 2004. Biosynthesis of nonribosomal peptides. Annu. Rev. Microbiol. **58**:453-488.

84. **Kraas FI, Helmetag V, Wittmann M, Strieker M, Marahiel MA.** 2010. Functional dissection of surfactin synthetase initiation module reveals insights into the mechanism of lipoinitiation. Chem. Biol. **17**:872-880.

85. **Wittmann M, Linne U, Pohlmann V, Marahiel MA.** 2008. Role of DptE and DptF in the lipidation reaction of daptomycin. FEBS J. **275**:5343-5354.

86. **Choi SK, Park SY, Kim R, Kim SB, Lee CH, Kim JF, Park SH.** 2009. Identification of a polymyxin synthetase gene cluster of *Paenibacillus polymyxa*

and heterologous expression of the gene in *Bacillus subtilis*. J. Bacteriol. **191**:3350-3358.

87. **Maget-Dana R, Ptak M.** 1995. Interactions of surfactin with membrane models. Biophys. J. **68**:1937-1943.

88. **Sheppard JD, Jumarie C, Cooper DG, Laprade R.** 1991. Ionic channels induced by surfactin in planar lipid bilayer membranes. Biochim. Biophys. Acta **1064**:13-23.

89. **Heerklotz H, Seelig J.** 2007. Leakage and lysis of lipid membranes induced by the lipopeptide surfactin. Eur. Biophys. J. **36**:305-314.

90. **Pogliano J, Pogliano N, Silverman JA.** 2012. Daptomycin-mediated reorganization of membrane architecture causes mislocalization of essential cell division proteins. J. Bacteriol. **194**:4494-4504.

91. **Tiwari BK, Valdramidis VP, O'Donnell CP, Muthukumarappan K, Bourke P, Cullen PJ.** 2009. Application of natural antimicrobials for food preservation. J. Agric. Food Chem. **57**:5987-6000.

92. **Bhunia AK, Johnson MC, Ray B.** 1988. Purification, characterization and antimicrobial spectrum of a bacteriocin produced by *Pediococcus acidilactici*. J. Appl. Bacteriol. **65**:261-268.

93. **Goldstein BP, Wei J, Greenberg K, Novick R.** 1998. Activity of nisin against *Streptococcus pneumoniae*, in vitro, and in a mouse infection model. J. Antimicrob. Chemother. **42**:277-278.

94. **Kruszewska D, Sahl HG, Bierbaum G, Pag U, Hynes SO, Ljungh A.** 2004. Mersacidin eradicates methicillin-resistant *Staphylococcus aureus* (MRSA) in a mouse rhinitis model. J. Antimicrob. Chemother. **54**:648-653.

95. **Ryan MP, Flynn J, Hill C, Ross RP, Meaney WJ.** 1999. The natural food grade inhibitor, lacticin 3147, reduced the incidence of mastitis after experimental challenge with *Streptococcus dysgalactiae* in nonlactating dairy cows. J. Dairy Sci. **82**:2108-2114.

96. **Howell TH, Fiorellini JP, Blackburn P, Projan SJ, de la Harpe J, Williams RC.** 1993. The effect of a mouthrinse based on nisin, a bacteriocin, on developing plaque and gingivitis in beagle dogs. J. Clin. Periodontol. **20**:335-339.

97. **Vaara M.** 2010. Polymyxins and their novel derivatives. Curr. Opin. Microbiol. **13**:574-581.

98. **Vaara M, Fox J, Loidl G, Siikanen O, Apajalahti J, Hansen F, Frimodt-Moller N, Nagai J, Takano M, Vaara T.** 2008. Novel polymyxin derivatives carrying only three positive charges are effective antibacterial agents. Antimicrob. Agents Chemother. **52**:3229-3236.

99. **Fowler VGJ, Boucher HW, Corey GR, Abrutyn E, Karchmer AW, Rupp ME, Levine DP, Chambers HF, Tally FP, Vigliani GA, Cabell CH, Link AS, DeMeyer I, Filler SG, Zervos M, Cook P, Parsonnet J, Bernstein JM, Price CS, Forrest GN, Fatkenheuer G, Gareca M, Rehm SJ, Brodt HR, Tice A, Cosgrove SE.** 2006. Daptomycin versus standard therapy for bacteremia and endocarditis caused by *Staphylococcus aureus*. N. Engl. J. Med. **355**:653-665.

100. **Raja A, LaBonte J, Lebbos J, Kirkpatrick P.** 2003. Daptomycin. Nat. Rev. Drug Discov. **2**:943-944.

101. **Arias CA, Panesso D, McGrath DM, Qin X, Mojica MF, Miller C, Diaz L, Tran TT, Rincon S, Barbu EM, Reyes J, Roh JH, Lobos E, Sodergren E, Pasqualini R, Arap W, Quinn JP, Shamoo Y, Murray BE, Weinstock GM.** 2011. Genetic basis for in vivo daptomycin resistance in enterococci. N. Engl. J. Med. **365**:892-900.

102. **Seydlová G, Svobodová J.** 2008. Review of surfactin chemical properties and the potential biomedical applications. Cent. Eur. J. Med. **3**:123-133.

103. **Takahashi T, Ohno O, Ikeda Y, Sawa R, Homma Y, Igarashi M, Umezawa K.** 2006. Inhibition of lipopolysaccharide activity by a bacterial cyclic lipopeptide surfactin. J. Antibiot. **59**:35-43.

104. **Mireles JR, Toguchi A, Harshey RM.** 2001. *Salmonella enterica* serovar typhimurium swarming mutants with altered biofilm-forming abilities: surfactin inhibits biofilm formation. J. Bacteriol. **183**:5848-5854.

105. **Dufour S, Deleu M, Nott K, Wathelet B, Thonart P, Paquot M.** 2005. Hemolytic activity of new linear surfactin analogs in relation to their physico-chemical properties. Biochim. Biophys. Acta **1726**:87-95.

106. **Symmank H, Franke P, Saenger W, Bernhard F.** 2002. Modification of biologically active peptides: production of a novel lipohexapeptide after engineering of *Bacillus subtilis* surfactin synthetase. Protein Eng. **15**:913-921.

107. **Lohans CT, van Belkum MJ, Cochrane SA, Huang Z, Sit CS, McMullen LM, Vederas JC.** 2014. Biochemical, structural, and genetic characterization of

tridecaptin A(1), an antagonist of *Campylobacter jejuni*. ChemBioChem **15**:243-249.

108. **Lohans CT, Huang Z, van Belkum MJ, Giroud M, Sit CS, Steels EM, Zheng J, Whittal RM, McMullen LM, Vederas JC.** 2012. Structural characterization of the highly cyclized lantibiotic paenicidin A via a partial desulfurization/reduction strategy. J. Am. Chem. Soc. **134**:19540-19543.
109. **Tulini FL, Lohans CT, Bordon KC, Zheng J, Arantes EC, Vederas JC, De Martinis EC.** 2014. Purification and characterization of antimicrobial peptides from fish isolate *Carnobacterium maltaromaticum* C2: Carnobacteriocin X and carnolysins A1 and A2. Int. J. Food Microbiol. **173**:81-88.
110. **Lohans CT, Towle KM, Miskolzie M, McKay RT, van Belkum MJ, McMullen LM, Vederas JC.** 2013. Solution structures of the linear leaderless bacteriocins enterocin 7A and 7B resemble carnocyclin A, a circular antimicrobial peptide. Biochemistry **52**:3987-3994.
111. **Sit CS, Lohans CT, van Belkum MJ, Campbell CD, Miskolzie M, Vederas JC.** 2012. Substitution of a conserved disulfide in the type IIa bacteriocin, leucocin A, with L-leucine and L-serine residues: effects on activity and three-dimensional structure. ChemBioChem **13**:35-38.
112. **Abriouel H, Franz CMAP, Ben Omar N, Galvez A.** 2011. Diversity and applications of Bacillus bacteriocins. FEMS Microbiol. Rev. **35**:201-232.
113. **Ash C, Priest FG, Collins MD.** 1993. Molecular identification of rRNA group 3 bacilli (Ash, Farrow, Wallbanks and Collins) using a PCR probe test. Proposal for the creation of a new genus *Paenibacillus*. Antonie van Leeuwenhoek **64**:253-260.

114. **Raza W, Yang W, Shen QR.** 2008. *Paenibacillus polymyxa*: antibiotics, hydrolytic enzymes and hazard assessment. J. Plant Pathol. **90**:419-430.

115. **Fluhe L, Knappe TA, Gattner MJ, Schafer A, Burghaus O, Linne U, Marahiel MA.** 2012. The radical SAM enzyme AlbA catalyzes thioether bond formation in subtilosin A. Nat. Chem. Biol. **8**:350-357.

116. **Kawulka K, Sprules T, McKay RT, Mercier P, Diaper CM, Zuber P, Vederas JC.** 2003. Structure of subtilosin A, an antimicrobial peptide from *Bacillus subtilis* with unusual posttranslational modifications linking cysteine sulfurs to α-carbons of phenylalanine and threonine. J. Am. Chem. Soc. **125**:4726-4727.

117. **Sit CS, van Belkum MJ, McKay RT, Worobo RW, Vederas JC.** 2011. The 3D solution structure of thurincin H, a bacteriocin with four sulfur to α-carbon crosslinks. Angew. Chem. Int. Ed. Engl. **50**:8718-8721.

118. **Oman TJ, Boettcher JM, Wang H, Okalibe XN, van der Donk WA.** 2011. Sublancin is not a lantibiotic but an S-linked glycopeptide. Nat. Chem. Biol. **7**:78-80.

119. **Wang H, Oman TJ, Zhang R, Garcia De Gonzalo CV, Zhang Q, van der Donk WA.** 2014. The glycosyltransferase involved in thurandacin biosynthesis catalyzes both O- and S-glycosylation. J. Am. Chem. Soc. **136**:84-87.

120. **Huang E, Yousef AE.** 2014. Paenibacterin, a novel broad-spectrum lipopeptide antibiotic, neutralises endotoxins and promotes survival in a murine model of *Pseudomonas aeruginosa*-induced sepsis. Int. J. Antimicrob. Agents **44**:74-77.

121. **World Health Organization**. 2012. The global view of campylobacteriosis: report of an expert consultation, (1st ed.), Utrecht, Netherlands.

122. **Zhao S, Young SR, Tong E, Abbott JW, Womack N, Friedman SL, McDermott PF.** 2010. Antimicrobial resistance of Campylobacter isolates from retail meat in the United States between 2002 and 2007. Appl. Environ. Microbiol. **76**:7949-7956.

123. **Hoang KV, Stern NJ, Lin J.** 2011. Development and stability of bacteriocin resistance in *Campylobacter* spp. J. Appl. Microbiol. **111**:1544-1550.

124. **Svetoch EA, Stern NJ, Eruslanov BV, Kovalev YN, Volodina LI, Perelygin VV, Mitsevich EV, Mitsevich IP, Pokhilenko VD, Borzenkov VN, Levchuk VP, Svetoch OE, Kudriavtseva TY.** 2005. Isolation of *Bacillus circulans* and *Paenibacillus polymyxa* strains inhibitory to *Campylobacter jejuni* and characterization of associated bacteriocins. J. Food. Prot. **68**:11-17.

125. **Kato T, Hinoo H, Shoji J.** 1978. The structure of tridecaptin A (studies on antibiotics from the genus Bacillus. XXIV). J. Antibiot. **31**:652-661.

126. **Massart-Leen AM, DePooter H, Decloedt M, Schamp N.** 1981. Composition and variability of the branched-chain fatty acid fraction in the milk of goats and cows. Lipids **16**:286-292.

127. **Lohans CT, Vederas JC.** 2014. Structural characterization of thioether-bridged bacteriocins. J. Antibiot. **67**:23-30.

128. **Chatterjee C, Paul M, Xie L, van der Donk WA.** 2005. Biosynthesis and mode of action of lantibiotics. Chem. Rev. **105**:633-684.

129. **Fuchs SW, Jaskolla TW, Bochmann S, Kotter P, Wichelhaus T, Karas M, Stein T, Entian KD.** 2011. Entianin, a novel subtilin-like lantibiotic from *Bacillus*

subtilis subsp. *spizizenii* DSM 15029T with high antimicrobial activity. Appl. Environ. Microbiol. **77**:1698-1707.

130. **Ross AC, Liu H, Pattabiraman VR, Vederas JC.** 2010. Synthesis of the lantibiotic lactocin S using peptide cyclizations on solid phase. J. Am. Chem. Soc. **132**:462-463.
131. **Liu W, Chan AS, Liu H, Cochrane SA, Vederas JC.** 2011. Solid supported chemical syntheses of both components of the lantibiotic lacticin 3147. J. Am. Chem. Soc. **133**:14216-14219.
132. **Brotz H, Sahl H-G.** 2000. New insights into the mechanism of action of lantibiotics--diverse biological effects by binding to the same molecular target. J. Antimicrob. Chemother. **46**:1-6.
133. **Shin SH, Kim S, Kim JY, Song HY, Cho SJ, Kim DR, Lee KI, Lim HK, Park NJ, Hwang IT, Yang KS.** 2012. Genome sequence of *Paenibacillus terrae* HPL-003, a xylanase-producing bacterium isolated from soil found in forest residue. J. Bacteriol. **194**:1266.
134. **Kaneda T.** 1991. Iso- and anteiso-fatty acids in bacteria: biosynthesis, function, and taxonomic significance. Microbiol. Rev. **55**:288-302.
135. **Kaneda T.** 1967. Fatty acids in the genus Bacillus. I. Iso- and anteiso-fatty acids as characteristic constituents of lipids in 10 species. J. Bacteriol. **93**:894-903.
136. **Rawlings BJ.** 1997. Biosynthesis of fatty acids and related metabolites. Nat. Prod. Rep. **14**:335-358.
137. **Kim JF, Jeong H, Park SY, Kim SB, Park YK, Choi SK, Ryu CM, Hur CG, Ghim SY, Oh TK, Kim JJ, Park CS, Park SH.** 2010. Genome sequence of the

polymyxin-producing plant-probiotic rhizobacterium *Paenibacillus polymyxa* E681. J. Bacteriol. **192**:6103-6104.

138. **Jeong H, Park SY, Chung WH, Kim SH, Kim N, Park SH, Kim JF.** 2011. Draft genome sequence of the *Paenibacillus polymyxa* type strain (ATCC 842T), a plant growth-promoting bacterium. J. Bacteriol. **193**:5026-5027.
139. **Schwarzer D, Mootz HD, Linne U, Marahiel MA.** 2002. Regeneration of misprimed nonribosomal peptide synthetases by type II thioesterases. Proc. Natl. Acad. Sci. U. S. A. **99**:14083-14088.
140. **Kato T, Sakazaki R, Hinoo H, Shoji J.** 1979. The structures of tridecaptins B and C (studies on antibiotics from the genus Bacillus. XXV). J. Antibiot. **32**:305-312.
141. **Cochrane SA, Lohans CT, Brandelli JR, Mulvey G, Armstrong GD, Vederas JC.** 2014. Synthesis and structure-activity relationship studies of N-terminal analogues of the antimicrobial peptide tridecaptin A(1). J. Med. Chem. **57**:1127-1131.
142. **Naghmouchi K, Baah J, Hober D, Jouy E, Rubrecht C, Sane F, Drider D.** 2013. Synergistic effect between colistin and bacteriocins in controlling Gram-negative pathogens and their potential to reduce antibiotic toxicity in mammalian epithelial cells. Antimicrob. Agents Chemother. **57**:2719-2725.
143. **Draper LA, Cotter PD, Hill C, Ross RP.** 2013. The two peptide lantibiotic lacticin 3147 acts synergistically with polymyxin to inhibit Gram negative bacteria. BMC Microbiol. **13**:212.
144. **Stern NJ, Svetoch EA, Eruslanov BV, Kovalev YN, Volodina LI, Perelygin VV, Mitsevich EV, Mitsevich IP, Levchuk VP.** 2005. *Paenibacillus polymyxa* purified

bacteriocin to control *Campylobacter jejuni* in chickens. J. Food Prot. **68**:1450-1453.

145. **Jett BD, Huycke MM, Gilmore MS.** 1994. Virulence of enterococci. Clin. Microbiol. Rev. **7**:462-478.

146. **Van Tyne D, Martin MJ, Gilmore MS.** 2013. Structure, function, and biology of the *Enterococcus faecalis* cytolysin. Toxins **5**:895-911.

147. **Brock TD, Davie JM.** 1963. Probable identity of a group D hemolysin with a bacteriocine. J. Bacteriol. **86**:708-712.

148. **Ike Y, Hashimoto H, Clewell DB.** 1984. Hemolysin of *Streptococcus faecalis* subspecies *zymogenes* contributes to virulence in mice. Infect. Immun. **45**:528-530.

149. **Haas W, Gilmore MS.** 1999. Molecular nature of a novel bacterial toxin: the cytolysin of *Enterococcus faecalis*. Med. Microbiol. Immunol. **187**:183-190.

150. **Booth MC, Bogie CP, Sahl HG, Siezen RJ, Hatter KL, Gilmore MS.** 1996. Structural analysis and proteolytic activation of *Enterococcus faecalis* cytolysin, a novel lantibiotic. Mol. Microbiol. **21**:1175-1184.

151. **Gilmore MS, Segarra RA, Booth MC, Bogie CP, Hall LR, Clewell DB.** 1994. Genetic structure of the *Enterococcus faecalis* plasmid pAD1-encoded cytolytic toxin system and its relationship to lantibiotic determinants. J. Bacteriol. **176**:7335-7344.

152. **Haas W, Shepard BD, Gilmore MS.** 2002. Two-component regulator of *Enterococcus faecalis* cytolysin responds to quorum-sensing autoinduction. Nature **415**:84-87.

153. **Coburn PS, Hancock LE, Booth MC, Gilmore MS.** 1999. A novel means of self-protection, unrelated to toxin activation, confers immunity to the bactericidal effects of the *Enterococcus faecalis* cytolysin. Infect. Immun. **67**:3339-3347.

154. **Knerr PJ, van der Donk WA.** 2013. Chemical synthesis of the lantibiotic lacticin 481 reveals the importance of lanthionine stereochemistry. J. Am. Chem. Soc. **135**:7094-7097.

155. **Quadri LE, Sailer M, Roy KL, Vederas JC, Stiles ME.** 1994. Chemical and genetic characterization of bacteriocins produced by *Carnobacterium piscicola* LV17B. J. Biol. Chem. **269**:12204-12211.

156. **Gursky LJ, Martin NI, Derksen DJ, van Belkum MJ, Kaur K, Vederas JC, Stiles ME, McMullen LM.** 2006. Production of piscicolin 126 by *Carnobacterium maltaromaticum* UAL26 is controlled by temperature and induction peptide concentration. Arch. Microbiol. **186**:317-325.

157. **Martin-Visscher LA, van Belkum MJ, Garneau-Tsodikova S, Whittal RM, Zheng J, McMullen LM, Vederas JC.** 2008. Isolation and characterization of carnocyclin A, a novel circular bacteriocin produced by *Carnobacterium maltaromaticum* UAL307. Appl. Environ. Microbiol. **74**:4756-4763.

158. **Stoffels G, Nissen-Meyer J, Gudmundsdottir A, Sletten K, Holo H, Nes IF.** 1992. Purification and characterization of a new bacteriocin isolated from a *Carnobacterium* sp. Appl. Environ. Microbiol. **58**:1417-1422.

159. **Margulies M, Egholm M, Altman WE, Attiya S, Bader JS, Bemben LA, Berka J, Braverman MS, Chen YJ, Chen Z, Dewell SB, Du L, Fierro JM, Gomes XV, Godwin BC, He W, Helgesen S, Ho CH, Irzyk GP, Jando SC, Alenquer ML,**

Jarvie TP, Jirage KB, Kim JB, Knight JR, Lanza JR, Leamon JH, Lefkowitz SM, Lei M, Li J, Lohman KL, Lu H, Makhijani VB, McDade KE, McKenna MP, Myers EW, Nickerson E, Nobile JR, Plant R, Puc BP, Ronan MT, Roth GT, Sarkis GJ, Simons JF, Simpson JW, Srinivasan M, Tartaro KR, Tomasz A, Vogt KA, Volkmer GA, Wang SH, Wang Y, Weiner MP, Yu P, Begley RF, Rothberg JM. 2005. Genome sequencing in microfabricated high-density picolitre reactors. Nature **437**:376-380.

160. **Leonard MT, Panayotova N, Farmerie WG, Triplett EW, Nicholson WL.** 2013. Complete genome sequence of *Carnobacterium gilichinskyi* strain WN1359T (DSM 27470T). Genome Announc. **1**:e00985-13.

161. **Quadri LE, Kleerebezem M, Kuipers OP, de Vos WM, Roy KL, Vederas JC, Stiles ME.** 1997. Characterization of a locus from *Carnobacterium piscicola* LV17B involved in bacteriocin production and immunity: evidence for global inducer-mediated transcriptional regulation. J. Bacteriol. **179**:6163-6171.

162. **Tulini FL, De Martinis EC.** 2010. Improved adsorption-desorption extraction applied to the partial characterization of the antilisterial bacteriocin produced by *Carnobacterium maltaromaticum* C2. Braz. J. Microbiol. **41**:493-496.

163. **Coburn PS, Pillar CM, Jett BD, Haas W, Gilmore MS.** 2004. *Enterococcus faecalis* senses target cells and in response expresses cytolysin. Science **306**:2270-2272.

164. **Wuthrich K**. 1986. NMR of Proteins and Nucleic Acids, (1st ed.), John Wiley & Sons, New York.

165. **Sambrook J, Russell DW.** 2006. Directional cloning into plasmid vectors. CSH Protoc. **2006**

166. **Coburn PS, Gilmore MS.** 2003. The *Enterococcus faecalis* cytolysin: a novel toxin active against eukaryotic and prokaryotic cells. Cell Microbiol. **5**:661-669.

167. **Hauge HH, Mantzilas D, Eijsink VG, Nissen-Meyer J.** 1999. Membrane-mimicking entities induce structuring of the two-peptide bacteriocins plantaricin E/F and plantaricin J/K. J. Bacteriol. **181**:740-747.

168. **Rogne P, Fimland G, Nissen-Meyer J, Kristiansen PE.** 2008. Three-dimensional structure of the two peptides that constitute the two-peptide bacteriocin lactococcin G. Biochim. Biophys. Acta **1784**:543-554.

169. **Nissen-Meyer J, Oppegard C, Rogne P, Haugen HS, Kristiansen PE.** 2010. Structure and mode-of-action of the two-peptide (class-IIb) bacteriocins. Probiotics Antimicrob. Proteins **2**:52-60.

170. **Martin-Visscher LA, Gong X, Duszyk M, Vederas JC.** 2009. The three-dimensional structure of carnocyclin A reveals that many circular bacteriocins share a common structural motif. J. Biol. Chem. **284**:28674-28681.

171. **Gonzalez C, Langdon GM, Bruix M, Galvez A, Valdivia E, Maqueda M, Rico M.** 2000. Bacteriocin AS-48, a microbial cyclic polypeptide structurally and functionally related to mammalian NK-lysin. Proc. Natl. Acad. Sci. U. S. A. **97**:11221-11226.

172. **Gong X, Martin-Visscher LA, Nahirney D, Vederas JC, Duszyk M.** 2009. The circular bacteriocin, carnocyclin A, forms anion-selective channels in lipid bilayers. Biochim. Biophys. Acta **1788**:1797-1803.

173. **Galvez A, Maqueda M, Martinez-Bueno M, Valdivia E.** 1991. Permeation of bacterial cells, permeation of cytoplasmic and artificial membrane vesicles, and channel formation on lipid bilayers by peptide antibiotic AS-48. J. Bacteriol. **173**:886-892.

174. **Liu X, Vederas JC, Whittal RM, Zheng J, Stiles ME, Carlson D, Franz CM, McMullen LM, van Belkum MJ.** 2011. Identification of an N-terminal formylated, two-peptide bacteriocin from *Enterococcus faecalis* 710C. J. Agric. Food Chem. **59**:5602-5608.

175. **Johnson BA.** 2004. Using NMRView to visualize and analyze the NMR spectra of macromolecules. Methods Mol. Biol. **278**:313-352.

176. **Guntert P.** 2004. Automated NMR structure calculation with CYANA. Methods Mol. Biol. **278**:353-378.

177. **Dolinsky TJ, Nielsen JE, McCammon JA, Baker NA.** 2004. PDB2PQR: an automated pipeline for the setup of Poisson–Boltzmann electrostatics calculations. Nucleic Acids Res. **32**:W665-W667.

178. **Rea MC, Sit CS, Clayton E, O'Connor PM, Whittal RM, Zheng J, Vederas JC, Ross RP, Hill C.** 2010. Thuricin CD, a posttranslationally modified bacteriocin with a narrow spectrum of activity against *Clostridium difficile*. Proc. Natl. Acad. Sci. U. S. A. **107**:9352-9357.

179. **Chen Y, Ludescher RD, Montville TJ.** 1997. Electrostatic interactions, but not the YGNGV consensus motif, govern the binding of pediocin PA-1 and its fragments to phospholipid vesicles. Appl. Environ. Microbiol. **63**:4770-4777.

180. **Fleury Y, Dayem MA, Montagne JJ, Chaboisseau E, Le Caer JP, Nicolas P, Delfour A.** 1996. Covalent structure, synthesis, and structure-function studies of mesentericin Y 105(37), a defensive peptide from gram-positive bacteria *Leuconostoc mesenteroides*. J. Biol. Chem. **271**:14421-14429.

181. **Derksen DJ, Stymiest JL, Vederas JC.** 2006. Antimicrobial leucocin analogues with a disulfide bridge replaced by a carbocycle or by noncovalent interactions of allyl glycine residues. J. Am. Chem. Soc. **128**:14252-14253.

182. **Derksen DJ, Boudreau MA, Vederas JC.** 2008. Hydrophobic interactions as substitutes for a conserved disulfide linkage in the type IIa bacteriocins, leucocin A and pediocin PA-1. ChemBioChem **9**:1898-1901.

183. **Sprules T, Kawulka KE, Gibbs AC, Wishart DS, Vederas JC.** 2004. NMR solution structure of the precursor for carnobacteriocin B2, an antimicrobial peptide from *Carnobacterium piscicola*. Eur. J. Biochem. **271**:1748-1756.

184. **Makrides SC.** 1996. Strategies for achieving high-level expression of genes in *Escherichia coli*. Microbiol. Rev. **60**:512-538.

185. **Vuister GW, Bax AD.** 1993. Quantitative J correlation: a new approach for measuring homonuclear three-bond J (HNH. alpha.) coupling constants in 15N-enriched proteins. J. Am. Chem. Soc. **115**:7772-7777.

186. **Cornilescu G, Delaglio F, Bax A.** 1999. Protein backbone angle restraints from searching a database for chemical shift and sequence homology. J. Biomol. NMR **13**:289-302.

187. **Pace CN, Scholtz JM.** 1998. A helix propensity scale based on experimental studies of peptides and proteins. Biophys. J. **75**:422-427.

188. **Roccatano D, Colombo G, Fioroni M, Mark AE.** 2002. Mechanism by which 2,2,2-trifluoroethanol/water mixtures stabilize secondary-structure formation in peptides: a molecular dynamics study. Proc. Natl. Acad. Sci. U. S. A. **99**:12179-12184.

189. **Yau WM, Wimley WC, Gawrisch K, White SH.** 1998. The preference of tryptophan for membrane interfaces. Biochemistry **37**:14713-14718.

190. **Wiegand I, Hilpert K, Hancock RE.** 2008. Agar and broth dilution methods to determine the minimal inhibitory concentration (MIC) of antimicrobial substances. Nat. Protoc. **3**:163-175.

191. **Hanahan D.** 1983. Studies on transformation of *Escherichia coli* with plasmids. J. Mol. Biol. **166**:557-580.

192. **Sievers F, Wilm A, Dineen D, Gibson TJ, Karplus K, Li W, Lopez R, McWilliam H, Remmert M, Soding J, Thompson JD, Higgins DG.** 2011. Fast, scalable generation of high-quality protein multiple sequence alignments using Clustal Omega. Mol. Syst. Biol. **7**:539.

193. **Ansari MZ, Yadav G, Gokhale RS, Mohanty D.** 2004. NRPS-PKS: a knowledge-based resource for analysis of NRPS/PKS megasynthases. Nucleic Acids Res. **32**:W405-13.

194. **Rottig M, Medema MH, Blin K, Weber T, Rausch C, Kohlbacher O.** 2011. NRPSpredictor2--a web server for predicting NRPS adenylation domain specificity. Nucleic Acids Res. **39**:W362-7.

195. **Dai Y, Whittal RM, Li L.** 1999. Two-layer sample preparation: a method for MALDI-MS analysis of complex peptide and protein mixtures. Anal. Chem. **71**:1087-1091.

196. **Rutherford K, Parkhill J, Crook J, Horsnell T, Rice P, Rajandream MA, Barrell B.** 2000. Artemis: sequence visualization and annotation. Bioinformatics **16**:944-945.

197. **Delaglio F, Grzesiek S, Vuister GW, Zhu G, Pfeifer J, Bax A.** 1995. NMRPipe: a multidimensional spectral processing system based on UNIX pipes. J. Biomol. NMR **6**:277-293.

198. **Inoue H, Nojima H, Okayama H.** 1990. High efficiency transformation of *Escherichia coli* with plasmids. Gene **96**:23-28.